Deutsches Diabetes-Zentrum

Heinrich Heine
Universität Düsseldorf

Characterization of the exercise-induced secretome of insulin sensitive and insulin resistant skeletal muscle cells

Inaugural-Dissertation

zur Erlangung des Doktorgrades
der Mathematisch-Naturwissenschaftlichen Fakultät
der Heinrich-Heine-Universität Düsseldorf

Vorgelegt von

Pia Marlene Förster

aus Berlin

Düsseldorf, April 2024

aus dem Institut für Klinische Biochemie und Pathobiochemie
des Deutschen Diabetes-Zentrums (DDZ)
Leibniz-Zentrum für Diabetes-Forschung
an der Heinrich-Heine-Universität Düsseldorf

Gedruckt mit der Genehmigung der
Mathematisch-Naturwissenschaftlichen Fakultät der
Heinrich-Heine-Universität Düsseldorf

Berichterstatter:

1. Prof. Dr. Hadi Al-Hasani
2. Prof. Dr. Jürgen Scheller

Tag der mündlichen Prüfung: 27.06.2024

Summary

Skeletal muscle is an endocrine organ that secretes proteins (myokines) to communicate with other organs in an autocrine, paracrine, and endocrine manner. Contraction-induced myokines are released from skeletal muscle cells and are thought to mediate the health-promoting effects of exercise. Electrical pulse stimulation (EPS) is a widely used method to stimulate contractile activity in skeletal muscle cells *in vitro*. Recent studies have identified contraction-induced myokines released in response to EPS, however, the knowledge about the composition of the muscle secretome of contracting skeletal muscle cells is limited.

In the present thesis, the muscle secretomes of the two most commonly used cell culture models, murine C2C12 cells and human skeletal muscle cells (HSkMCs), were investigated after acute (6h) low-frequency EPS. In both cell culture models, EPS induced contractile activity concurrent with activation of the AMPK signaling pathway. Analysis of muscle secretomes by high-resolution mass spectrometry (MS) identified 1,440 and 385 novel myokines secreted by murine and human myotubes, respectively. While EPS induced the secretion of hundreds of proteins, the overlap of myokines in both murine and human secretomes was moderate, suggesting that EPS induced a distinct myokine secretion profile in both cell models.

Secondly, the effect of EPS on the muscle secretome of insulin sensitive and insulin resistant HSkMCs was investigated. An *in vitro* protocol was established by exposing human myotubes to high levels (800 µM) of palmitic acid. Insulin resistance was characterized by impaired insulin signaling and reduced insulin-stimulated glycogen synthesis in HSkMCs. MS analysis revealed differences in the secretomes of resting and contracting insulin sensitive and resistant myotubes, indicating that the myokine secretion profile is altered in the insulin resistant state. A comprehensive analysis of the secreted proteins revealed a distinct myokine pattern in contracting human myotubes, comprising 70 myokines exclusively secreted in insulin sensitive cells and 93 myokines exclusively secreted in insulin resistant cells. Lastly, bioinformatics analysis suggests that several different secretory pathways are altered in insulin resistant cells, leading to a different balance of classical and unconventional protein secretion (UPS). In conclusion, insulin resistant HSkMCs exhibit distinct alterations in myokine secretion, which may affect, at least in part, the metabolic response to exercise in type 2 diabetes. Moreover, comparative analysis of the secretomes underscore the importance of studies using HSkMCs to translate the knowledge gained to the human system. Further studies are needed to investigate i) the underlying mechanisms that cause the changes in the myokine profile of insulin resistant HSkMCs, and ii) the impact of differentially secreted myokines on human metabolism.

Zusammenfassung

Der Skelettmuskel ist ein endokrines Organ, das Proteine (Myokine) sekretiert, um mit anderen Organen auf auto-, para- und endokrine Weise zu kommunizieren. Durch die Muskelkontraktion werden Myokine freigesetzt, von denen angenommen wird, dass sie an den gesundheitsfördernden Effekten körperlicher Aktivität beteiligt sind. Die Elektrische Puls Stimulation (EPS) ist eine weit verbreitete Methode, um die kontraktile Aktivität von Skelettmuskelzellen *in vitro* zu simulieren. Mehrere Studien haben bereits kontraktionsinduzierte Myokine identifiziert, jedoch ist das bisherige Wissen über die Zusammensetzung des Muskelsekretoms kontrahierender Skelettmuskelzellen begrenzt.

In der vorliegenden Arbeit wurden die Sekretomprofile der beiden am häufigsten verwendeten Zellkulturmodelle, murine C2C12 Skelettmuskelzellen und humane Skelettmuskelzellen (HSkMCs), nach akuter (6h) Niederfrequenz-EPS untersucht. In beiden Zellkulturmodellen führte die EPS zu einer kontraktilen Aktivität, die mit der Aktivierung des AMPK-Signalweges einherging. Die Analyse der Muskelsekretome mittels hochauflösender Massenspektrometrie (MS) identifizierte 1440 (C2C12) bzw. 385 (HSkMCs) bislang nicht beschriebene Myokine. Obwohl die EPS die Sekretion von Hunderten von Proteinen induzierte, war die Überlappung der Myokine beider Sekretome moderat. Des Weiteren wurde die Wirkung von der EPS auf das Muskelsekretom von insulinsensitiven und insulinresistenten HSkMCs untersucht. Insulinresistenz wurde *in vitro* durch die Behandlung von humanen Myotuben mit Palmitinsäure erzeugt, welche durch eine Beeinträchtigung der Insulinsignaltransduktion sowie einer reduzierten insulin-stimulierten Glykogensynthese im Skelettmuskel charakterisiert wurde. Die MS-Analyse ergab Unterschiede in den Sekretomen von ruhenden und kontrahierenden insulinsensitiven und resistenten Myotuben, was darauf hindeutet, dass das Myokin-Sekretionsprofil im insulinresistenten Zustand verändert ist. Insgesamt induzierte die EPS die Sekretion von 70 Myokinen ausschließlich von insulinsensitiven und 93 Myokinen ausschließlich von insulinresistenten Zellen. Des Weiteren zeigten bioinformatische Analysen des insulinresistenten Sekretoms Veränderungen innerhalb der konventionellen und unkonventionellen Sekretionswege. Zusammenfassend lässt sich sagen, dass insulinresistente HSkMCs deutliche Veränderungen in der Myokinsekretion aufweisen, die zumindest teilweise die metabolische Reaktion auf körperliche Betätigung bei Diabetes mellitus Typ 2 beeinflussen können. Darüber hinaus unterstreicht die vergleichende Analyse der Sekretome beider Spezies die Bedeutung von Studien mit HSkMCs, um die gewonnenen Erkenntnisse auf das menschliche System zu übertragen. Weitere Studien sind erforderlich, um i) die zugrundeliegenden Mechanismen zu untersuchen, die die Veränderungen im Myokinprofil von insulinresistenten HSkMCs verursachen, und ii) die Auswirkungen der unterschiedlich sezernierten Myokine auf den menschlichen Stoffwechsel.

Table of contents

1 Introduction

1.1 Diabetes mellitus

Diabetes mellitus is a chronic metabolic disease with a steadily increasing prevalence worldwide, posing a major challenge to the human population of today´s world. In 2021, diabetes affected approximately 537 million adults aged 20-79 years worldwide and was responsible for 6.7 million deaths, yet a large number of cases remain undiagnosed (1, 2). Current numbers are projected to increase to 643 million affected adults by 2030 and to 783 million by 2045. In Germany, 6.2 million adults (20-79 years) are currently living with diabetes, corresponding an age-adjusted prevalence of 6.9%, which is expected to rise steadily to 7.9% by 2035 and 8.4% by 2045. In addition, 1.35 million people in Germany remained undiagnosed with diabetes in 2021, which accounts for 21.7% (2).

Type 1 diabetes mellitus (T1DM) and type 2 diabetes mellitus (T2DM) are the two main forms of diabetes mellitus, which are both characterized by a decrease in functional beta cell mass, but their pathogenesis is quite different (3). T1DM is considered an autoimmune disease that leads to the destruction of the insulin-producing pancreatic beta cells. This results in absolute insulin deficiency and hyperglycemia, requiring lifelong treatment with insulin substitution medication. It is diagnosed by an elevated glycated hemoglobin (HbA_{1C}) level (6.5% or higher), often at an early age as it is one of the most prevalent chronic diseases in childhood, but it can also be diagnosed in adulthood (4).

T2DM is a metabolic disease that affects the majority (90%) of patients with diabetes mellitus and also has a significant impact on their quality of life (1). Glucose homeostasis is impaired by defective insulin secretion and a poor response of insulin sensitive tissue to insulin (termed insulin resistance), leading to a metabolic imbalance (5, 6). As a consequence, hyperglycemia is responsible for causing micro- and macrovascular complications such as retinopathy, nephropathy, neuropathy and cardiovascular comorbidities. In addition to genetic predisposition, the pathogenesis of T2DM is mainly driven by environmental factors such as a sedentary lifestyle and unhealthy diet, both of which promote obesity and insulin resistance (5). Prevention and treatment of T2DM therefore include lifestyle interventions, such as a healthy diet and regular exercise in conjunction with pharmacotherapy. While the benefits of exercise have been extensively studied, there remains a subset of individuals who do not experience the expected beneficial effects of exercise (e.g., lowering of blood glucose levels), referred to as “non-responders” (7). The reasons why certain individuals do not respond to exercise are not fully understood, underscoring the importance of understanding the mechanisms that drive the beneficial health effects of exercise (8). Exploring molecular predictors such as genetic, epigenetic and metabolic factors may shed light on why non-

responders fail to benefit from exercise (7). Moreover, it is probable that individuals will respond differently to specific exercise intervention, as it was shown that aerobic exercise activates different signaling pathways than resistance exercise (9). Therefore, understanding the different mechanisms driving the health promoting effects of exercise could potentially lead to tailored exercise interventions to ensure that these individuals receive appropriate therapies (7, 10). Such personalized approaches could complement pharmacotherapy and a balanced diet to maximize the overall effectiveness of treatment regimens (7).

In addition to the two main forms of diabetes, there are also other types of diabetes, such as gestational diabetes, which can occur during pregnancy without a history of the disease, or secondary diabetes, which is caused by other medical conditions (11).

1.2 Insulin resistance

Environmental factors such as a sedentary lifestyle, unhealthy diet and lack of physical activity are the main factors contributing to the development of insulin resistance, which often results as a consequence of obesity (excessive accumulation of adipose tissue, body mass index of over 30 kg/m^2) (12, 13). Insulin resistance is often diagnosed in late adulthood but is becoming increasingly common in young people as more overweight children develop obesity (14). Insulin resistance is defined by a decreased metabolic response to the hormone insulin, which is produced and secreted by the beta cells of the pancreas to regulate circulating blood glucose levels and promote the uptake of glucose into cells (15). In healthy individuals, the binding of insulin to its receptors on the plasma membrane activates a signaling cascade in target cells that promotes cellular glucose uptake and glycogen storage, particularly in muscle and adipose tissue (16). In insulin resistance, insulin signaling is impaired, characterized by a diminished response to insulin, which renders target tissues unable to properly remove blood glucose, inhibit lipolysis, stimulate glycogen synthesis, and inhibit hepatic glucose production, resulting in elevated blood glucose levels (called hyperglycemia). To compensate for the steadily rising circulating blood glucose levels, pancreatic beta cells produce and secrete more insulin, resulting in hyperinsulinemia (17). The resulting vicious cycle of hyperglycemia and hyperinsulinemia eventually leads to decompensation of the insulin-producing beta cells in the pancreas, leading to the development of T2DM (5, 15, 18).

In obesity, excess body fat, particularly visceral fat, promotes the release of large amounts of free fatty acids from adipose tissue because insulin fails to inhibit lipolysis (the hydrolysis of lipid triglycerides (TG) to glycerol and free fatty acids (FFA)), directly contributing to impaired insulin signaling in skeletal muscle and liver (19, 20). In addition, the accumulation of excess lipids and toxic lipid metabolites such as FFA, diacylglycerol (DAG) and ceramide in non-

adipose tissues (ectopic fat disposition) leads to lipid-induced toxicity (lipotoxicity), which is another major reason for the development of insulin resistance in liver and muscle tissue (16, 21). Under physiological conditions, insulin stimulates the uptake of circulating glucose and its storage as glycogen in skeletal muscle and liver, but in insulin resistance, proximal insulin signaling is disrupted, including by higher levels of DAG, leading to reduced glucose uptake, which results in elevated circulating glucose levels (21). In addition, insulin-mediated suppression of gluconeogenesis (*de novo* glucose production) in the liver is disrupted, leading to further production of glucose, resulting in higher circulating glucose levels (17, 22).

1.3 The skeletal muscle

1.3.1 Skeletal muscle anatomy

Skeletal muscle is a highly dynamic and plastic tissue, accounting for about 40% of total body weight in humans and representing 50-75% of all body proteins. It is a versatile organ involved in many immunometabolic processes and is part of the locomotor system, responsible for the movement of the joints by contraction (23). The structure of skeletal muscle is defined by a specific arrangement of muscle fibers, also known as myofibers. Each myofiber represents a muscle cell that develops during the differentiation of uninucleated myoblasts into multinucleated myotubes (called myogenesis) (24, 25). To generate force during muscle contraction, the basic cellular contractile unit, the sarcomere, is required, which develops during myogenesis and is formed by differentiated, multinucleated myofibers (26). Sarcomeres are arranged in visible rows in cylindrical bundles and form myofibrils, which is why skeletal muscle is categorized as striated muscle (27). It is a molecular machinery that extends from Z-disk to Z-disk, comprising an A-band (thick filaments with myosin) and half I-bands (thin filaments with actin) (24, 27, 28). Myosin, the force-generating motor protein at the sarcomere center, along with regulatory proteins such as the troponin complex and tropomyosin, drive force generation and movement (23, 24, 27). The structure of a myofiber and its sarcomere is simplified illustrated in Figure 1.

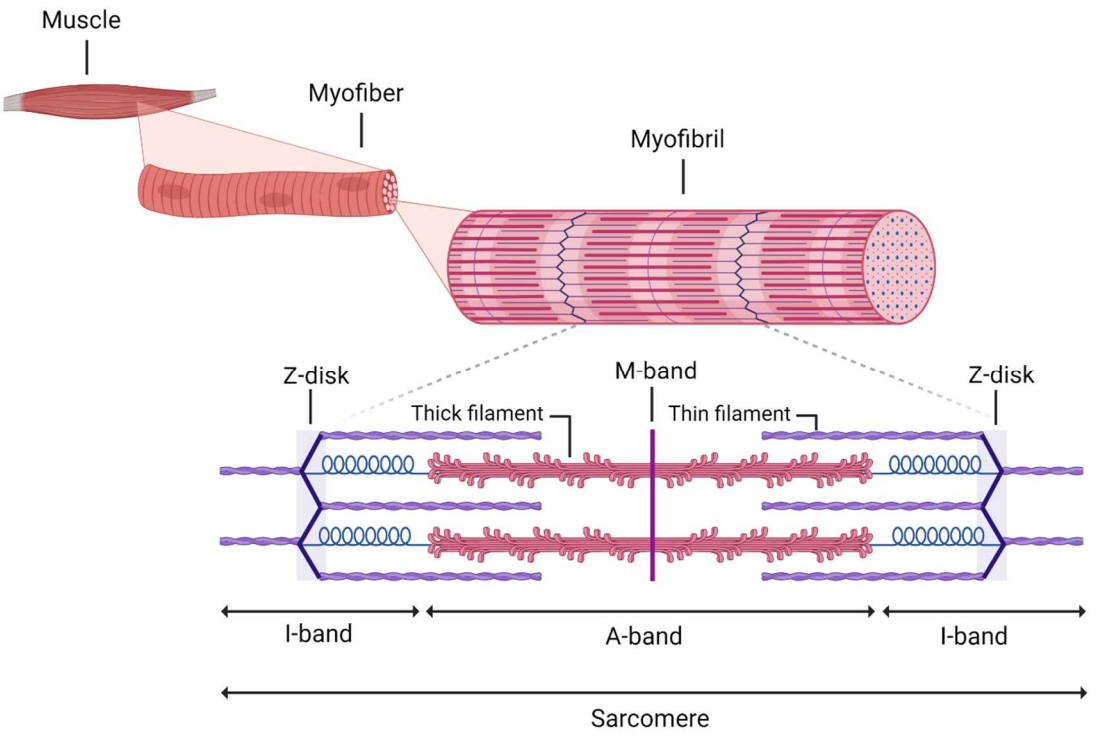

Figure 1: The structure of skeletal muscle, simplified representation of a single myofiber and its contractile unit, the sarcomere. The figure was created with BioRender.com

Skeletal muscle is characterized by its capacity for self-renewal and therefore responds to injury by activating quiescent satellite cells that proliferate and differentiate into multinucleated myofibers to allow skeletal muscle repair and regeneration (25, 29). Satellite cells are located between the sarcolemma and the basal lamina and represent the adult stem cells of the skeletal muscle (30). They are activated by transcription factors such as myogenic regulatory factors (MRF), which regulate the expression of molecular markers representing different stages of myogenesis (31, 32). Indeed, satellite cell biogenesis, survival and self-renewal processes involve paired box (Pax) family transcription factors such as *Pax3* and *Pax7* (33), while in the early stages of myogenesis the expression of myoblast determination protein 1 (*MyoD*) is crucial, as it activates the expression of other myogenesis-associated proteins such as myogenin (*MyoG*), myogenic factor 5 (*Myf5)* and *Mrf4 (34-36)*. The latter are representative of later stages of differentiation, where *MyoG* is responsible for the fusion of myoblasts into multinucleated myotubes (28). Furthermore, terminal differentiation is characterized by the downregulation of *Myf5*, which is highly abundant in myoblasts, and later by *MyoD (24, 25)*. The process of myogenesis is simplified illustrated in Figure 2.

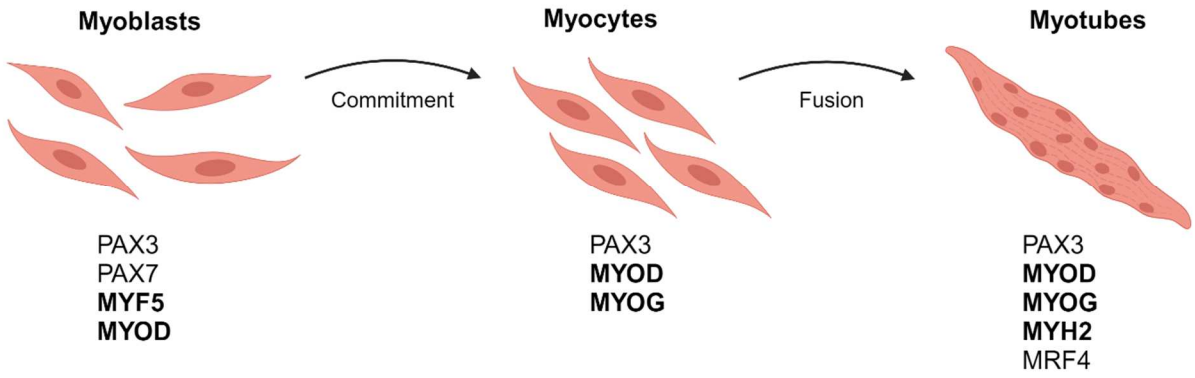

Figure 2: Representative genes for different stages of myogenesis. After the initiation of differentiation, mononuclear myoblasts begin to arrange themselves to myocytes and fuse to multinucleated myotubes, eventually. Representative differentiation markers used in this thesis for myoblasts and myotubes are highlighted in bold. The figure was created with BioRender.com

1.3.2 Skeletal muscle as an endocrine organ

In addition to muscle contraction, skeletal muscle has long been known to function as an endocrine organ by producing and releasing proteins known as myokines (37, 38). The first muscle-derived protein was described in 1997 by McPherron et al., who identified myostatin as a member of the transforming growth factor beta (TGF-β) superfamiliy and a negative autocrine regulator of skeletal muscle growth (39). In 2003, Pederson et al. first proposed to define these muscle-specific secreted proteins as “myokines” (40). Since then, hundreds of myokines have been identified and investigated in targeted and non-targeted studies addressing their role and function in communication between skeletal muscle and other organs during exercise and disease (41-43). Investigation of their auto-, para- and endocrine effects on metabolic regulation is essential as it may contribute to address and understand the consequences associated with insulin resistance and T2DM (44, 45). During muscle contraction, skeletal muscle responds by releasing proteins that mediate the beneficial health effects of exercise, but the underlying mechanisms remain unclear (46). Contraction-induced secreted proteins have recently been described as “exerkines” (47) and represent potential candidates to be used as biomarkers for the prevention and treatment of cardiovascular diseases, T2DM or obesity (48, 49). Furthermore, it has been observed that myokine secretion is altered and impaired during physical inactivity, which marks the onset of metabolic diseases such as T2DM (46, 50). In addition to myokines, the skeletal muscle secretome contains other valuable markers such as extracellular vesicles (EV) (e.g. exosomes), which contain coding and non-coding RNAs, DNA and various metabolites that are also engaged in muscle-organ crosstalk and metabolic regulation (51). Previous proteomic studies have analyzed the muscle secretome (the myokinome) using non-targeted approaches and revealed a large number of secreted proteins (52, 53), but the biological function of these myokines remains to be elucidated and has only been described for about 5% of all known myokines (38, 49).

1.3.3 Myokines – skeletal muscle-derived secreted proteins

During metabolic disease, the signaling pathway of certain myokines was altered at the mRNA and protein levels in skeletal muscle, suggesting that changes in the myokinome play a critical role in the onset of insulin resistance and T2DM (43, 53). Using targeted approaches, the concentration of selected circulating pro-inflammatory myokines was measured in T2DM patients and non-diabetic subjects, revealing increased levels of the pro-inflammatory cytokines TNF-α, interleukins such as IL-6, IL-8, IL-15, follistatin and MCP-1 in T2DM patients compared to healthy subjects (50). In addition, the myokine secretion profile is also affected and altered in response to exercise and as myokines play a central role in muscle-organ crosstalk, they are thought to be involved in mediating the health-promoting effects of exercise (38, 42, 54, 55). Therefore, previous studies have investigated the myokinome after exercise, resulting in the identification of contraction-induced myokines such as IL-6, IL-8 and IL-15, fibroblast growth factor 21 (FGF-21), leukemia inhibitory factor (LIF), irisin, myostatin, angiopoietin-like 4 (ANGPTL4), brain-derived neurotrophic factor (BDNF), follistatin-like 1 (FSTL1), vascular endothelial growth factor (VEGF) and secreted protein acidic and rich in cysteine (SPARC) (48, 56-58). The following sections present a selection of myokines that have been described and investigated as exerkines and therefore may contribute to the health-promoting effects of exercise, however, some are also secreted by other tissues, such as adipose tissue, where they show pro-inflammatory properties.

1.3.3.1 IL-6

IL-6 and its dual role as an exerkine and mediator of systemic inflammation has been intensively studied over the past decades and is undoubtedly the most thoroughly characterized myokine at present (37, 58). During muscle contraction, increased levels of circulating IL-6 are secreted in response to exercise, but the amount of IL-6 secreted depends on the type of exercise (endurance vs resistance training, acute vs chronic exercise) (44, 46). Muscle contraction-induced IL-6 exerts its health-promoting effects (e.g. increased glucose uptake) in an endocrine and paracrine manner (56, 59, 60). Furthermore, previous studies have shown that IL-6 stimulates the expression of other anti-inflammatory cytokines, while suppressing the expression of the pro-inflammatory cytokine TNF-α (61). In contrast, chronic secretion of IL-6 leads to negative regulation of metabolic homeostasis, resulting in insulin resistance and T2DM (43, 59, 62, 63). IL-6 enters the cell via two receptors, either via the membrane-bound receptor (IL-6R), which induces the classical signaling, or by binding to the soluble form of the IL-6 receptor (sIL-6R), which induces trans signaling. While classical signaling mediates the anti-inflammatory effects of IL-6, trans signaling is responsible for promoting the pro-inflammatory effects of IL-6 (64), a process that causes the activation of inflammatory cells (macrophages) that express glycoprotein (gp)130 but lack the IL-6 receptor

(65). Pharmacological targeting of IL-6 trans signaling could control IL-6-mediated inflammation.

1.3.3.2 IL-8 and IL-15

Shortly after IL-6 was classified as a myokine, IL-8 (also known as chemokine ligand 8 (CXCL8)) and IL-15 were also recognized as such. Both are generally considered pro-inflammatory cytokines, but they also respond to exercise with increased mRNA and plasma levels and have recently been categorized as exerkines (37, 66). Both resistance and endurance training have been reported to stimulate IL-15 expression and secretion (46, 54, 56, 67), while IL-8 expression levels were increased by endurance training (68)and plasma levels were increased by electrical pulse stimulation (EPS), an *in vitro* muscle contraction method, after 24 hours (69) and 48 hours (70). IL-8 acts locally as an angiogenic factor in an autocrine and paracrine manner (67), while IL-15 contributes to the regulation of glucose metabolism and muscle development (37, 66). Cell culture studies using murine skeletal muscle cells (C2C12 cell line) have shown increased glucose uptake in skeletal muscle after treatment with IL-15 (71). Therefore, it may be a potential target for the prevention and treatment of metabolic diseases such as T2DM and obesity.

1.3.3.3 ANGPTL4

ANGPTL4 is an exercise-induced myokine involved in various physiological processes such as insulin sensitivity, lipid metabolism, and adipogenesis, and is also secreted by other organs such as adipose tissue, liver, and intestine (46). In myotubes, increased gene expression of ANGPTL4 was measured in response to four hours of EPS, and an increase in protein content was measured in the supernatant after eight hours of stimulation (69). In contrast, elevated circulating levels of ANGPTL4 were also observed in obese patients with or without T2DM (72), suggesting that it plays a dual role that is not yet fully understood in the context of glucose metabolism and obesity, so its potential role as a therapeutic target requires further investigation.

1.3.3.4 MCP-1

Another well-studied secreted protein is the adipo-myokine MCP-1, which acts as an inflammatory mediator when secreted by adipocytes and as an exerkine when secreted by skeletal muscle (66), but its role and function is controversial in the literature and still not fully understood (73). Cell culture studies with human myotubes from T2DM patients showed increased gene expression (74) and protein levels in the cell culture supernatant (50) of MCP-1. In addition, Sell et al. reported that incubation of human myotubes with MCP-1 resulted in impaired insulin signaling and glucose uptake in skeletal muscle (75). In contrast, other studies reported that MCP-1 was increased in response to different types of exercise (resistance

training, treadmill training, or cycling). Resistance training led to a strong increase in MCP-1 mRNA expression in skeletal muscle (76) and protein levels (77). Similar results have been reported after endurance training such as cycling (78) and treadmill exercise (79).

1.3.4 Protein secretion pathways

Classical protein secretion is defined by the trafficking of cargo proteins along the conventional secretion pathway, the ER to Golgi complex. The cargo proteins carry a signal peptide sequence (also known as a “leader sequence”, consisting of short amino acid sequences) at the N-terminus or a transmembrane domain, which facilitates their recognition and selection for the classical secretion pathway (80). Here, they travel from the ER via COPII-coated vesicles to the Golgi apparatus before reaching the plasma membrane (81, 82). Recently, studies have revealed alternative secretion pathways that secrete a large number of proteins into the extracellular space through unconventional routes (82-84). Unconventional protein secretion (UPS) pathways include cytosolic proteins that do not carry a signal peptide sequence (“leaderless proteins”) and transmembrane proteins that contain a signal peptide and are secreted bypassing the Golgi apparatus (85). There are four types of UPS: Type I and II include cytoplasmic leaderless non-vesicular proteins that are released directly into the extracellular space either by pore-mediated translocation across the plasma membrane (86-88) or via ATP-binding cassette (ABC) transporters (89). The formation of plasma membrane pores (Type I secretion), which mediates the translocation of cargo proteins across the plasma membrane, is either self-sustained or induced by inflammation. A prominent example of self-sustained lipid pore formation is the constitutively secreted fibroblast growth factor 2 (FGF2). It is recruited to the inner leaflet of the plasma membrane where it interacts with phosphatidylinositol-4,5-bisphosphate ($PI(4,5)P_2$), triggering self-oligomerization leading to membrane insertion and lipid pore formation, which mediates translocation of FGF2 across the plasma membrane into the extracellular space (84, 90). Another important discovery was that the membrane-bound heparan sulfates on the outer leaflet of the plasma membrane are required for the release of FGF2 into the extracellular space (82, 84). Inflammation is another key factor for lipid pore formation, which promotes the secretion of cytokines from the macrophage cytoplasm. A prominent example is IL-1β, which uses the Type I pathway when secreted from macrophages during inflammation (82, 90). Type II secretion remains poorly understood, but ABC transporter-mediated secretion is mainly used for the secretion of acylated peptides (82). The Type III secretion pathway is characterized by leaderless cytoplasmic vesicular proteins that are enveloped in membrane-bound organelles such as autophagosomes, lysosomes, endosomes, micovesicular bodies (MVB and is mainly triggered by stress (82, 91). MVB are important components of the endolysosomal system that package cytosolic proteins into vesicles and form intraluminal vesicles (ILV). This process is regulated by endosomal sorting complexes required for transport 0-III (ESCRT 0-III) proteins, which are

required for fusion of vesicles with the plasma membrane (90). Through exocytosis, small extracellular vesicles such as exosomes are released into the extracellular space. Recently, the study of extracellular vesicles such as exosomes has become of great interest, since their contents (e.g. genetic material DNA, mRNA, miRNA, lipids, carbohydrates, even entire organelles such as mitochondria) can be altered in disease (51, 92). Moreover, another double-membrane organelle called autophagosomes is often used to secrete cargo proteins into the extracellular space (90). In particular, autophagosomes are often used by cytokines and other inflammatory mediators for UPS, such as the pro-inflammatory cytokine IL-β (93, 94). Notably, IL-1β secretion is induced by a variety of stimuli, with inflammation inducing secretion via the Type I pathway and starvation (stress) inducing secretion via vesicular structures via the Type III pathway (82). Moreover, Golgi reassembly and stacking proteins (GRASP), such as GRASP55 and GRASP65 play a role in the formation of secretory autophagosomes and IL-1β secretion (82, 90)

Proteins assigned to Type IV of the UPS pathway are recognized by the signal recognition particle by carrying a signal peptide sequence. Similar to classically secreted proteins, they are synthesized in the ER on the ribosome, but when secreted into the extracellular space, they bypass the Golgi (82, 95). Type IV secretion is mostly triggered by various cellular stresses, including ER stress, mechanical stress, and nutrient starvation (95). Prominent examples of transmembrane proteins using Type IV UPS pathway are pendrin and cystic fibrosis transmembrane conductance regulator (CFRT). Mutations in both proteins lead to misfolding and ER retention. When ER-Golgi trafficking is blocked or under ER stress conditions, immature core-glycosylated CFTR and pendrin are transported to the plasma membrane by bypassing the Golgi. The underlying mechanisms facilitating this transport via the Type IV UPS pathway seem comparable for both proteins, as both are promoted by activation of the inositol-requiring enzyme 1 α (IRE1α) kinase pathway (85, 95). Taken together, it should be considered that certain cargo proteins are secreted via different types of UPS pathways, but some proteins undergo various UPS pathways to reach the extracellular space, such as IL-1β, which uses both Type I and III UPS pathways (91).

Another alternative secretion pathway is known as ectodomain shedding (96). Shedding is an irreversible post-translational modification process in which a protease known as a sheddase (e.g. ADAM proteases) cleaves a membrane protein substrate located either near or within its transmembrane domain (97). Subsequently, the soluble extracellular domain, called the ectodomain, of the membrane protein is released into the extracellular space. Regulated shedding is an important cellular mechanism that controls processes like adhesion, migration and proliferation ensuring proper functioning in both development and inflammation (98). It controls the activation or inactivation of surface proteins, such as the release of growth factors

or cytokines (e.g. TGF-α, IL-6-receptor) attached to the plasma membrane (97). However, when dysregulated, shedding can be implicated in the development of several diseases, including Alzheimer´s disease, cancer, infections and inflammatory diseases (96, 98). An overview of the different secretion pathways is shown below in Figure 3.

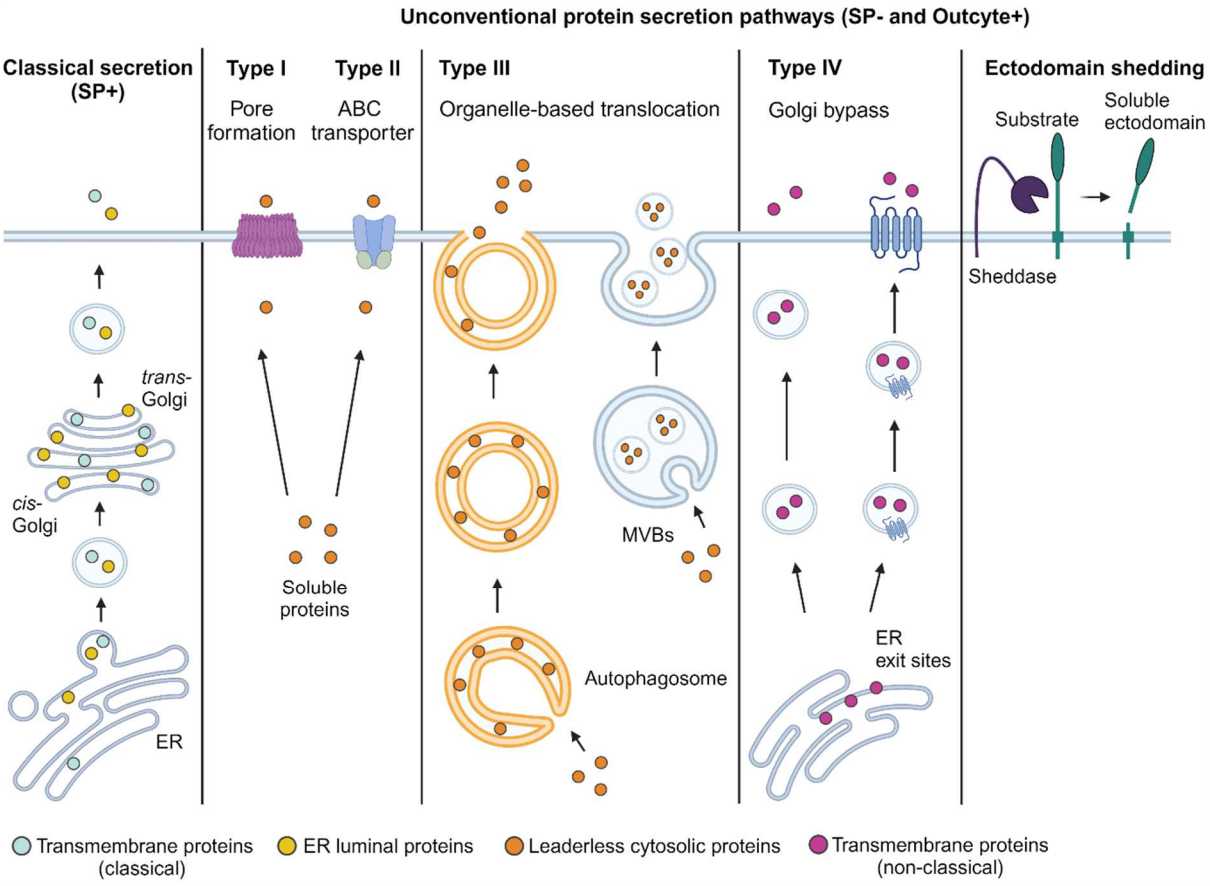

Figure 3: Classical protein secretion versus UPS pathways. Classical secretion pathway (ER-to-Golgi) involves proteins that carry a SP sequence at the N-terminus. UPS pathways involves trafficking of leaderless proteins (Type I-III) and trafficking of proteins containing a SP sequence but bypass the Golgi (Type IV). UPS: unconventional protein secretion; ER: endoplasmic reticulum; SP: signal peptide, MVBs: multivesicular bodies. The figure was created with BioRender.com

1.3.4.1 Bioinformatical analysis tools for the prediction of secretion pathways

The web-based tools SignalP 6.0, SecretomeP 2.0 and, more recently Outcyte 1.0 are bioinformatics tools that enable computational prediction and classification of secreted proteins in terms of their secretion pathways (99, 100). SignalP is a machine learning program that first identifies proteins carrying a cleavable signal peptide (SP) sequence and then detects the position of the SP cleavage site. It is used to predict classically secreted proteins, referred to as “SP+ proteins” in this thesis (101, 102). Another sequence-based program is SecretomeP, which allows the prediction of leaderless proteins secreted via UPS pathways. The program is based on the hypothesis that extracellular proteins share common characteristics regardless of their secretion pathway. A dataset consisting of classically secreted proteins is used as a

positive reference for extracellular proteins with the signal peptide part of the sequence removed, allowing the prediction of non-classically secreted proteins, referred to in this thesis as “SP- proteins” (103, 104). The latest tool, Outcyte 1.0, is also applicable for the prediction of proteins secreted via UPS pathways. It has an integrated tool (Outcyte-SP) that first identifies proteins with a signal peptide or a transmembrane domain within the first 70 amino acids. The remaining proteins are further filtered by comparing them to the Outcyte-UPS database, which is based on in-house experimental secretome data from different cell lines and uses physicochemical features derived directly from protein sequences to enable the prediction of UPS proteins (100). USP proteins detected by Outcyte are referred to as “Outcyte+” in this thesis. Bioinformatic classification and different secretion pathways are shown above in Figure 3.

1.4 AKT/ PI3K and AMPK signaling in skeletal muscle

1.4.1 Insulin-induced signaling

The insulin receptor (IR) is expressed on the plasma membrane at the cell surface of insulin-responsive tissues and is a tetrameric protein consisting of two extracellular insulin-binding alpha subunits coupled to two transmembrane beta subunits. When the polypeptide hormone insulin binds to the receptor, autophosphorylation activates an intracellular tyrosine kinase domain located on the beta subunits (105, 106). The conformational change of the IR and consequently its activation leads to the recruitment of new receptor substrates to the membrane, such as those of the insulin receptor substrate (IRS) protein family (IRS1-6), which are scaffold proteins responsible for mediating insulin signaling (107, 108). In skeletal muscle, the two most important IRS proteins involved in metabolic regulation are IRS-1 and IRS-2. While IRS-1 is crucial for myoblasts differentiation and glucose metabolism, IRS-2 plays an important role in lipid metabolism and extracellular signal-regulated kinase (ERK) activation (109, 110). The catalytic subunit of IRS1 is then activated, leading to the phosphorylation of phosphatidylinositol-4,5-bisphosphate (PIP_2), which generates the lipid messenger phosphatidylinositol (3,4,5)-trisphosphate (PIP_3). Protein kinase B (PKB/AKT) is then recruited to the plasma membrane by PIP_3 and activated by phosphorylation (106, 111). The 3-phosphoinositide-dependent protein kinase 1 (PDK-1), an upstream kinase of AKT, is activated by binding its pleckstrin homology (PH) domain to membrane-bound PIP_3 and subsequently phosphorylating AKT at Thr-308 (112). However, full activation of AKT is only achieved by phosphorylation at Ser-473, which is mediated by the mammalian target of rapamycin complex 2 (mTORC2) (113, 114). In total, there are three different isoforms of AKT, in particular AKT2 plays an important role in mediating insulin action as it is the most prominent isoform in insulin sensitive tissues (106, 115). AKT mediates the activation and phosphorylation of many downstream targets, such as mTORC1, through its downstream target proline-rich AKT

substrate 40 kDa (PRAS40), leading to the abrogation of mTOR1 inhibition. In addition, mTOR1 activation can result from phosphorylation of tuberous sclerosis complex 2 (TCS-2) at Thr-1642, which leads to degradation of a complex consisting of TCS-1 and TCS-2. Following this, the 4E-binding protein 1 (4E-BP1) is phosphorylated and inhibited, while the ribosomal protein S6 kinases S6K1 and S6K2 as well as SREBP1 are activated, which have an influence on various genes involved in metabolism, protein synthesis and cell growth (116, 117). Furthermore, AKT phosphorylates transcription factors of the forkhead box O (FOXO) family, which are responsible for the regulation of lipogenic and gluconeogenic genes (118). For insulin-stimulated glucose uptake, phosphorylation of RabGTPase-activating proteins (RabGAPs), TBC1 domain family 4 (TBC1D4), also known as AKT substrate of 160 kDa (AS160), and its homologue TBC1D1, by AKT is indispensable to promote the translocation of glucose transporter type 4 (GLUT4) vesicles to the plasma membrane. GLUT4 storage vesicle (GSV) trafficking is initiated by the activation of various serine and threonine phosphorylation sites of TBC1D1 and TBC1D4, which promote the interaction between TBC1D1/TBC1D4 and 14-3-3 proteins (119). As a result, Rab is predominantly loaded with GTP rather than GDP, which facilitates the translocation and fusion of GSV with the plasma membrane, thereby promoting glucose uptake (119-122). Importantly, RabGAPs represent a major signaling node between insulin and contraction-induced signaling, which will be discussed in more detail in Section 1.4.2 and is illustrated below in Figure 4. In addition, activated AKT facilitates the phosphorylation of glycogen synthase kinase 3 (GSK3) at Ser-21 (GSK3α) and Ser-9 (GSK3β) to inactivate it, promoting the activation of glycogen synthase and the storage of glycogen in muscle and liver (123, 124). The insulin-induced signaling pathway is shown in Figure 4.

1.4.2 Contraction-induced signaling

The discovery of the signaling molecule 5'-adenosine monophosphate-activated protein kinase (AMPK), an intracellular energy sensor, elucidated another pathway involved in glucose metabolism in skeletal muscle (60). The heterotrimer AMPK consists of the catalytic subunit alpha (α) and two regulatory subunits beta and gamma (β, γ). The alpha subunit carries the kinase domain along with the major regulatory phosphorylation site Thr-172, which must be phosphorylated for full activation. Two primary upstream kinases in skeletal muscle are thought to be responsible for AMPK activation, with liver kinase B1 (LKB1) being the major upstream kinase and Ca^{2+}/ calmodulin-dependent protein kinase kinase (CaMKK), a sensor of intracellular Ca^{2+} concentration, being considered as an alternative kinase (125-129). AMPK is activated when intracellular levels of adenosine monophosphate (AMP) increase during energy stress. AMP sensitivity is mediated by the gamma subunit, which provides four cystathionine β-synthase (CBS) domains that can bind AMP, adenosine diphosphate (ADP) or adenosine triphosphate (ATP). When ATP is dephosphorylated to ADP, AMP is generated (130, 131). The LKB1 complex mediates phosphorylation of AMPK at Thr-172 by binding AMP

to the gamma subunit, which enhances phosphorylation and inhibits dephosphorylation (132, 133).

Downstream of AMPK, the contracting muscle activates the two closely related RabGAPs TBC1D1 and TBC1D4 through phosphorylation, leading to the translocation of GSV to the plasma membrane and subsequently increasing glucose uptake into the muscle cell (116, 134, 135). Both TBC1D1 and TBC1D4 play an essential role in insulin- and contraction-induced glucose uptake in skeletal muscle cells, but the regulatory mechanisms underlying the activation of RabGAPs remain to be elucidated (129, 136-138). Insulin- and contraction-induced signaling is illustrated in Figure 4.

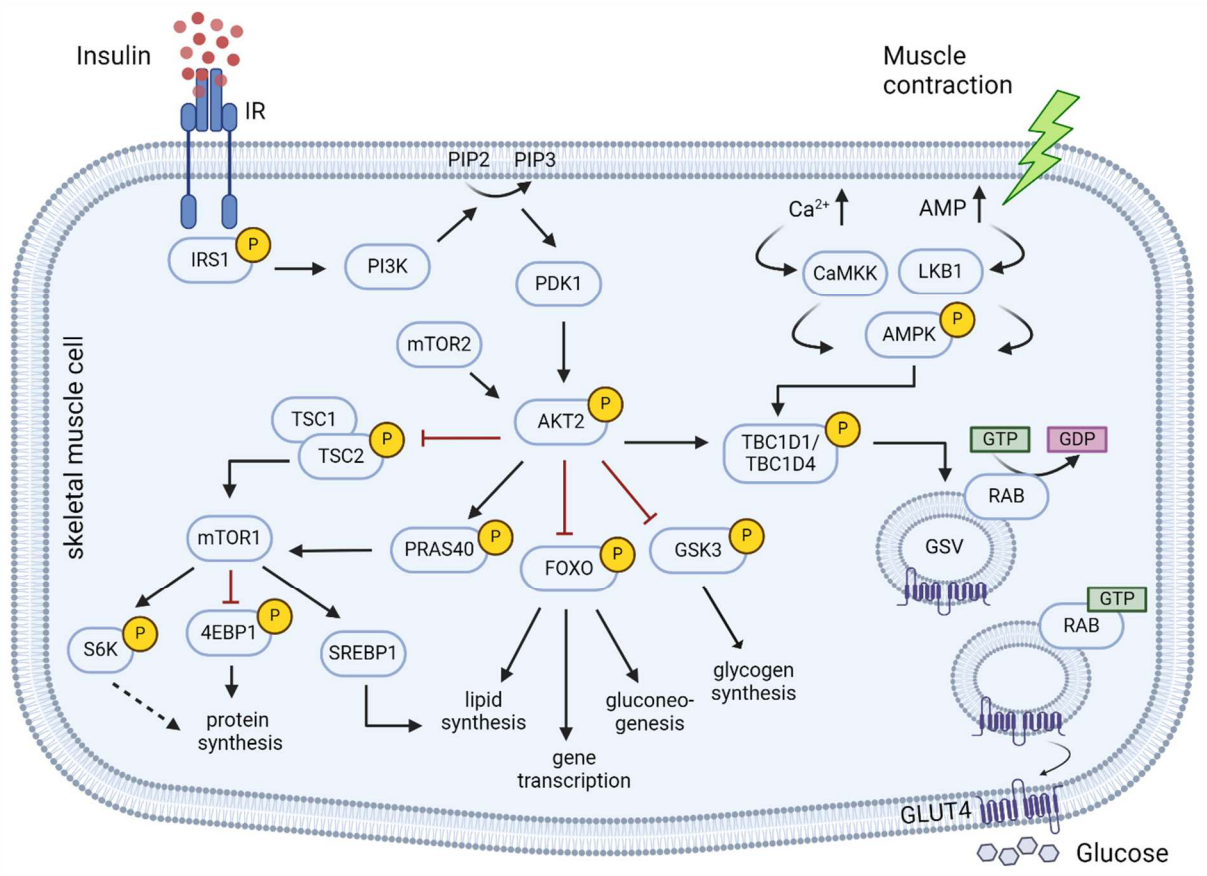

Figure 4: Illustration of insulin- and contraction-mediated signaling in skeletal muscle. Insulin and exercise-mediated muscle contraction induce an autophosphorylation cascade that promotes the translocation of GSV to the plasma membrane mediating glucose uptake. IR: insulin receptor; IRS-1: insulin receptor substrate-1; PI3K: phosphoinositide 3-kinase: PIP2, phosphatidylinositol 4,5-bisphosphate; PIP3: phosphatidylinositol (3,4,5)-triphosphate; PDK1: phosphoinositide-dependent kinase-1; mTORC1/2, mechanistic/mammalian target of rapamycin complex 1/2; AKT: protein kinase B; TSC-1/2: tuberous sclerosis-1/2; S6K: S6 Kinase; 4E-BP1, 4E-binding protein 1; SREBP-1c, sterol-regulatory element-binding protein-1c; PRAS40: proline-rich AKT substrate 40 kDa; FOXO: Forkhead box O transcription factors; GSK-3: glycogen synthase kinase-3; AMP: adenosine monophosphate; LKB1: liver kinase B1; CaMKK: Ca2+/ calmodulin-dependent protein kinase kinase; AMPK: adenosine monophosphate-activated protein kinase; TBC1D1/D4: TBC1 domain family D1/D4; GDP: guanosine diphosphate; GTP: guanosine triphosphate; RabGAPs: Rab guanosine triphosphate-activating; GSV: GLUT4 storage vesicle; GLUT4: glucose transporter 4. The figure was created with BioRender.com

1.4.3 Skeletal muscle insulin resistance at the molecular level

The primary role of insulin in skeletal muscle is to facilitate cellular glucose uptake, which is achieved by translocation of GSV to the plasma membrane. Insulin-mediated glucose uptake in muscle is particularly vulnerable to insulin resistance, which is a central aspect of insulin resistance associated with obesity and type 2 diabetes (T2D) (139, 140). Skeletal muscle insulin resistance primarily results from impairments at proximal levels the of insulin signaling pathway, including the IR, IRS1, PI3K, and AKT, ultimately leading to decreased glucose uptake (17). Several intracellular mechanisms contribute to insulin resistance in skeletal muscle at the molecular level, which are described in more detail in the following secretions and are shown in Figure 5.

1.4.3.1 Lipotoxicity

The accumulation of fats in peripheral non-adipose tissues (e.g. skeletal muscle), known as ectopic lipid accumulation, is a result of excessive dietary intake and is considered the primary cause of lipid-induced insulin resistance (141, 142). In skeletal muscle insulin resistance, intramyocellular lipids (IMCL) such as DAG and ceramides accumulate due to the impaired inhibitory effect of insulin on lipolysis (143, 144). Thus, lipolysis of TG by lipoprotein lipase (LPL) increases FFA, which are taken up by fatty acid transporters (FAT/CD36) in skeletal muscle, increasing IMCL levels and ultimately disrupting insulin signaling (145, 146). Protein kinase C isoform theta (PKC-θ) is activated by elevated DAG levels and stimulates phosphorylation of IRS-1 at its Ser-307 residue, thereby blocking insulin-mediated phosphorylation of IRS-1 at its tyrosine residues, leading to impaired insulin signaling and insulin resistance (111, 147).

1.4.3.2 Lipid-induced inflammation

One of the major lipid mediators of diet-induced inflammation is saturated FFA palmitate (C16) (148), which constitutes 27% of the total FFA present in plasma (149). Chandra et al. reviewed several studies on circulating FFA levels in T2DM patients and concluded that palmitate levels were elevated in T2DM patients in all studies (150). Palmitate is mainly taken up by the cell via the membrane-bound fatty acid transporter CD36, but it can also enter the cell by other mechanisms (151). It promotes the accumulation of ceramides, another specific lipid metabolite associated with obesity and insulin resistance, via *de novo biosynthesis* (Figure 5), which takes place in the endoplasmic reticulum (ER). First, serine palmitoyl transferase (SPT) catalyzes the reaction of palmitoyl-CoA with serine to form 3-ketodihydrosphingosine, which is rapidly reduced to dihydrosphingosine by 3-ketodihydrosphingosine reductase (KDHR). Different isoforms of ceramides synthases (CerS 1-6) then acylate dihydrosphingosine to form dihydroceramides of different chain lengths. Next, dihydroceramide D4-desaturase (DES1) desaturates dihydroceramides to ceramides. Bandet et al. reviewed multiple studies that

confirmed that elevated ceramides levels lead to the onset of muscle insulin resistance (152). Intracellularly, elevated ceramide concentrations activate protein phosphatase 2 A (PP2A), which negatively regulates insulin signaling by blocking the PI3K/AKT pathway. Cell culture studies using murine C2C12 skeletal muscle cells showed that exposure to palmitate increased PP2A activity and induced a reduction in insulin-stimulated phosphorylation of AKT (21, 152). In addition, palmitate inhibits AMPK phosphorylation, resulting in phosphorylation of ribosomal protein S6 kinase beta-1 (S6K1) and phosphorylation of IRS1, contributing to impaired insulin signaling in skeletal muscle (153). Also, insulin-induced glycogen synthesis and glucose oxidation were negatively affected by increased palmitate levels in skeletal muscle (154). Moreover, chronic elevated levels of palmitate and ER stress cause protein unfolding or misfolding. This imbalance in the ER triggers an adaptive mechanism known as “unfolded protein response” that initiates the formation of the IREa-TRAF2-IKK complex, which leads to the activation of nuclear factor-κB (NFκB) and promotes its translocation to the nucleus, ultimately leading to the downregulation of GLUT4 gene expression (155-157). In addition, NFκB promotes nuclear mRNA expression of pro-inflammatory chemokines and cytokines such as TNF-α, IL-1β, IL-6 and many others in skeletal muscle (156, 158-160).

1.4.3.3 Reactive oxygen species

Furthermore, the primary mechanisms underlying palmitate-induced lipotoxicity involve the excessive generation of reactive oxygen species (ROS) and the dysregulation of calcium levels. Increased intracellular ceramide levels promote the activation of the mitochondrial respiratory chain, which stimulates the overproduction of ROS (161). Fatty acid oxidation of palmitoyl-CoA in mitochondria leads to ROS emission resulting in increased intracellular ROS levels (162). In addition to ceramides, elevated DAG levels lead to PKC activation, which also promotes ROS generation. As a result of increased ROS levels, the redox status of the ER is impaired, leading to disruption of calcium homeostasis and dysregulation of calcium release from the ER, inducing ER stress and overproduction of ROS (163).

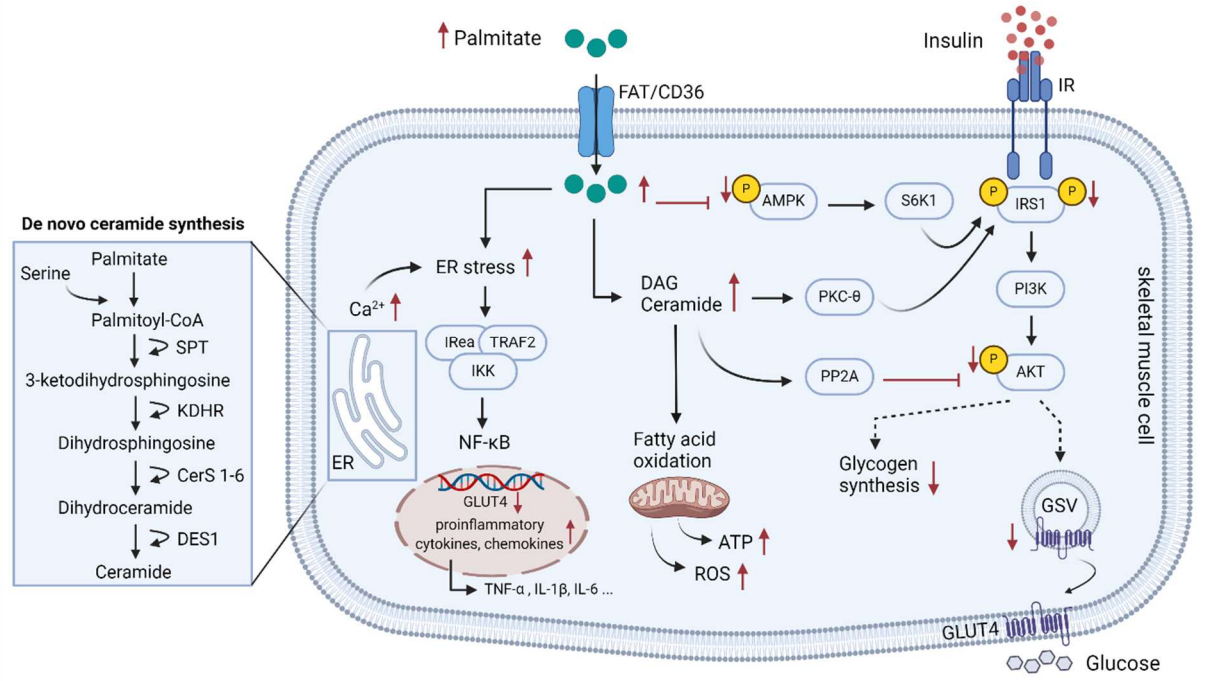

Figure 5: Illustration of palmitate-induced insulin resistance in skeletal muscle. Chronic exposure to palmitate causes lipotoxicity, a process that leads to multiple intracellular dysfunctions promoting skeletal muscle insulin resistance. FAT: fatty acid translocase; CD36: cluster of differentiation 36; ER, endoplasmatic reticulum; IRea: serine/threonineprotein kinase/endoribonuclease; TRAF2: TNF receptor-associated factors; IKK: I kappa B kinase; NFκB: nuclear factor kappa B; TNF-α: tumor necrosis factor alpha; IL-1β/6: Interleukin-1 beta/6; DAG: diacylglycerols; ROS, reactive oxygen species; ATP: adenosine triphosphate; AMPK: adenosine monophosphate-activated protein kinase; S6K1: ribosomal S6 kinase 1; IRS1: insulin receptor substrate1 1; IR: insulin receptor; PI3K: phosphoinositide 3-kinases; PKC-θ: protein kinase C theta; PP2A: protein phosphatase 2A; AKT: protein kinase B; GSV: GLUT4 storage vesicle; GLUT4: glucose transporter type 4; SPT: Serine palmitoyl transferase; KDHR: 3-ketodihydrosphingosine reductase; CerS: Ceramides synthases; DES1: Dihydroceramide △4-desaturase. The figure was created with BioRender.com

1.5 Skeletal muscle cell culture models

To study muscle-specific effects related to exercise or T2DM and insulin resistance, murine skeletal muscle cells (immortalized C2C12 myoblast cell line) and primary HSkMCs serve as *in vitro* cell culture models (49). Both C2C12 myoblasts and primary human myoblasts are derived from muscle precursor satellite cells, express muscle specific regulatory markers (e.g. *Myf5*, *MyoD*), and are easily cultured in appropriate media. Initially, myoblasts appear as mononucleated spindle-shaped cells that differentiate into multinucleated myotubes as they reach 90-95% confluence and transition from growth to differentiation medium. Within three to six days, myoblasts fuse to form elongated fiber-shaped myotubes. These morphological transformations, including the presence of multiple nuclei and changes in cytoskeletal actin, have been validated by confocal microscopy and immunofluorescence staining analysis (164-166). In cell culture studies, another advantage is the strict control of the extracellular environment, and a notable advantage of HSkMCs is the ability to distinguish between genetic and environmental factors (donor variability), since it is not an immortalized cell line, as is the case with C2C12 cells (165). Moreover, fully differentiated myotubes show features of native

muscle such as contractile activity, increased GLUT4 mRNA expression and intact insulin signaling (165, 167). Furthermore, they provide a relevant *in vitro* system to study the myokine secretion patterns under different physiological and pathological conditions (52).

1.5.1 An *in vitro* exercise model: EPS in skeletal muscle

The most commonly used cell culture models for exercise studies are primary HSkMCs, obtained from the thigh muscle (e.g. *vastus lateralis*) of donors, and C2C12 cells, also obtained from murine thigh muscle (49, 164, 168). EPS is an *in vitro* muscle contraction method to investigate contraction-related changes in skeletal muscle signaling pathways (60, 169, 170), metabolism (171, 172), myokine secretion (69, 70, 173), and morphology (174). Although the application of EPS dates back to the 1970s (175), its specific use as an *in vitro* muscle contraction model has only developed in the last two decades, when Nedachi et al. first proposed EPS as an *in vitro* exercise model, observing exercise-induced effects such as activation of AMPK and increased glucose uptake and insulin sensitivity in murine C2C12 myotubes (169). In addition, several studies have investigated the EPS-mediated cross talk between skeletal muscle cells and other organs such as adipocytes and pancreatic beta islet cells (176-178). Apparently, the skeletal muscle response to EPS depends on the selected EPS parameters (168, 179). Several studies have suggested that a duration of less than 24 hours corresponds to an acute bout of exercise (172, 176, 177, 180-184), while chronic exercise is mimicked either by continuous stimulation from 24 to 48 hours (172, 176, 185, 186) or by administering an acute EPS protocol on consecutive days (182). Furthermore, some EPS protocols using a wide frequency range from 1 Hz to 100 Hz defined their exercise type as resistance training (69, 174, 177, 182, 187, 188), as others referred to similar EPS parameters as endurance training (189). Therefore, there is a lack of consensus in the literature regarding which EPS protocol represents which type of exercise (179). In fact, the terms “high-frequency” and “low-frequency” are more commonly used to describe EPS-induced changes in the skeletal muscle and seem to be decisive parameters, for example to determine which signaling pathways are activated. While acute (183, 190) and chronic (169, 171, 177, 191) low-frequency EPS (< 5 Hz) protocols promote the activation of AMPK signaling, high-frequency EPS mediates the activation of p70S6K1, more simulating resistance training (69). To investigate the effects of EPS on the myokine secretion pattern, recent studies have rather used acute three to six hours (171, 176, 177) or chronic over 24 hours (70, 176, 192) low-frequency (0.1 Hz - 1 Hz) EPS protocols. Lambernd et al. showed that IL-6 secretion was significantly increased after both eight and 24 hours of EPS in primary HSkMCs (171). However, EPS did not significantly increase IL-6 secretion after six hours, but only after 24 hours in murine C2C12 cells (192). Therefore, EPS protocols consisting of different parameters (duration, voltage, pulse duration, frequency) make a direct comparison rather difficult. A common protocol used in previous studies is the following: 1 Hz, 2 ms, 11.5 V for two to 24 hours (171, 173, 191-194).

Taken together, EPS parameters are crucial and may be adjusted to the specific research question.

1.5.2 An *in vitro* insulin resistant model: Palmitate treatment in skeletal muscle

Previous studies using murine C2C12 cells or primary HSkMCs were designed to investigate palmitate-induced changes in cellular signaling and metabolism at the molecular level. Exposure of C2C12 myotubes to higher palmitate concentrations (400 - 750 µM) over a continuous stimulation period of 16 to 18 hours was shown to significantly impair insulin-stimulated phosphorylation of AKT and its downstream target GSK3 (154, 195-198). As a consequence, insulin-stimulated glycogen synthesis was also significantly decreased in palmitate-treated C2C12 cells (750 µM palmitate, 16 - 18 hours) (195, 198) and HSkMCs (400 µM palmitate, 18 hours) (199). The same palmitate conditions also promoted the accumulation of the lipid metabolites ceramide and DAG, higher levels of which were measured in C2C12 myotubes (195, 198) and primary human myotubes (199). As shown in Figure 5 (1.4.3), higher PP2A levels resulted in inhibition of AKT activity. Cazzolli et al. showed that palmitate-treated C2C12 myotubes (750 µM, 18 hours) resulted in increased PP2A activity compared to control cells under basal and insulin conditions (197). Thus, previous studies characterizing the effects of palmitate on skeletal muscle cells *in vitro* have shown that insulin signaling and glucose and lipid metabolism are disrupted, making palmitate an excellent choice for generating insulin resistance in cell culture models.

1.5.3 LC-MS/MS secretome studies using different cell culture models

Recent studies have focused on characterizing the secretome profile of skeletal muscle cells under various physiological and pathological conditions using a non-targeted mass spectrometry (liquid chromatography, LC-MS/MS) based approach. Deshmukh et al. generated insulin-resistant skeletal muscle cells by exposing C2C12 myotubes to 500 µM palmitate in serum-free medium for 16 hours, followed by a further 12-hour starvation period in the absence of palmitate, before collecting the supernatant (“conditioned media”, CM) for MS analysis (200). Palmitate is coupled to bovine serum albumin (BSA), so the final 12-hour incubation step is critical to obtain serum-free CM for MS analysis. The in-depth secretome analysis revealed that 4,491 proteins were identified in the CM, of which 1,073 proteins were considered to be secretory proteins according to bioinformatic tools (SignalP, SecretomeP). Furthermore, they were able to show that the secretomes of palmitate- and BSA-treated (control) myotubes differed from each other, indicating that the secretion patterns of myokines are significantly distinct (200). The first attempt to study the EPS-induced muscle secretome by in-depth MS analysis was made in 2021 by Gonzalez-Franquesa et al. who subjected C2C12 myotubes to a continuous low-frequency EPS protocol (24h, 1 Hz, 2 ms, 11.5 V). They quantified 1,724 myokines in the CM, of which 67% were classified as secretory proteins. In

addition, they confirmed that the secretomes of EPS-stimulated and non-stimulated cells segregate from each other (192). Mengeste et al. sought to explore EPS-related effects on the muscle secretome of healthy primary HSkMCs using another chronic low-frequency EPS protocol (24h, 0.1 Hz, 2 ms, 10 V) and quantified 1,215 proteins, of which 137 were significantly regulated by EPS (54 upregulated, 83 downregulated) (70). Proteomic profiling of the secretome of contracting skeletal muscle cells may help to uncover and understand crucial mechanisms driven by myokine secretion during exercise or in the pathogenesis of T2DM/insulin resistance, thus further approaches to explore the muscle secretome are needed.

1.6 Objectives

Many previous studies have shown that EPS is a valid method to simulate exercise-like effects *in vitro* (179). Recently, first attempts have been made to investigate the EPS-induced myokine secretion profile of skeletal muscle cells using a non-targeted approach (MS) to expand the knowledge on myokine-mediated health-promoting effects (70, 192). For this approach, both studies used chronic (24h) low-frequency EPS protocols in which cells were continuously stimulated for 24 hours (70, 192). In fact, C2C12 cells and HSkMCs are the most commonly used cell models to study myokine secretion and contraction-induced changes in the muscle secretome, but relatively little is known about the extent to which the secretomes of C2C12 cells and primary HSkMCs are similar or distinct. Therefore, the first aim of this thesis was to investigate and compare the myokine secretion profile of both cell models under acute (6h) low-frequency EPS conditions with the following hypothesis:

1. **The myokine secretion profile of C2C12 myotubes and primary human myotubes that were exposed to acute low-frequency EPS differs.**

The FFA palmitate has been used for over two decades to artificially induce insulin resistance in skeletal muscle cells *in vitro* (167). Deshmukh et al. performed the first MS-based secretome analysis of palmitate-pretreated C2C12 myotubes, which provided a deep insight into the secretome of potentially insulin resistant skeletal muscle cells (200). In contrast to C2C12 cells, primary human skeletal muscle cells provide characteristics that are more similar to native muscle (e.g. donor variability). Therefore, the second aim of this thesis was to establish an insulin resistant cell culture model that would subsequently allow MS-based secretome analysis. The following hypothesis was addressed:

2. **The muscle secretome of insulin sensitive versus insulin resistant primary human myotubes differs.**

It is known that exercise can also increase the insulin sensitivity of insulin resistant skeletal muscle. We hypothesized that the EPS-induced secretomes of insulin sensitive and resistant myotubes differ. Therefore, the third aim of this thesis was to evaluate the effect of acute low-frequency EPS (6h) on the myokine secretion profile of insulin resistant cells compared to insulin sensitive cells using an MS-based approach.

3. **The skeletal muscle secretome of insulin sensitive and insulin resistant primary human myotubes differs after exposure to acute low-frequency EPS.**

2 Material and Methods

2.1 Material

2.1.1 Instruments and disposals

Conventional instruments and disposals that are part of the standard laboratory equipment are not listed in the following tables (Table 1 and 2).

Table 1: Instruments.

Instruments	Manufacturer
Acclaim™ PepMap™ 100 - C18 HPLC Columns (ID: 75 µm, 2 cm length)	Thermo Scientific™ (Waltham, MA, USA)
Analytical balance	Sartorius AG (Göttingen, Germany)
Bandelin Sonorex	GEO-Reinigungstechnik (Ahaus-Ottenstein, Germany)
Bio-Plex® 200 System, Luminex	Bio-Rad Laboratories, Inc. (Hercules, CA, USA)
C-Dish™ (carbon electrodes for EPS)	IonOptix LLC (Westwood, MA, USA)
Centrifugal vacuum concentrator Savant™ SpeedVac™ SPD 1030	Thermo Scientific™ (Waltham, MA, USA)
Centrifuge 5810 R	Eppendorf GmbH (Hamburg, Germany)
ChemiDoc XRS+	Bio-Rad Laboratories, Inc. (Hercules, CA, USA)
C-Pace EM Culture Stimulator	IonOptix LLC (Westwood, MA, USA)
Gen2 Aurora Series column with nanoZero® product details (25 cm, C18)	IonOpticks (Fitzroy, Victoria, Australia)
Heracell™ 240i CO2 Incubator	Thermo Scientific™ (Waltham, MA, USA)
Heraeus® Multifuge 3S+	Thermo Scientific™ (Waltham, MA, USA)
Herasafe 2030i Biosafety Cabinet	Thermo Scientific™ (Waltham, MA, USA)
iMark™ Microplate Absorbance Reader	Bio-Rad Laboratories, Inc. (Hercules, CA, USA)
Infinite® 200 PRO	Tecan Trading AG (Männedorf, Switzerland)
MicroBeta® Counter	PerkinElmer (Waltham, MA, USA)
Microliter Syringes	Hamilton Company (Reno, NV, USA)

Milli-Q® (MQ) Advantage A10 Water (H_2o) Purification System	Millipore, Merck KGaA (Darmstadt, Germany)
Mini-PROTEAN Tetra Vertical Electrophoresis Cell	Bio-Rad Laboratories, Inc. (Hercules, CA, USA)
MLS-50 Swinging-Bucket Rotor	Beckman Coulter (Brea, CA, USA)
NanoDrop™ 2000/2000c Spectrophotometer	Thermo Scientific™ (Waltham, MA, USA)
Nanospray Flex™ Ion Sources	Thermo Scientific™ (Waltham, MA, USA)
Optima-MAX-XP Ultracentrifuge	Beckman Coulter (Brea, CA, USA)
Orbitrap Exploris™ 480 mass spectrometer	Thermo Scientific™ (Waltham, MA, USA)
Orbitrap Fusion™ Lumos™ mass spectrometer	Thermo Scientific™ (Waltham, MA, USA)
PowerPac™ Basic Power Supply	Bio-Rad Laboratories, Inc. (Hercules, CA, USA)
QuantStudio™ 7 Flex	Thermo Scientific™ (Waltham, MA, USA)
Thermomixer comfort	Eppendorf GmbH (Hamburg, Germany)
UltiMate™ 3000 LC Systems	Thermo Scientific™ (Waltham, MA, USA)
Uniprep gyrator-24	UniEquip (Martinsried, Germany)

Table 2: Disposals.

Disposals	**Manufacturer**
Amicon® Ultra 0.5 ml Centrifugal Filter P/N UFC5030	Millipore, Merck KGaA (Darmstadt, Germany)
Amicon® Ultra 4 ml Centrifugal Filter Unit (3K)	Millipore, Merck KGaA (Darmstadt, Germany)
Combitips® advanced	Eppendorf GmbH (Hamburg, Germany)
Criterion™ TGX Stain-Free™ Precast Gel	Bio-Rad Laboratories, Inc. (Hercules, CA, USA)
Cryo tubes 1.8 ml	Thermo Scientific™ (Waltham, MA, USA)
EPS-plates Greiner CELLSTAR® multiwell culture plates (6-well)	Greiner Bio-One GmbH (Frickenhausen, Germany)
Greiner centrifuge tubes, 50 ml	Greiner Bio-One GmbH (Frickenhausen, Germany)

LDH-assay plates, Nunclon™ Delta Surface, (96-well)	Thermo Scientific™ (Waltham, MA, USA)
MicroAmp™ Optical Adhesive Film	Thermo Scientific™ (Waltham, MA, USA)
Neubauer counting chambers	Assistant, glassware factory Karl Hecht GmbH & Co. KG (Sondheim vor der Röhn, Germany)
Nitrocellulose membrane	Cytiva Europe GmbH (Freiburg im Breisgau, Germany)
Open-Top Thinwall Polypropylene Tube, 6 ml	Beckman Coulter (Brea, CA, USA)
PCR-Plates (FrameStar® 384-well)	4titude (Berlin, Germany)
Protein LoBind® Tubes 1.0 ml,1.5 ml, 15 ml	Eppendorf GmbH (Hamburg, Germany)
Safe-Lock tubes 1.0 ml,1.5 ml, 2.0 ml	Eppendorf GmbH (Hamburg, Germany)
SureSTART™ 1.5 ml Total Recovery Glass Snap Top Microvials for <2 ml Samples	Thermo Scientific™ (Waltham, MA, USA)
SureSTART™ 11 mm Snap Caps	Thermo Scientific™ (Waltham, MA, USA)
Tissue Culture Flasks 75 cm^2, 150 cm^2	TPP Techno Plastic Products AG (Trasadingen, Switzerland)
Tissue Culture Test Plates (6-well)	TPP Techno Plastic Products AG (Trasadingen, Switzerland)
Whatman papers	Whatman plc (Maidstone, UK)
Western Lightning® ECL Pro	PerkinElmer Inc. (Waltham, MA, USA)
Western Lightning® Ultra	PerkinElmer Inc. (Waltham, MA, USA)

2.1.2 Chemicals and reagents

Table 3 lists all chemicals and reagents used in this thesis.

Table 3: Chemicals.

Chemicals	**Manufacturer**
4-(2-Hydroxyethyl)-piperazine-1-ethanesulfonic acid (HEPES)	Sigma-Aldrich (St. Louis, MO, USA)
Acetic acid	Merck KGaA (Darmstadt, Germany)
Acetonitrile (MeCN)	Sigma-Aldrich (St. Louis, MO, USA)

Acrylamide 30%	AppliChem GmbH (Darmstadt, Germany)
Ammonium bicarbonate	AppliChem GmbH (Darmstadt, Germany)
Ammonium Peroxodisulfate	AppliChem GmbH (Darmstadt, Germany)
Ammonium persulfate (APS)	Serva (Heidelberg, Germany)
Bovine Serum Albumin (BSA)	Merck KGaA (Darmstadt, Germany)
Bromophenol blue	AppliChem GmbH (Darmstadt, Germany)
BSA Control for BSA-Fatty Acid Complexes (5 mM)	Cayman Chemical (Ann Arbor, MI, USA)
BSA-Palmitate Saturated Fatty Acid Complex (5 mM)	Cayman Chemical (Ann Arbor, MI, USA)
Calcium chloride dehydrate ($CaCl_2$ x $2H_2O$)	Sigma-Aldrich (St. Louis, MO, USA)
cOmplete™ Protease Inhibitor Cocktail	Roche (Basel, Switzerland)
Coomassie® Brilliant Blue R-250	AppliChem GmbH (Darmstadt, Germany)
Dimethyl Sulfoxide (DMSO) for cell culture	AppliChem GmbH (Darmstadt, Germany)
Disodium hydrogen phosphate (Na_2HPO_4)	Merck KGaA (Darmstadt, Germany)
Dithiothreitol (DTT)	Carl Roth GmbH & Co. KG (Karlsruhe, Germany)
Dulbecco´s Modified Eagle Medium (DMEM), high glucose, no glutamine, no phenol red, 31053028	Gibco®, Thermo Scientific™ (Waltham, MA, USA)
DMEM, high glucose, pyruvate, 11995065	Gibco®, Thermo Scientific™ (Waltham, MA, USA)
DMEM, low glucose, GlutaMAX™ Supplement, 10567014	Gibco®, Thermo Scientific™ (Waltham, MA, USA)
Dulbecco´s Phosphate Buffered Saline (DPBS), 14040091	Gibco®, Thermo Scientific™ (Waltham, MA, USA)
DMEM, low glucose, pyruvate, no glutamine, no phenol red, 11880028	Gibco®, Thermo Scientific™ (Waltham, MA, USA)
Ethanol, absolute (EtOH)	Merck (Darmstadt, Germany)
Ethylenediaminetetraacetic acid (EDTA)	Carl Roth GmbH & Co. KG (Karlsruhe, Germany)
Ethyleneglycol-bis(aminoethyl ether)-N,N,N′,N′-tetraacetic acid (EGTA)	Carl Roth GmbH & Co. KG (Karlsruhe, Germany)

GlutaMAX™ (L-Glutamine)	Gibco®, Thermo Scientific™ (Waltham, MA, USA)
Glycerol	MP Biomedicals (Solon, OH, USA)
Glycine	AppliChem GmbH (Darmstadt, Germany)
Glycogen from bovine liver, G0885	Sigma-Aldrich (St. Louis, MO, USA)
GoScript™ Reverse Transcriptase System	Promega Corporation (Madison, WI, USA)
Hexanucleotide primers	Roche (Basel, Switzerland)
Horse serum (HS)	ATCC (Manassas, VA, USA)
Hydrochloric acid (HCl)	Carl Roth GmbH & Co. KG (Karlsruhe, Germany)
Insulin	Sigma-Aldrich (St. Louis, MO, USA)
Iodoacetamide (IAA)	AppliChem GmbH (Darmstadt, Germany)
Isopropyl	Carl Roth GmbH & Co. KG (Karlsruhe, Germany)
LY294002 #9901	Cell Signaling (Danvers, MA, USA)
Magnesium sulphate heptahydrate ($MgSO_4$ x $7H_2O$)	Merck KGaA (Darmstadt, Germany)
Methanol (MeOH)	Carl Roth GmbH & Co. KG (Karlsruhe, Germany)
N,N,N′,N′-Tetramethyl-ethylendiamin (TEMED)	Carl Roth GmbH & Co. KG (Karlsruhe, Germany)
Ortho-phosphoric acid 85% (o-H_3PO_4)	AppliChem GmbH (Darmstadt, Germany)
Palmitate	Sigma-Aldrich (St. Louis, MO, USA)
Penicillin/ Streptomycin (P/S) 10.000 U/ml P, 10.000 µg/ml S	Gibco®, Thermo Scientific™ (Waltham, MA, USA)
PhosSTOP™	Roche (Basel, Switzerland)
Potassium chloride (KCl)	Merck KGaA (Darmstadt, Germany)
Potassium hydroxide (KOH)	Merck KGaA (Darmstadt, Germany)
Powdered milk	Carl Roth GmbH & Co. KG (Karlsruhe, Germany)
RLT Buffer	Qiagen GmbH (Hilden, Germany)

Rotiszint®eco plus	Carl Roth GmbH & Co. KG (Karlsruhe, Germany)
SkGM™-2 Skeletal Muscle Cell Growth Medium-2 BulletKit™	Lonza, (Basel, Switzerland)
Sodium chloride (NaCl)	Carl Roth GmbH & Co. KG (Karlsruhe, Germany)
Sodium dodecyl sulfate (SDS)	Carl Roth GmbH & Co. KG (Karlsruhe, Germany)
Sodium hydrogen carbonate ($NaHCO_3$)	Carl Roth GmbH & Co. KG (Karlsruhe, Germany)
Sodium pyruvate (100 mM)	Gibco®, Thermo Scientific™ (Waltham, MA, USA)
SYBR Green qPCR primer (gene specific)	Eurogentec (Seraing, Belgium)
Trifluoroacetic acid (TFA) (0.1%) in H_20	Thermo Scientific™ (Waltham, MA, USA)
TFA (0.1%) in MeCN	Thermo Scientific™ (Waltham, MA, USA)
Tris ultrapure, A1086	AppliChem GmbH (Darmstadt, Germany)
Triton™ X-100	Sigma-Aldrich (St. Louis, MO, USA)
Trypan blue 0.4%	Gibco®, Thermo Scientific™ (Waltham, MA, USA)
Trypsin/Lys-C Mix	Promega Corporation (Madison, WI, United States)
Trypsin-EDTA solution	Gibco®, Thermo Scientific™ (Waltham, MA, USA)
TWEEN® 20 (Polysorbat 20)	MP Biomedicals (Solon, OH, United States)

2.1.3 Radioactive Isotope

As a radiochemical [^{14}C]-D-glucose was used to determine glycogen synthesis in insulin sensitive and insulin resistant primary HSkMCs.

Table 4: Radioactive chemical.

Radiochemical	**Manufacturer**
[^{14}C]-D-glucose, NEC042X	PerkinElmer (Waltham, MA, USA)

2.1.4 Buffers and solutions

Table 5 summarizes all buffers and solutions used in this thesis.

Table 5: Buffers and solutions.

Buffers and solutions	Ingredients
APS-solution 50%	50 mg APS + 100 µl MQ-H_2O
Blocking buffer TBS-T	TBS-T (1x) + 5% non-fat dry milk powder (MP)
Cell lysis buffer (RT-qPCR)	RLT Buffer
cOmplete™ solution	1 tablet dissolved in 2 ml H_2O
Electrophoresis buffer (10x)	25 mM Tris, 192 mM glycine, 0.1% SDS, 20 Vol % glycerol, 1% SDS, 10 mM EDTA
Fling-Gregerson-buffer	50 mM Tris, 192 mM Glycine, 0.1 % SDS
High Performance Liquid Chromatography(HPLC)-buffer A	0.1% formic acid dissolved in water (Thermo Scientific™, Waltham, MA, USA)
HPLC-buffer B	80% acetonitrile, 0.1% formic acid Dilution of 0.1% formic acid in acetonitrile with 0.1% formic acid in water (Thermo Scientific™, Waltham, MA, USA)
Insulin stock solution	100 µM insulin in 5 mM HCl
Laemmli running buffer (1x)	25 mM Tris, 192 mM Glycine, 0.1% SDS
Laemmli sample buffer (4x)	0.25 M Tris, 6% DTT, 0.2% bromophenol blue (pH 6.8)
LDH-Storage Buffer	200 mM Tris-HCl, 10% glycerol, 1% BSA (pH 7.3)
Palmitate, stock solution (5 mM)	10% BSA solution: 10 g BSA + 100 ml PBS, incubate overnight at 4°C; 20 mM palmitate solution: add 7.7 mg palmitate to 1.5 ml 0.1 M NaOH; 5 mM palmitate stock solution: add 20 mM palmitate solution to 10% BSA solution.
Phosphate buffered saline (PBS) without Mg^{2+} and Ca^{2+}	136.9 mM NaCl, 2.7 mM KCl, 1.5 mM KH_2PO_4, 8.06 mM Na_2HPO_4 x $2H_2O$ (pH = 7.4)
SDS lysis buffer (proteomics)	4% SDS, 100 mM Tris (pH = 8.0), 100 mM DTT, 1x phosphatase-inhibitor 2, 1x phosphatase-inhibitor 3, 1x cOmplete™

SDS sample buffer (1x)	62.5 mM Tris/HCl (pH = 6.8), 10% glycerol, 2 mM EDTA, 2 % SDS, 100 mM DTT, 0.01% bromophenol blue
SDS sample buffer (5x)	312.5 mM Tris/HCl (pH = 6.8), 50% glycerol, 10 mM EDTA, 10% SDS, 500 mM DTT, 0.05% bromophenol blue
Separating gel buffer (western blot) Separating gel buffer (proteomics)	1.5 M Tris, 0.4% SDS (pH 8.8) 3 M Tris/HCl, 0.8% SDS (pH 8.8)
Stacking gel buffer (western blot) Stacking gel buffer (proteomics)	0.5 M Tris, 0.4% SDS (pH 6.8) 0.5 M Tris/HCl, 0.8% SDS; pH = 6.8
Transfer buffer	25 mM Tris, 192 mM glycine, 20% methanol
Trypan blue cell culture solution	0.2% Trypan blue in PBS
Urea buffer	8M urea, 100 mM Tris-HCl (pH 8.0)
Western blot lysis buffer	20 mM Tris-HCl (pH = 7.5), 150 mM NaCl, 1 mM EDTA (pH = 8), 1 mM EGTA (pH = 8), 1% Triton. 40 µl/ 1 ml of cOmplete™ solution and 100 µl/ 1 ml of PhosSTOP™ solution were added to the lysis buffer before usage each time

2.1.5 Cell culture

In this thesis, primary human skeletal muscle myoblasts (HSMM) from five healthy, insulin sensitive male donors between the ages of 16 to 35 years and a BMI between 19 to 26 kg/m^2 were included (Supplemental Table 1). Moreover, further experiments were conducted with the immortalized murine C2C12 myoblast cell line (Table 6).

2.1.5.1 Skeletal muscle cell models

Table 6: Cell culture models.

Cell model	Muscle tissue	Cell type	Manufacturer
Primary HSMM, CC-2580	Quadriceps femoris	Myoblasts	Lonza, (Basel, Switzerland)
Murine C2C12 cell line (CRL-1772™)	Thigh muscle from C3H mouse	Myoblasts	ATCC (Manassas, VA, USA)

2.1.5.2 Cell culture and assay media

All cell culture media used for the cultivation and maintenance of cell cultures are listed below as well as all assay media used in this thesis (Table 7).

Table 7: Cell culture media

Media	Supplements
DMEM, high glucose, no glutamine, no phenol red, 31053028, **starvation medium** (C2C12)	1% P/S, 2% GlutaMAX™, 1% sodium pyruvate
DMEM, high glucose, pyruvate, 11995065, **differentiation medium** (C2C12)	1% sodium pyruvate, 1% P/S, 2% HS
DMEM, high glucose, pyruvate, 11995065, **growth medium** (C2C12)	1% sodium pyruvate, 1% P/S, 10% FBS
DMEM, low glucose, 11880028, **starvation medium** (HSkMCs)	1% P/S, 2% GlutaMAX™
DMEM, low glucose, 11880028, **differentiation medium** (HSkMCs)	2% HS, 1% P/S, 2% GlutaMAX™
DMEM, low glucose, 21885025, **basal medium** (HSkMCs)	-
DPBS, 14040091, (washing medium)	-
SkGM™-2 Skeletal Muscle Cell Growth Medium-2, **growth medium** (HSkMCs)	BulletKit™: Gentamicin Sulfate Amphotericin-B (GA-)1000, 0.50 ml, Epidermal Growth Factor Human, recombinant (rhEGF), 0.50 ml, Dexamethasone, 0.50 ml, L-Glutamine, 10.00 ml, fetal bovine serum (FBS), 50.00 ml

HS: Horse serum, P/S: Penicillin / Streptomycin, FBS: fetal bovine serum

Table 8: Assay media.

Assay media	Supplements
[14C(U)]glucose basal	Basal medium + [14C(U)]glucose (100 µCi/ml), final conc.: 2 µCi/ml
[14C(U)]glucose basal + insulin	Basal medium + [14C(U)]glucose (100 µCi/ml), final conc.: 2 µCi/ml; + insulin (100 µM), final conc.: 100 nM
BSA (control)	Starvation medium + BSA Control for BSA-Fatty Acid Complexes (5 mM) (formulation: 0.8 mM BSA in 150 mM NaCl, pH 7.4); final conc.: 400 µM or 800 µM

DMSO (control)	Starvation medium + DMSO, final conc: 0.08%
Insulin	Starvation medium + insulin, final conc.: 10 µM or 100 µM
LY294002	Starvation medium + LY294002 (formulation: 1.5 mg in 98 µM DMSO); final conc.: 40 µM
Palmitate 300 µM	Differentiation medium + palmitate stock solution (5 mM); final conc.: 300 µM
Palmitate 800 µM	Starvation medium + BSA-Palmitate Saturated Fatty Acid Complex (5mM), (formulation: 5 mM Palmitate:0.8 mM BSA (6:1 palmitate:BSA) in 150 mM NaCl, pH 7.4); final conc.: 800 µM

Final conc.: Final concentration

2.1.6 Commercial kits

The following table shows all reaction kits used in this thesis (Table 9).

Table 9: Reaction kits.

Reaction kit	Manufacturer
BCA Protein Assay Kit	Pierce (Rockford, IL, USA)
Bio-Plex® Pro Human Cytokine Screening Panel, 48-Plex, #12007283	Bio-Rad Laboratories, Inc. (Hercules, CA, USA)
GoScript™ Reverse Transcriptase	Promega (Madison, WI, USA)
LDH-Glo™ Cytotoxicity Assay	Promega (Madison, WI, USA)
MILLIPLEX® MAP Human Myokine Magnetic Bead Panel, HMYOMAG-56K	Millipore, Merck KGaA (Darmstadt, Germany)
miRNeasy Mini Kit	Qiagen GmbH (Hilden, Germany)
Pierce™ Quantitative Colorimetric Peptide Assay	Thermo Scientific™ (Waltham, MA, USA)
RNase-free DNase Set	Qiagen GmbH (Hilden, Germany)

2.1.7 Antibodies

All antibodies listed below were used for Western blot analysis (Table 10).

Table 10: Antibodies.

Antibodies	Source	Dilution[1]	Product Number	Manufacturer
Primary				
AKT	Rabbit	1:1,000 (v/v) 5% MP	#9272	Cell Signaling (Danvers, MA, USA)
AMPKα	Rabbit	1:1,000 (v/v) 5% BSA	#2532	Cell Signaling (Danvers, MA, USA)
GAPDH	Rabbit	1:2,000 (v/v) 5% MP	#2118	Cell Signaling (Danvers, MA, USA)
GSK3α/β	Rabbit	1:1,000 (v/v) 5% BSA	#5676	Cell Signaling (Danvers, MA, USA)
Phospho-GSK3α/β-Ser21/9	Rabbit	1:1,000 (v/v) 5% BSA	#9331	Cell Signaling (Danvers, MA, USA)
Phospho-AKT-Ser472	Rabbit	1:1,000 (v/v) 5% MP	#9271	Cell Signaling (Danvers, MA, USA)
Phospho-AKT-Thr308	Rabbit	1:1,000 (v/v) 5% MP	#9275	Cell Signaling (Danvers, MA, USA)
Phospho-AMPKα-Thr172	Rabbit	1:1,000 (v/v) 5% BSA	#2531	Cell Signaling (Danvers, MA, USA)
Phospho-PRAS40-Thr246	Rabbit	1:1,000 (v/v) 5% BSA	#2640	Cell Signaling (Danvers, MA, USA)
PRAS40	Rabbit	1:1,000 (v/v) 5% BSA	#2610	Cell Signaling (Danvers, MA, USA)
α-Tubulin	Mouse	1:2,000 (v/v) 5% MP	T6199	Sigma-Aldrich (St. Louis, MO, USA)

Secondary				
Anti-mouse IgG, HRP-linked	Goat	1:20,000	A6531	Sigma-Aldrich (St. Louis, MO, USA)
Anti-rabbit IgG, HRP-linked	Goat	1:10,000 1:20,000	111-035-003	Jackson ImmunoResearch (West Grove, PA, USA)

[1] Both buffers, 5% nonfat dry milk powder (MP) and 5% BSA, were diluted in 1x TBS-T; HRP: Horseradish peroxidase; IgG: Immunoglobulin G.

2.1.8 Primers

Table 11 lists all used primers in this thesis.

Table 11: SYBR gene qPCR Primers.

Primer/ target	Sequence 5´→ 3´
HSkMCs	
Beta-2-microglobulin (*B2M*)	Fwd: CTATCCAGCGTACTCCAAAG Rev: GAAAGACCAGTCCTTGCTGA
Myoblast determination protein 1 (*MYOD*)	Fwd: CGGCATGATGGACTACAGCG Rev: CAGGCAGTCTAGGCTCGAC
Myogenic factor 5 (*MYF5*)	Fwd: CCACCTCCAACTGCTCTGAT Rev: GCAATCCAAGCTGGATAAGG
Myogenin (*MYOG*)	Fwd: ACCCTACAGATGCCCACAAC Rev: TGGTTTCATCTGGGAAGGCC
Myosin heavy chain 2 (*MYH2*)	Fwd: GAAAGTCTGAAAGGGAACGCA Rev: CGCCACAAAGACAGATGTTTTG
C2C12 cells	
Myoblast determination protein 1 (*MyoD*)	Fwd: CTTCTATCGCCGCCACTC Rev: AAGTCGTCTGCTGTCTCAA
Myogenic factor 5 (*Myf5*)	Fwd: CCACCTCCAACTGCTCTGAC Rev: GCACATGCATTTGATACATCAGG
Myogenin (*MyoG*)	Fwd: GTGCCCAGTGAATGCAACTC Rev: CGAGCAAATGATCTCCTGGGA
Myosin heavy chain 2 (*Myh2*)	Fwd: GCCCTGGACAAGAAGCAGAGAA Rev: TCGCTTCAGGGTTTCTAGCT

TATA binding protein (*Tbp*)	Fwd: GCGGCACTGCCCATTTATTT Rev: GGCGGAATGTATCTGGCACA

2.1.9 Molecular weight size markers

The following molecular weight size markers were used in this thesis (Table 12).

Table 12: Molecular weight size markers.

Molecular weight size marker	Manufacturer
PageRuler™ Prestained Protein Ladder	Thermo Scientific™ (Peqlab, Wilmington MA, USA)
Precision Plus Protein™ All Blue Prestained Protein Standards	Bio-Rad Laboratories, Inc. (Hercules, CA, USA)
Precision Plus Protein™ Unstained Protein Standards	Bio-Rad Laboratories, Inc. (Hercules, CA, USA)

2.1.10 Softwares

The following softwares were used in this thesis (Table 13).

Table 13: Softwares.

Software	Manufacturer
Bio-Plex Manager™ 6.0	Bio-Rad Laboratories, Inc. (Hercules, CA, USA)
GraphPad Prism 10.0.2	GraphPad Software Inc (San Diego, CA, USA)
Image Lab™ 6.0.1	Bio-Rad Laboratories, Inc. (Hercules, CA, USA)
i-control™ 2.0	Tecan Trading AG (Männedorf, Switzerland)
Microplate Manager® 6.0	Bio-Rad Laboratories, Inc. (Hercules, CA, USA)
NanoDrop™ 2000	Thermo Scientific™ (Waltham, MA, USA)
Proteome Discover™ (PD™) 3.0	Thermo Scientific™ (Waltham, MA, USA)
QuantStudio™ 7 Flex	Thermo Scientific™ (Waltham, MA, USA)

2.2 Methods

2.2.1 Cell culture techniques

2.2.1.1 Cultivation of murine C2C12 cells

In this thesis, the immortalized murine C2C12 myoblast cell line from ATCC (Table 6) was used. For the following experiments, myoblasts from passage four to ten were cultured and expanded at a density of $2x10^5$ cells in T75 flasks in a humidified atmosphere with 5% CO_2 at 37 °C. The growth medium (Table 7) was changed every two to three days. When sufficient cells were generated for each experiment, myoblasts were seeded into 6-well plates at a density of $2x10^5$ cells per well. Cell culture experiments with C2C12 cells were kindly performed by Moira Pottgießer.

2.2.1.2 Cultivation of primary HSkMCs

In this thesis, primary HSMM isolated from the quadriceps muscle of five healthy male donors aged 16 to 35 years with a body mass index (BMI) between 19 to 26 kg/m^2 (Supplemental Table 1) were purchased from Lonza (Table 6). Myoblasts were used from passage two to a maximum of passage ten for all experiments and were grown at a density of either $2x10^5$ to $4x10^5$ in T75 flasks or $4x10^5$ to $1x10^6$ in T150 flasks (Table 2) in a humidified atmosphere with 5% CO_2 at 37 °C. Growth medium (Table 7) was changed every two days at 2 ml/well, and cells were passaged at 60-65% confluence.

2.2.1.3 Passage and determination of cell count

At 60-65% confluence, myoblasts (HSMM and C2C12) were passaged and either transferred to new flasks or seeded into 6-well plates (Table 2) for the respective experiments. Cells were washed 1x with PBS (Table 5), either 10 ml for T75 flasks or 20 ml for T150 flasks (Table 2). Subsequently, the cells (HSMM and C2C12) were incubated with the respective trypsin/ EDTA mixture (Table 3) for approximately 3 ½ minutes in the incubator (5% CO_2, 37 °C) (Table 1) to detach the cells from the surface, either 2 ml (T75) or 4 ml (T150) of trypsin/ EDTA mixture was applied for the HSMM and 1 ml of trypsin/ EDTA mixture was applied for the C2C12 cells. The trypsin/EDTA reaction was stopped by adding 8 ml (T75) to 16 ml (T150) growth medium (Table 7) to the cell suspension (depending on the volume of trypsin/ EDTA mixture), which was then transferred to 50 ml tubes (Table 2). The cell suspension from HSMM was centrifuged at 485 xg for 5 min, while the cell suspension from C2C12 cells was centrifuged at 216 xg for 5 minutes (Table 1). An aliquot of the cell suspension was mixed with trypan blue stain (1:2) (Table 5) to exclude apoptotic cells from counting. Cell number was determined using Neubauer chamber (Table 2) and calculated as follows:

$$cell\ count = number\ of\ cells : 8\ x\ 2\ x\ 10{,}000 = cells/\ ml$$

The number of cells was then multiplied by the volume of cell suspension media. For further expansion, cells were seeded in T75 or in T150 flasks, for all experiments, cells were seeded in 6-well plates at a density of $2x10^5$ cells/ well (HSkMCs and C2C12 cells) and grown in the incubator with 5% CO_2 at 37 °C. The growth media were changed every two days with 2 ml/ well (Table 7).

2.2.1.4 Differentiation to myotubes

After three to five days of proliferation (donor dependent) in 6-well plates (Table 2), HSMM (Table 6) reached 90-95% confluence and differentiation was initiated by replacing growth medium with differentiation medium (2 ml/well) (Table 7). Medium was changed every two days and experiments were performed after five or six days of differentiation. Murine C2C12 myoblasts grew rapidly very dense and confluent (95%), so differentiation was initiated one day after seeding into 6-well plates. Differentiation medium (2 ml/well) was changed every three days (Table 7) and experiments were performed on day six of differentiation.

2.2.1.5 Induction of insulin resistance in primary HSkMCs

To artificially induce insulin resistance in insulin sensitive primary HSkMCs and thereby impair the insulin signaling cascade, several approaches have been pursued.

2.2.1.5.1 Exposure of human myotubes to LY294002

On day six of differentiation, multinucleated myotubes were incubated in starvation medium for four hours (Table7) and then incubated with 40 µM PI3K-inhibitor LY294002 (LY) for another 1 ½ hours in starvation medium (Table 8). Since LY was reconstituted in DMSO, control myotubes were also exposed to the same amount of DMSO (0.08%) as well (Table 8). After 1 ½ hours of incubation, the cells were acutely stimulated with insulin as described in 2.2.1.6.

2.2.1.5.2 Exposure of human myotubes to 300 µM palmitate

Since higher levels of circulating FFA such as palmitic acid are associated with a higher risk of T2DM resulting in insulin resistance, we established different protocols using palmitate to impair insulin signaling. In the first protocol, myotubes were exposed to 300 µM palmitate in differentiation medium (Table 8) for 18 hours on day five of differentiation. The next day, the cells were incubated in starvation medium (Table 7) for six hours without the presence of palmitate and either acutely stimulated with insulin (2.2.1.6) or stimulated with insulin for three hours to measure glycogen synthesis (2.2.4.1).

2.2.1.5.3 Exposure of human myotubes to 800 µM palmitate

The second protocol consisted of stimulating the myotubes on the fifth day of differentiation with 800 µM palmitate (6:1 palmitate:BSA complex) (Table 8) for 12 hours, only this time in starvation medium (Table 8). Control cells were exposed to the same amount of BSA

(Table 8) as palmitate-treated cells. The next day, the medium was replaced with fresh starvation medium (Table 7) without palmitate and the myotubes were either starved for six hours before acute stimulation with insulin (2.2.1.6) or exposure to EPS (2.2.1.7) for six hours.

2.2.1.6 Acute insulin stimulation

For acute insulin stimulation after the respective experiments, myotubes from control and treatment groups were exposed to either 10 nM or 100 nM insulin-containing starvation medium (Table 8) or insulin-free starvation medium (Table 7) (basal cells) for 15 minutes in the incubator (5% CO_2, 37 °C).

2.2.1.7 Electrical Pulse Stimulation

To mimic physical exercise *in vitro*, myotubes were exposed to an acute low-frequency EPS protocol on day six of differentiation. Before starting the EPS treatment, C-Dish™ carbon electrodes (Table 1) were briefly pre-soaked in the respective starvation medium (for HSkMCs or C2C12 cells) (Table 7) and the cells were washed three times with DPBS (Table 7) to remove any kind of serum residues (FBS, HS, BSA) in the supernatant. Subsequently, the media were changed to the respective starvation medium (1 ml/well) (Table 7), C-Dish™ was placed on 6-well plates (Table 2) and all together were placed in the incubator (Table 1). Under similar conditions, the control group was also exposed to C-Dish™ carbon electrodes, but not connected to the power supply. EPS parameters were adjusted for HSkMCs (40 V, 2 ms, 1 Hz) and murine C2C12 cells (11.5 V, 2 ms, 1 Hz), respectively followed by an acute stimulation period of six hours for both cell models. After stimulation, each cell supernatant (conditioned media, CM) was collected in 15 ml LoBind® tubes (Table 2) for mass spectrometry analysis and centrifuged at 1,000 xg for 10 minutes at 4 °C (Table 1) to remove any cell debris. Next, supernatant was then transferred into new LoBind® tubes, yielding approximately 5 to 5.5 ml of CM per condition, and stored at -80 °C until further analysis. An aliquot of 120 µl of the centrifuged CM was taken for Multiplex immunoassay (MIA) (2.2.4.3) and was stored in LoBind® tubes at -80°C. Cells were placed on ice and washed 1x with cold DPBS. For cellular proteomic analyses, HSkMCs were lysed at 50 µl/ well and C2C12 cells at 200 µl/well in SDS lysis buffer (Table 5), shock frozen in liquid nitrogen and stored at – 80°C until further analysis. For Western blot analyses cell lysates were generated as described in section 2.2.3.1. In this experiment, each EPS-stimulated or unstimulated plate represents one technical replicate (*n*).

2.2.2 Molecular biological methods

2.2.2.1 RNA isolation and cDNA synthesis

For RNA isolation, myoblasts (HSMM and C2C12) were grown to 90-95% confluence in 6-well plates (Table 2), washed once with PBS (Table 5) at day zero of differentiation, and harvested in 120 µl/well RLT-buffer (Table 5). Samples were shock frozen in liquid nitrogen and stored at -20 °C until further analysis. Myoblasts were differentiated into multinucleated myotubes by switching from starvation medium to differentiation medium (Table 7) and were harvested on day six of differentiation using the same procedure as previously described for the myoblasts. RNA from human and murine myoblasts and myotubes was isolated using the RNeasy-Mini Kit (Table 9) according to the manufacturer´s instructions. RNA concentration and purity were determined using the NanoDrop™ spectrophotometer (Table 1) by measuring optical density at a wavelength of 260 nm. For cDNA synthesis, 1 µg of RNA was transferred into a reaction tube together with 1 µl of deoxynucleotide triphosphates (dNTPs) and 2 µl of pre-diluted (1:10) hexanucleotide primers (Table 11). Samples were incubated for 5 minutes at 65 °C in the thermomixer comfort (Table 1), then cooled down on ice for one minute and briefly centrifuged for 10 seconds (Table 1). A total of 7 µl of master mix containing 4 µl of GoScript™ 5x buffer, 2 µl of magnesium chloride ($MgCl_2$) and 1 µl of reverse transcriptase (Table 3) was added to each sample, briefly spun down, and reaction tubes were loaded into the thermomixer according to the following protocol. RNA isolation and cDNA synthesis were kindly performed by Didi Humpert.

Table 14: cDNA synthesis protocol.

Reaction	Temperature	Duration
Annealing	25 °C	5 min
Elongation	42 °C	60 min
RT-inactivation	70 °C	15 min
Hold	+4 °C	

Once the run was completed, cDNA was diluted in nuclease free water (1:10) and stored at - 20 °C until further analysis.

2.2.2.2 Quantitative reverse transcription polymerase chain reaction (qRT-PCR)

To validate the differentiation from myoblasts to myotubes, qRT-PCR was performed on representative genes in HSkMCs and C2C12 cells for different stages of myogenesis was performed. The latter is a fluorescence-based method that assesses the change in emission of accumulated PCR amplicons in real time. There are target-specific fluorescent dyes that

label oligonucleotides such as primers or probes, and there are DNA-binding dyes such as SYBR Green that emit a fluorescence signal proportional to the accumulated PCR amplicons in the sample. Using the GoScript™ Reverse Transcriptase kit (Table 9), 4 µl of diluted cDNA (2.2.2.1) was added to 5 µl of Master Mix containing 0.5 µl of diluted forward and reverse labeled-SYBR Green primer (Table 11) in a reaction tube and subsequently transferred to a 384-well plate (Table 2). The plate was covered with MicroAmp adhesive films (Table 2) and briefly centrifuged (Table 1) before placed in the QuantStudio™ 7 Flex (Table 1) PCR System machine applying the protocol described below (Table 15).

Table 15: qPCR protocol.

Reaction	Temperature	Duration	Cycle
Hot Start	95 °C	2 min	1x
Denaturation	95 °C	15 sec	40x
Annealing	60 °C	60 sec	
Dissociation	60-95 °C	90 sec	1x

To quantify transcript abundance, the exponential phase threshold was set to 0.2. The calculated Ct values were first normalized to the housekeeping gene *B2M* (ΔCt) (HSkMCs) or *Tpb* (C2C12 cells) and then further normalized to the control of each experiment (2-ΔCt). Therefore, the final results were presented as relative normalized gene expression (2-ΔΔCt). RT-qPCR was kindly performed by Didi Humpert.

2.2.3 Biochemical Methods

2.2.3.1 Cell lysis and determination of protein concentration via Bicinchonic acid assay

After acute stimulation with insulin as described in 2.2.1.6, HSkMCs in 6-well plates (Table 2) were rinsed on ice with cold PBS (Table 5) once and subsequently lysed in 70 µl/well using Western blot lysis buffer (Table 5). Samples were pooled and cell lysates were transferred to a 1.5 ml reaction tube (Table 2), then homogenized in Uniprep gyrator-24 (Table 1) for 10 min. Next, samples were centrifuged at 25,000 xg for 10 minutes at 4 °C to pellet (Table 1) to remove any cell debris, then the clear supernatant was transferred to a new reaction tube and samples were stored at -20 °C until further analysis. C2C12 cells were processed in the same way as the HSkMCs, except that they were lysed in 200 µl/well of Western blot lysis buffer. Next, the assay was performed using bicinchonic acid (BCA) Protein Assay Kit (Table 9), which allows photometric and quantitative determination of protein concentration by reducing Cu^{2+} ions to Cu^{+} ions, which then form a chelate complex with 2 bicinchonic acid molecules each.

This colored complex will then be photometrically detected at a wavelength of 560 nm. After applying the standard curve (Table 16) to the 96-well plate (Table 2), protein lysates were added in a dilution of 1:5 (HSkMCs) or 1:20 (C2C12) in MQ-H_2O, all applied as duplicate technical replicas. Before reading the plate in iMark™ Microplate Absorbance Reader (Table 1) it was incubated for 30 minutes in a humid atmosphere (5% CO_2, 37 °C) to initiate the reaction. The pipetting scheme of the BSA standard curve is listed in Table 16.

Table 16: Standard series BSA assay.

Amount [µg/well]	Concentration [µg/well]	BSA stock solution [µl]	MQ-H_2O [µl]
0.5	0.025	1.5	118.5
1.0	0.050	3	117.0
2.0	0.100	6	114.0
3.0	0.150	9	111.0
4.0	0.200	12	108.0
5.0	0.250	15	105.0
6.0	0.300	18	102.0
7.0	0.350	21	99.0

2.2.3.2 Sodium-dodecylsulfate-polyacrylamide gel electrophoresis

Electrophoretic separation of proteins according to their size was obtained by denaturing sodium-dodecylsulfate-polyacrylamide gel electrophoresis (SDS-PAGE). Therefore, SDS (Table 3) was added to the protein lysates in order to generate a negative charge, allowing the proteins to migrate to the anode of the electric field. The polyacrylamide gel matrix separates the proteins based on their molecular mass, hence larger proteins are retained by the matrix whereas smaller proteins reach the anode more quickly. Firstly, protein lysates were diluted with 4x Laemmli buffer (Table 5) and MQ-H_2O, in order to load 10-20 µg of total protein on the gel. Next, samples were vortexed and denatured for five minutes at 95 °C in thermomixer comfort (Table 1), thus secondary and tertiary structures of the proteins are broken, which then allows SDS to cover the protein with its own negative charge that is proportional to the protein mass. Afterwards, samples were briefly cooled on ice, shorty spun down and loaded on a 12% SDS gel (Table 17) or stored at -20 °C until further analysis. Additionally, PageRuler™ Prestained Protein Ladder (Table 12) was applied on the gel, serving as a control to assess the protein size of the proteins of interest. Electrophoresis was performed using Mini-

PROTEAN Tetra Vertical Electrophoresis Cell systems (Table 1) filled with electrophoresis buffer (Table 5) starting at 50 V for approximately 15 min, then switching to 150 V for another 50 to 60 minutes until protein ladder was widely separated.

Table 17: Composition of stacking and separation gel for western blot analysis.

Compound	Volume
Stacking gel	
Stacking gel buffer	780 µl
Acrylamide (30 %)	390 µl
ddH_2O	1.83 µl
APS	6 µl
TEMED	3 µl
Separation gel	
Separation buffer (Table X)	2.34 ml
Acrylamide (30%)	3.6 ml
ddH_2O	3.06 ml
APS	18 µl
TEMED	9 µl

The specifications listed in the table refer to one 12% gel.

2.2.3.3 Western Blot analysis

After gel electrophoresis, separated proteins were transferred onto a nitrocellulose membrane (Table 2) using a wet-tank blotting system. Therefore, membrane, gel together with Whatman papers (Table 2) and two sponges were stacked in a cassette, followed by a two hours of transfer at 0.2 A and 4 °C in a tank blot containing transfer buffer (Table 5). The transfer of the negatively charged proteins to the membrane was towards the anode. Afterwards, unspecific antibody binding sites were blocked, by incubating the membrane with the Tris-buffered saline with Tween® (TBS-T) blocking buffer (Table 5) supplemented with 5% MP for approximately one hour at room temperature. Membranes were washed with TBS-T and incubated overnight at 4 °C with specific primary antibodies (Table 10) during rotation. The next day, membranes were washed with TBS-T and incubated with secondary HRP-coupled antibody (Table 10) in either 5% MP or BSA for another hour at room temperature. After one more washing step (TBS-T), proteins were detected using Western Lightning® ECL chemiluminescent substrate

(Table 2) according to manufacturer instructions. Both compounds (1:1) of the kit initiate HRP to catalyze the conversion of luminol to 3-aminophthalate. This reaction emits a signal which was then detected by the transilluminator ChemiDoc XRS+ (Table 1) and quantified using Image Lab software (Table 13). Protein bands were either normalized to the housekeeping protein Glyceraldehyde 3-phosphate dehydrogenase (GAPDH) or α-Tubulin.

2.2.4 Cell-based assays

2.2.4.1 Glycogen synthesis

Primary human skeletal muscle myotubes were treated with 300 µM palmitate for 18 hours in differentiation medium overnight in a humidified atmosphere with 5% CO_2 at 37 °C (2.2.1.5.2). To access the level of insulin resistance in the cells, measurement of insulin-induced glycogen synthesis was used to detect insulin resistance at a functional level. After pretreatment with 300 µM palmitate, cells were incubated for six hours in starvation medium (Table 7) and then starved for another three hours in basal medium supplemented with D-[^{14}C(U)]-glucose (2 µCi/mL) in the presence or absences of 100 nM insulin (Table 8). The myotubes were then rinsed twice with cold PBS (Table 5) on ice and stored at -20 °C for further analysis. For sample solubilization, cells were thawed on ice and harvested in 1M KOH (5.6mg/100 ml) (Table 3) at 400 µl/well. Next, 60% KOH and glycogen (20 mg/ml) (Table 3) were added, samples were vortexed and incubated at 80 °C for 20 min. By adding 1 ml of ice-cold absolute EtOH (Table 2) to the samples, glycogen was precipitated. The samples were centrifuged at 10,000 xg for 20 minutes at 4 °C (Table 1), the supernatant was discarded and the samples were washed again with 1 ml 70% EtOH, vortexed and centrifuged again at 10,000 xg for 20 minutes at 4 °C. The supernatant was discarded and the pellet was dried at 37 °C in a thermomixer (Table 1) for approximately 30 to 45 min. Finally, the pellet was resuspended in 500 µl H_2O. For the determination of incorporated D-[^{14}C(U)]-glucose in the skeletal muscle, 300 µl of sample was mixed with 2.5 ml of scintillation liquid Rotiszint®eco plus (Table 3), incubated for 20 minutes at rotation in the dark and then the radioactivity was counted in a MicroBeta® counter (Table 1). Protein concentration was measured by BCA assay as described in 2.2.3.1, except that samples and standard were diluted in 1M KOH.

2.2.4.2 Assessment of cell viability and cytotoxicity

To assess the level of cytotoxicity in primary human myotubes after treatment with either LY294002, palmitate or EPS, the release of the cytosolic enzyme lactate dehydrogenase (LDH) into the cell culture media was measured. When the plasma membrane is damaged, LDH is quickly released into the cell culture media and therefore serves as an excellent biomarker for cell damage. The assay was performed using the LDH-Glo™ Cytotoxicity Assay kit (Table 9), according to manufacturer´s instructions. The kit uses a bioluminescent method to quantify LDH by converting the compound luciferin to a bioluminescent signal using Ultra-

Glo™rLuciferase that is proportional to the amount of LDH in the cell culture media. Luciferin is generated by the reduction of nicotinamide adenine dinucleotide (NAD+) to NADH (-hydrogen) and the concomitant oxidation of lactate, which is catalyzed by LDH. NADH is used by the reductase enzyme together with reductase substrate to produce luciferin. For the maximum LDH release control, myotubes were treated with 10% Triton X-100 (2 µl/100 µl) (Table 3) and incubated for 15 minutes, resulting in irreversible permeabilization of the membrane and release of LDH into the cell culture medium. For the assay, an aliquot of the supernatant was collected after each treatment (2.2.1.5.1, 2.2.1.5.3, 2.2.1.7), diluted 1:20 in LDH storage buffer and immediately stored at -20 °C until further analysis. Subsequently, samples were further diluted in LDH Storage Buffer at a ratio of 1:50 (samples with starvation medium as background) or 1:300 (samples with Triton X100), transferred to a 96-well plate and applied as technical duplicates. Standards and controls were each run as technical triplicates. LDH detection reagent was added to the wells and the plate was incubated for one hour at room temperature. Luminescence was recorded using Infinite® 200 PRO (Table 1) and analyzed using i-control™ 2.0 software (2.1.1.0), the plate was read with an integration time of 0.5 seconds. The absolute values of LDH release measured in the samples were compared to the maximum release control used as a reference.

2.2.4.3 Multiplex immunoassay

In a targeted approach, the concentration of specific analytes was measured in the cell culture supernatant of insulin sensitive and insulin resistant HSkMCs from five donors after exposure to palmitate and EPS treatment (2.2.1.5.3, 2.2.1.7). Therefore, MIA were performed using MILLIPLEX® MAP Human Myokine Magnetic Bead Panel, HMYOMAG-56K (15-Plex) and Bio-Plex® Pro Human Cytokine Screening Panel (48-Plex) (Table 9). The MILLIPLEX® myokine assay screens for the presence of IL-6, Oncostatin M, BDNF, IL-15, FGF21, LIF, fatty acid-binding protein 3 (FABP3), fractalkine, osteocrin/ musclin, apelin, irisin, myostatin, FSTL-1, and SPARC. The Bio-Plex® assay quantifies 48 cytokines, chemokines and growth factors present in the supernatant, including TNF-α, IL-8, MCP-1, macrophage migration inhibitory factor (MIF) and VEGF-A. MIA use internally color-coded microspheres (magnetic beads) with fluorescent dyes that are coated with a specific capture antibody. The beads react with the sample to capture an analyte, followed by several wash steps to remove unbound proteins, and then a biotinylated detection antibody is added to the multiplexed suspension. This is incubated with a streptavidin-phycoerythrin conjugate to complete the reaction. This technique allows the simultaneous quantification of all analytes in the sample. For the MILLIPLEX® assay 25 µl (undiluted) and for the Bio-Plex® 50 µl (undiluted) of each sample were used, 25 µl (undiluted) of cell culture starvation medium with or without palmitate or BSA served as controls. All reagents were allowed to equilibrate to room temperature and the MIA was conducted according to the manufacturer´s instructions. For data acquisition and analysis,

assays were read on a Bio-Plex® 200 System and results were quantified based on fluorescent reporter signals (phycoerythrin). The mean fluorescence intensity (MFI) of the phycoerythrin signal is proportional to the concentration of analyte bound to each microsphere, allowing the Bio-Plex Manager™ software to report the data as MFI or concentration (pg/ml or ng/ml). This assay was kindly performed by Martina Schiller.

2.2.5 Bottom-up proteomics workflow and mass spectrometry analyses

The following sections describe the processing of samples of either HSkMCs or C2C12 cells prepared for MS analysis. Skeletal muscle cells were expanded in cell culture (2.2.1.1, 2.2.1.2, 2.2.1.3) and differentiated (2.2.1.4) into multinucleated myotubes. Insulin sensitive and resistant human myotubes were generated (2.2.1.5.3) and subjected to acute low-frequency EPS, while control cells remained unstimulated (2.2.1.7). Murine C2C12 myotubes were also treated with acute low-frequency EPS or left unstimulated (CON) (2.2.1.7). Subsequently, supernatant (CM) and cell lysates from both cell models were processed within a bottom-up proteomics workflow and analyzed by high-resolution MS as shown in Figure 6. The proteomics analyses were performed in collaboration with our proteome analysis unit headed by Dr. S. Lehr. The sample preparation of the C2C12 samples and the BSA- and palmitate-treated samples from five donors was performed by the two technical assistants M. Schiller and U. Kittel, the MS analyses (PD™ result files) were performed by Dr. S. Hartwig.

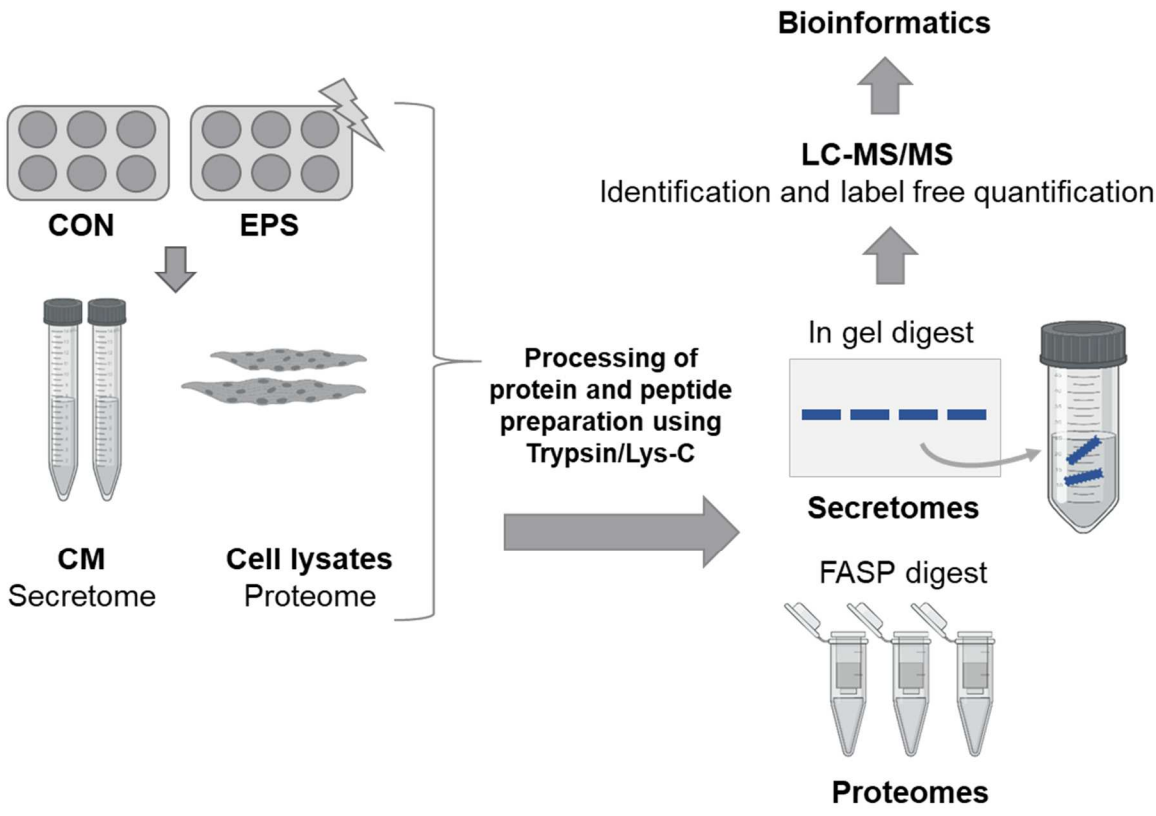

Figure 6: Simplified overview of a bottom-up proteomics workflow of secretome and proteome samples for MS analysis. CON: control (unstimulated), EPS: Electrical pulse stimulation, CM: conditioned media, LC: Liquid

chromatography, MS: Mass spectrometry, FASP: Filter-aided sample preparation. This figure was created with BioRender.

2.2.5.1 Sample preparation for secretome analysis

In this thesis, secretome and cellular proteome samples were processed within a bottom-up proteomics workflow, meaning that the complex mixture of proteins was first enzymatically digested into peptides, which were then separated by LC prior to MS analysis (Figure 6). Cell culture supernatants from HSkMCs and C2C12 cells (2.2.1.7) were thawed and kept on ice throughout the sample preparation process. Samples were transferred to polypropylene tubes (Table 2) and centrifuged at 85,000 xg for 30 minutes at 4 °C (Table 1). High speed centrifugation removed larger molecules such as apoptotic bodies and cell debris, while smaller molecules such as EV were not pelleted. The entire sample volume was then transferred to Amicon® ultra-4 centrifugal tubes (filter unit 3K) to concentrate the proteins in the samples by reducing the initial volume from approximately 5.5 ml to 50 to 100 µl. Prior to sample transfer, 1 ml DPBS (Table 3) was used to activate the Amicon® columns and discarded shortly thereafter. Samples were centrifuged at 3,220 xg for approximately 2 to 2 ½ h (Table 1) until no supernatant eluted through the filter columns. The concentrated samples were transferred to new reaction tubes and the protein concentration was measured using the NanoDrop™ spectrophotometer (Table 1) at a wavelength of 280 nm.

Next, a gradient SDS-PAGE gel was run, which concentrated the samples into a single band required for subsequent in-gel digestion. The composition of the SDS-PAGE gel is shown in Table 18.

Table 18: Composition of MS-gel for enzymatic protein digestion procedure.

Stacking gel 4%	Separation gel 10%	Separation gel 25%
2.275 ml MQ-H_2O	0.75 ml MQ-H_2O	0.625 ml MQ-H_2O
0.875 ml 0.5 M Tris pH 6.8/ 0.8% SDS (4x)	0.375 ml 3 M tris pH 8.8/ 0.8% SDS (4x)	1.25 ml 3 M tris pH 8.8/ 0.8% SDS (4x)
0.35 ml acrylamide (40%)	0.375 ml acrylamide (40%)	3.125 ml acrylamide (40%)
13.15 µl APS (10%)	7.5 µl APS (10%)	25 µl APS (10%)
2.65 µl TEMED	1.5 µl TEMED	5 µl TEMED

The solutions were poured in the following order: 25% separation gel, 10% separation gel, and 4% stacking gel. A total of 25 µg of protein was loaded on the gel for in gel digestion of C2C12 supernatant samples. For HSkMC, supernatants from two different experiments were used for MS analyses. For the first in gel digestion, samples from three donors were used, where the protein yield in the cell culture supernatant was very low, therefore approximately 1 µg of

protein was loaded on the gel for digestion. For the second in gel digestion, samples from five donors were used, where a higher yield was achieved, allowing a total of 4.2 µg of protein to be loaded onto the gel. The samples were then diluted with MQ-H2O and 5x SDS sample buffer (Table 5), followed by denaturation at 95°C for 5 minutes with BSA (500 ng) (Table 3). All Blue Prestained Protein Standard (Table 12) diluted in 1x SDS sample buffer (Table 5), BSA (reference band) and samples were applied to the gel and electrophoresis was performed at 100 V in Fling-Gregerson buffer (Table 5). Compressed protein bands were then visualized by staining with Coomassie® Brilliant Blue R-250 dye (Table 3) as described in Table 19. The gel was incubated in the appropriate solution (100 ml) with shaking at room temperature. Finally, the gel was imaged using the ChemiDoc XRS+ Gel Imaging System (Table 1).

Table 19: MS-gel staining protocol with Coomassie® Brilliant Blue R-250 dye.

Staining	Chemicals	Procedure
Fixation	40% MeOH, 2% o- H_3PO_4, ad. MQ-H_2O	Incubation time 1h
Washing	MQ-H_2O	Change MQ-H_2O every 20 min
Equilibration	34% MeOH, 2% o- H_3PO_4, 17% $(NH_4)_2SO_4$ ad. MQ-H_2O	Incubation time 1h
Staining	34% MeOH, 2% o- H_3PO_4, 17% $(NH_4)_2SO_4$, 0.066% Coomassie® Brilliant Blue R-250 ad. MQ-H_2O	Dyeing overnight, next day change staining solution and incubate for another 3 - 4h
Destaining	MQ-H_2O	Destaining of background

All instructions refer to 100 ml total volume. (MeOH, methanol; o- H_3PO_4, o-phosphoric acid; $(NH_4)_2SO_4$, ammonium sulfate)

After the staining, the compressed gel bands were excised from the gel, cut into 4 equal pieces and transferred to a 1.5 ml reaction tube. Each sample was washed alternately with 200 µl of 25 mM ammonium bicarbonate ($(NH_4)HCO_3$) and 200 µl of 25 mM 50% acetonitrile (v/v) (MeCN, methyl cyanide) for 10 minutes until the blue color disappeared. For dehydration, the gel pieces were washed with 200 µl 100% MeCN (v/v) for 15 minutes and dried for another 15 minutes. Then, 80 µl dithiothreitol (DTT, dissolved in 25 mM $(NH_4)HCO_3$) was added to break the disulfide bonds of the proteins, and the samples were heated at 50 °C for 15 minutes with shaking. The samples were cooled on ice and the DTT solution was discarded. Samples were again incubated with 200 µl 100% MeCN for 15 minutes, followed by a 15 minutes drying process, before samples were incubated in the dark with 80 µl iodoacetamide (IAA, dissolved in 25 mM $NH_4)HCO_3$) for irreversible alkylation. Again, samples were washed alternately with 500 µl of 25 mM $(NH_4)HCO_3$) and 200 µl of 25 mM 50% MeCN (v/v), followed by a further

dehydration step with 200 µl of 100% MeCN for 15 minutes. The supernatant was discarded and the samples were dried at room temperature for 15 minutes until Trypsin/Lys-C mixture (Table 3) was added at a 1:25 (w/w) enzyme/protein ratio (diluted in 50 mM $(NH_4)HCO_3$) and 2% MeCN (v/v)). Enzymatic digestion was performed overnight at 37 °C (max. 16 hours). The next day, the samples were incubated with 1% trifluoroacetic acid (TFA) (Table 3) for approximately 60 minutes and then with 0.1% TFA/90% MeCN (v/v) for another 30 minutes to elute the peptides from the gel pieces. The eluted peptides were lyophilized at 45°C in the Savant™ SpeedVac™ SPD 1030 centrifugal vacuum concentrator (Table 1) and stored at 4°C until further analysis.

2.2.5.2 LC-MS/MS analyses of secretomes

For high-resolution LC-MS/MS analyses, lyophilized peptides from C2C12 cells and HSkMCs (2.2.1.7) were reconstituted in 1% TFA (v/v) and separated on an LC UltiMate™ 3000 (Table 1) connected to an Orbitrap Exploris™ 480 mass spectrometer (Table 1). Peptides were trapped and desalted on an Acclaim™ PepMap™ C18-LC-column (ID: 75 µm, 2 cm length), followed by separation on an Aurora C18 column (Table 1) using a 2 hours three step gradient at a total flow rate of 300 nl/ minutes with buffer A (0.1% formic acid) and buffer B (80% ACN, 0.1% formic acid). First, linear from 2-19% buffer B for 72 min, second from 19-29% buffer B for 28 min, then from 29-41% buffer B for 20 minutes and a 1 min linear gradient increasing buffer B to 95%. MS data were acquired in data dependent acquisition (DDA) mode at 120,000 resolution (2 seconds cycle time), m/z range of 350-1,200 and a normalized AGC target value of 300%. Fragmentation precursor selection filters were set to charge state between two and six and dynamic exclusion of 45 seconds. Fragmentation of precursors was performed with an isolation window (m/z) of 1.6, a higher-energy collisional dissociation (HCD) energy of 30%, and a resolution of 15,000 with automatic adjustment of the automatic gain control (AGC) target value and injection time.

2.2.5.3 Sample preparation for cellular proteome analyses

Cell lysates from C2C12 and human myotubes for proteome analyses (2.2.1.7) were further solubilized in denaturing SDS buffer (Table 5) by 10 strokes through an insulin syringe (Table 1, needle 26 gauge) followed by sonification (two times pulse 0.09sec_10sec). The samples were then centrifuged at 75,000 xg for 30 minutes at 4 °C and the supernatants were transferred to new reaction tubes. Protein concentrations were determined using the NanoDrop™ spectrophotometer (Table 1). Protease digestion was performed according to the filter-aided sample preparation (FASP) procedure (201) with some adaptations. Shortly, protein samples (100 µg) were incubated at 96 °C for 10 minutes and then diluted 1:10 (v/v) with urea buffer (Table 5). Samples were then centrifuged at 10,000 xg using Amicon® Ultra 0.5 ml centrifugal filter devices (Table 1) and alkylated by incubation with 50 mM IAA for 15

minutes at room temperature. Washing steps with urea buffer were repeated three times (including centrifugation at 10,000 xg for 16 minutes), protein lysates were digested using Trypsin/Lys-C mixture (Table 3) in a 1:25 (w/w) enzyme/protein ratio overnight at 37 °C. The next day, filter devices were centrifuged and the peptides were collected and acidified with TFA to a final concentration of 0.1% (v/v). Purification was obtained using C18 solid phase extraction (Strata C18-E, 200 mg/ml, Phenomenex) according to manufacturer´s instructions. Eluates were lyophilized and stored as aliquots at -80°C.

2.2.5.4 Pierce™ Quantitative Colorimetric Peptide Assay

The lyophilizates (2.2.5.3) for cellular proteome analysis of C2C12 cells and HSkMCs were solubilized in 1% TFA (v/v) and peptide concentration was determined using Pierce™ Quantitative Peptide Assay according to manufacturer´s instructions. This assay is characterized by copper reduction (Cu^{2+} to Cu^{1+}) caused by amide bonds of the peptides under alkaline conditions. A chelating agent combines with the reduced copper ions to form a red complex with an absorbance at 480 nm. For this colorimetric assay, only a small amount of sample (5 µl) was used in a 1:4 dilution in MQ-H_2O with a working peptide concentration range of 25 to 1,000 µg/mL.

2.2.5.5 LC-MS/MS analyses of cellular proteomes

For LC-MS/MS analyses, lyophilized peptides were reconstituted in 1% TFA (v/v) and peptide concentrations were determined using Quantitative Colorimetric Peptide Assay (Table 9) as described in 2.2.5.4. Samples (400 ng) were run in triplicates on an LC UltiMate™ 3000 (Table 1) as described in 2.2.5.2. MS analysis was performed on an Orbitrap Fusion™ Lumos™ mass spectrometer (Table 1) coupled to a Nanospray Flex™ ion source (Table 1) and equipped with a high-field asymmetric waveform ion mobility spectrometry (FAIMS Pro) interface. MS data were obtained in DDA mode using FAIMS compensation voltages (CV) of -40, -60 and -80 V. MS spectra were acquired at 120,000 resolution (3 seconds cycle time) and m/z range of 350-1,600. Fragmentation precursor selection filters were set to charge state between two and seven, dynamic exclusion of 30 seconds and an intensity threshold of 2.5E4. Fragmentation of precursors was done with an isolation window (m/z) of 3.6, HCD energy of 30% at 15,000 resolution with automatic adjustment of AGC target and injection time.

2.2.6 Quantitative analyses of MS-based data

Proteome Discoverer™ (PD™) 3.0 software (Table 13) was used to analyze the MS raw files. For spectral recalibration, the SpectrumRC node was used with the FASTA database (UniProtKB database, reviewed SwissProt, *Homo sapiens* TaxID=9606, v2022-12-14 and v2023-06-28, *Mus musculus* TaxID=10090, v2023-03-01). The minora feature detector node was used for quantification with default settings (minimum trace length 5, maximum delta RT

of isoptope pattern multiplets of 0.2 min, and only high confidence PSMs were used for feature-ID association). CHIMERYS search was performed against UniProtKB database (reviewed SwissProt, *Homo sapiens* TaxID=9606, v2022-12-14 and v2023-06-28, *Mus musculus* TaxID=10090, v2023-03-01 and an in-house contaminant fasta file). Enzymatic digestion was performed using trypsin, allowing a maximum of two missed cleavage sites, and b and y ions were selected for HCD fragmentation with a fragment mass tolerance of 0.02 Da. Carbamidomethylation of cysteine was set as the static modification, while N-terminal acetylation, N-terminal methionine loss, N-terminal methionine loss/acetylation and methionine oxidation were allowed as variable modifications. Percolator (included in PD™, max delta Cn: 0.01) was applied for data validation. Label-free quantification was performed on precursor intensities present in at least 20% of replicate features. Protein ratios were calculated either on a pairwise ratio basis (t-test, background based) or by ANOVA (individual proteins).

2.2.6.1 Bioinformatic analyses of MS-based data

MS data were filtered for “master proteins”, proteins with high levels of “false discovery rate” (FDR), proteins with at least one “unique peptide” and the species map was chosen for either “*Homo sapiens*” or “*Mus musculus*” using PD™. Potential myokines were then analyzed using bioinformatic prediction tools, including as SignalP 6.0 (102), SecretomeP 2.0 (104) and Outcyte 1.0 (100). The SignalP algorithm screens for proteins that carry a signal peptide sequence at the N-terminus and are therefore predicted to be secreted via the classical ER-to-Golgi pathway. SecretomeP (nn-score<0.6) and Outcyte predict putative secretory proteins that are secreted via unconventional secretory pathways, such as intracellular- or transmembrane proteins. Moreover, gene ontology cellular component (GOCC) analyses were performed using the generic GO term mapper (202). Comparative analyses between C2C12 cells and primary HSkMCs were performed on the basis of gene symbols, and comparative analyses within the same species were performed on the basis of primary UniProtKB accessions. For further analysis of the large MS datasets, Venn diagrams were created using the web-based tool InteractiVenn (203), and heatmap and PCA analyses were performed using either ClustVis (204) or R 4.3.2.

2.2.6.2 Cross-species literature research of MS data

The literature search was performed using the PubMed® database. For the comparative analyses, only papers published in English that performed non-targeted secretome analyses of skeletal muscle cells (C2C12 or primary HSkMCs) were considered. Keywords such as “secretome analysis”, “secreted proteins”, “mass spectrometry”, “skeletal muscle cells”, “myokines”, “exercise” and “electrical pulse stimulation” were selected for PubMed® database search. The given data from different MS secretome studies provided a diverse and broad data

set. Data alignment of C2C12 cells and primary HSkMCs and comparative analyses were performed based on gene symbols.

2.2.7 Statistical analysis

In this thesis, data from all experiments are presented as mean ± standard error of the mean (SEM). The figure legend indicates the number of samples (*n*) used for each experiment, and at least three individual experiments (n=3) were performed to determine statistical significance. An unpaired two-tailed t-test with Welch's correction was used to ensure statistical significance between two groups. To test for multiple comparisons between two groups ordinary one-way ANOVA or two-way ANOVA were conducted following recommended the Dunnett or Sidak post hoc tests. Correlation analyses were performed by calculating Pearson correlation coefficients or performing linear regression analysis. In all statistical analyses, p-values<0.05 were considered statistically significant and are indicated in the figure legends as follows *p<0.05, **p<0.01, ***p<0.001, p****<0.0001. The GraphPad Prism 10 software was used for graphical illustration and statistical calculation.

3 Results

Recent studies have investigated the muscle secretome by non-targeted approaches using high-resolution MS. Of particular interest are contraction-induced myokines (exerkines), which are associated with the health-promoting effects of exercise. Exerkine secretion can be simulated *in vitro* by EPS of skeletal muscle cells in culture. To date, only two MS-based studies have analyzed the contraction-induced secretome of skeletal muscle cells (C2C12 and HSkMCs), both using chronic (24h) low-frequency EPS protocols (70, 192), however no comparative analyses have yet been carried out between these two cell models. In this thesis, the first aim was to investigate the similarities and differences of the contraction-induced muscle secretomes of the two most commonly used cell models for skeletal muscle metabolism, C2C12 cells and primary HSkMCs. Therefore, both cell models were subjected to acute (6h) low-frequency EPS protocols and myokine secretion profiles were studied and compared using high-resolution MS. The second and third aim of this thesis was to study the human muscle secretome under pathological conditions (insulin resistance) and to further explore the effects of acute (6h) low-frequency EPS on the myokine secretion profile of contracting insulin resistant human myotubes compared to insulin sensitive human myotubes. Therefore, we have established a protocol that simulates insulin resistance *in vitro* by treating skeletal muscle cells with the FFA palmitate. This in-depth MS-secretome analysis of contracting insulin sensitive and resistant human myotubes is the first of its kind.

3.1 Establishment and validation of an *in vitro* contraction model

3.1.1 Generation of differentiating murine myotubes

During myogenesis, various genes representing different stages of differentiation are expressed in skeletal muscle (1.3.1, Figure 2). To monitor differentiation of C2C12 cells *in vitro*, the mRNA expression of *Myf5* and *MyoD*, genes representing the early stages of differentiation, as well as *MyoG* and myosin heavy chain 2 (*Myh2*), which are expressed in differentiated myotubes, was determined. Murine C2C12 cells were cultured (2.2.1.1), myoblasts were harvested at day zero and myotubes at day six of differentiation (2.2.2.1) and mRNA levels were analyzed using RT-qPCR (2.2.2.2). As expected, *Myf5* mRNA expression was significantly increased in C2C12 myoblasts compared to myotubes (Figure 7A), while MyoD mRNA expression was significantly upregulated in C2C12 myotubes compared to myoblasts (Figure 7B). Furthermore, fully differentiated myotubes showed significantly increased mRNA levels of *MyoG* (Figure 7D) and *Myh2* (Figure 7E) compared to myoblasts. Moreover, light microscopic observation during the entire differentiation process showed how

mononucleated myoblasts (Figure 7C) fused to multinucleated myotubes (Figure 7F) over the course of 6 days.

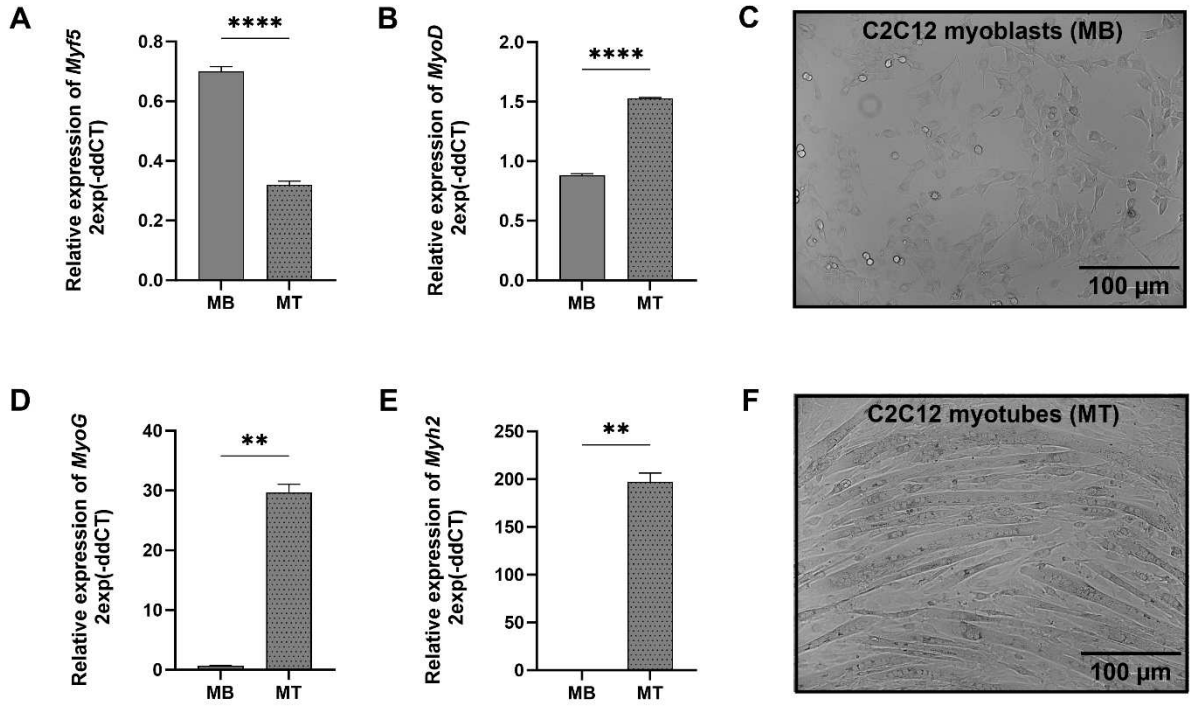

Figure 7: Validation of differentiation of murine C2C12 cells using RT-qPCR to measure gene expression profiles of representative genes of various differentiation stages. MB were harvested at day zero of differentiation and MT at day six of differentiation in RLT-lysis buffer for RNA isolation. **(A)** Gene expression profile of *Myf5*. **(B)** Gene expression profile of *MyoD*. **(C)** Bright field microscopy images of MB. (**D)** Gene expression profile of *MyoG*. **(E)** Gene expression profile of *Myh2*. **(F)** Bright field microscopy images of MT. Quantified data was normalized to housekeeping gene *Tbp*, data are mean ±SEM from three individual experiments (*n=3*) in C2C12 cells, and were analyzed by unpaired t test (Welch´s correction), **p < 0.01, ****p < 0.0001. Bright field microscopy images, scale bars = 100 µm. Dark grey bars represent MB and grey dotted bars display MT. MB: myoblasts; MT: myotubes; Myf5: myogenic factor 5; MyoD: myoblast determination protein 1; MyoG: myogenin; Myh2: myosin heavy chain 2; Tbp: TATA-box binding protein

3.1.2 Generation of differentiating human myotubes

The same myogenic factors (1.3.1, Figure 2) previously determined for C2C12 cells (3.1.1) during differentiation were also measured for HSkMCs. Primary HSkMCs from five donors were cultured (2.2.1.2), myoblasts were harvested at day zero and myotubes at day six of differentiation (2.2.2.1) and subsequently mRNA levels were analyzed by RT-qPCR (2.2.2.2). As expected, *MYF5* gene expression was significantly higher in human myoblasts than in myotubes (Figure 8A), while *MYOD* mRNA expression was nearly the same in human myoblasts and myotubes (Figure 8B). Furthermore, *MYOG* and *MYH2* were significantly increased in human myotubes compared to myoblasts (Figure 8D-E). Also, the differentiation process was captured by light microscopy showing mononucleated myoblasts at day zero of differentiation (Figure 8C) and multinucleated myotubes at day six of differentiation (Figure 8F).

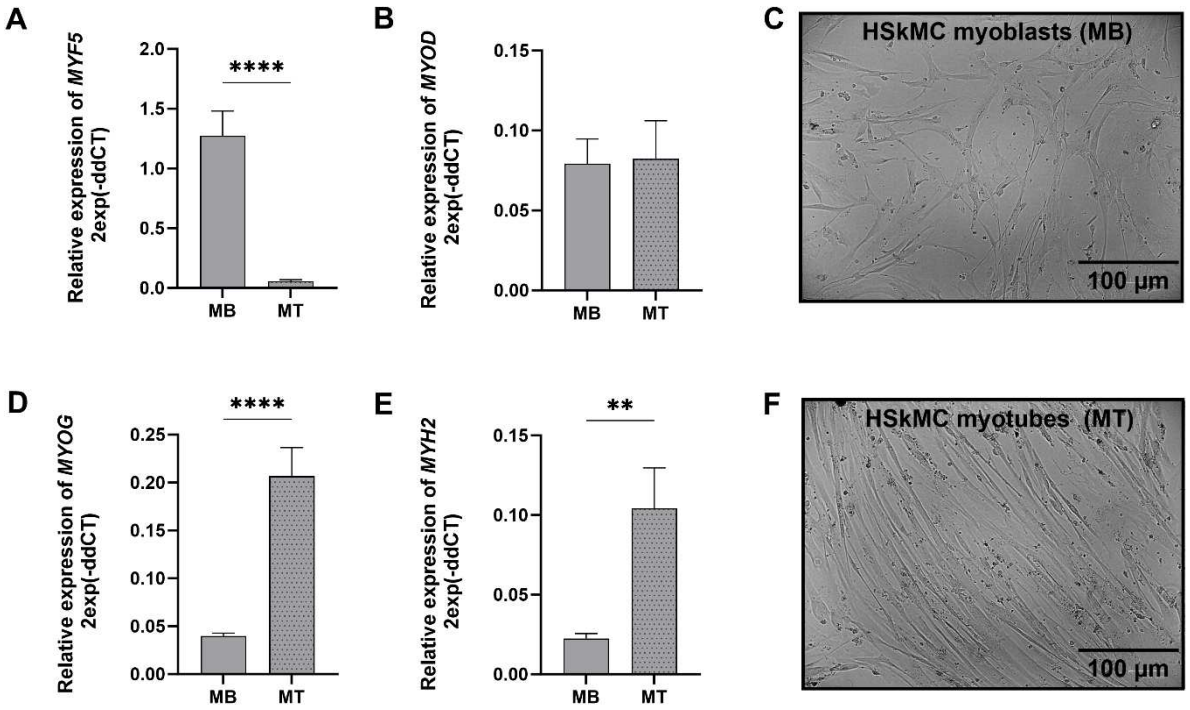

Figure 8: Validation of differentiation of primary HSkMCs using RT-qPCR to measure gene expression profiles of representative genes of various differentiation stages. MB were harvested at day zero of differentiation and MT at day six of differentiation in RLT-lysis buffer for RNA isolation. **(A)** Gene expression profile of *MYF5*. **(B)** Gene expression profile of *MYOD*. **(C)** Bright field microscopy images of MB. **(D)** Gene expression profile of *MYOG*. **(E)** Gene expression profile of *MYH2*. **(F)** Bright field microscopy images of MT. Quantified data was normalized to housekeeping gene *B2M*, data are mean ±SEM from 15 individual experiments (*n=15*) from HSkMCs obtained from five different donors. Data were analyzed by unpaired *t* test (Welch´s correction), **$p < 0.01$, ****$p < 0.0001$. Bright field microscopy images, scale bars = 100 µm. Light grey bars represent MB and grey dotted bars MT. MB: myoblasts; MT: myotubes; HSkMCs: human skeletal muscle cells; MYF5: myogenic factor 5; MYOD: myoblast determination protein 1; MYOG: myogenin; MYH2: myosin heavy chain 2; B2M: β2-Mikroglobulin

3.1.3 EPS-induced phosphorylation of AMPKα-Thr172

The intracellular energy sensor AMPK is activated in response to muscle contraction, therefore immunoblotting of AMPK activity at its main regulatory phosphorylation site (Thr-172) has long been a method to verify exercise-induced signaling (1.4.2, Figure 4). To validate our *in vitro* acute low-frequency EPS protocols, murine and human myotubes were exposed to EPS for six hours (2.2.1.7) and cell lysates were processed for Western blot analysis (2.2.3.1, 2.2.3.2, 2.2.1.3). EPS treatment showed no effect on total AMPKα protein abundance in both murine (Figure 9A) and human (Figure 9C) myotubes. As expected, we observed an increase in EPS-mediated phosphorylation of AMPK-Thr172 in both murine (Figure 9B) and human myotubes, whereas in HSkMCs the effect was statistically significant (Figure 9D).

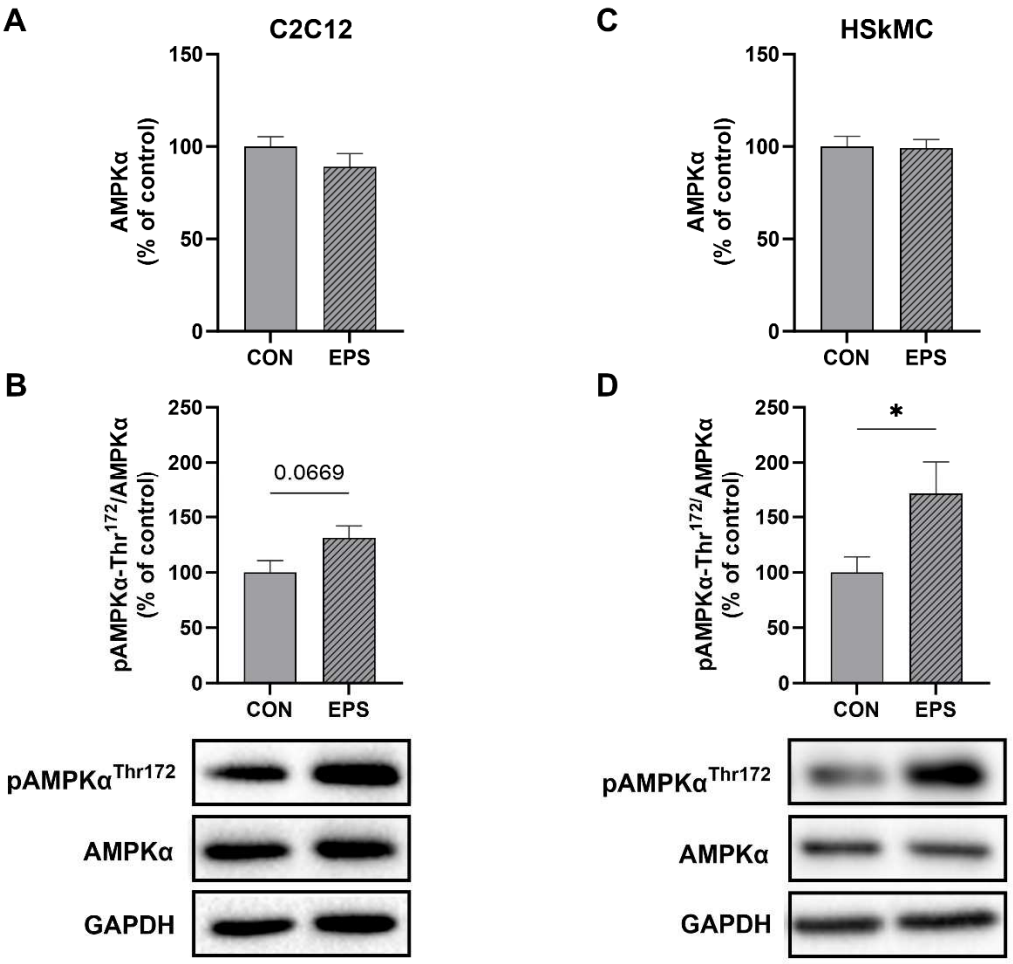

Figure 9: Validation of EPS-induced muscle contraction in murine C2C12 cells and primary HSkMCs. C2C12 cells and HSkMCs were differentiated to multinucleated myotubes until day six of differentiation followed by acute (6h) low-frequency EPS on human (40 V, 1 Hz, 2 ms) and murine (11.5 V, 1 Hz, 2 ms) myotubes, control cells were exposed to electrodes but remained unstimulated. Cell lysates were analyzed for total AMPKα abundance and for changes at AMPKα-Thr172 phosphosite after EPS-induced muscle contraction. **(A)** Protein abundance of total AMPKα in C2C12 cells. **(B)** EPS-induced phosphorylation of AMPKα-Thr172 in C2C12 cells. **(C)** Protein abundance of total AMPKα in HSkMCs. **(D)** EPS-induced phosphorylation of AMPKα-Thr172 in HSkMCs. All graphs shown are mean ±SEM from nine individual experiments (*n=9*) in HSkMCs from three different donors and from six individual experiments (*n=6*) in C2C12 cells. Expression levels were normalized for the protein abundance of GAPDH and unstimulated cells were regarded as control and set at 100%. Data were analyzed by unpaired t test (Welch´s correction), *p < 0.05. Grey bars represent control cells and grey striped bars show EPS-treated cells, for both cell models respectively. CON: control, EPS: electrical pulse stimulation, HSkMCs: human skeletal muscle cells, AMPK: adenosine monophosphate-activated protein kinase, GAPDH: glyceraldehyde-3-phosphate dehydrogenase

3.2 LC-MS/MS analyses of insulin sensitive murine C2C12 cells versus primary HSkMCs following acute low-frequency EPS

Recently, first attempts have been made to investigate the EPS-induced muscle secretome of C2C12 cells and HSkMCs using a non-targeted approach. Murine and human myotubes were exposed to chronic (24h) low-frequency EPS protocols and cell culture supernatants were analyzed by high-resolution MS (70, 192). Little is known about the contraction-induced muscle secretome. To date, there are no comparative studies of the muscle secretomes of C2C12 cells and HSkMCs. Since it is known that different types of exercise affect the myokine

secretion profile differently, the first aim of this thesis was to analyze and compare the contraction-induced muscle secretomes of the two most commonly used skeletal muscle cell culture models, murine C2C12 cells and primary HSkMCs. Therefore, HSMM and C2C12 myoblasts were expanded in cell culture (2.2.1.1, 2.2.1.2, 2.2.1.3) and differentiated to multinucleated myotubes (2.2.1.4). On the sixth day of differentiation, murine and human myotubes were exposed to an acute low-frequency EPS protocol (2.2.1.7), then supernatants (conditioned media: CM) and cell lysates were processed in the bottom-up proteomics workflow (2.2.5, Figure 6) and analyzed by high-resolution MS (2.2.5.2, 2.2.5.5).

3.2.1 Characterization of murine and human muscle secretomes

To categorize the large MS datasets, bioinformatic analyses were performed as described in 2.2.6.1. Computational analysis of the murine C2C12 muscle secretome resulted in the identification of 5,710 potential myokines, of which 2,874 proteins were predicted as secretory myokines. Moreover, 674 proteins (12%) were considered as classically secreted (SP+) proteins, while 1,204 (21%) and another 996 myokines (17%) were recognized as unconventionally secreted proteins (Figure 10A-B). Furthermore, GOCC analysis revealed that most murine secreted proteins were annotated as “plasma membrane proteins”, “vesicles” and “mitochondrial proteins” (Figure 10C).

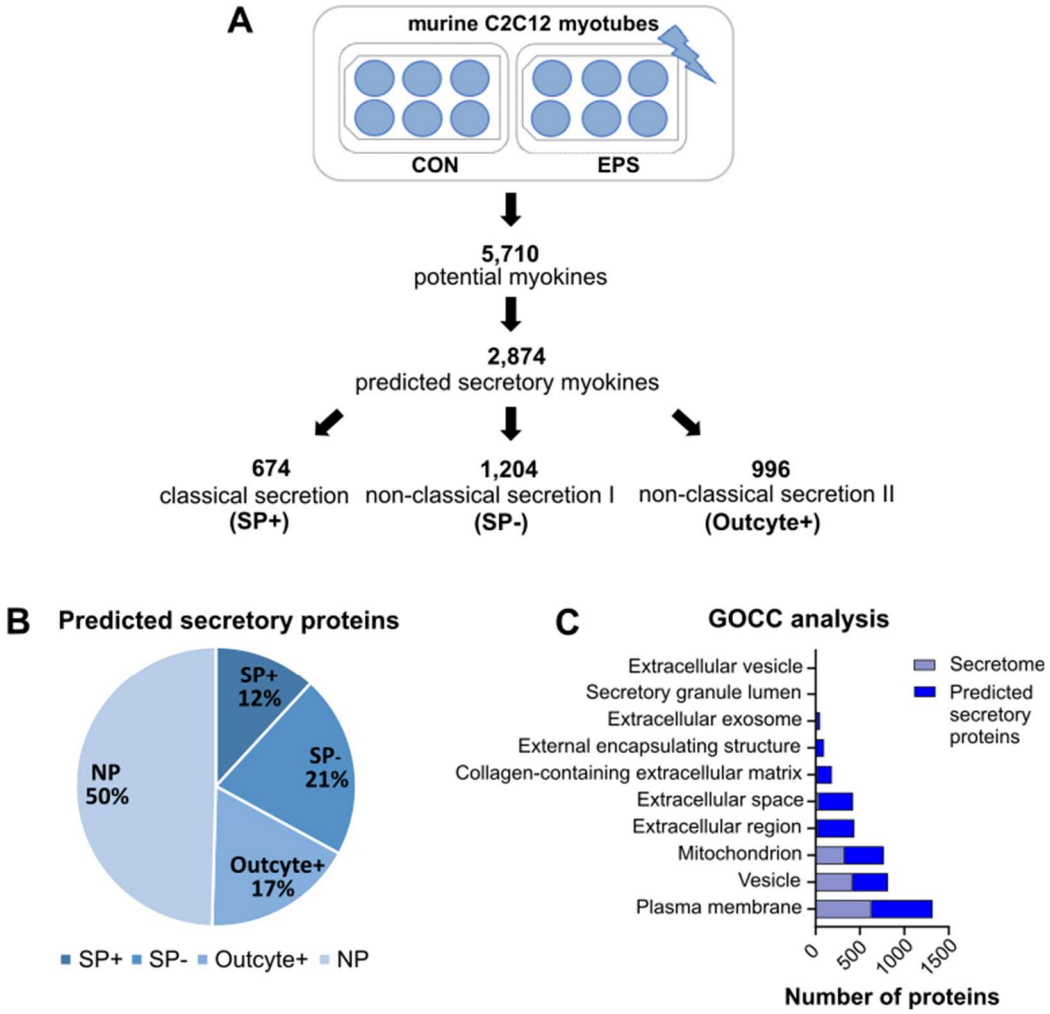

Figure 10: Bioinformatic prediction analysis of murine C2C12 muscle secretome after acute low-frequency EPS. Proteome DiscovererTM (PD) software 3.0 was used for proteomics analyses. **(A)** Bioinformatic prediction analysis using SignalP 6.0, SecretomeP 2.0 and Outcyte 1.0. **(B)** Percentage of "predicted secretory myokines". **(C)** GOCC analysis of the entire muscle secretome and the subgroup "predicted secretory myokines". Samples from C2C12 cells (*n=3*) are demonstrated in blue. CON: control, EPS: electrical pulse stimulation, GOCC: gene ontology cellular component, NP: non-predicted, SP+: signal peptide positive, SP-: signal peptide negative

Furthermore, MS-based secretome analysis identified 3,285 potential myokines in the CM of HSkMCs, of which 2,105 proteins were predicted to be secretory myokines. Moreover, 779 proteins (24%) were considered as classically secreted (SP+) proteins, while 650 (20%) and another 676 myokines (20%) were recognized as unconventionally secreted proteins (Figure 11A-B). According to GOCC analysis most proteins were assigned to the GO terms "extracellular exosome", "plasma membrane" as well as "extracellular space" and "region" (Figure 11C).

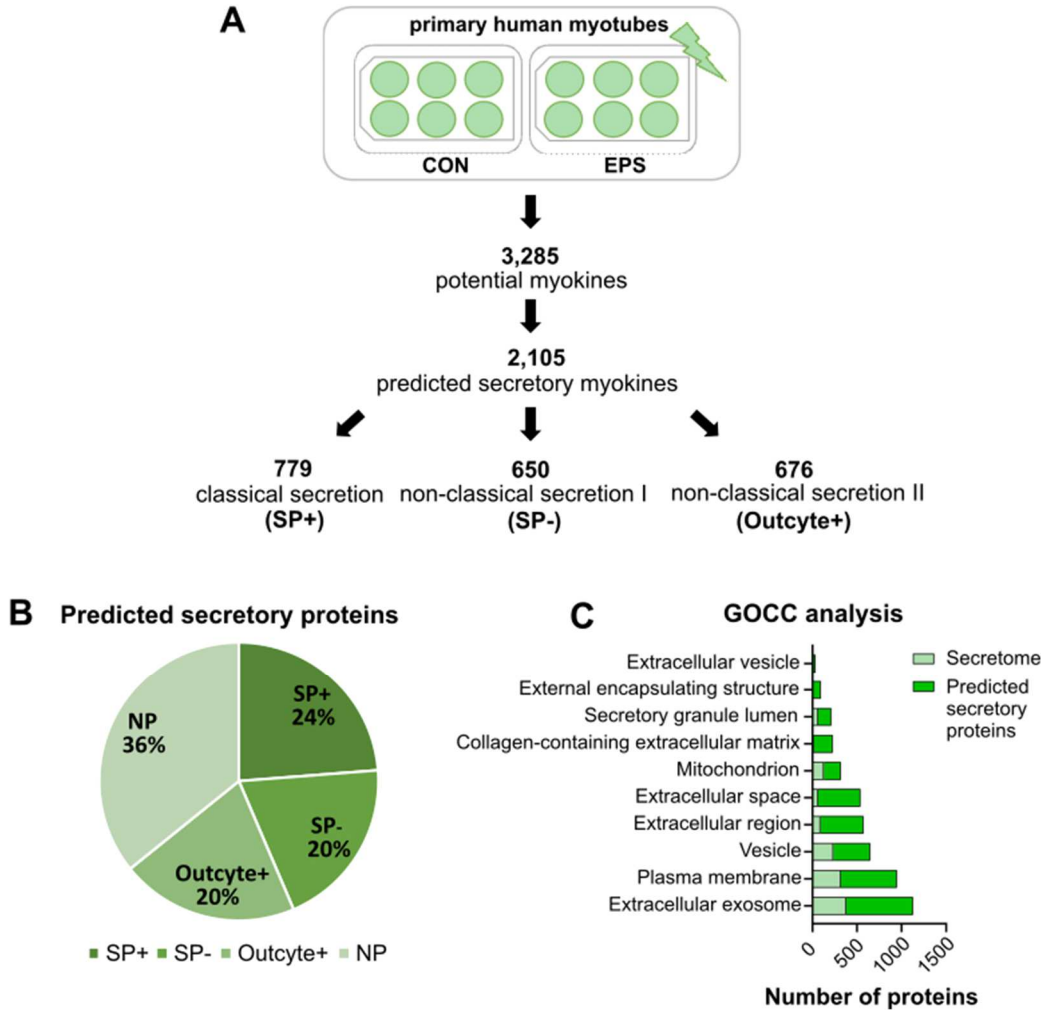

Figure 11: Bioinformatic prediction analysis of primary HSkMCs secretome after acute low-frequency EPS. Proteome DiscovererTM (PD) software 3.0 was used for proteomics analyses. **(A)** Bioinformatic prediction analysis using SignalP 6.0, SecretomeP 2.0 and Outcyte 1.0. **(B)** Percentage of "predicted secretory myokines". **(C)** GOCC analysis of the entire muscle secretome and the subgroup "predicted secretory myokines". Samples from HSkMCs from three donors (*n=3*) are displayed in green. CON: control, EPS: electrical pulse stimulation, GOCC: gene ontology cellular component, NP: non-predicted, SP+: signal peptide positive, SP-: signal peptide negative

3.2.2 Comparative analyses of muscle secretomes and proteomes

To assess the similarities and differences between murine C2C12 cells and primary HSkMCs, we directly compared the proteomes and secretomes of both cell models. MS data were analyzed as described in 2.2.6.1. The interspecies comparative analysis of muscle secretomes revealed an overlap of 2,556 proteins that were present in the CM of both C2C12 cells and HSkMCs, while a greater number of proteins were secreted from C2C12 myotubes (5,571) than from human myotubes (3,213) (Figure 12A). Comparison of the proteomes revealed an overlap of 4,929 proteins, indicating that the C2C12 and human proteomes have a similar distribution of proteins (Figure 12B).

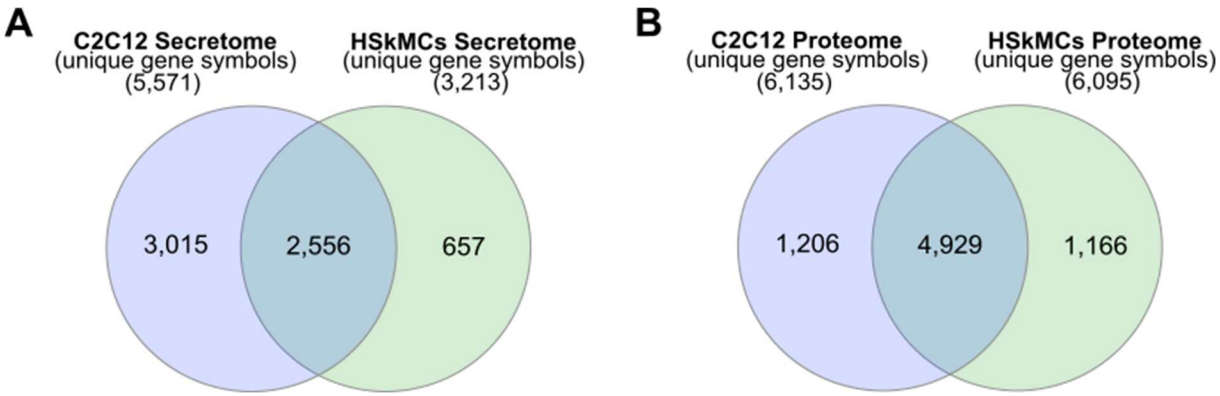

Figure 12: Venn diagram analyses showing interspecies comparison of muscle secretomes and cellular proteomes. (A) Comparison of murine and human secretomes based on their gene symbols. **(B)** Comparison of murine and human proteomes based on their gene symbols. Data from C2C12 cells (*n=3*) are shown in blue and from HSkMCs from three different donors (*n=3*) in green.

Next, a comparison of the secretome and proteome data within the same species was performed as described in 2.2.6.1. Comparative analysis of the muscle secretome (5,710 proteins) and proteome (6,215 proteins) of C2C12 myotubes resulted in an overlap of 4,718 proteins, showing that 83% of all secreted proteins were also detected in the cellular proteome (Figure 13A). Also, a large number of proteins (1,714) previously categorized as “predicted secretory myokines” (a subset of the secretome) overlapped with the C2C12 proteome (Figure 13A). Similar results were observed for the HSkMCs. The secretome and the proteome of human myotubes show an overlap of 2,702 proteins, which corresponds to 82 % of all secreted proteins that were also detected in the cellular proteome (Figure 13B). The “predicted secretory myokines” of the human muscle secretome overlapped with the human proteome with 2,260 proteins (Figure 13B). To gain insight into the protein distribution within versatile GO terms for intracellular and extracellular components, a GOCC analysis was performed for both cell models. Interestingly, proteins annotated for intracellular GO terms such as “nucleus, cytosol and cytoskeleton” were nearly identical in murine secretome and proteome (Figure 13C), while the number of proteins for these GO terms in the humane secretome was remarkably lower in comparison to the human proteome (Figure 13D). The number of proteins annotated as GO “extracellular matrix” and “non-structural extracellular” proteins were comparable in the secretome and proteome dataset of both C2C12 cells and HSkMCs (Figure 13C-D).

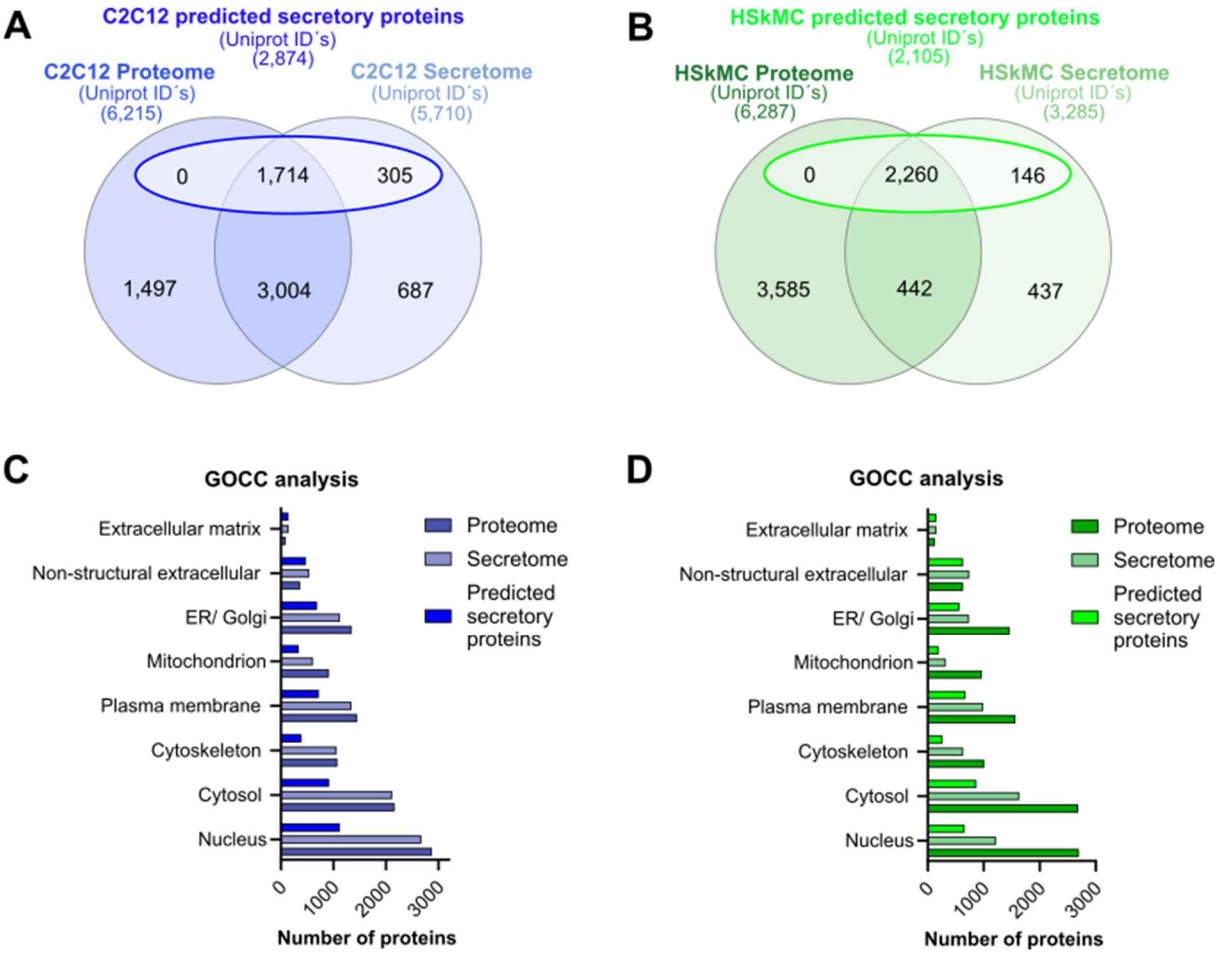

Figure 13: Secretome and proteome analysis of C2C12 cells and HSkMCs. Proteome DiscovererTM software 3.0 was used for proteomics analyses. Alignment of proteome data with either total secretome or a subgroup of secretome data ("predicted secretory myokines") from C2C12 cells **(A)** or HSkMCs **(B).** GOCC analyses of C2C12 **(C)** and HSkMCs **(D)** proteome, secretome and "predicted secretory proteins" data was conducted. Venn analyses were performed based on UniprotKB IDs for *Mus musculus* and *Homo sapiens*. Data shown in blue represent C2C12 cells (*n=3*) while data displayed in green represent HSkMCs from three subjects (*n=3*). HSkMCs: human skeletal muscle cells, GOCC: gene ontology cellular component, ER: endoplasmic reticulum

To determine the abundance distribution of the proteins detected in the secretome and proteome and whether the same proteins are similarly distributed in C2C12 cells and HSkMCs, the top 100 candidates were ranked according to their peptide spectrum match (PSM). It was observed that 52% of the top 100 abundant proteins were present in both murine secretome and proteome (Figure 14A). Similarly, the human secretome and proteome shared 47% of the top 100 proteins (Figure 14B).

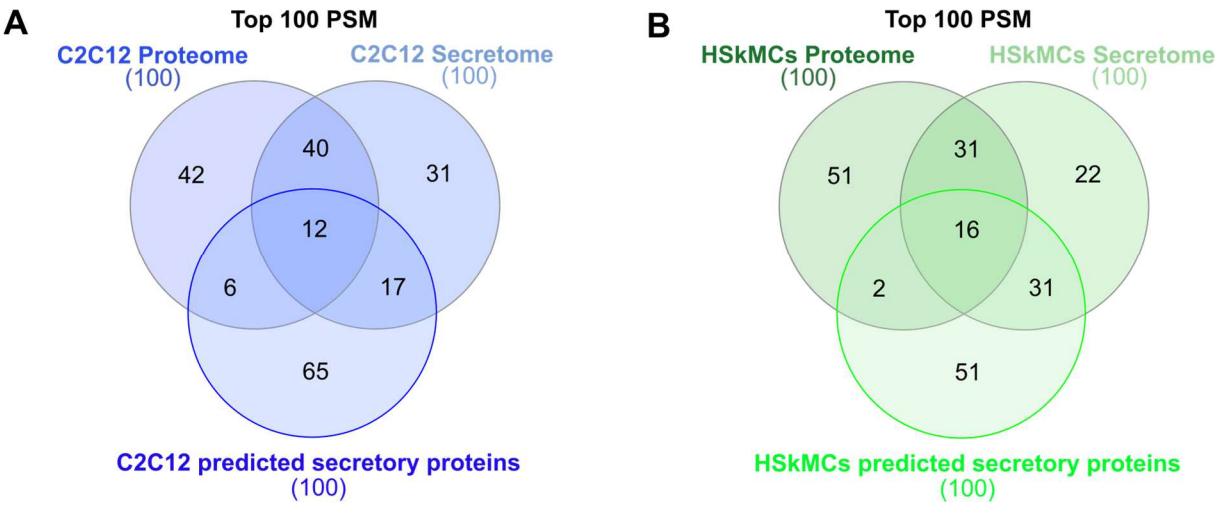

Figure 14: The top 100 most abundant proteins from proteome and secretome data, ranked by their PSM (A) Overlap of the top 100 proteins in the proteome and secretome as well as for the "predicted secretory proteins" of C2C12 cells. **(B)** Overlap of the top 100 proteins in the proteome and secretome as well as for the "predicted secretory proteins" of HSkMCs. Venn analyses were performed based on UniprotKB accession number for *Mus musculus* and *Homo sapiens*. Data displayed in blue represent C2C12 cells (*n=3*) while green data represents HSkMCs from three donors (*n=3*). HSkMCs: human skeletal muscle cells, PSM: peptide spectrum match

3.2.3 Comparison of murine and human secretome data with the literature

To put the MS data of this study in context with the results of previous MS-based secretome studies of C2C12 cells and HSkMCs, a comparison with the literature was performed (2.2.6.1, 2.2.6.2). The comparative analysis revealed that 1,440 myokines identified in the CM of C2C12 myotubes in this study have not yet been described in the literature. Furthermore, additional 20 proteins were identified in the secretome of C2C12 cells that were previously only mentioned in human MS-secretome studies, while a further 186 proteins were found exclusively in the CM of C2C12 cells and HSkMCs in this study. Comparison with the literature on human cells resulted in the identification of 385 novel myokines in the CM of human myotubes that were unique to this study and had not been described in other MS-based studies. Moreover, 1,393 common proteins were found in the human and murine secretome of this study as well as in previously characterized murine secretome data from the literature. Additionally, 111 myokines were discovered in the human secretome in this study that were previously only described in the literature for C2C12 cells (Figure 15A). In this study, we confirmed the presence of known secreted myokines such as IL-6, decorin, desmin, SPARC and VEGFA in both murine and human muscle secretomes. Interestingly, other known myokines such as follistatin (FST), meteorin (METRN), sestrin-1 (SESN1) and insulin-like growth factor I (IGF-1) were only detected in the CM of C2C12 cells, whereas others such as LIF were exclusively identified in the CM of HSkMCs. All MS-based secretome studies that were considered for literature comparison are shown in Figure 15B. The comparison of MS data from this study with literature data from C2C12 cells revealed an overlap of 3,906

myokines, while the comparison of data from HSkMCs revealed an overlap of 1,163 proteins (Figure 15B).

A

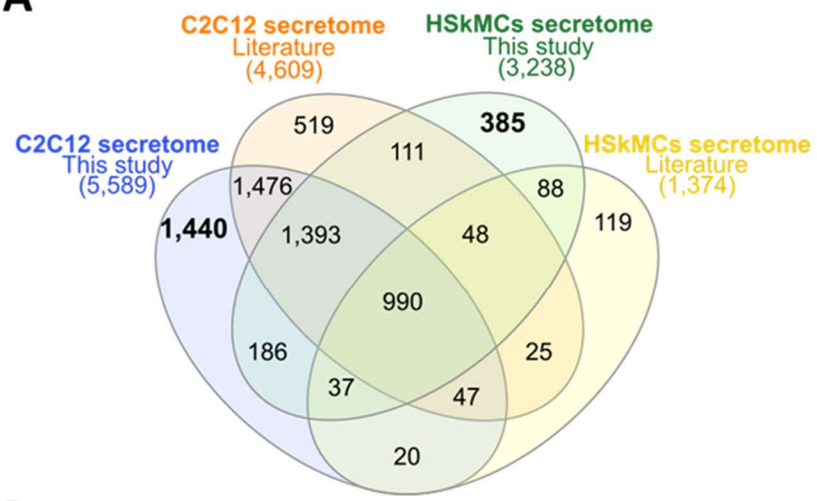

B

Literature	Source	Identified unique gene symbols	
Chan et al. 2007	C2C12	65	Overlap 3,906 proteins
Henningsen et al. 2010		599	
Chan et al. 2011		191	
Deshmukh et al. 2015		4,335	
Grube et al. 2018		666	
Gonzalez-Franquesa et al. 2021		1,739	
This study	**C2C12**	**5,589**	
Hittel et al. 2009	HSkMCs	44	Overlap 1,163 proteins
Norheim et al. 2011		232	
Le Bihan et al. 2012		952	
Hartwig et al. 2013		530	
Whitham et al. 2018		306	
Mengeste et al. 2022		151	
This study	**HSkMCs**	**3,238**	

Figure 15: Comparison of MS data from this study with the literature. A) MS data of C2C12 cells and HSkMCs from this study compared to MS-data from the literature **(B)** Overview of the MS studies used for the comparative analysis. The data from this study are shown in blue for C2C12 cells (*n=3*) and in green for HSkMCs from three donors (*n=3*). Data from the literature on C2C12 cells are represented in orange and on HSkMCs in yellow. GOCC: gene ontology cellular component, NP: non-predicted, SP+: signal peptide positive, SP-: signal peptide negative

Bioinformatic prediction analyses were then performed (2.2.6.1) to obtain information on the newly identified myokines identified for the first time in the CM of C2C12 and human myotubes in this study. Of the newly identified myokines in the murine muscle secretome, 51% were identified as “predicted secretory myokines”, of which a minority (5%) were secreted via the classical secretion pathway (SP+), while the majority (46%) were secreted via UPS pathways (SP- and Outcyte+) (Figure 16A). In contrast, 42% of the newly identified myokines of the human secretome were predicted to be “classically secreted proteins” (SP+), while 34% were secreted via UPS pathways (SP-, Outcyte) (Figure 16B). GOCC analysis of novel myokines revealed that the majority of proteins in both cell models were annotated with the GO term

"plasma membrane". In the murine secretome, most proteins were annotated as "mitochondrion" and "vesicle", while in the human secretome most common GO terms were "extracellular space", "extracellular exosome" and "extracellular region" (Figure 16C-D).

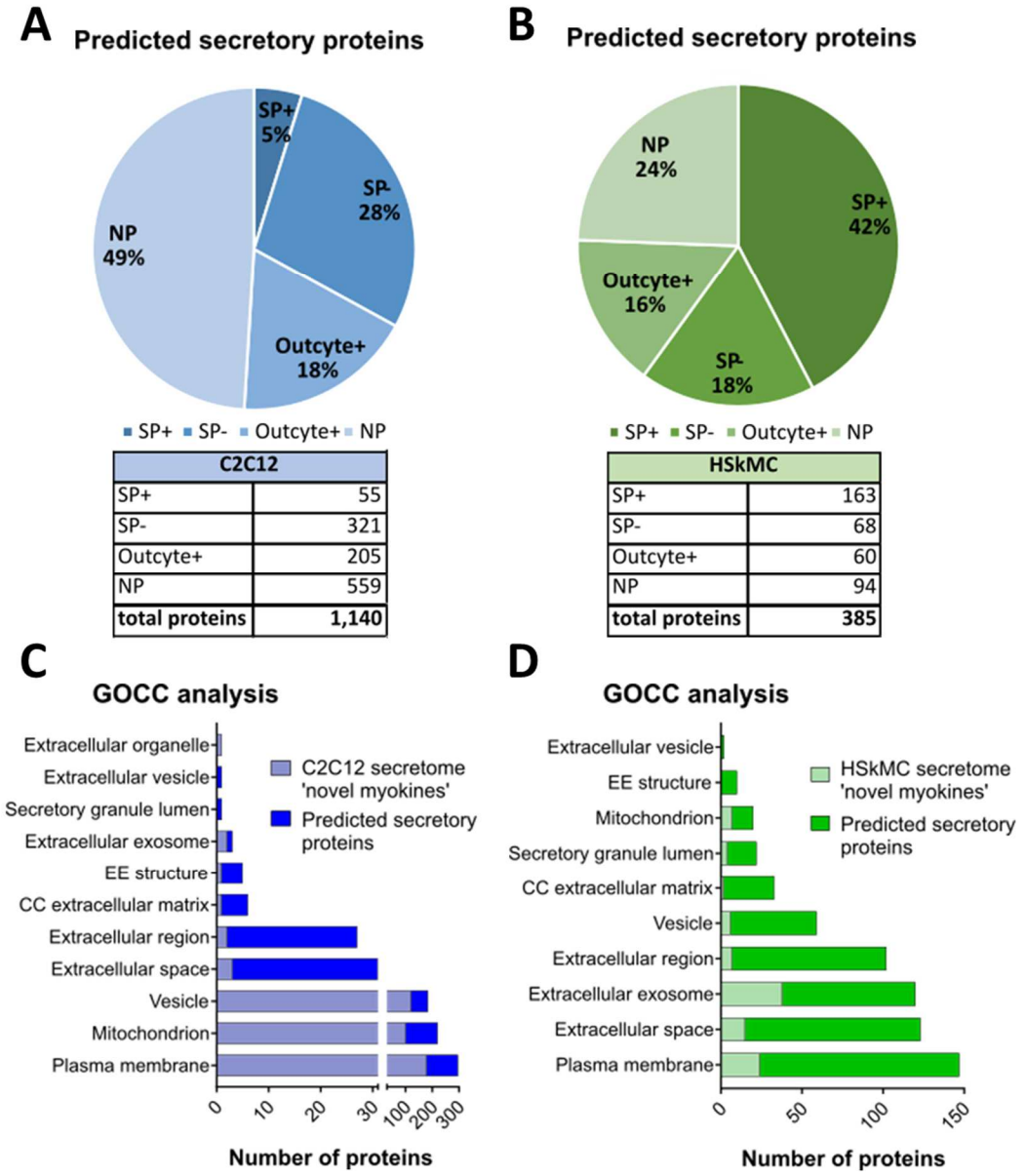

C2C12	
SP+	55
SP-	321
Outcyte+	205
NP	559
total proteins	**1,140**

HSkMC	
SP+	163
SP-	68
Outcyte+	60
NP	94
total proteins	**385**

Figure 16: Bioinformatic analyses of novel identified myokines. (A) Bioinformatic prediction analysis for the newly described myokines in the CM of C2C12 cells. **(B)** Bioinformatic prediction analysis for the newly described myokines in the CM of HSkMCs. **(C)** GOCC analysis of the newly described proteins in the CM of C2C12 cells. **(D)** GOCC analysis of the newly described proteins in the CM of HSkMCs. HSkMCs: human skeletal muscle cells, NP: non-predicted, SP+: signal peptide positive, SP-: signal peptide negative; GOCC: gene ontology cellular component, EE structure: external encapsulating structure, CC extracellular matrix: collagen-containing CC extracellular matrix

3.2.4 EPS-induced myokines in the murine and human muscle secretome

MS datasets were analyzed as described in 2.2.6.1 and filtered for significantly regulated proteins (p-value<0.05). Acute low-frequency EPS induced differential changes in 518 myokines quantified in the CM of C2C12 myotubes, of which 172 proteins were significantly downregulated while 346 proteins were significantly upregulated (Figure 17A). In comparison,

336 myokines were differentially regulated by acute low-frequency EPS in the CM of primary human myotubes, of which 199 proteins were significantly downregulated and 137 proteins were significantly upregulated (Figure 17B). Interestingly, comparative analysis of both muscle secretomes revealed that EPS induced different myokine secretion profiles in both cell models, as indicated by a relatively low overlap of myokines in both secretomes (Supplemental Figure 2). Bioinformatic prediction analysis revealed that 56% were considered as “predicted secretory myokines” in the CM of C2C12 cells, of which 11% were categorized as classically secreted proteins (SP+), while 45% were secreted through UPS pathways (SP-, 29%; Outcyte+, 16%) (Figure 17C). Similar results were obtained for HSkMCs-derived secreted proteins, as bioinformatic tools predicted 58% as secreted proteins, of which 16% were considered as classically secreted proteins (SP+) and 42 % (SP-, 26%; Outcyte+, 16%) as non-classically secreted proteins (Figure 17D). All classically secreted proteins (SP+) derived from C2C12 or human myotubes are listed in Table 20 and Table 21, respectively. All unconventionally secreted myokines from C2C12 and human myotubes are listed in Supplemental Table 2 and Supplemental Table 3, respectively. GOCC analysis of contraction-induced myokines in the CM of C2C12 myotubes proposed enrichment of proteins annotated as “plasma membrane”, “mitochondrion”, “vesicle”, “extracellular space” and “region” (Figure 17E). In contrast, contraction-induced myokines in the CM of HSkMCs were enriched in the following GO terms: “extracellular exosomes”, “plasma membrane”, “vesicle”, “extracellular region” and “extracellular space” (Figure 17F).

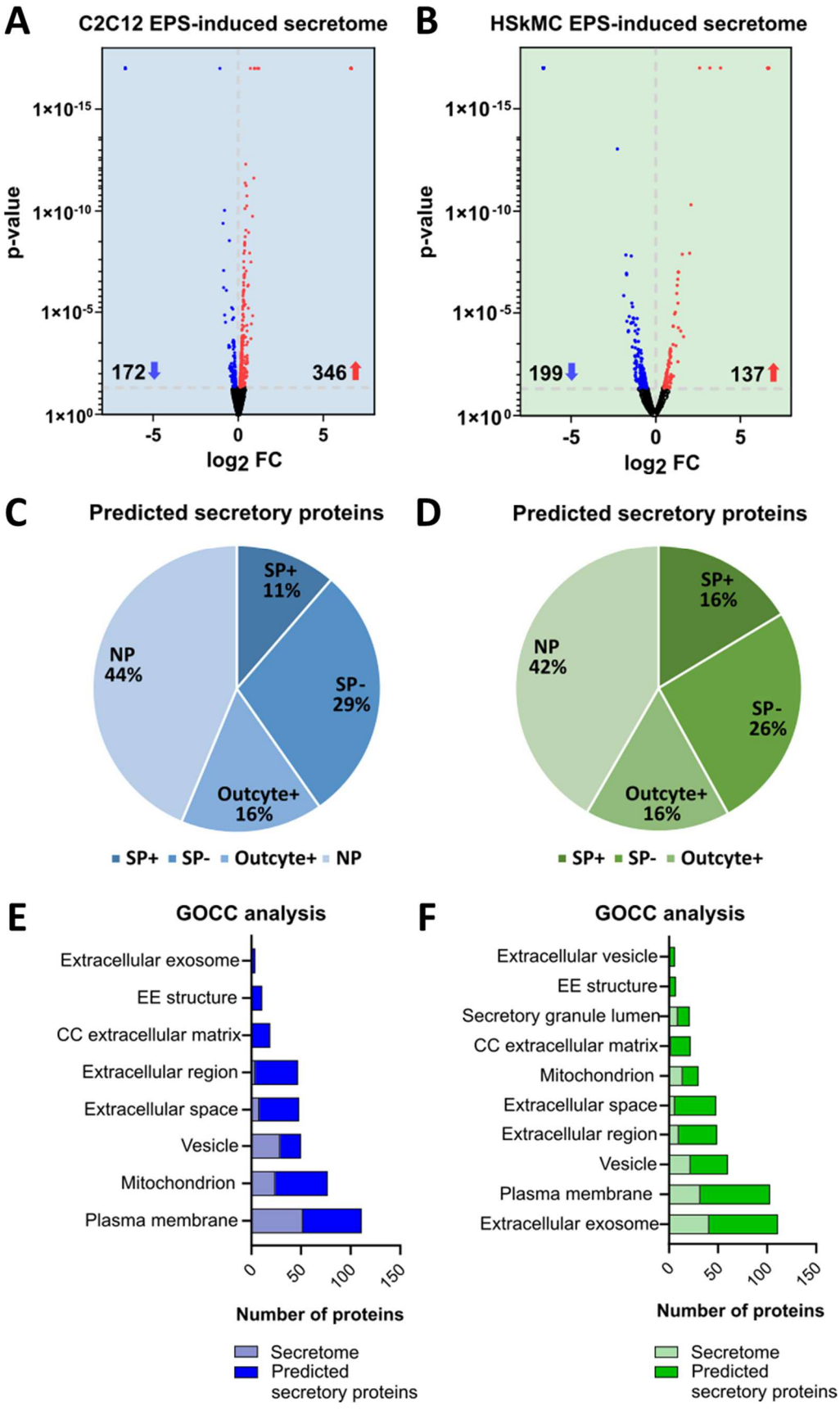

Figure 17: Contraction-induced myokines in the murine und human muscle secretome following acute low-frequency EPS. Volcano plot analysis of murine C2C12 secretome **(A)** or human secretome **(B)** displaying the differentially regulated proteins. Bioinformatic prediction analysis of contraction-induced myokines from C2C12 **(C)** or human muscle secretome **(D).** GOCC analysis of contraction-induced myokines in the CM of C2C12 **(E)** and

HSkMCs **(F).** Data from C2C12 cells (*n=3*) are shown in blue and data of HSkMCs from three donors (*n=3*) are presented in green. EPS: electrical pulse stimulation, GOCC: gene ontology cellular component, NP: non-predicted, SP+: signal peptide positive, SP-: signal peptide negative, CM: conditioned media, EE structure: external encapsulating structure, CC extracellular matrix: collagen-containing CC extracellular matrix

Table 20 below lists all predicted classically secreted myokines (SP+) quantified in the CM of C2C12 cells and induced by acute low-frequency EPS.

Table 20: EPS-regulated classically secreted proteins in the muscle secretome of C2C12 cells (EPS/CON).

UniProtKB	Gene symbol	Protein description	*p*-value	Log_2FC	Secretion type
P58022	Loxl2	Lysyl oxidase homolog 2	1.00E-17	6.64	SP+
Q91WU0	Ces1f	Carboxylesterase 1F	1.00E-17	6.64	SP+
P10923	Spp1	Osteopontin	1.00E-17	1.21	SP+
Q9Z0M6	Adgre5	Adhesion G protein-coupled receptor E5	1.00E-17	1.13	SP+
O09161	Casq2	Calsequestrin-2	1.00E-17	0.96	SP+
P70158	Smpdl3a	Acid sphingomyelinase-like phosphodiesterase 3a	3.16E-08	0.75	SP+
Q8CA71	Shisa4	Protein shisa-4	1.15E-08	0.67	SP+
A6X935	Itih4	Inter alpha-trypsin inhibitor, heavy chain 4	1.68E-03	0.56	SP+
Q00560	Il6st	Interleukin-6 receptor subunit beta	8.98E-03	0.52	SP+
O09165	Casq1	Calsequestrin-1	1.82E-11	0.51	SP+
O35143	Atp5if1	ATPase inhibitor, mitochondrial	5.66E-12	0.47	SP-
P19788	Mgp	Matrix Gla protein	7.62E-11	0.40	SP+
P15208	Insr	Insulin receptor	2.90E-02	0.39	SP+
Q9Z1W4	Gdf11	Growth/differentiation factor 11	3.58E-02	0.38	SP+
P47931	Fst	Follistatin	9.65E-07	0.30	SP+
Q501P1	Fbln7	Fibulin-7	3.52E-02	0.28	SP+
Q8BNJ2	Adamts4	A disintegrin and metalloproteinase with thrombospondin motifs 4	6.65E-04	0.26	SP+
Q06335	Aplp2	Amyloid beta precursor like protein 2	3.28E-04	0.25	SP+
Q9JM99	Prg4	Proteoglycan 4	3.24E-02	0.25	SP+
O54819	Tfpi	Tissue factor pathway inhibitor	9.56E-04	0.22	SP+
P29788	Vtn	Vitronectin	1.91E-03	0.22	SP+
P47880	Igfbp6	Insulin-like growth factor-binding protein 6	6.11E-04	0.21	SP+
Q61982	Notch3	Neurogenic locus notch homolog protein 3	2.80E-03	0.20	SP+
O70326	Grem1	Gremlin-1	1.93E-03	0.19	SP+
Q9QZJ6	Mfap5	Microfibrillar-associated protein 5	3.47E-03	0.19	SP+
P12850	Cxcl1	Growth-regulated alpha protein	1.08E-02	0.19	SP+
Q9CYK2	Qpct	Glutaminyl-peptide cyclotransferase	1.16E-02	0.19	SP+
P16882-2	Ghr	Isoform 2 of Growth hormone receptor	3.77E-02	0.19	SP+
Q80TS3	Adgrl3	Adhesion G protein-coupled receptor L3	1.10E-02	0.17	SP+

O35664-3	Ifnar2	Isoform 3 of Interferon alpha/beta receptor 2	1.57E-02	0.17	SP+
P01887	B2m	Beta-2-microglobulin	6.77E-03	0.15	SP+
Q9Z121	Ccl8	C-C motif chemokine 8	4.16E-02	0.15	SP+
Q61810	Ltbp3	Latent-transforming growth factor beta-binding protein 3	2.57E-02	0.14	SP+
P04925	Prnp	Major prion protein	3.54E-02	0.13	SP+
Q8CG19	Ltbp1	Latent-transforming growth factor beta-binding protein 1	4.19E-02	0.13	SP+
Q60994	Adipoq	Adiponectin	2.68E-02	0.12	SP+
P21460	Cst3	Cystatin-C	2.85E-02	0.12	SP+
P47879	Igfbp4	Insulin-like growth factor-binding protein 4	4.02E-02	0.12	SP+
P28798	Grn	Progranulin	4.27E-02	0.11	SP+
Q9Z0J0	Npc2	NPC intracellular cholesterol transporter 2	4.41E-02	0.11	SP+
P19324	Serpinh1	Serpin H1	4.10E-02	-0.14	SP+
P11087	Col1a1	Collagen alpha-1(I) chain	2.34E-02	-0.15	SP+
Q05186	Rcn1	Reticulocalbin-1	2.45E-02	-0.15	SP+
O08746	Matn2	Matrilin-2	1.22E-02	-0.16	SP+
O35887	Calu	Calumenin	2.01E-02	-0.16	SP+
Q8VHI3	Pofut2	GDP-fucose protein O-fucosyltransferase 2	3.95E-02	-0.16	SP+
P15379	Cd44	CD44 antigen	1.03E-02	-0.17	SP+
Q62059-2	Vcan	Isoform V1 of Versican core protein	2.94E-02	-0.17	SP+
Q9ER41	Tor1b	Torsin-1B	2.65E-02	-0.18	SP+
A2AVA0	Svep1	Sushi, von Willebrand factor type A, EGF and pentraxin domain-containing protein 1	3.51E-02	-0.18	SP+
P11688	Itga5	Integrin alpha-5	1.60E-03	-0.19	SP+
O08807	Prdx4	Peroxiredoxin-4	1.28E-02	-0.24	SP+
Q8K007	Sulf1	Extracellular sulfatase Sulf-1	1.38E-03	-0.28	SP+
P21237	Bdnf	Brain-derived neurotrophic factor	6.40E-03	-0.32	SP+
P04756	Chrna1	Acetylcholine receptor subunit alpha	4.09E-02	-0.32	SP+
Q8K297	Colgalt1	Procollagen galactosyltransferase 1	4.98E-03	-0.35	SP+
P50608	Fmod	Fibromodulin	3.13E-05	-0.75	SP+
Q8R180	Ero1a	ERO1-like protein alpha	1.00E-17	-6.64	SP+
Q9CQU0	Txndc12	Thioredoxin domain-containing protein 12	1.00E-17	-6.64	SP+
Q61475	Cd55	Complement decay-accelerating factor, GPI-anchored	1.00E-17	-6.64	SP+

Table 21 below lists all predicted classically secreted myokines (SP+) quantified in the CM of primary HSkMCs and induced by acute low-frequency EPS.

Table 21: EPS-regulated classically secreted proteins in the muscle secretome of HSkMCs obtained from three donors (EPS/CON).

UniProtKB	Gene symbol	Protein description	*p*-value	Log_2FC	Secretion type
P15309	ACP3	Prostatic acid phosphatase	1.00E-17	6.64	SP+
Q02487-2	DSC2	Isoform 2B of Desmocollin-2	1.00E-17	6.64	SP+
Q16610-2	ECM1	Isoform 2 of Extracellular matrix protein 1	1.00E-17	6.64	SP+
A8MVW0	FAM171A2	Protein FAM171A2	1.00E-17	6.64	SP+
O95867	LY6G6C	Lymphocyte antigen 6 complex locus protein G6c	1.00E-17	6.64	SP+
Q9HB40	SCPEP1	Retinoid-inducible serine carboxypeptidase	1.00E-17	6.64	SP+
P49908	SELENOP	Selenoprotein P	1.00E-17	6.64	SP+
P24821-4	TNC	Isoform 4 of Tenascin	1.00E-17	6.64	SP+
P23280	CA6	Carbonic anhydrase 6	1.00E-17	3.83	SP+
P13500	CCL2	C-C motif chemokine 2	1.25E-08	1.57	SP+
O75339	CILP	Cartilage intermediate layer protein 1	1.18E-02	1.05	SP+
O95969	SCGB1D2	Secretoglobin family 1D member 2	3.43E-04	1.02	SP+
Q6E0U4	DMKN	Dermokine	1.25E-02	0.96	SP+
Q9Y2I2	NTNG1	Netrin-G1	2.60E-02	0.88	SP+
P43307	SSR1	Translocon-associated protein subunit alpha	2.28E-02	0.85	SP+
Q86WD7	SERPINA9	Serpin A9	1.09E-03	0.83	SP+
Q03405	PLAUR	Urokinase plasminogen activator surface receptor	1.29E-02	0.83	SP+
Q6Y288	B3GLCT	Beta-1,3-glucosyltransferase	3.82E-02	0.83	SP+
P08138	NGFR	Tumor necrosis factor receptor superfamily member 16	7.48E-03	0.67	SP+
Q9UMX5	NENF	Neudesin	3.56E-02	0.67	SP+
P0DUB6	AMY1A	Alpha-amylase 1A	1.25E-02	0.66	SP+
Q14703	MBTPS1	Membrane-bound transcription factor site-1 protease	1.41E-02	0.66	SP+
Q96S86	HAPLN3	Hyaluronan and proteoglycan link protein 3	2.21E-02	0.65	SP+
P08246	ELANE	Neutrophil elastase	1.03E-02	0.64	SP+
Q15517	CDSN	Corneodesmosin	9.32E-03	0.63	SP+
Q8TCT8	SPPL2A	Signal peptide peptidase-like 2A	1.26E-02	0.63	SP+
O43240	KLK10	Kallikrein-10	3.99E-02	0.63	SP+
P49862	KLK7	Kallikrein-7	1.54E-02	0.62	SP+
Q9H4F8	SMOC1	SPARC-related modular calcium-binding protein 1	9.59E-03	0.61	SP+
O60911	CTSV	Cathepsin L2	1.57E-02	0.61	SP+
Q08554-2	DSC1	Isoform 1B of Desmocollin-1	2.07E-02	0.58	SP+
Q9H1E1	RNASE7	Ribonuclease 7	2.11E-02	0.57	SP+
Q9P121-4	NTM	Isoform 4 of Neurotrimin	2.66E-02	0.55	SP+
P25311	AZGP1	Zinc-alpha-2-glycoprotein	2.71E-02	0.55	SP+
Q8WWX9	SELENOM	Selenoprotein M	3.81E-02	0.52	SP+
Q07507	DPT	Dermatopontin	4.45E-02	0.51	SP+
P12273	PIP	Prolactin-inducible protein	4.40E-02	0.50	SP+

P05067	APP	Amyloid-beta precursor protein	2.26E-02	-0.59	SP+
P18065	IGFBP2	Insulin-like growth factor-binding protein 2	1.38E-02	-0.64	SP+
P12111	COL6A3	Collagen alpha-3(VI) chain	1.04E-02	-0.67	SP+
P14625	HSP90B1	Endoplasmin	8.58E-03	-0.68	SP+
O43854	EDIL3	EGF-like repeat and discoidin I-like domain-containing protein 3	1.51E-02	-0.76	SP+
P08648	ITGA5	Integrin alpha-5	1.02E-02	-0.87	SP+
Q4V9L6	TMEM119	Transmembrane protein 119	1.77E-02	-0.89	SP+
P13667	PDIA4	Protein disulfide-isomerase A4	1.86E-05	-1.10	SP+
Q9BXX0	EMILIN2	EMILIN-2	2.31E-03	-1.15	SP+
P07093	SERPINE2	Glia-derived nexin	2.15E-04	-1.23	SP+
Q13361	MFAP5	Microfibrillar-associated protein 5	1.48E-05	-1.57	SP+
P55854	SUMO3	Small ubiquitin-related modifier 3	1.37E-07	-1.72	SP-
Q8TAV4	STOML3	Stomatin-like protein 3	1.16E-07	-1.73	SP-
P02458	COL2A1	Collagen alpha-1(II) chain	1.00E-17	-6.64	SP+
P25445	FAS	Tumor necrosis factor receptor superfamily member 6	1.00E-17	-6.64	SP+
Q9Y639	NPTN	Neuroplastin	1.00E-17	-6.64	SP+
Q15063-7	POSTN	Isoform 7 of Periostin	1.00E-17	-6.64	SP+
P07602-3	PSAP	Isoform Sap-mu-9 of Prosaposin	1.00E-17	-6.64	SP+
P20062	TCN2	Transcobalamin-2	1.00E-17	-6.64	SP+
P02766	TTR	Transthyretin	1.00E-17	-6.64	SP+

3.2.5 Acute vs chronic low-frequency EPS-induced muscle secretomes

MS datasets from this study and the literature were analyzed as described in 2.2.6.1 and 2.2.6.2. To date, two MS-based secretome studies that have investigated the effects of EPS on the muscle secretome, both using chronic low-frequency EPS protocols (70, 192). To explore whether the type of exercise (acute vs chronic) has an effect on the contraction-induced muscle secretome, our acute (6h) low-frequency EPS protocols were compared with chronic (24h) low-frequency EPS protocols from the literature. We observed that indeed different myokines were regulated by low-frequency EPS after acute (6h) versus chronic (24h) stimulation of C2C12 myotubes (Figure 18A). Comparison of the MS data of this study with those of Gonzalez-Franquesa et al., who used the same EPS parameters (11.5 V, 2 ms, 1 Hz) but stimulated for a total of 24 hours, showed an overlap of nine proteins (Figure 18A) (192). Similar results were obtained when comparing MS data from HSkMCs. Mengeste et al. also used a low-frequency EPS protocol, but with different parameters compared to those used in this study (24h, 10 V, 0.1 Hz, single, 2 ms) (70). MS data alignment resulted in an overlap of ten proteins that were found in the CM of acutely and chronically stimulated human myotubes (Figure 18B).

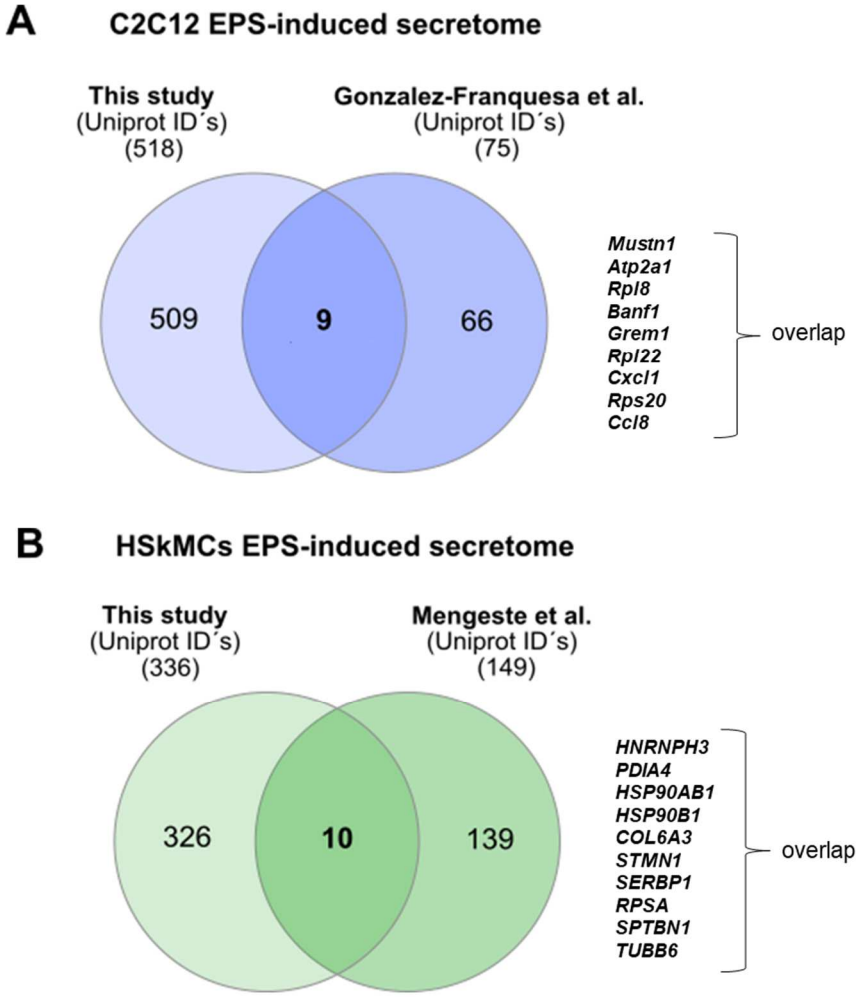

Figure 18: Comparative analyses of EPS-induced myokines in the CM of C2C12 and human myotubes following acute versus chronic low-frequency EPS protocols. (A) EPS-induced secretome of C2C12 cells from this study compared to the literature. **(B)** EPS-induced secretome of HSkMCs from this study compared to the literature. Venn diagram analyses show data from C2C12 cells (*n=3*) in blue (light blue: this study, dark blue: literature) and of HSkMCs from three donors (*n=3*) in green (light green: this study, dark green: literature). EPS: electrical pulse stimulation, HSkMCs: human skeletal muscle cells, CM: conditioned media

3.3 Establishment and validation of *in vitro* insulin resistance in HSkMCs

The second aim of this thesis was to establish an *in vitro* protocol for the generation of insulin resistant HSkMCs defined by an impairment of the insulin signaling cascade (Figure 5, 1.4.3). Therefore, HSMM were expanded in cell culture (2.2.1.2, 2.2.1.3) and differentiated into multinucleated myotubes (2.2.1.4), which were subsequently exposed to different external stimuli (LY294002, palmitate) to induce skeletal muscle insulin resistance *in vitro* (2.2.1.5.1, 2.2.1.5.2, 2.2.1.5.3). The generation of insulin resistant human myotubes was required to further explore and compare the muscle secretomes of contracting insulin sensitive and insulin resistant human myotubes after exposure to EPS, which was the third aim of this thesis (3.4).

3.3.1 PI3K inhibitor LY294002 impairs insulin signaling in primary human myotubes

In order to impair the insulin signaling cascade, primary human myotubes were starved for four hours in starvation medium and subsequently exposed to 40 µM of the chemical PI3K-inhibitor LY294002 (LY), while control cells were treated with the same amount of DMSO (2.2.1.5.1) prior to acute stimulation with insulin (2.2.1.6). Impairment of the insulin signaling cascade was assessed by immunoblotting changes in the phosphorylation of AKT using specific antibodies, a key member of the insulin signaling pathway in skeletal muscle as demonstrated in Figure 4 (1.4.2). As shown in Figure 19A, pretreatment with LY had no effect on total AKT protein abundance, however insulin-mediated phosphorylation of AKT-Ser473 (Figure 19B) and AKT-Thr308 (Figure 19C) was significantly impaired in LY-treated myotubes compared to control cells. Insulin-stimulated phosphorylation of AKT-Ser473 was reduced by 37% and phosphorylation of AKT-Thr308 was reduced by 40% in LY-treated human myotubes (Figure 19B-C). To exclude any detrimental effects of LY on primary human myotubes, the abundance of LDH, a commonly used marker for cell damage, was measured in the supernatant of human myotubes under all conditions. Therefore, supernatants of each condition were collected and processed as described in 2.2.4.2. Myotubes that were treated with 10% Triton X100, a detergents that initiates the maximal release of LDH, served as a positive control and was therefore set at 100%. Figure 19D shows cytotoxicity levels below 5% in both LY-treated and control cells, indicating no significant detrimental effects of treatment with 40 µM LY on primary HSkMCs.

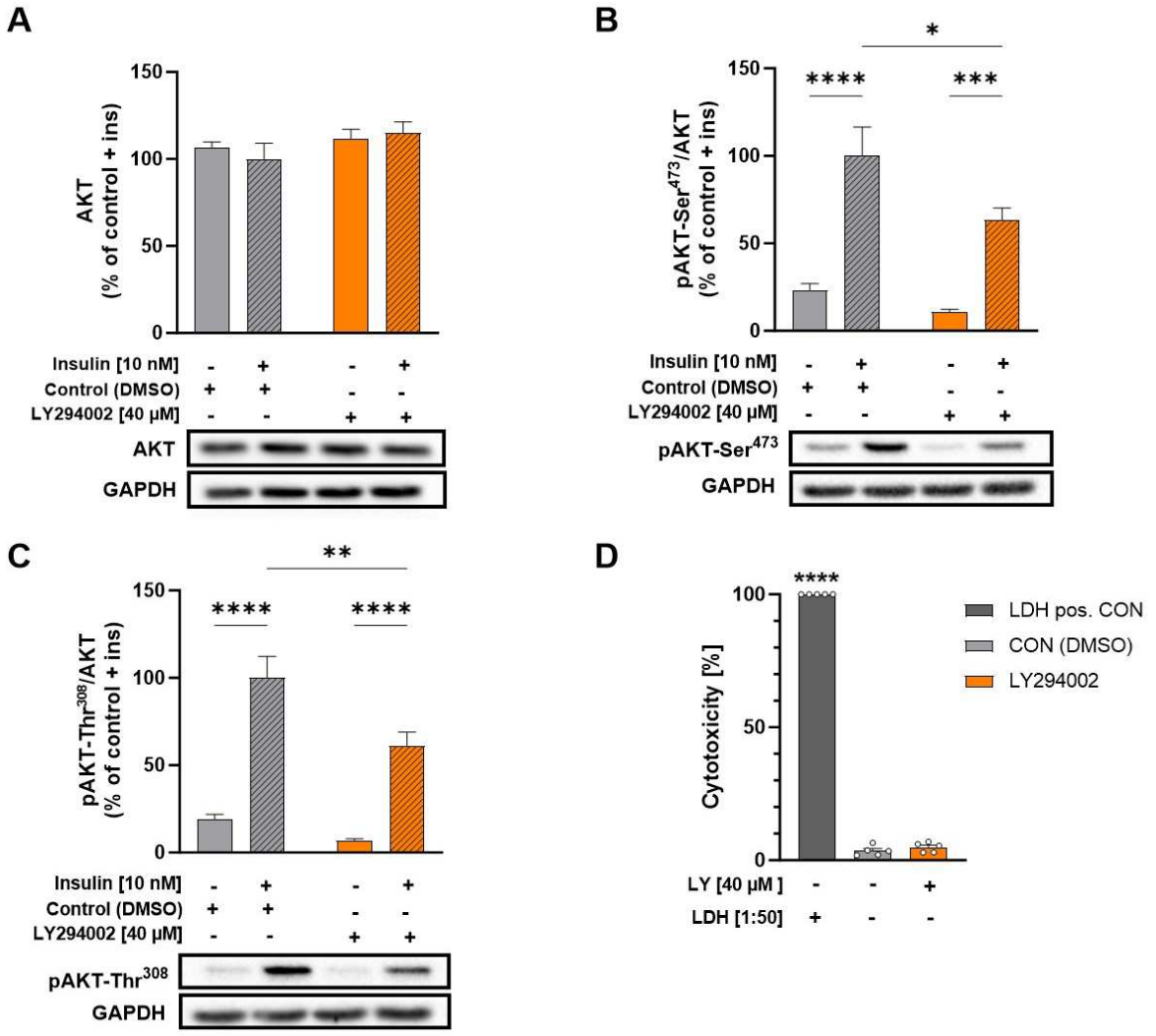

Figure 19: Effect of PI3K-inhibitor LY294002 on insulin signaling and cytotoxicity in primary HSkMCs. Human myotubes were starved for 4h followed by 1 ½h of incubation with 40 µM LY in starvation medium prior to 15 min of stimulation with insulin. Cell lysates were analyzed for total AKT protein abundance **(A)** and for LY-induced changes on insulin-stimulated phosphorylation of AKT-Ser473 **(B)** and AKT-Thr308 **(C).** Data shown are mean ±SEM from 15 (*n=15*) (AKT, AKT-Ser473) and 12 (*n=12*) (AKT-Thr308) individual experiments in primary HSkMCs obtained from five different donors. Expression levels were normalized for the protein abundance of GAPDH and DMSO treated insulin-stimulated cells were regarded as control and set at 100%. Data were analyzed by two-way ANOVA with Sidak post-hoc test for multiple comparisons. *p<0.05, **p<0.01 with vs without LY, ***p<0.001, ****p<0.0001, with vs without insulin stimulation. **(D)** Cellular cytotoxicity in primary HSkMCs (LY- and DMSO-treated) was determined by bioluminescent detection of LDH in the cell culture supernatant using the LDH-Glo™ cytotoxicity assay. Data shown are mean ±SEM from five (*n=5*) individual experiments in primary HSkMCs obtained from five different donors. Data were analyzed by one-way ANOVA with Dunnett post-hoc test for multiple comparisons. ****p<0.0001, LY- and DMSO-treated cells vs LDH positive control. Grey bars represent DMSO-treated control cells and orange bars display LY-treated cells. Striped bars represent insulin-stimulated cells. HSkMCs: human skeletal muscle cells, LDH: lactate dehydrogenase, LY: LY294002, DMSO: dimethyl sulfoxide, AKT: protein kinase B, GAPDH: glyceraldehyde-3-phosphate dehydrogenase

3.3.2 Effects of palmitate on insulin signaling and glucose metabolism in primary human myotubes

3.3.2.1 Treatment with 300 µM palmitate shows mitigated effect on phosphorylation of AKT and its downstream targets in insulin signaling

In order to impair the insulin signaling cascade, primary human myotubes were pretreated with FFA palmitate (300 µM) for 18 hours in differentiation medium and subsequently starved for six hours in starvation medium (2.2.1.5.2) prior to acute stimulation with insulin (2.2.1.6). Impairment of the insulin signaling cascade was assessed by immunoblotting changes in the phosphorylation of AKT, a key member of the insulin signaling pathway, as well as its downstream targets GSK3 and PRAS40 in skeletal muscle (Figure 4, 1.4.2). Figure 20A-D shows that 300 µM palmitate had no effect on the total protein abundance of AKT, GSK3α, GSK3β and PRAS40. Insulin-stimulated phosphorylation of AKT-Ser473 hardly differed from untreated control cells (Figure 20E), while phosphorylation levels of GSK3α-Ser21, GSK3β-Ser9 and PRAS40-Thr246 were reduced by 19%, 15% and 10%, respectively, in palmitate-treated cells compared to the untreated controls (Figure 20F-H).

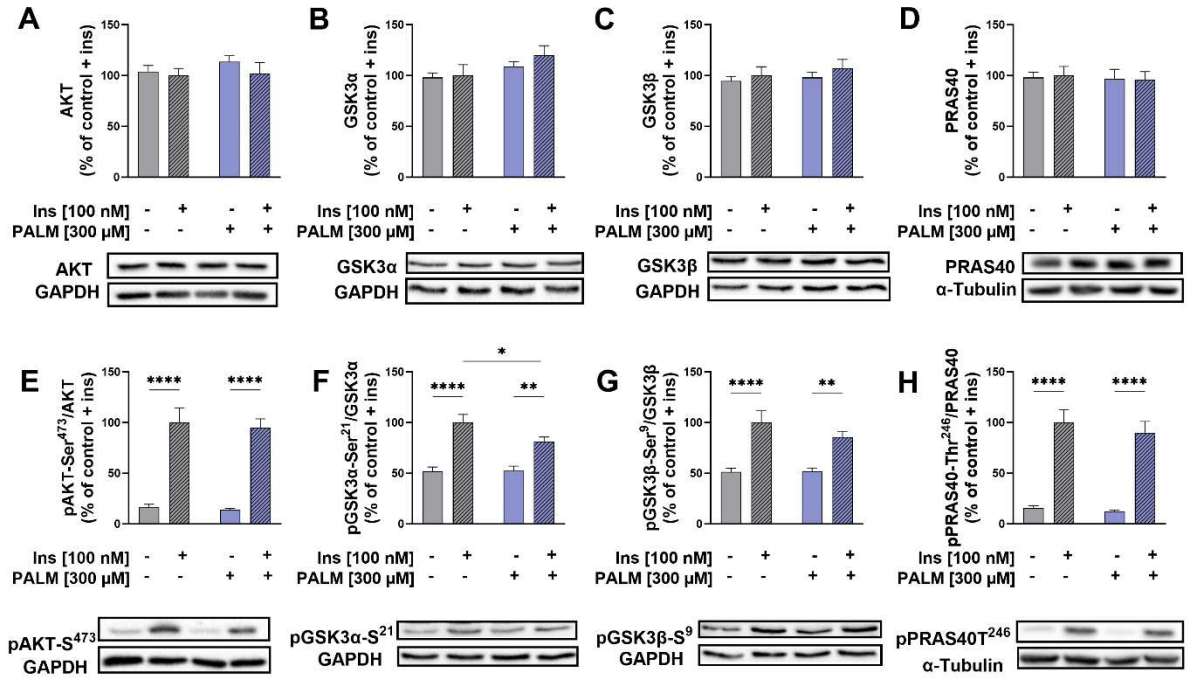

Figure 20: Effect of 300 µM palmitate on insulin signaling in primary HSkMCs. Human myotubes were pretreated with 300 µM palmitate for 18h in differentiation medium, followed by 6h of starvation in the absence of palmitate prior to 15 min of stimulation with insulin. Cell lysates were analyzed for total AKT **(A),** GSK3α **(B),** GSK3β **(C)** and PRAS40 **(D)** protein abundance and for palmitate-induced changes on insulin-stimulated phosphorylation of AKT-Ser473 **(E)**, GSK3α-Ser21 **(F)**, GSK3β-Ser9 **(G)** and PRAS40-Thr246 **(H).** Data shown are mean ±SEM from nine (*n=9*) individual experiments in primary HSkMCs obtained from three different donors. Expression levels were normalized for the protein abundance of GAPDH or α-Tubulin and non-palmitate-treated insulin-stimulated cells were regarded as control and set at 100%. Data were analyzed by two-way ANOVA with Sidak post-hoc test for multiple comparisons. *p<0.05, with vs without palmitate, **p<0.01, ****p<0.0001, with vs without insulin stimulation. Grey bars represent control cells (untreated) and light blue bars show PALM-treated cells. Striped bars represent insulin-stimulated cells. HSkMCs: human skeletal muscle cells, Ins: insulin, PALM: palmitate, AKT: protein

kinase B, GAPDH: glyceraldehyde-3-phosphate dehydrogenase, GSK3: glycogen synthase kinase-3, PRAS40: proline-rich AKT substrate of 40 kDa

3.3.2.2 Treatment with 300 µM palmitate leads to a reduction in insulin-stimulated glycogen synthesis in primary human myotubes

Furthermore, the impairment of insulin signaling in human insulin resistant myotubes was demonstrated at a functional level by measuring insulin-stimulated glycogen synthesis. To generate insulin resistant cells, human myotubes were pretreated with 300 µM palmitate for 18 hours in differentiation medium and subsequently starved for six hours in the absence of palmitate (2.2.1.5.2). Next, HSkMCs were starved for a further three hours in starvation medium supplemented with radiolabeled D-[^{14}C(U)]-glucose in the presence or absence of 100 nM insulin (2.2.4.1), and glycogen synthesis was measured as incorporation of radioactive glucose into glycogen in skeletal muscle cells. Glycogen synthesis was significantly increased in insulin-stimulated human myotubes (untreated cells) compared to basal conditions, whereas this effect was completely abolished in palmitate-treated myotubes, where insulin-stimulated glycogen synthesis was significantly reduced compared to untreated cells (Figure 21).

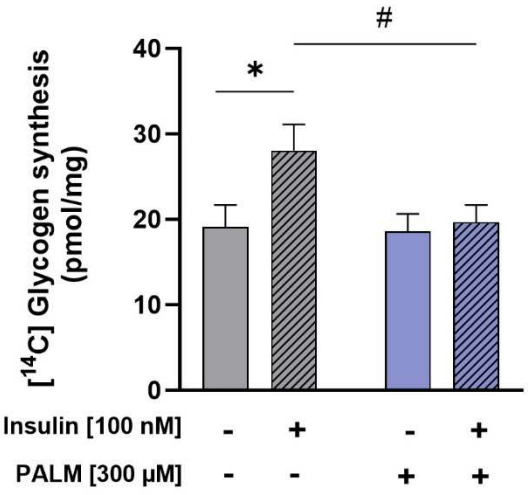

Figure 21: Effect of 300 µM palmitate on insulin-stimulated glycogen synthesis in primary HSkMCs. Myotubes were pretreated for 18h with 300 µM palmitate in differentiation medium and subsequently starved for 6h in the absence of palmitate prior to 3h incubation with D-[14C(U)]-glucose in the presence or absence of 100 nM insulin. All data shown are mean ±SEM from seven (*n=7*) independent experiments in primary HSkMCs obtained from three different individuals. Data shown were analyzed by two-way ANOVA with Sidak post-hoc test, *p<0.05, with vs without insulin, #p<0.05 with vs without palmitate. Grey bars represent control cells and light blue bars show PALM-treated cells. Striped bars represent insulin-stimulated cells. HSkMCs: human skeletal muscle cells, PALM: palmitate

3.3.3 EPS-induced IL-6 secretion is reduced after pretreatment with 300 µM palmitate in primary human myotubes

To test our hypothesis that the human muscle secretome is altered in insulin resistance and to determine the effects of exercise, we first used a targeted approach to analyze the muscle

secretome under pathological conditions. Therefore, insulin resistant human myotubes were generated by exposure to 300 µM palmitate (2.2.1.5.2) and subsequently subjected to acute (6h) low-frequency EPS (2.2.1.7). The well-studied exercise-induced myokine IL-6 was then measured in the supernatant of human myotubes by MIA (2.2.4.3), which is a widely used method to verify the contractile activity of skeletal muscle cells (59). Figure 22 shows that IL-6 secretion was significantly increased in the CM of insulin sensitive control cells after acute low-frequency EPS, while this effect was completely mitigated in palmitate-treated myotubes.

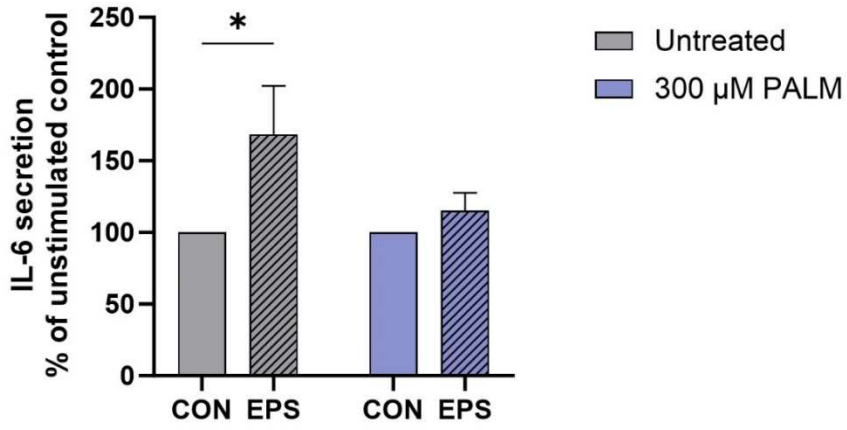

Figure 22: Effect of 300 µM palmitate on EPS-induced IL-6 secretion in primary HSkMCs. Human myotubes were pretreated with 300 µM palmitate for 18h in differentiation medium prior to exposure of acute low-frequency EPS in the absence of palmitate in starvation medium. Control cells remained untreated and unstimulated. IL-6 protein secreted in the CM of human myotubes was measured using multiplex immunoassay. Data shown were normalized to unstimulated control cells for insulin sensitive (untreated) and insulin resistant (PALM) cells, respectively. Data are expressed as mean ±SEM from six individual experiments (*n=6*) and primary HSkMCs were obtained from three different individuals. Data shown were analyzed by two-way ANOVA with Sidak post-hoc test, *$p < 0.05$, CON vs EPS. Grey bars represent control cells and light blue bars show PALM-treated cells. Striped bars represent EPS-stimulated cells. CM: conditioned media, CON: control, EPS: electrical pulse stimulation, HSkMCs: human skeletal muscle cells, IL-6: interleukin-6, PALM: palmitate, IL-6: Interleukin-6

3.3.4 Treatment with 800 µM palmitate impairs insulin signaling in primary human myotubes

Since the impairment of the insulin signaling cascade was not effective with the first protocol (300 µM palmitate), a second protocol was established in which the palmitate concentration was increased to 800 µM. In addition, the incubation time was reduced from 18 hours to 12 hours and the incubation was performed in starvation medium (serum-free), instead of differentiation medium (2.2.1.5.3). The last step was important since incubation in differentiation medium can affect the amount of unbound free fatty acids due to the presence of horse serum (albumin binding to palmitate), thus reducing the lipotoxic effect of palmitate. Therefore, insulin resistant human myotubes were generated by pretreatment with 800 µM palmitate, while control cells were treated with BSA (2.2.1.5.3). Subsequently, insulin sensitive and resistant myotubes were starved for six hours and subjected to acute insulin stimulation (2.2.1.6). Impairment of the insulin signaling cascade was assessed by immunoblotting

phosphorylation of AKT, a key member of the insulin signaling pathway, and its downstream targets GSK3 and PRAS40 (Figure 4, 1.4.2). Figure 23A shows that 800 µM palmitate had no effect on total AKT protein abundance, however we observed a significant reduction in insulin-mediated phosphorylation of AKT-Ser473 (Figure 23B) and AKT-Thr308 (Figure 23C) in palmitate-treated myotubes compared to BSA-treated control cells. Insulin-stimulated phosphorylation was statistically significant in both BSA-treated (control) and palmitate-treated cells, however phosphorylation levels were reduced by 30% at the AKT-Ser473 and by 26% at AKT-Thr308 phosphosite (Figure 23 B-C).

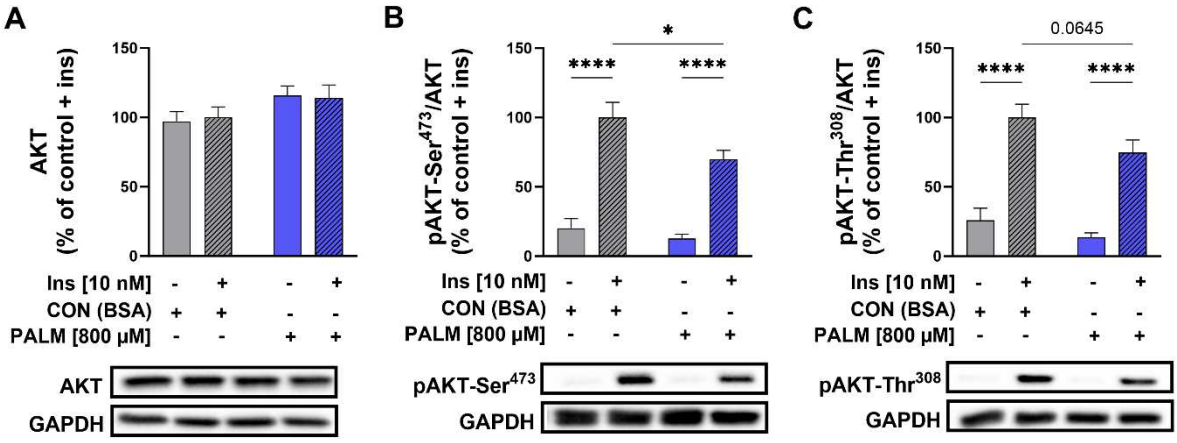

Figure 23: Effect of 800 µM palmitate on insulin signaling in primary HSkMCs. Human myotubes were pretreated with 800 µM palmitate for 12h in starvation medium, followed by 6h of starvation in the absence of palmitate prior to 15 min of stimulation with insulin. Cell lysates were analyzed for total AKT protein abundance **(A)** and for palmitate-induced changes on insulin-stimulated phosphorylation of AKT-Ser473 **(B)** and AKT-Thr308 **(C).** Data shown are mean ±SEM from 15 *(n=15)* individual experiments in primary HSkMCs obtained from five different donors. Expression levels were normalized for the protein abundance of GAPDH and BSA-treated insulin-stimulated control cells were regarded as control and set at 100%. Data were analyzed by two-way ANOVA with Sidak post-hoc test for multiple comparisons. *p<0.05, with *vs* without palmitate, **p<0.01, ****p<0.0001, with *vs* without insulin stimulation. Grey bars represent BSA-treated control cells and blue bars show PALM-treated cells. Striped bars represent insulin-stimulated cells. BSA: bovine serum albumin, ins: insulin, PALM: palmitate, AKT: protein kinase B, GAPDH: glyceraldehyde-3-phosphate dehydrogenase

Similarly, the total protein abundance of GSK3α, GSK3β and PRAS40 in human myotubes was not affected by pretreatment with 800 µM palmitate (Figure 24A-C). Furthermore, insulin significantly increased the phosphorylation of GSK3α-Ser21, GSK3β-Ser9, and PRAS40-Thr246 in BSA-treated (control) cells, whereas the phosphorylation levels of GSK3α-Ser21, GSK3β-Ser9, and PRAS40-Thr246 were decreased in palmitate-treated cells compared to control (BSA-treated) cells (Figure XD-F).

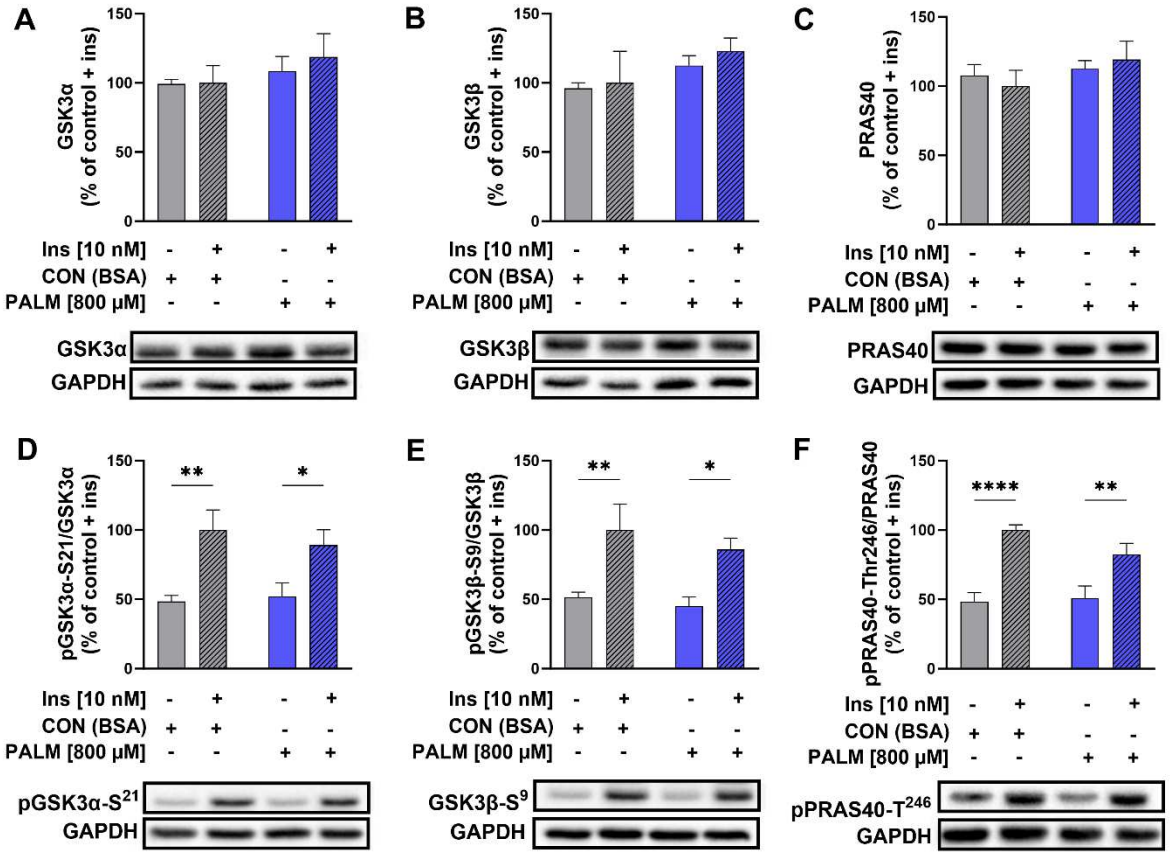

Figure 24: Effect of palmitate on downstream targets of AKT/PKB signaling in primary HSkMCs. Differentiated myotubes were pretreated with 800 µM palmitate for 12h in starvation medium, followed by 6h of starvation without the presence of BSA or palmitate prior to 15 min of stimulation with insulin. Cell lysates were analyzed for total GSK3α **(A)**, GSK3β **(B)** and PRAS40 **(C)** protein abundance and for palmitate-induced changes on insulin-stimulated phosphorylation of GSK3α-Ser21 **(D)**, GSK3β-Ser9 **(E)** and PRAS40-Thr246 **(F)** by Western blot analysis. Data shown are mean ±SEM from six to eight *(n=6-8)* individual experiments in primary HSkMCs obtained from four to five different donors. Expression levels were normalized for the protein abundance of GAPDH and BSA-treated insulin-stimulated control cells were regarded as control and set at 100%. Data were analyzed by two-way ANOVA with Sidak post-hoc test for multiple comparisons. *p<0.05, **p<0.01, ****p<0.0001, with *vs* without insulin stimulation. Grey bars represent BSA-treated control cells and blue bars show PALM-treated cells. Striped bars represent insulin-stimulated cells. BSA: bovine serum albumin, ins: insulin, PALM: palmitate, GAPDH: glyceraldehyde-3-phosphate dehydrogenase, GSK3: glycogen synthase kinase-3, PRAS40: proline-rich Akt substrate of 40 kDa

3.3.5 Pretreatment with 800 µM palmitate followed by EPS does not exert damaging effects on primary human myotubes

To ensure the absence of cytotoxic effects following palmitate and EPS treatment, the abundance of LDH, a marker for cell damage, was measured in the supernatant of HSkMCs. In order to generate insulin resistant cells, human myotubes were pretreated with 800 µM palmitate for 12 hours (2.2.1.5.3) and subsequently subjected to acute low-frequency EPS for six hours in the absence of palmitate (2.2.1.7). Supernatants from each condition were collected and LDH levels were measured as described in 2.2.4.2. Myotubes that were treated with 10% Triton X100 were referred to as a positive control, as Triton, a detergent, induces the maximal release of LDH in the cell culture media, therefore values were set at 100%. Figure

25 shows that the cytotoxicity levels in all conditions were below 10% compared to the LDH positive control, indicating that neither palmitate nor EPS treatment exerted detrimental effects.

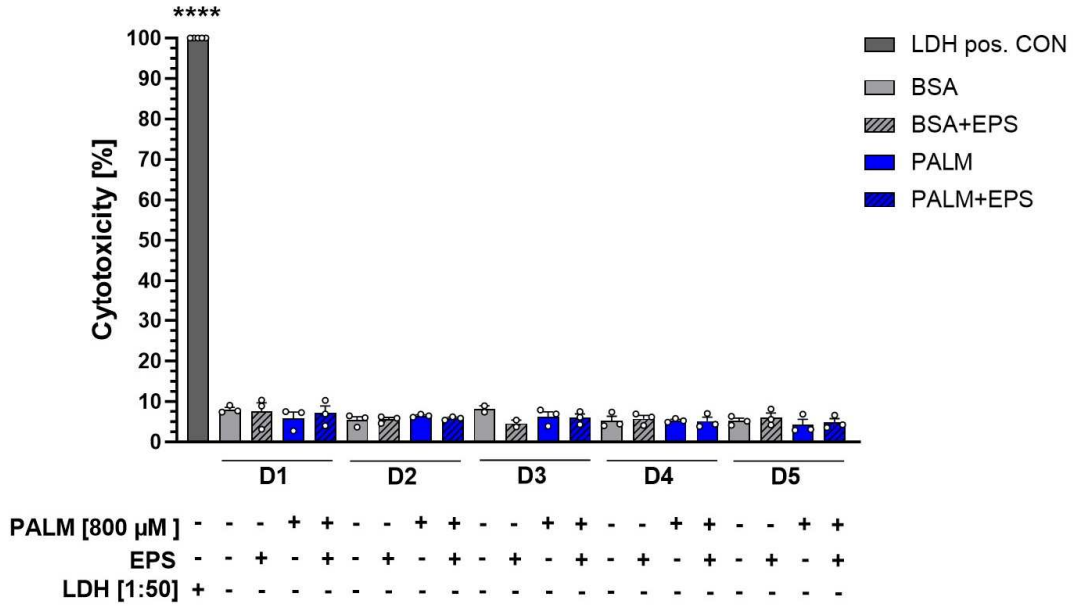

Figure 25: Pretreatment with palmitate and subsequent EPS do not show damaging effects on HSkMCs. Primary myotubes were pretreated with 800 µM palmitate for 12h in starvation medium, followed by 6h of low-frequency EPS without in the absence of palmitate in the starvation medium. Supernatant was harvested after treatment with palmitate and EPS, respectively. Cellular cytotoxicity in primary HSkMCs was assessed by bioluminescent detection of LDH in the supernatants using LDH-Glo™ Cytotoxicity assay. Data shown are mean ±SEM from 15 (*n=15*) individual experiments in primary HSkMCs obtained from five different donors. Cells from each donor treated with 10% triton for maximal LDH release were considered as LDH positive control and set as 100%. Data were analyzed by one-way ANOVA with Dunnett post-hoc test for multiple comparisons. ****p<0.0001 for all treatments vs LDH positive control. Grey bars represent BSA-treated control cells and blue bars show PALM-treated cells. Striped bars represent EPS-stimulated cells. BSA: bovine serum albumin, CON: control, D: donor, EPS: electrical pulse stimulation, HSkMCs: human skeletal muscle cells, LDH: lactate dehydrogenase, PALM: palmitate

3.3.6 EPS-induced IL-6 secretion is reduced after pretreatment with 800 µM palmitate in primary human myotubes

To evaluate the effects of the second established protocol for muscle insulin resistance (800 µM) on the secretome and to further investigate the effects of acute low-frequency EPS on contraction-induced myokine secretion in insulin resistant cells, we measured protein secretion of the exercise-induced myokine IL-6. Therefore, human myotubes were pretreated with 800 µM palmitate for 12 hours (2.2.1.5.3) and then subjected to EPS for six hours in the absence of palmitate (2.2.1.7). The supernatants of each condition were then collected and analyzed using Multiplex Immunoassy (MIA) (2.2.4.3). As expected, contraction-induced myokine secretion of IL-6 was significantly increased following acute low-frequency EPS in both BSA-treated (control) and palmitate-treated cells. However, IL-6 protein secretion was significantly decreased in palmitate-treated myotubes compared to control myotubes (Figure 26).

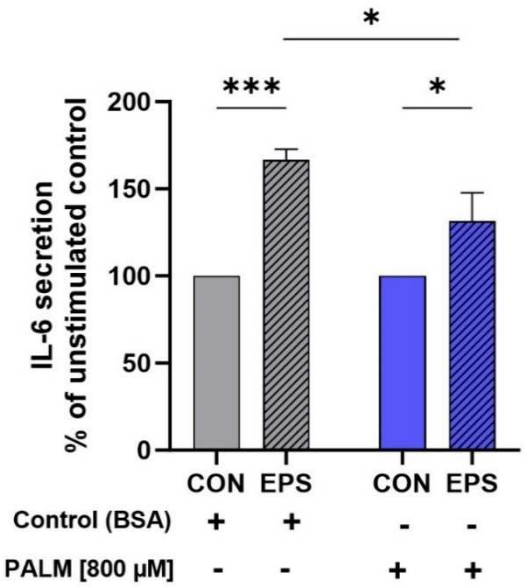

Figure 26: Effect of 800 µM palmitate treatment on EPS-induced IL-6 secretion in primary HSkMCs. Human myotubes were pretreated with 800 µM palmitate for 12h in starvation medium, followed by 6h of low-frequency EPS in starvation medium without the presence of palmitate. Supernatant was harvested post EPS and myokine protein concentration of IL-6 were measured using multiplex immunoassay. Data are expressed as mean ±SEM from five (*n=5*) individual experiments in primary HSkMCs obtained from five different donors and were normalized to unstimulated BSA-treated or palmitate-treated control cells. All data shown were analyzed by two-way ANOVA with Sidak post-hoc test for multiple comparisons. *p<0.05, ***p<0.001, with vs without EPS. Grey bars represent BSA-treated control cells and blue bars show PALM-treated cells. Striped bars represent EPS-stimulated cells. BSA: bovine serum albumin, CON: control, EPS: electrical pulse stimulation, HSkMCs: human skeletal muscle cells, PALM: palmitate, IL-6: Interleukin-6

3.3.7 Myokine secretion in insulin sensitive versus insulin resistant HSkMCs is affected by donor variability

Prior to studying the secretomes of insulin sensitive and insulin resistant human myotubes using a non-targeted approach, the response of known myokines to *in vitro* exercise was evaluated using a targeted approach. The aim was to explore whether there are differences in myokine secretion of human muscle cells in the insulin sensitive and insulin resistant state after acute low-frequency EPS treatment. Insulin resistant cells were generated by exposing human myotubes to 800 µM palmitate for 12 hours (2.2.1.5.3). Subsequently, human myotubes were exposed to acute low-frequency EPS for six hours in the absence of palmitate (2.2.1.7), the supernatant was collected and several myokines were measured by MIA (2.2.4.3).

3.3.7.1 Exercise-induced secreted myokines

Secretion profiles of known exerkines like LIF, SPARC, VEGF and FABP3 were analyzed in the CM of insulin sensitive and insulin human myotubes. Acute low-frequency EPS did not significantly induce protein secretion of exerkines in stimulated myotubes compared to unstimulated in either insulin sensitive or insulin resistant human myotubes (Figure 27A-D). The myokines LIF and VEGF showed a slight increase in insulin sensitive cells exposed to

EPS compared to non-stimulated cells, however this tendency was donor dependent and was not observed in insulin resistant cells (Figure 27A and 27C). SPARC and FABP3 showed no difference between stimulated and non-stimulated myotubes, however a strong increase in FABP3 secretion was observed in insulin resistant myotubes after EPS treatment, at least for one donor (Figure 27B and 27D). Yet the results also show a large donor variability as the secretion of myokines varies greatly within the five donors (represented by dots).

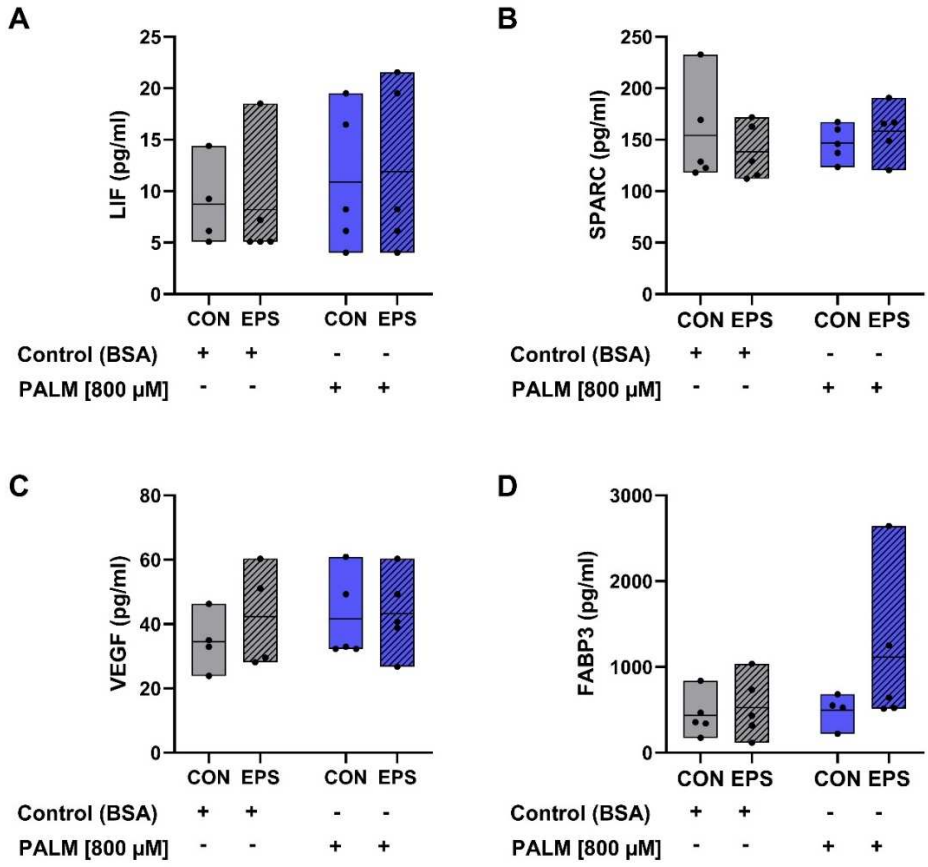

Figure 27: Effect of donor variability on exercise-induced protein secretion in HSkMCs. Human myotubes were pretreated with 800 µM palmitate for 12h in starvation medium, followed by 6h of low-frequency EPS in starvation medium in the absence of palmitate. Supernatant was harvested post EPS treatment and myokine concentrations **(A)** LIF, **(B)** SPARC, **(C)** VEGF, **(D)** FABP3 were measured by multiplex immunoassay. Data are expressed as mean ±SEM from four to five (*n=4-5*) individual experiments in primary HSkMCs obtained from four to five different donors and are shown as absolute values. All data shown were analyzed by two-way ANOVA with Sidak post-hoc test for multiple comparisons. Grey bars represent insulin sensitive (BSA-treated) control cells and blue bars represent insulin resistant (palmitate-treated) cells. Striped bars represent EPS-stimulated cells, each dot represents one donor. BSA: bovine serum albumin, CON: control, EPS: electrical pulse stimulation, HSkMCs: human skeletal muscle cells, PALM: palmitate, LIF: leukemia inhibitory factor, SPARC: secreted protein acidic and rich in cysteine, VEGF: vascular endothelial growth factor, FABP3: fatty acid-binding protein 3

3.3.7.2 Secreted pro-inflammatory myokines

Further secretion profiles of known pro-inflammatory cytokines and chemokines were assessed. Again, protein secretion was highly variable between donors. Protein secretion of the pro-inflammatory cytokines MIF, MCP-1 and IL-8 was strongly increased in the CM of insulin resistant (palmitate-treated) human myotubes compared to insulin sensitive (BSA-treated) control cells (Figure 28A-C). In particular, MCP-1 and IL-8 showed increased secreted protein levels in response to acute low-frequency EPS, since they are also known as exercise-induced myokines (Figure 28B and 28C). MCP-1 protein levels were also increased in insulin sensitive myotubes in response to EPS, however this was not observed for IL-8 secretion (Figure 28B and 28C). Other myokines such as M-CSF and SCGF-β showed an increase in protein secretion after EPS in insulin sensitive cells for some donors, while this effect was completely attenuated in insulin resistant cells (Figure 28G and 28I).

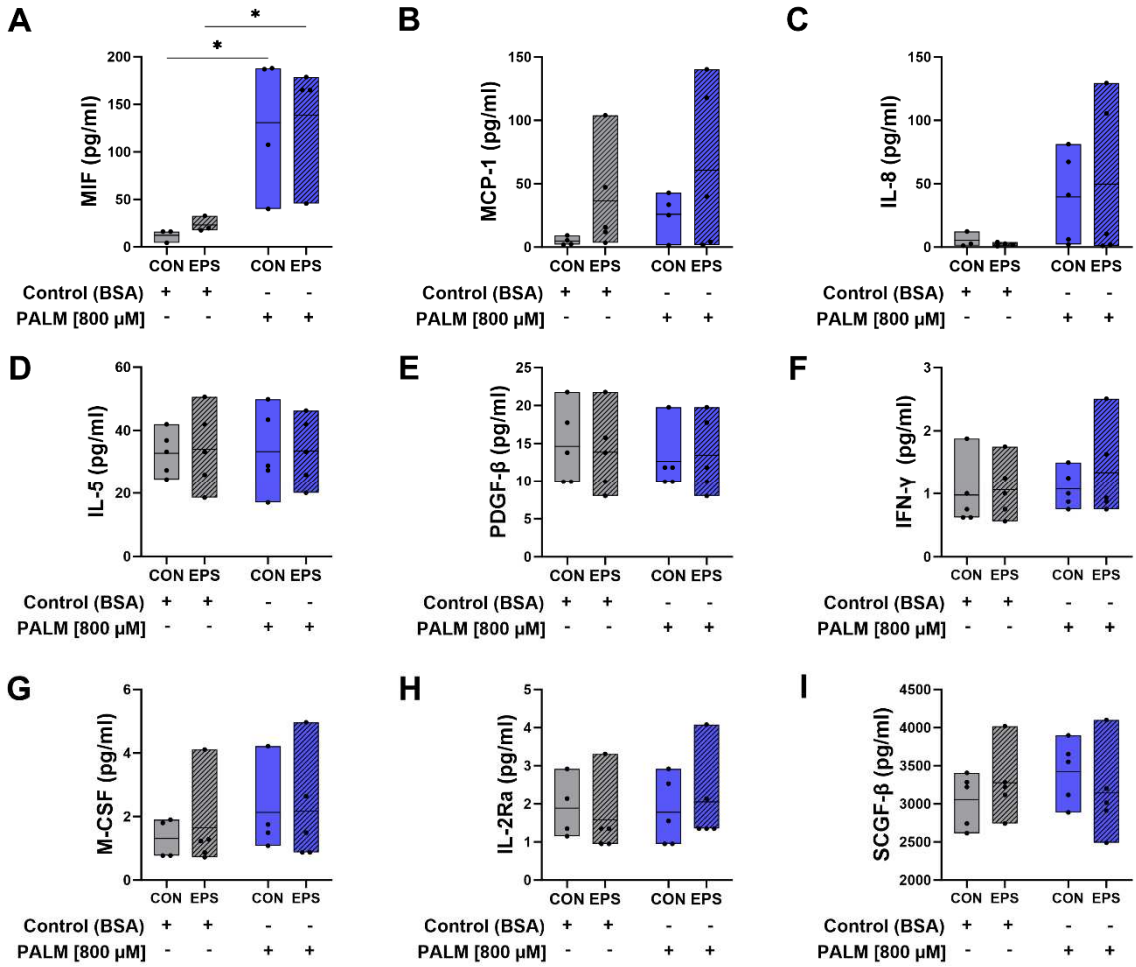

Figure 28: Effect of donor variability on pro-inflammatory cytokine secretion in HSkMCs. Human myotubes were pretreated with 800 µM palmitate for 12h in starvation medium, followed by 6h of low-frequency EPS in starvation medium in the absence of palmitate. Supernatant was harvested post EPS treatment and myokine concentrations **A)** MIF, **(B)** MCP-1, **(C)** IL-8, **(D)** IL-5, **(E)** PDGF-β, **(F)** IFN-γ, **(G)** M-CSF, **(H)** IL-2Ra, **(I)** SCGF-β were measured by multiplex immunoassay. Data are expressed as mean ±SEM from four to five (*n=4-5*) individual experiments in primary HSkMCs obtained from four to five different donors and are shown as absolute values. All

data shown were analyzed by two-way ANOVA with Sidak post-hoc test for multiple comparisons. *p<0.05, ***p<0.001, with vs without EPS. Grey bars represent BSA-treated control cells and blue bars show PALM-treated cells. Striped bars represent EPS-stimulated cells, each dot represents one donor. BSA: bovine serum albumin, CON: control, EPS: electrical pulse stimulation, HSkMCs: human skeletal muscle cells, PALM: palmitate, MIF: macrophage migration inhibitory factor; MCP-1: monocyte chemoattractant protein-1, IL-8/15: interleukin-8/15, PDGF-β: platelet-derived growth factor receptor beta, IFN-γ: recombinant human Interferon-gamma, M-CSF: human macrophage colony stimulating factor, IL-2Ra: interleukin-2 receptor alpha chain, SCGF-β: serum stem cell growth factor beta

3.4 LC-MS/MS analyses of insulin sensitive versus insulin resistant primary HSkMCs following acute low-frequency EPS

The second aim of this thesis was to induce insulin resistance in HSkMCs *in vitro* and subsequently compare the secretomes of insulin sensitive and insulin resistant human myotubes. To date, only a few proteomic secretome studies investigated the composition of the secretome in muscle insulin resistance, however, these studies were conducted using rodent cell culture models (200, 205). To further extend the knowledge of the myokine secretion profile in an insulin resistant state and to translate it to the human system, we established an *in vitro* insulin resistant model as described in section 3.3. The third aim of this thesis was to test our hypothesis that the secretome of contracting insulin sensitive and insulin resistant myotubes differs. As it is known from recent studies that the muscle secretome is altered by EPS (70, 192), we sought to determine the effect of EPS on the secretome of insulin resistant HSkMCs. Primary HSMM were cultured and expanded as described in sections 2.2.1.2 and 2.2.1.3. Myoblasts were differentiated into multinucleated myotubes (2.2.1.4) and pretreated with 800 µM palmitate for 12 hours in starvation medium (2.2.1.5.3). The next day, myotubes were either subjected to acute low-frequency EPS (2.2.1.7) or remained unstimulated (control). Subsequently, CM from each condition were collected for secretome analysis and cell lysates for cellular proteome analysis (2.2.1.7). Samples were processed in the bottom-up proteomics workflow, hence proteins were enzymatically digested with trypsin prior to MS analysis (2.2.5, Figure 6). By using a non-targeted approach, we were able to identify and quantify a large number of proteins detected in the CM. In the following sections, the results regarding the similarities and differences of the different secretomes are presented.

3.4.1 Characterization of different human muscle secretomes

3.4.1.1 Bioinformatic prediction analyses revealing different secretion types

MS data were analyzed as described in 2.2.6. In order to filter and analyze the high throughput molecular data, bioinformatic tools were used to predict different types of secretion and to gain insight into the representation of proteins within different cellular components (2.2.6.1). MS secretome analysis of insulin sensitive human myotubes previously exposed to acute low-frequency EPS identified 4,121 potential myokines in the in the CM, of which 2,325 proteins

were identified as “predicted secretory myokines” (Figure 29A). A total of 865 (SP+, 21%) proteins were assigned to the classical secretion pathway, while 1,460 (SP-, 18%; Outcyte+, 17%) myokines were unconventionally secreted (UPS) (Figure 29A-B). GOCC analysis revealed that most myokines were annotated as “extracellular exosome” (28%), “plasma membrane proteins” (27%), and “vesicles” (18%)“, of which more than half were also identified by bioinformatic analysis as “predicted secretory proteins” highlighted in green (Figure 29C).

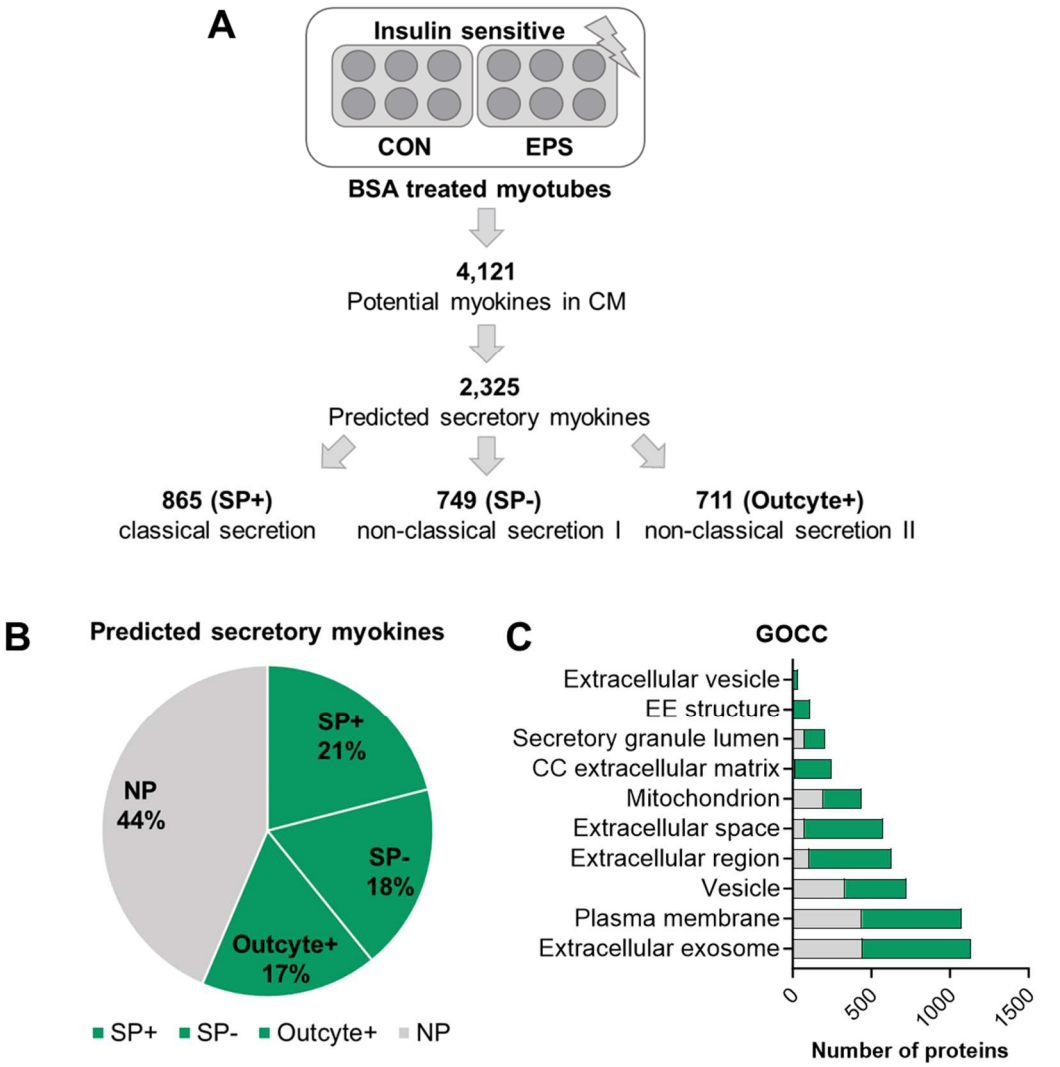

Figure 29: Bioinformatic prediction analysis of insulin sensitive human myotubes following EPS. Human myotubes from five donors (*n=5*) were pretreated with BSA (insulin sensitive cells) and then subjected to 6h of low-frequency EPS. **(A)** Bioinformatic prediction analysis using SignalP 6.0, SecretomeP 2.0 and Outcyte 1.0. **(B)** Percentage of “predicted secretory myokines”**. (C)** GOCC analysis of the entire muscle secretome and the subgroup “predicted secretory myokines”. Insulin sensitive cells are represented in dark grey. Predicted secretory myokines are represented in green, while NP proteins are represented in light grey. CON: control, EPS: electrical pulse stimulation, GOCC: gene ontology cellular component, NP: non-predicted, SP+: signal peptide positive, SP-: signal peptide negative, EE structure: external encapsulating structure, CC extracellular matrix: collagen-containing CC extracellular matrix

MS secretome analysis of insulin sensitive and insulin resistant myotubes identified 4,185 potential myokines in the CM, of which 2,336 proteins were considered “predicted secretory

myokines" (Figure 30A). Bioinformatic prediction analysis resulted in 865 classically secreted myokines (SP+, 21%) and 1,471 unconventionally secreted myokines (SP-, 18%; Outcyte+, 17%) (Figure 30A-B). The results of the GOCC analysis were nearly the same (Figure 30C) as previously shown in Figure 29C for insulin sensitive myotubes subjected to EPS.

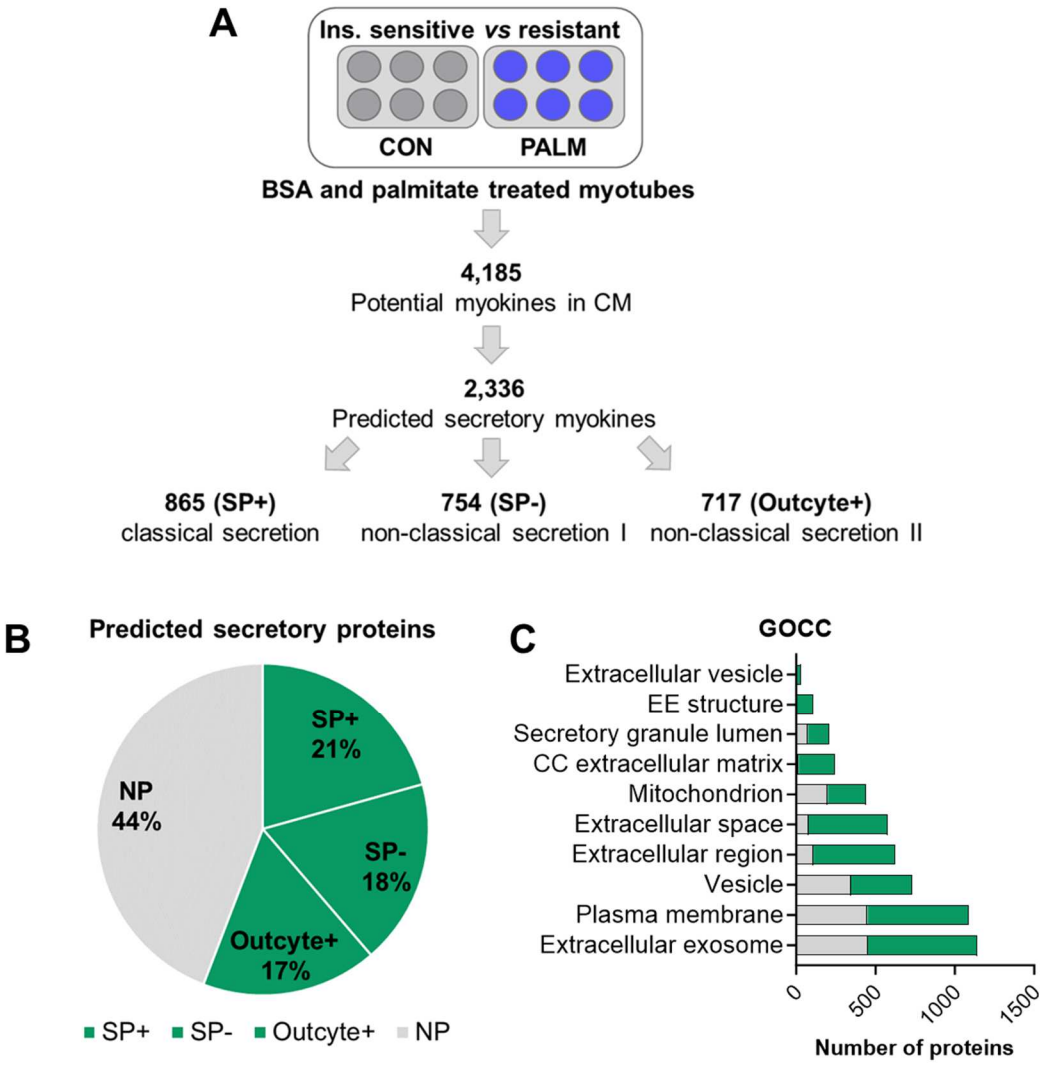

Figure 30: Bioinformatic prediction analysis of insulin sensitive and insulin resistant myotubes. Human myotubes from five donors (*n=5*) were pretreated with either BSA (insulin sensitive cells) or 800 µM palmitate (insulin resistant cells) and subsequently starved for 6h in starvation medium. **(A)** Bioinformatic prediction analysis using SignalP 6.0, SecretomeP 2.0 and Outcyte 1.0. **(B)** Percentage of "predicted secretory myokines". **(C)** GOCC analysis of the entire muscle secretome and the subgroup "predicted secretory myokines". Insulin sensitive cells are represented in dark grey, while insulin resistant cells are shown in blue. Predicted secretory myokines are represented in green, while NP proteins are represented in light grey. CON: control, EPS: electrical pulse stimulation, GOCC: gene ontology cellular component, NP: non-predicted, SP+: signal peptide positive, SP-: signal peptide negative, EE structure: external encapsulating structure, CC extracellular matrix: collagen-containing CC extracellular matrix

The MS secretome analysis of insulin resistant myotubes exposed to acute low-frequency EPS showed quite similar results as described for the two previous secretome analyses. A total of 4,239 potential myokines were identified in the CM, of which 2,350 proteins were predicted as "secretory myokines". Bioinformatics considered 858 myokines (SP+, 20%) as classically

secreted and 1,492 myokines (SP-, 18%; Outcyte+, 17%) as unconventionally secreted (Figure 31A-B). The GOCC analysis of this secretome was also similar to the results of the two previously described secretome analyses shown in Figure 29C and 30C (Figure 31C).

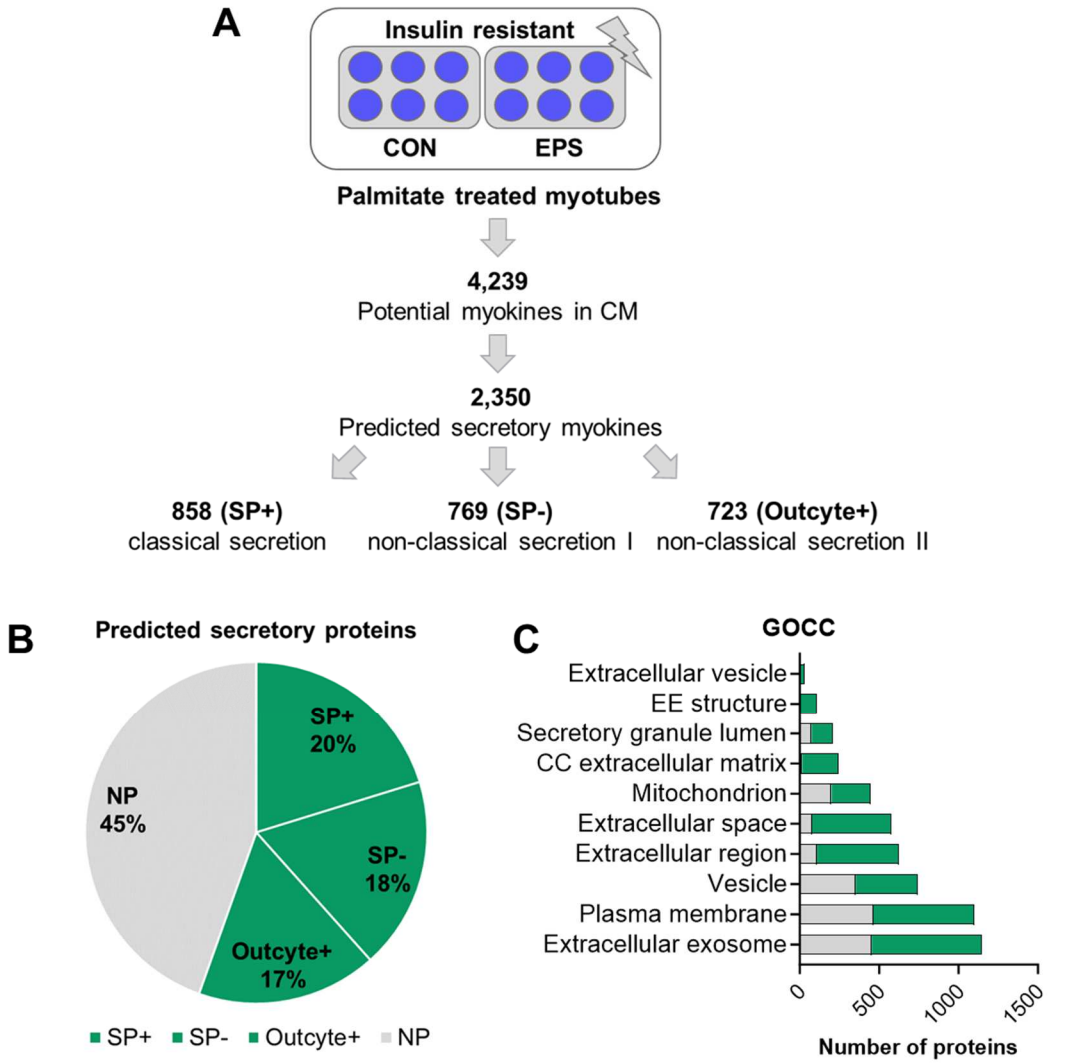

Figure 31: Bioinformatic prediction analysis of insulin resistant human myotubes following EPS. Human myotubes from five donors (*n=5*) were pretreated with 800 µM palmitate (insulin resistant cells) and then subjected to 6h of low-frequency EPS. **(A)** Bioinformatic prediction analysis using SignalP 6.0, SecretomeP 2.0 and Outcyte 1.0. **(B)** Percentage of "predicted secretory myokines". **(C)** GOCC analysis of the entire muscle secretome and the subgroup "predicted secretory myokines". Insulin resistant cells are represented in blue. Predicted secretory myokines are represented in green, while NP proteins are represented in light grey. CON: control, EPS: electrical pulse stimulation, GOCC: gene ontology cellular component, NP: non-predicted, SP+: signal peptide positive, SP-: signal peptide negative, EE structure: external encapsulating structure, CC extracellular matrix: collagen-containing CC extracellular matrix

3.4.1.2 Muscle secretome and proteome analysis: a comparison

MS data were analyzed and filtered as described in 2.2.6 and 2.2.6.1. To evaluate the overlap between muscle secretome and proteome, comparative analyses were conducted. As expected, we observed a large overlap between the muscle secretome and proteome data (Figure 32A, C, E). In total, 83-84% of all secreted proteins were also detected in the

corresponding cellular proteome (Figure 32A, C, E). Comparison of the subset of "predicted secretory myokines" with the proteome also showed an overlap of 78-79% (Figure 32A). Furthermore, GOCC analysis showed that the most abundant proteins in the proteome were annotated as nuclear and cytosolic proteins, while these were notably reduced in the muscle secretome (Figure 32B, D, F). Interestingly, the distribution of proteins in the cellular components "extracellular matrix" and "non-structural extracellular" was nearly the same in both, proteome and secretome (Figure 32B, D, F).

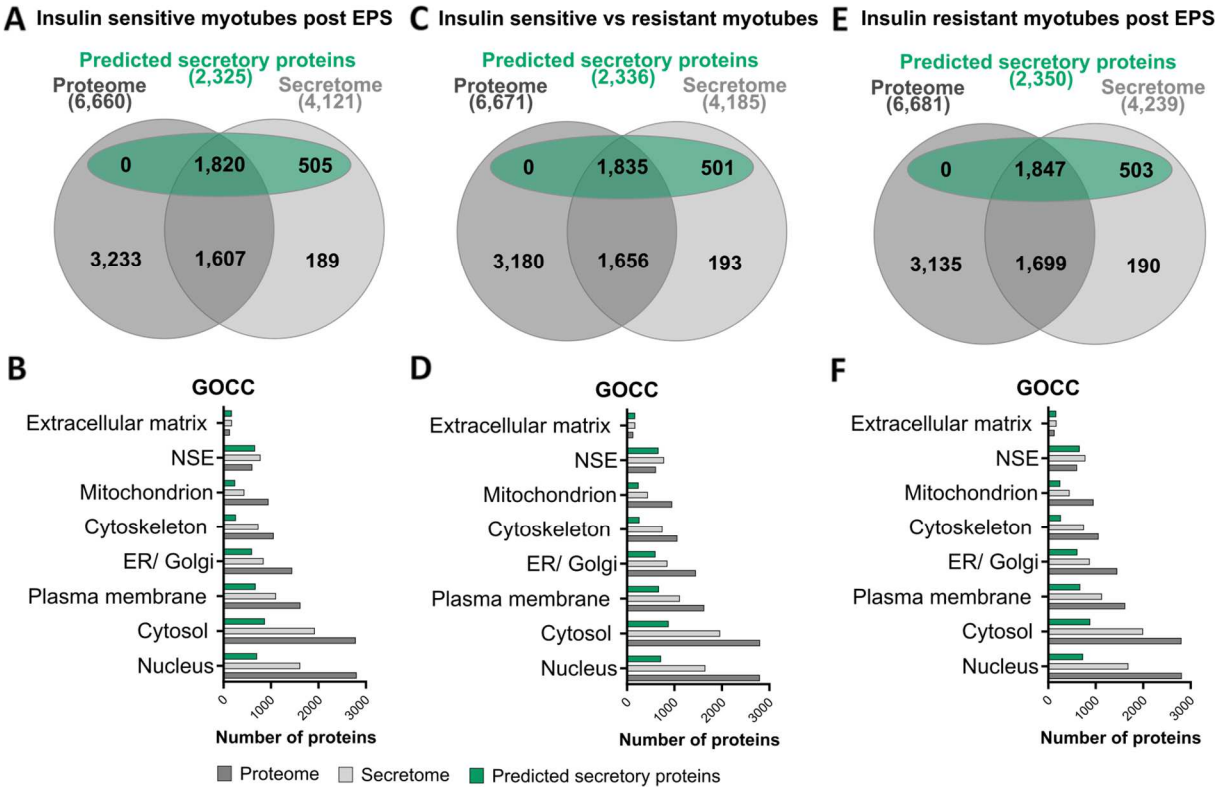

Figure 32: Secretome and proteome analysis of insulin sensitive and insulin resistant HSkMCs. Human myotubes from five donors (*n=5*) were pretreated with either BSA (insulin sensitive cells) or 800 µM palmitate (insulin resistant cells) and then subjected to 6h of low-frequency EPS. (A, C, E) Venn diagram analyses of muscle secretome and proteome as well as with the secretome subgroup "predicted secretory proteins". (B, D, F) GOCC analysis of the entire muscle secretome and the subgroup "predicted secretory myokines". Proteomes are colored in dark grey and secretomes in light grey, "predicted secretory proteins" are colored in green. BSA: bovine serum albumin, CON: control, EPS: electrical pulse stimulation, GOCC: gene ontology cellular component, PALM: palmitate, NSE: non-structural extracellular, ER: endoplasmic reticulum

To evaluate the correlations between proteome and secretome data, scatter plots were generated showing the intensities of common proteins detected in CM and cell lysates of each condition (Figure 33 A-D). We observed a rather moderate positive correlation (R^2 0.13-0.29, *p*-value <0.0001) between protein abundances of secretomes and proteomes. Proteins predicted as "secretory myokines" are colored in green (Figure 33 A-D).

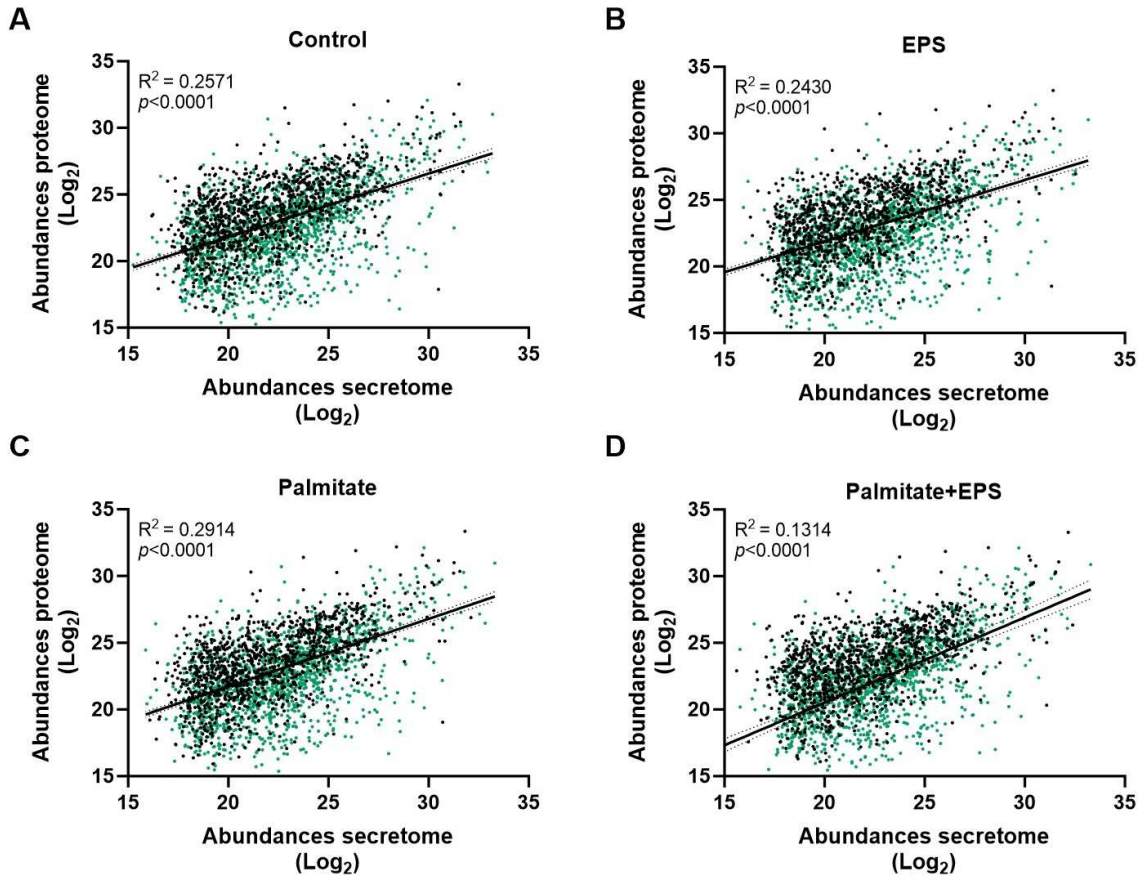

Figure 33: Scatterplot analyses of common proteins that occurred in the secretome and cellular proteome of each condition. Human myotubes were pretreated with either BSA (insulin sensitive cells) or 800 µM palmitate (insulin resistant cells) and then subjected to 6h of low-frequency EPS. **(A-D)** Abundances of the common proteins in the secretome and proteome for the respective conditions were correlated with each other, as shown by the correlation coefficient R^2. All proteins described as "predicted secretory myokines" were colored in green and all NP proteins are shown in black. Simple linear regression analyses were performed, data shown are abundances expressed as mean from five *(n=5)* different subjects. Pearson correlation analysis of protein abundances resulted in **(A)** R^2=0,2571, r=0,5071, p<0.0001 **(B)** R^2=0,2430, r=0,4929, p<0.0001 **(C)** R^2=0,2914, r=0,5398, p<0.0001 **(D)** R^2=0,1314, r=0,3624, p<0.0001. EPS: electrical pulse stimulation, NP: non-predicted

3.4.1.3 Label free-quantification analyses of muscle secretome and cellular proteome

The MS datasets were analyzed (2.2.6) and filtered (2.2.6.1) as described previously. In total, approximately 4,200 proteins were identified in the muscle secretome and 6,600 proteins in the cellular proteome of insulin sensitive and insulin resistant myotubes. Furthermore, we aimed to determine the amount of quantified proteins in the muscle secretome and cellular proteome. Approximately 2,800 proteins were quantified in the CM of each donor under the respective conditions (Figure 34A). Overall, approximately 61% of all quantified proteins were categorized as "predicted secretory myokines", as shown in the green stacked diagram (Figure 34A). In comparison, approximately 5,700 proteins were quantified in the cellular proteome of each donor within the respective conditions, of which 32% were assigned as "predicted secretory proteins" (colored in green) (Figure 34B).

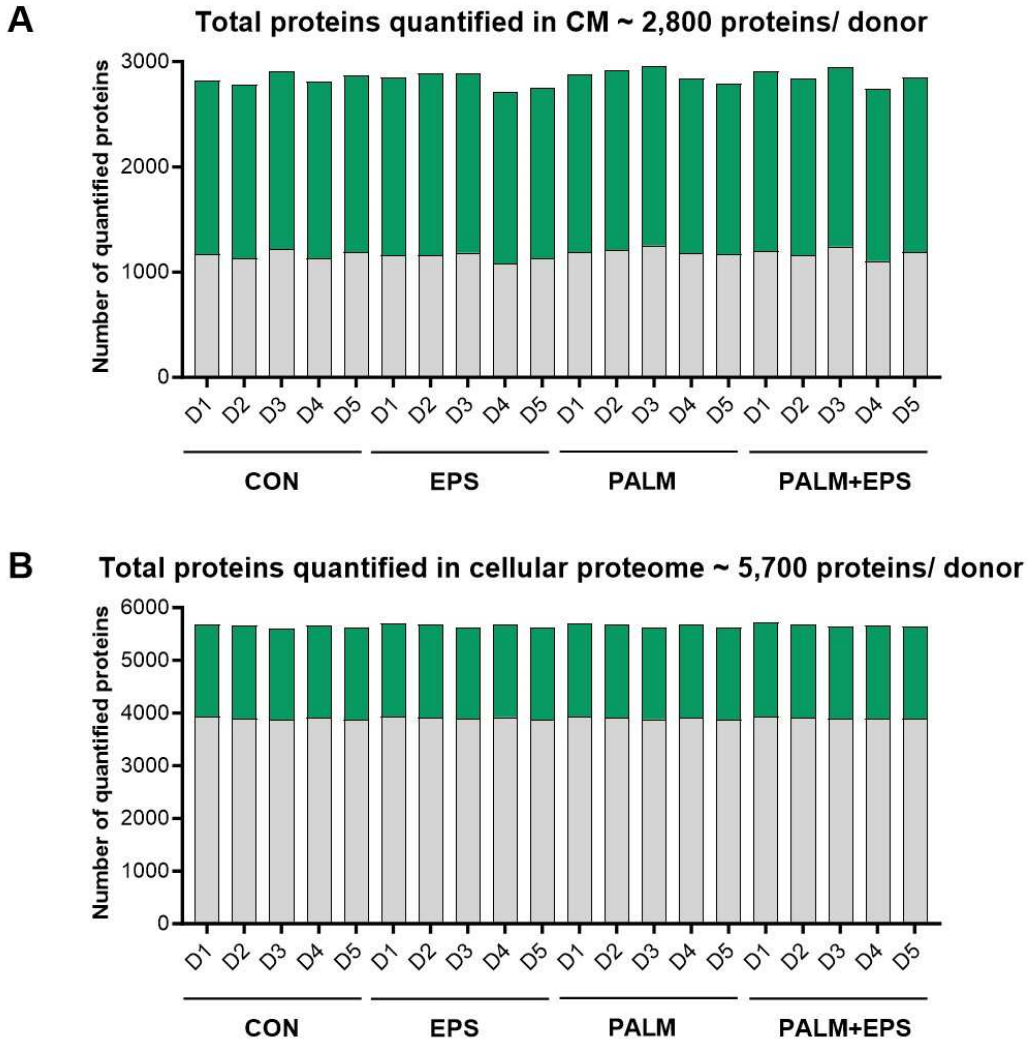

Figure 34: Label free-quantification analyses of proteins in the CM and cellular proteome. Human myotubes were pretreated with either BSA (insulin sensitive cells) or 800 µM palmitate (insulin resistant cells) and then subjected to 6h of low-frequency EPS. The bar graphs show the amount of quantified proteins of HSkMCs obtained from five donors (*n=5*), which were plotted for each condition for both, the secretome **(A)** and the proteome **(B).** All proteins annotated as "predicted secretory myokines" are colored in green in the stacked graph, NP proteins are shown in grey. CM: conditioned media, CON: control, D: donor, EPS: electrical pulse stimulation, HSkMCs: human skeletal muscle cells, NP: non-predicted, PALM: palmitate

3.4.2 EPS-regulated myokines in the muscle secretome of insulin sensitive primary HSkMCs

MS datasets were analyzed as previously described (2.2.6, 2.2.6.1), and secretome data were adjusted for differentially regulated proteins ($p<0.05$) in order to investigate the secretion of contraction-induced myokines from insulin sensitive human myotubes in response to acute low-frequency EPS. We observed that a total of 74 proteins were significantly regulated by EPS, of which 37 proteins were downregulated and 37 proteins were upregulated (Supplemental Figure 1, Figure 35A). All classically secreted myokines are listed in Table 22 below and all unconventionally secreted myokines are given in Supplemental Table 4. Moreover, bioinformatic prediction analysis revealed that 53% were classified as "predicted

secretory myokines", with 24% being classically secreted (SP+) and 29% being unconventionally secreted proteins (SP-, Outcyte+) (Figure 35B).

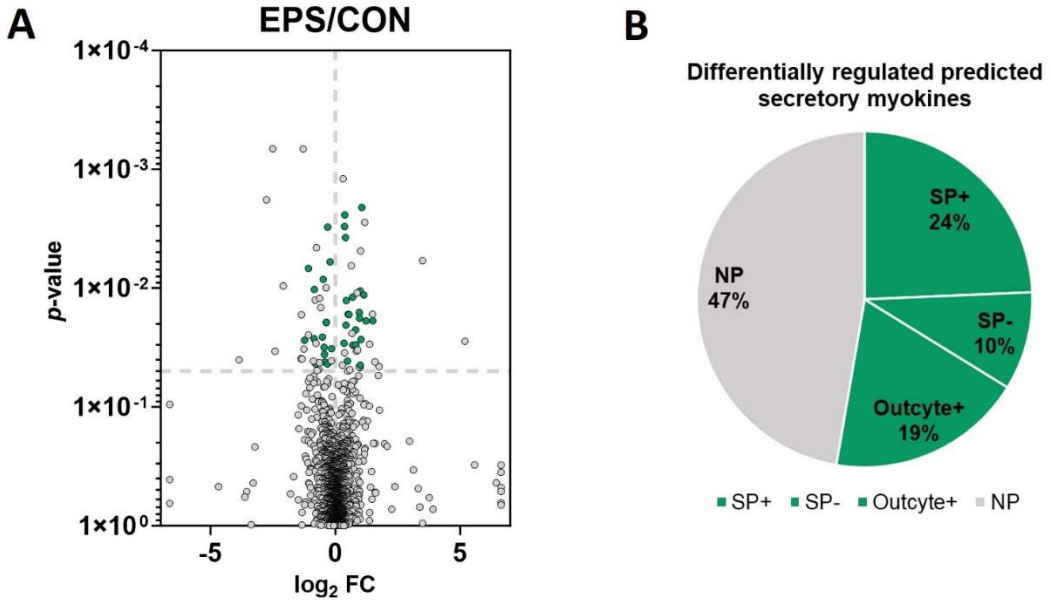

Figure 35: Characterization of the EPS-induced muscle secretome of insulin sensitive human myotubes. Human myotubes were pretreated with BSA (insulin sensitive cells) and then subjected to 6h of low-frequency EPS. **(A)** Volcano plot analysis. **(B)** Bioinformatic prediction analysis using SignalP 6.0, SecretomeP 2.0 and Outcyte 1.0. All proteins annotated as "predicted secretory myokines" are colored in green, while NP proteins are shown in grey. Primary HSkMCs were obtained from five donors *(n=5)*. CON: control, EPS: electrical pulse stimulation, HSkMCs: human skeletal muscle cells, NP: non-predicted, SP+: signal peptide positive, SP-: signal peptide negative

To visualize the EPS-induced differences in the secretome of insulin sensitive cells, Principle Component Analysis (PCA) was performed, which showed that control cells separated clearly from EPS-treated cells (Figure 36A). PCA also shows the variability of the donors with regard to the response to EPS. According to this, donor one (D1) shows the weakest response to EPS treatment compared to all other donors (D2-D5). This behavior is also reflected in the heatmap analysis, where all donors except D1 cluster within the respective condition (CON versus EPS), (Figure 36B).

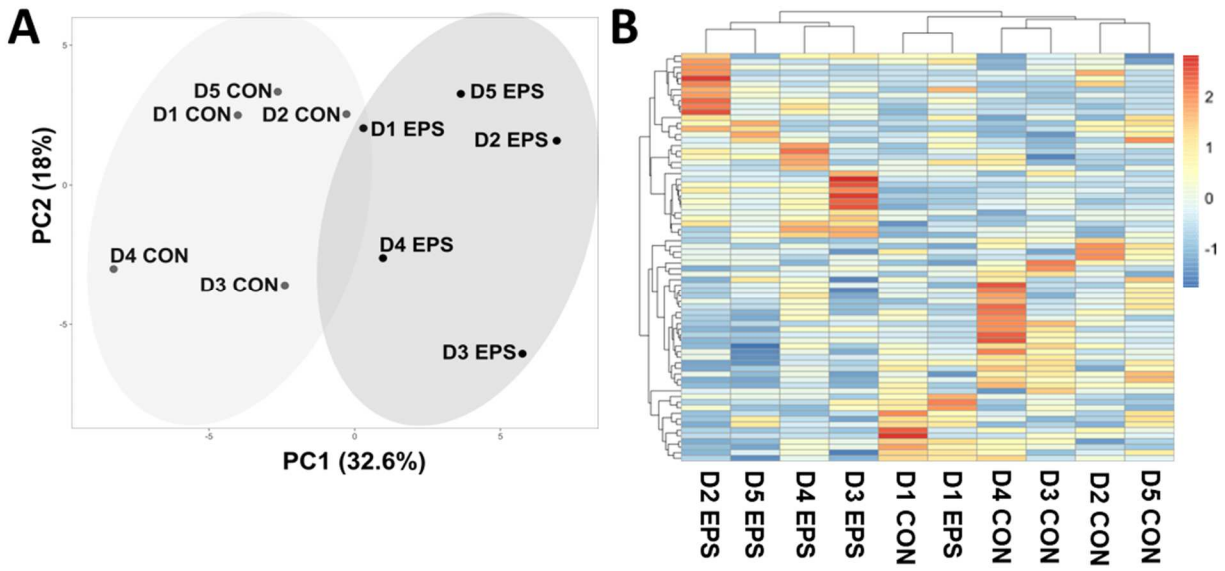

Figure 36: EPS-induced muscle secretome of insulin sensitive myotubes segregates from control. Human myotubes were pretreated with BSA (insulin sensitive cells) and then subjected to 6h of low-frequency EPS. **(A)** PCA of differentially regulated proteins. **(B)** Heat map analysis of differentially regulated proteins. Control secretome is shown in light grey, while EPS-induced secretome is represented in dark grey. Primary HSkMCs were obtained from five donors *(n=5)*. CON: control, EPS: electrical pulse stimulation, HSkMCs: human skeletal muscle cells, PC(A): principal componet (analysis), D: donor

The following Table 22 lists all classically secreted proteins (SP+) that were differentially regulated in response to acute-low frequency EPS in insulin sensitve human myotubes. Data are displayed in order of their log_2 fold change (log_2FC).

Table 22: EPS-regulated classically secreted proteins in the muscle secretome of insulin sensitive HSkMCs obtained from five donors (EPS/CON).

UniProtKB	Gene symbol	Protein description	*p*-value	Log_2FC	Secretion type
Q9BXJ4	C1QTNF3/ CTRP3	Complement C1q tumor necrosis factor-related protein 3	1.88E-02	1.23	SP+
Q14574	DSC3	Desmocollin-3	1.14E-02	1.14	SP+
O75095	MEGF6	Multiple epidermal growth factor-like domains protein 6	2.71E-02	1.03	SP+
A1L4H1	SSC5D	Soluble scavenger receptor cysteine-rich domain-containing protein SSC5D	1.05E-02	1.00	SP+
P05090	APOD	Apolipoprotein D	1.79E-02	0.97	SP+
P00746	CFD	Complement factor D	1.60E-02	0.96	SP+
P48740-2	MASP1	Isoform 2 of Mannan-binding lectin serine protease 1	2.99E-02	0.82	SP+
P05546	SERPIND1	Heparin cofactor 2	3.02E-02	0.7	SP+
Q9H1E1	RNASE7	Ribonuclease 7	1.19E-02	0.69	SP+
O60462	NRP2	Neuropilin-2	1.66E-02	0.51	SP+
P00734	F2	Prothrombin	3.02E-03	0.37	SP+
Q9NZV1	CRIM1	Cysteine-rich motor neuron 1 protein	2.91E-02	0.35	SP+

P07477	PRSS1	Trypsin-1	3.23E-02	-0.15	SP+
O95084	PRSS23	Serine protease 23	6.02E-03	-0.21	SP+
P02749	APOH	Beta-2-glycoprotein 1/ Apolipoprotein H	4.35E-02	-0.32	SP+
Q92484	SMPDL3A	Acid sphingomyelinase-like phosphodiesterase 3a	1.94E-02	-0.36	SP+
Q8WZ75	ROBO4	Roundabout homolog 4	8.41E-03	-0.49	SP+
P02746	C1QB	Complement C1q subcomponent subunit B	6.82E-03	-1.08	SP+

3.4.3 Palmitate-regulated myokines in the muscle secretome of insulin resistant primary HSkMCs

MS datasets were analyzed as previously described (2.2.6, 2.2.6.1), and secretome data were adjusted for differentially regulated proteins ($p<0.05$) in order to investigate alterations in the muscle secretome in insulin resistance. Palmitate-induced significant changes in 170 myokines, of which 81 proteins were downregulated and 89 proteins were upregulated (Supplemental Figure 1, Figure 37A). Bioinformatic predictions analysis revealed that 64% of the differentially regulated proteins were considered as "predicted secretory myokines", of which 22% were classically secreted (SP+) and a majority of 42% were unconventionally secreted (SP-, Outcyte+) (Figure 37B). All classically secreted myokines are listed in Table 23 below and all unconventionally secreted proteins are listed in Supplemental Table 5.

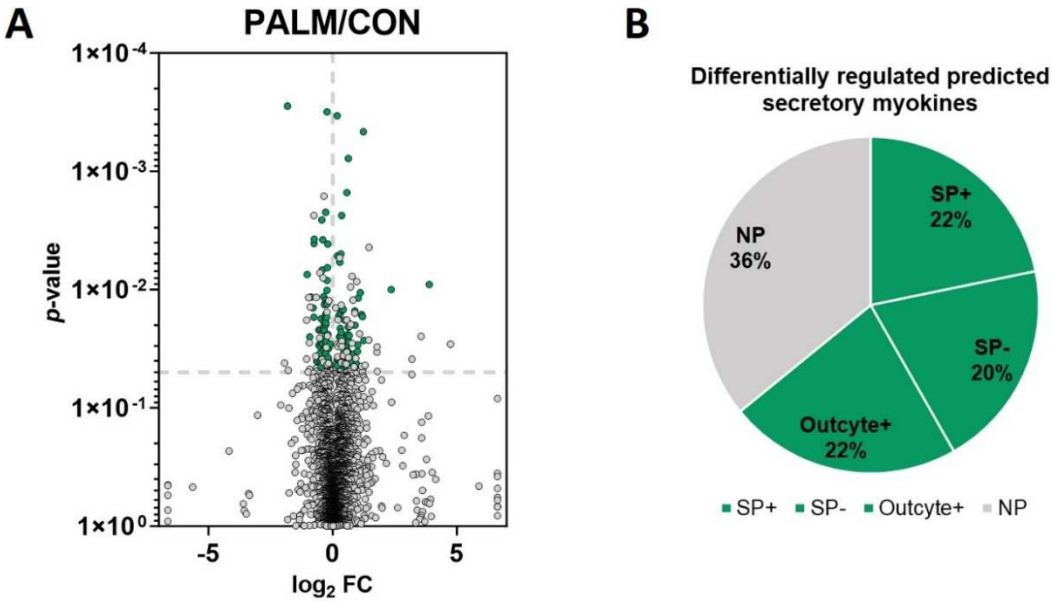

Figure 37: Characterization of the palmitate-induced muscle secretome of insulin resistant human myotubes. Human myotubes were pretreated with either BSA (insulin sensitive cells) or 800 µM palmitate (insulin resistant cells) and starved for 6h in starvation medium. **(A)** Volcano plot analysis. **(B)** Bioinformatic prediction analysis using SignalP 6.0, SecretomeP 2.0 and Outcyte 1.0. All proteins annotated as "predicted secretory myokines" are colored in green, while NP proteins are shown in grey. Primary HSkMCs were obtained from five

donors *(n=5)*. CON: control, PALM: palmitate, HSkMCs: human skeletal muscle cells, NP: non-predicted, SP+: signal peptide positive, SP-: signal peptide negative

PCA showed a clear separation of the palmitate-induced secretome from the control secretome (BSA-treated cells) (Figure 38A). The donor variability was also reflected in the heat map analysis, which showed that the clusters tended to rather group together within each donor, despite their condition (palmitate versus control) (Figure 38B).

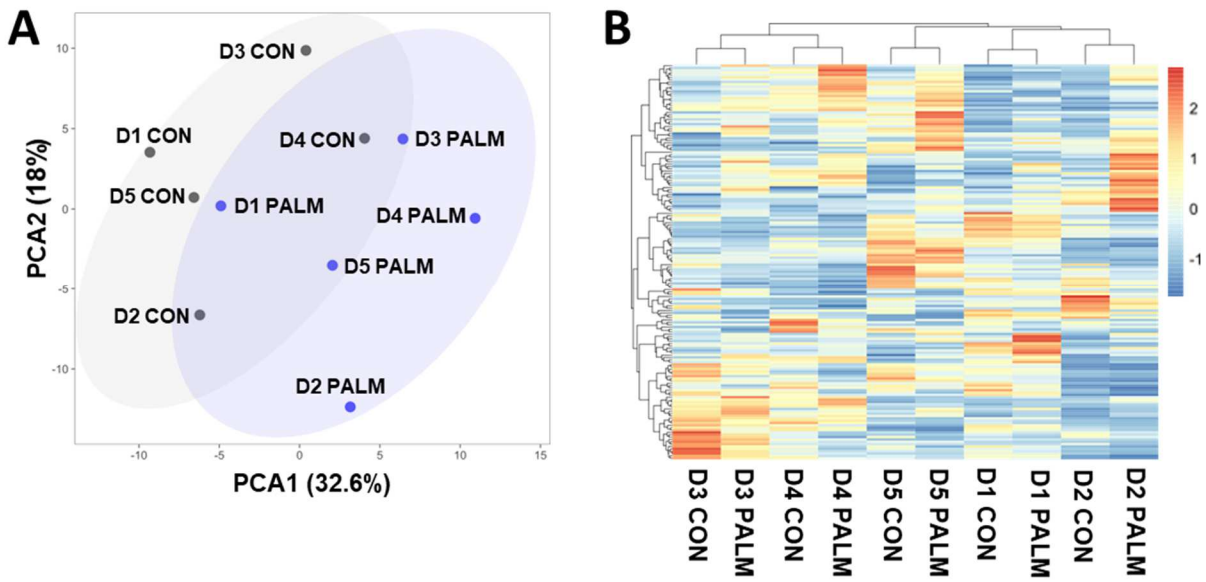

Figure 38: Palmitate-induced muscle secretome segregates from control secretome. Human myotubes were pretreated with either BSA (insulin sensitive cells) or 800 µM palmitate (insulin resistant cells) and starved for 6h in starvation medium. **(A)** PCA of differentially regulated proteins. **(B)** Heat map analysis of differentially regulated proteins. Control secretome is shown in light grey, while palmitate-induced secretome is represented in blue. Primary HSkMCs were obtained from five donors *(n=5)*. CON: control, PALM: palmitate, HSkMCs: human skeletal muscle cells, PC(A): principal componet (analysis), D: donor

Table 23 below lists all "classically secreted proteins" (SP+) that were differentially regulated in response to 12 hours of palmitate treatment in primary human myotubes. Data are presented in order of their log_2 fold change (log_2FC).

Table 23: Palmitate-regulated classically secreted proteins in the muscle secretome of insulin resistant HSkMCs obtained from five donors (PALM/CON).

UniProtKB	Gene symbol	Protein description	*p*-value	Log_2FC	Secretion type
Q14574	DSC3	Desmocollin-3	9.07E-03	3.89	SP+
P49257	LMAN1	Protein ERGIC-53	1.69E-02	1.2	SP+
Q9NS15	LTBP3	Latent-transforming growth factor beta-binding protein 3	3.52E-02	0.83	SP+
Q9BY76	ANGPTL4	Angiopoietin-related protein 4	3.54E-02	0.78	SP+
O15460-2	P4HA2	Isoform IIa of Prolyl 4-hydroxylase subunit alpha-2	4.13E-02	0.77	SP+
Q92896	GLG1	Golgi apparatus protein 1	7.77E-04	0.63	SP+
O75976	CPD	Carboxypeptidase D	1.81E-02	0.48	SP+

Q6UWY0	ARSK	Arylsulfatase K	4.49E-02	0.44	SP+
Q15063	POSTN	Periostin	4.00E-02	0.31	SP+
P11717	IGF2R	Cation-independent mannose-6-phosphate receptor	5.87E-03	0.29	SP+
O14672	ADAM10	Disintegrin and metalloproteinase domain-containing protein 10	2.40E-02	-0.19	SP+
P16070	CD44	CD44 antigen	3.97E-02	-0.2	SP+
P50895	BCAM	Basal cell adhesion molecule	1.32E-02	-0.23	SP+
O00462	MANBA	Beta-mannosidase	1.29E-02	-0.24	SP+
Q14118	DAG1	Dystroglycan 1	1.60E-02	-0.27	SP+
Q24JP5	TMEM132A	Transmembrane protein 132A	1.90E-02	-0.27	SP+
Q96SL4	GPX7	Glutathione peroxidase 7	1.23E-02	-0.28	SP+
P09486	SPARC	SPARC	2.22E-03	-0.28	SP+
Q6EMK4	VASN	Vasorin	3.80E-02	-0.3	SP+
P35555	FBN1	Fibrillin-1	1.34E-02	-0.33	SP+
Q9NWM8	FKBP14	Peptidyl-prolyl cis-trans isomerase FKBP14	2.90E-02	-0.4	SP+
P01008	SERPINC1	Antithrombin-III	2.62E-02	-0.4	SP+
P58215	LOXL3	Lysyl oxidase homolog 3	6.83E-03	-0.42	SP+
P01033	TIMP1	Metalloproteinase inhibitor 1	3.96E-02	-0.42	SP+
P55291	CDH15	Cadherin-15	2.57E-03	-0.44	SP+
P78504	JAG1	Protein jagged-1	2.81E-02	-0.45	SP+
O43155	FLRT2	Leucine-rich repeat transmembrane protein FLRT2	2.18E-02	-0.49	SP+
P20062	TCN2	Transcobalamin-2	3.48E-02	-0.52	SP+
Q8NBK3	SUMF1	Formylglycine-generating enzyme	2.20E-02	-0.56	SP+
Q8IW52	SLITRK4	SLIT and NTRK-like protein 4	4.04E-02	-0.64	SP+
Q9BRK3	MXRA8	Matrix remodeling-associated protein 8	3.74E-03	-0.74	SP+
Q14517	FAT1	Protocadherin Fat 1	4.07E-03	-0.75	SP+
Q92859	NEO1	Neogenin	1.16E-02	-0.87	SP+
Q12907	LMAN2	Vesicular integral-membrane protein VIP36	2.51E-02	-0.92	SP+
Q9UN70	PCDHGC3	Protocadherin gamma-C3	7.46E-03	-1.03	SP+
P09619	PDGFRB	Platelet-derived growth factor receptor beta	2.81E-04	-1.82	SP+

3.4.4 Palmitate-regulated proteins vary in the cellular proteome of different donors

MS datasets were analyzed as previously described (2.2.6, 2.2.6.1), and proteomic data were adjusted for differentially regulated proteins ($p<0.05$). Since the secretome of insulin resistant myotubes showed variability and divergence within the five donors (Figure 38A-B), we sought to determine whether this divergence was also reflected in the palmitate-induced insulin resistant proteome. Venn diagram analysis showed the proportionality of regulated proteins for each donor after treatment with palmitate. A total of 24 common proteins were found to be differentially regulated in all five donors. Most proteins were significantly regulated

(*p*-value<0.05) in donors two, three and five (approx. 1100 – 1900), whereas notably fewer proteins (approx. 500 – 600) were regulated by palmitate in donors one and four (Figure 39A).

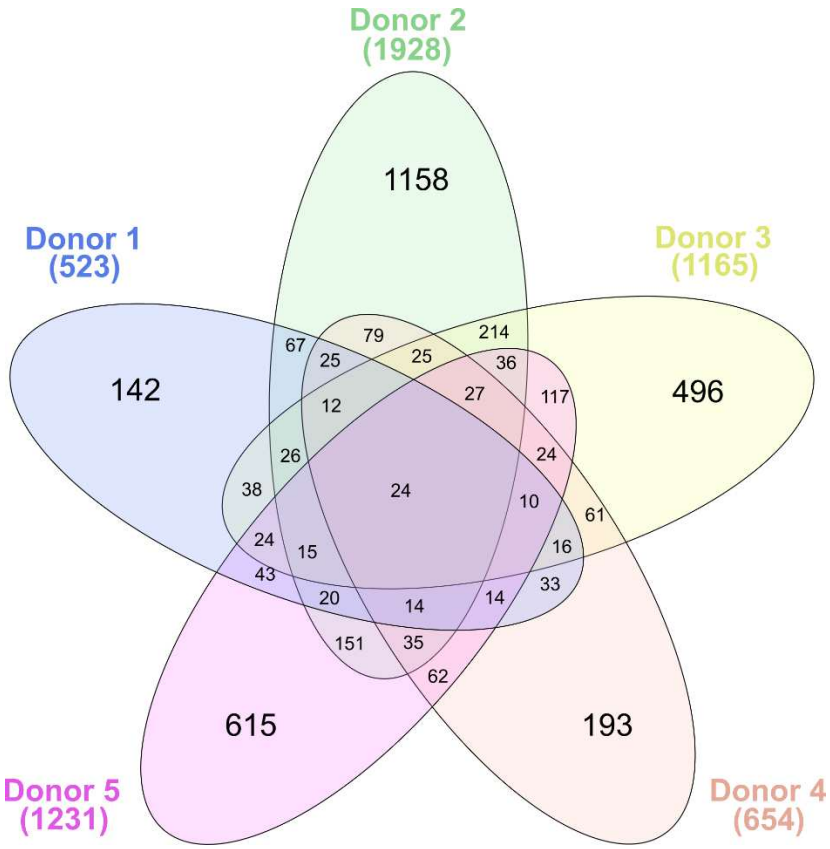

Figure 39: Palmitate-induced differentially regulated proteins in the cellular proteome of each donor. Human myotubes were pretreated with either BSA (insulin sensitive cells) or 800 µM palmitate (insulin resistant cells) and starved for 6h in starvation medium. Venn diagram shows differentially regulated proteins in the cellular proteome of each donor. **p*-value<0.05 was calculated for each donor using one sample *t*-test. The following colors represent the respective donors: blue: donor 1, green: donor 2, yellow: donor 3, orange: donor 4, pink: donor 5

3.4.5 EPS-regulated myokines in muscle secretome of insulin resistant primary HSkMCs

MS datasets were analyzed as previously described (2.2.6, 2.2.6.1), and secretome data were adjusted for differentially regulated proteins (*p*<0.05) in order to investigate alterations in the muscle secretome of insulin resistant human myotubes in response to acute low-frequency EPS. Secretome analysis of EPS-induced CM resulted in 97 differentially regulated myokines, of which 38 proteins were significantly downregulated and 59 proteins were significantly upregulated (Supplemental Figure 1, Figure 40A). Overall, 31% of the differentially regulated proteins were secreted via the classical secretion pathway (SP+), making this secretome dataset the one with the highest percentage of classically secreted proteins. In contrast, 38% (24%, SP-, 14%, Outcyte+) of myokines were classified as unconventionally secreted proteins (Figure 40B). All classically secreted proteins are listed in Table 24 and all unconventionally secreted myokines are listed in Supplemental Table 6.

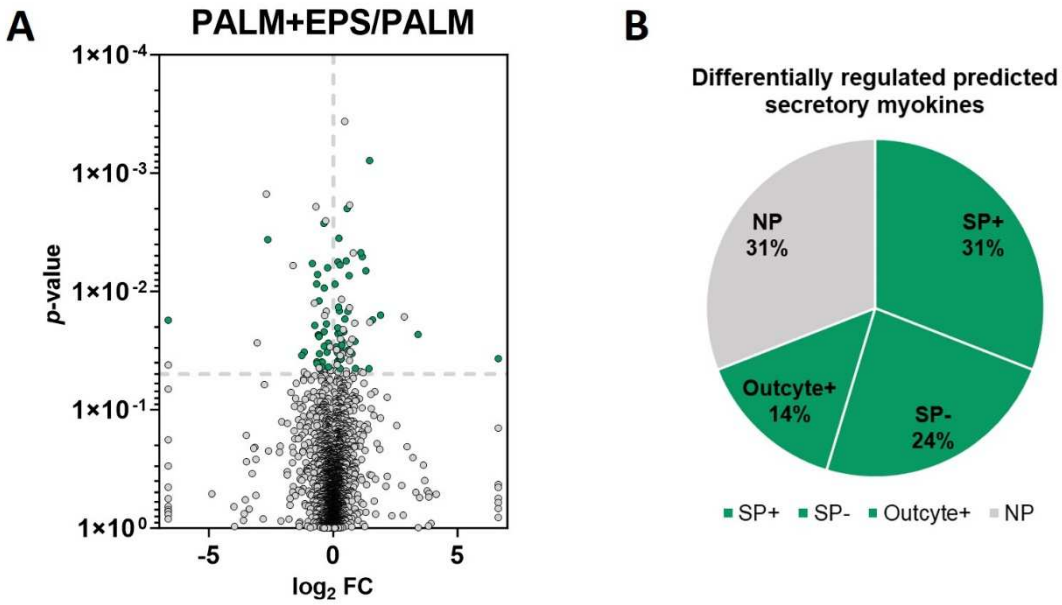

Figure 40: Characterization of the EPS-induced muscle secretome of insulin resistant human myotubes. Human myotubes were pretreated with 800 µM palmitate (insulin resistant cells) and then subjected to 6h of low-frequency EPS. **(A)** Volcano plot analysis. **(B)** Bioinformatic prediction analysis using SignalP 6.0, SecretomeP 2.0 and Outcyte 1.0. All proteins annotated as "predicted secretory myokines" are colored in green, while NP proteins are shown in grey. Primary HSkMCs were obtained from five donors *(n=5)*. PALM: palmitate, EPS: electrical pulse stimulation, HSkMCs: human skeletal muscle cells, NP: non-predicted, SP+: signal peptide positive, SP-: signal peptide negative

Moreover, PCA confirmed that the EPS-induced secretome from insulin resistant myotubes is clearly segregated from the secretome of unstimulated cells (Figure 41A). In this series of experiments, donor five (D5) can be considered an outlier as it does not cluster within the conditions as the other four donors. Heat map analysis showed that protein regulation was variable within the five donors, as protein regulation within the same donor was more similar than within the two conditions tested (Figure 41B).

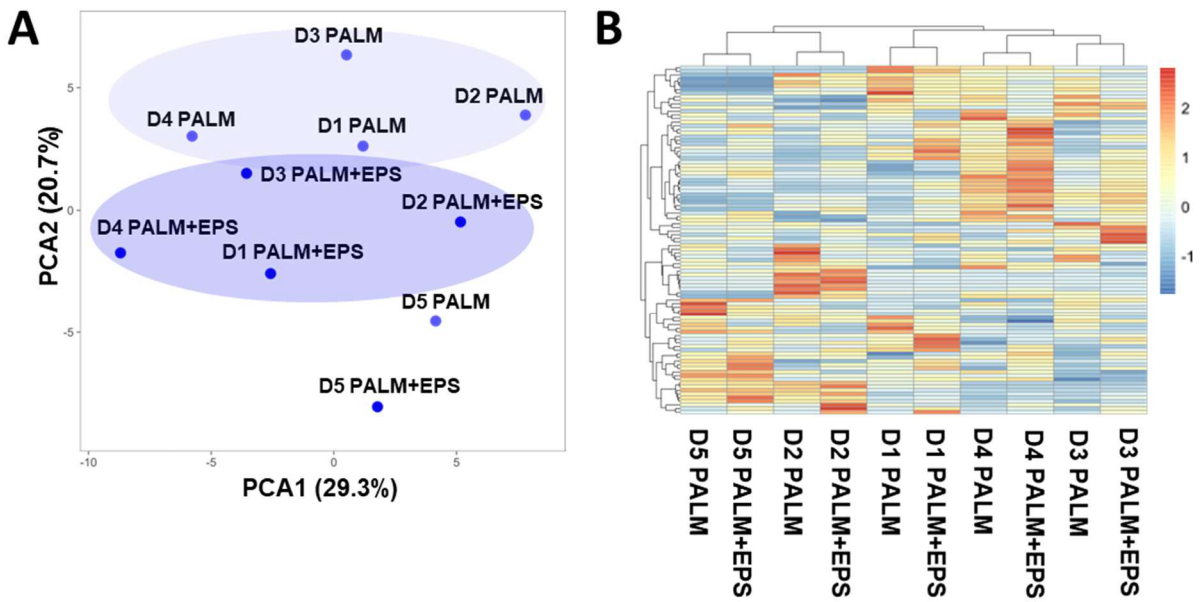

Figure 41: EPS-secretome of insulin resistant cells segregates from insulin resistant control secretome. Human myotubes were pretreated with 800 µM palmitate (insulin resistant cells) and then subjected to 6h of low-frequency EPS. **(A)** PCA of differentially regulated proteins. **(B)** Heat map analysis of differentially regulated proteins. Unstimulated secretome is shown in light blue, while EPS-induced secretome is represented in dark blue. Primary HSkMCs were obtained from five donors *(n=5)*. PALM: palmitate, EPS: electrical pulse stimulation, HSkMCs: human skeletal muscle cells, PC(A): principal componet (analysis), D: donor

Table 24 summarizes all "classically secreted proteins" (SP+) that were differentially regulated in response to acute low-frequency EPS in insulin resistant human myotubes. Data are presented in order of their log_2 fold change (log_2FC).

Table 24: EPS-regulated classically secreted proteins in the muscle secretome of insulin resistant HSkMCs obtained from five donors (PALM+EPS/PALM).

UniProtKB	Gene symbol	Protein description	*p*-value	Log_2FC	Secretion type
Q9P232	CNTN3	Contactin-3	3.70E-02	6.64	SP+
P00738	HP	Haptoglobin	1.59E-02	1.90	SP+
P55058	PLTP	Phospholipid transfer protein	4.50E-02	1.44	SP+
Q14517	FAT1	Protocadherin Fat 1	5.07E-03	1.17	SP+
Q7Z7M0	MEGF8	Multiple epidermal growth factor-like domains protein 8	2.64E-02	0.87	SP+
Q6UW63	POGLUT2	Protein O-glucosyltransferase 2	1.99E-03	0.56	SP+
Q495W5	FUT11	Alpha-(1,3)-fucosyltransferase 11	5.52E-03	0.52	SP+
Q14050	COL9A3	Collagen alpha-3(IX) chain	2.85E-02	0.35	SP+
Q68BL8	OLFML2B	Olfactomedin-like protein 2B	3.71E-02	0.31	SP+
Q6EMK4	VASN	Vasorin	3.56E-03	0.23	SP+
P00746	CFD	Complement factor D	2.27E-02	0.19	SP+
A0A075B6R9	IGKV2D-24	Probable non-functional immunoglobulin kappa variable 2D-24	3.87E-02	0.18	SP+
O95967	EFEMP2	EGF-containing fibulin-like extracellular matrix protein 2	8.66E-03	0.07	SP+

P19320	VCAM1	Vascular cell adhesion protein 1	4.35E-02	-0.19	SP+
Q9UBX5	FBLN5	Fibulin-5	2.72E-02	-0.20	SP+
P07339	CTSD	Cathepsin D	6.31E-03	-0.23	SP+
Q99538	LGMN	Legumain	1.88E-02	-0.27	SP+
P11021	HSPA5	Endoplasmic reticulum chaperone BiP	9.34E-03	-0.36	SP+
Q01459	CTBS	Di-N-acetylchitobiase	2.19E-02	-0.37	SP+
Q9UBP4	DKK3	Dickkopf-related protein 3	3.96E-02	-0.44	SP+
Q14554	PDIA5	Protein disulfide-isomerase A5	4.37E-02	-0.47	SP+
P35625	TIMP3	Metalloproteinase inhibitor 3	3.36E-02	-0.56	SP+
P43235	CTSK	Cathepsin K	2.37E-02	-0.57	SP+
P14314	PRKCSH	Glucosidase 2 subunit beta	7.18E-03	-0.63	SP+
Q96HD1-2	CRELD1	Isoform 2 of Protein disulfide isomerase CRELD1	3.93E-02	-0.66	SP+
O15460-2	P4HA2	Isoform IIa of Prolyl 4-hydroxylase subunit alpha-2	1.94E-02	-0.74	SP+
P25445	FAS	Tumor necrosis factor receptor superfamily member 6	5.81E-03	-0.84	SP+
P61812	TGFB2	Transforming growth factor beta-2 proprotein	3.26E-02	-1.17	SP+
Q14574	DSC3	Desmocollin-3	3.64E-03	-2.63	SP+
P19876	CXCL3	C-X-C motif chemokine 3	1.75E-02	-6.64	SP+

3.4.6 EPS-regulated myokines in muscle secretome of insulin sensitive versus insulin resistant primary HSkMCs

MS datasets were analyzed as previously described (2.2.6, 2.2.6.1), and secretome data were adjusted for differentially regulated proteins ($p<0.05$) to directly compare the EPS-induced secretomes of contracting insulin sensitive versus insulin resistant human myotubes. MS analysis of the CM revealed 304 myokines that were differentially regulated in response to EPS, of which 87 proteins were significantly downregulated and 217 were significantly upregulated (Supplemental Figure 1, Figure 42A). In total, 52% were predicted “secretory proteins”, of which 23% were classically secreted and 29% were unconventionally secreted (SP-, 14%; Outcyte+, 15%) myokines (Figure 42B). Classically secreted proteins are shown in Table 25 below and unconventionally secreted proteins are listed in Supplemental Table 7.

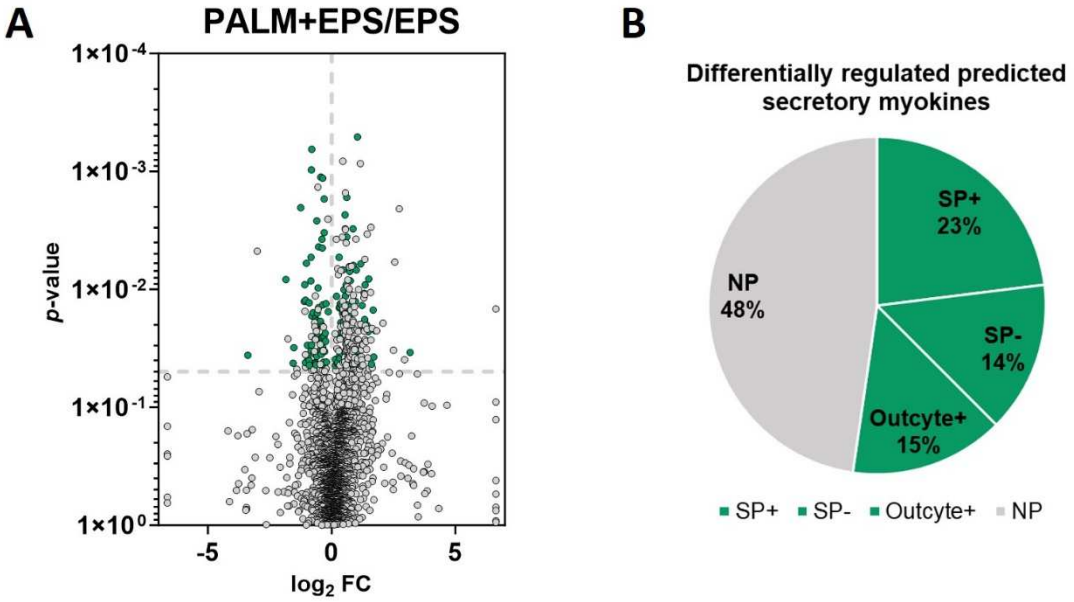

Figure 42: Characterization of the EPS-induced muscle secretome of insulin resistant versus insulin sensitive human myotubes. Human myotubes were pretreated with either BSA (insulin sensitive cells) or 800 µM palmitate (insulin resistant cells) and then subjected to 6h of low-frequency EPS. **(A)** Volcano plot analysis. **(B)** Bioinformatic prediction analysis using SignalP 6.0, SecretomeP 2.0 and Outcyte 1.0. All proteins annotated as "predicted secretory myokines" are colored in green, while NP proteins are shown in grey. Primary HSkMCs were obtained from five donors *(n=5)*. PALM: palmitate, EPS: electrical pulse stimulation, HSkMCs: human skeletal muscle cells, NP: non-predicted, SP+: signal peptide positive, SP-: signal peptide negative

PCA confirmed our hypothesis that the contraction-induced secretome of insulin resistant and insulin sensitive human myotubes differs, which was reflected in PCA by a clear segregation of both secretomes in response to acute low-frequency EPS (Figure 43A). Again, intra-donor variability was observed in response to EPS, with D4 and D3 being the most responsive to stimulation and also more similar in protein regulation than the other donors, as reflected in the heatmap analysis (Figure 43B).

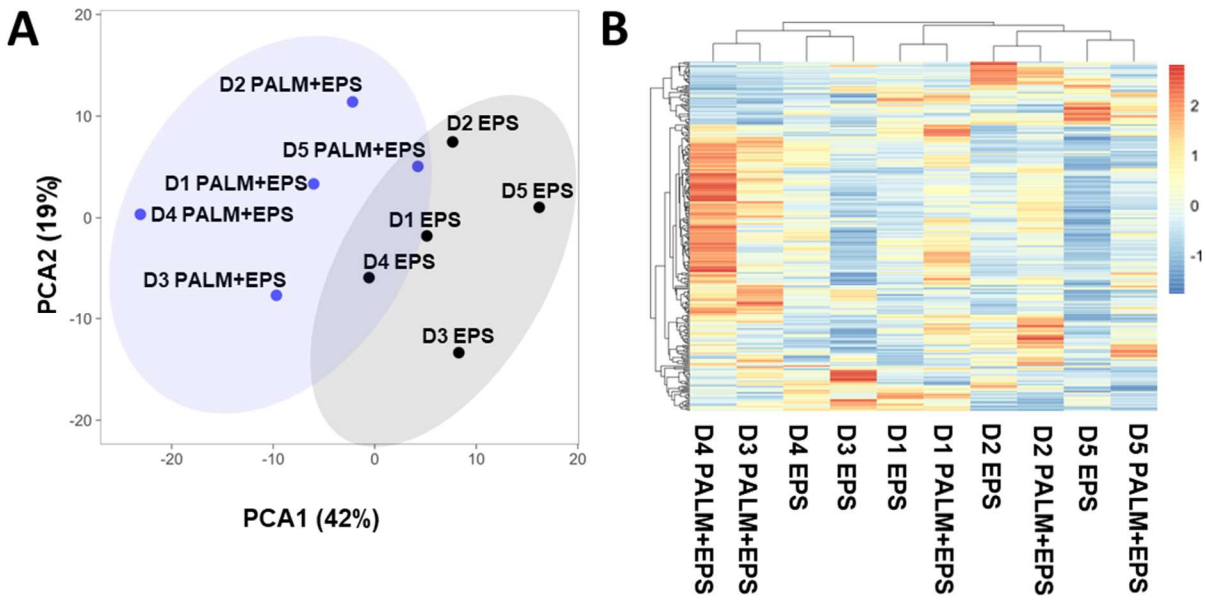

Figure 43: EPS-induced muscle secretome of insulin sensitive cells segregates from insulin resistant cells. Human myotubes were pretreated with either BSA (insulin sensitive cells) or 800 µM palmitate (insulin resistant cells) and then subjected to 6h of low-frequency EPS. **(A)** PCA of differentially regulated proteins. **(B)** Heat map analysis of differentially regulated proteins. EPS-induced secretome of insulin resistant cells is shown in light blue, while EPS-induced secretome of insulin sensitive cells is represented in grey. Primary HSkMCs were obtained from five donors *(n=5)*. PALM: palmitate, EPS: electrical pulse stimulation, HSkMCs: human skeletal muscle cells, PC(A): principal componet (analysis), D: donor

Table 25 shows all "classically secreted proteins" (SP+) that were differentially regulated in response to acute low-frequency EPS in insulin resistant and insulin sensitve human myotubes. Data are presented in order of their log_2 fold change (log_2FC).

Table 25: EPS-regulated classically secreted proteins in the muscle secretome of insulin resistant versus insulin sensitive HSkMCs obtained from five donors (PALM+EPS/EPS).

UniProtKB	Gene symbol	Protein description	*p*-value	Log_2FC	Secretion type
Q9BY76	ANGPTL4	Angiopoietin-related protein 4	9.16E-03	1.35	SP+
Q7Z7M0	MEGF8	Multiple epidermal growth factor-like domains protein 8	3.76E-02	1.10	SP+
Q6PCB0	VWA1	von Willebrand factor A domain-containing protein 1	3.34E-02	1.07	SP+
Q4ZHG4	FNDC1	Fibronectin type III domain-containing protein 1	4.28E-02	1.01	SP+
P50454	SERPINH1	Serpin H1	6.25E-03	0.88	SP+
Q9UBS4	DNAJB11	DnaJ homolog subfamily B member 11	3.79E-02	0.85	SP+
Q92841	DDX17	Probable ATP-dependent RNA helicase DDX17	2.67E-02	0.82	SP+
P11117	ACP2	Lysosomal acid phosphatase	1.66E-03	0.61	SP+
P13674	P4HA1	Prolyl 4-hydroxylase subunit alpha-1	9.15E-03	0.59	SP+
Q14697	GANAB	Neutral alpha-glucosidase AB	2.27E-02	0.56	SP+

Q9NYU2	UGGT1	UDP-glucose:glycoprotein glucosyltransferase 1	1.14E-02	0.55	SP+
Q9UNW1	MINPP1	Multiple inositol polyphosphate phosphatase 1	1.61E-02	0.51	SP+
P04062	GBA1	Lysosomal acid glucosylceramidase	1.01E-02	0.50	SP+
P30533	LRPAP1	Alpha-2-macroglobulin receptor-associated protein	1.33E-02	0.35	SP+
P43026	GDF5	Growth/differentiation factor 5	3.69E-02	0.32	SP+
P11717	IGF2R	Cation-independent mannose-6-phosphate receptor	1.43E-02	0.31	SP+
O00469-2	PLOD2	Isoform 2 of Procollagen-lysine,2-oxoglutarate 5-dioxygenase 2	4.23E-02	0.23	SP+
O60568	PLOD3	Multifunctional procollagen lysine hydroxylase and glycosyltransferase LH3	4.42E-02	0.15	SP+
Q6EMK4	VASN	Vasorin	4.13E-02	-0.21	SP+
P28799	GRN	Progranulin	1.32E-02	-0.23	SP+
Q9UBR2	CTSZ	Cathepsin Z	2.76E-02	-0.24	SP+
Q9NZV1	CRIM1	Cysteine-rich motor neuron 1 protein	3.36E-02	-0.29	SP+
Q16270	IGFBP7	Insulin-like growth factor-binding protein 7	3.30E-03	-0.30	SP+
Q06828	FMOD	Fibromodulin	1.71E-03	-0.30	SP+
P15151	PVR	Poliovirus receptor	2.49E-02	-0.31	SP+
P08123	COL1A2	Collagen alpha-2(I) chain	4.14E-02	-0.33	SP+
P49908	SELENOP	Selenoprotein P	1.14E-03	-0.36	SP+
O00115	DNASE2	Deoxyribonuclease-2-alpha	1.35E-02	-0.36	SP+
Q15262-4	PTPRK	Isoform 4 of Receptor-type tyrosine-protein phosphatase kappa	2.53E-02	-0.37	SP+
Q8NBK3	SUMF1	Formylglycine-generating enzyme	4.46E-03	-0.38	SP+
Q6NW40	RGMB	Repulsive guidance molecule B	2.04E-02	-0.38	SP+
P09486	SPARC	SPARC	3.77E-03	-0.39	SP+
O14672	ADAM10	Disintegrin and metalloproteinase domain-containing protein 10	2.62E-02	-0.42	SP+
Q9BZM5	ULBP2	UL16-binding protein 2	2.84E-02	-0.42	SP+
P43235	CTSK	Cathepsin K	1.12E-03	-0.44	SP+
P08603	CFH	Complement factor H	2.64E-02	-0.44	SP+
P01008	SERPINC1	Antithrombin-III	1.87E-02	-0.45	SP+
P01130	LDLR	Low-density lipoprotein receptor	3.27E-02	-0.46	SP+
P01033	TIMP1	Metalloproteinase inhibitor 1	1.43E-02	-0.53	SP+
Q8N158	GPC2	Glypican-2	1.92E-02	-0.55	SP+
Q9HAT2	SIAE	Sialate O-acetylesterase	9.72E-03	-0.55	SP+
P30530	AXL	Tyrosine-protein kinase receptor UFO	2.50E-02	-0.57	SP+
P78504	JAG1	Protein jagged-1	1.59E-02	-0.58	SP+
P05121	SERPINE1	Plasminogen activator inhibitor 1	2.49E-02	-0.61	SP+
Q9BRK3	MXRA8	Matrix remodeling-associated protein 8	1.84E-02	-0.61	SP+
P48307	TFPI2	Tissue factor pathway inhibitor 2	2.21E-02	-0.62	SP+

O94985	CLSTN1	Calsyntenin-1	4.36E-02	-0.63	SP+
P01034	CST3	Cystatin-C	4.26E-02	-0.65	SP+
P36222	CHI3L1	Chitinase-3-like protein 1	4.18E-02	-0.66	SP+
P24592	IGFBP6	Insulin-like growth factor-binding protein 6	1.77E-02	-0.66	SP+
Q9UN70	PCDHGC3	Protocadherin gamma-C3	3.50E-02	-0.72	SP+
Q96FE7	PIK3IP1	Phosphoinositide-3-kinase-interacting protein 1	1.68E-02	-0.80	SP+
P36955	SERPINF1	Pigment epithelium-derived factor	2.96E-02	-0.81	SP+
Q01459	CTBS	Di-N-acetylchitobiase	9.68E-04	-0.82	SP+
Q8TER0	SNED1	Sushi, nidogen and EGF-like domain-containing protein 1	3.33E-02	-0.83	SP+
O60462	NRP2	Neuropilin-2	5.34E-03	-0.83	SP+
P22304	IDS	Iduronate 2-sulfatase	8.49E-03	-0.84	SP+
P09958	FURIN	Furin	4.39E-02	-0.9	SP+
P32004	L1CAM	Neural cell adhesion molecule L1	1.30E-02	-0.91	SP+
P05155	SERPING1	Plasma protease C1 inhibitor	4.02E-02	-0.91	SP+
P34096	RNASE4	Ribonuclease 4	3.80E-02	-0.97	SP+
O95633	FSTL3	Follistatin-related protein 3	2.97E-02	-0.98	SP+
Q9BQT9	CLSTN3	Calsyntenin-3	5.99E-03	-1.02	SP+
Q13087	PDIA2	Protein disulfide-isomerase A2	4.18E-02	-1.06	SP+
Q12907	LMAN2	Vesicular integral-membrane protein VIP36	1.23E-02	-1.06	SP+
P04216	THY1	Thy-1 membrane glycoprotein	9.13E-03	-1.09	SP+
Q10588	BST1	ADP-ribosyl cyclase/cyclic ADP-ribose hydrolase 2	1.27E-02	-1.10	SP+
P13500	CCL2	C-C motif chemokine 2	2.03E-03	-1.25	SP+
P47972	NPTX2	Neuronal pentraxin-2	8.25E-03	-1.85	SP+
P52799	EFNB2	Ephrin-B2	3.61E-02	-3.39	SP+

Furthermore, we sought to evaluate the overlap of EPS-induced myokines in the secretome of insulin sensitive and insulin resistant human myotubes. The comparative analysis was performed as described in 2.2.6.1. Interestingly, only four myokines overlapped in the contraction-induced secretomes of both cell models, confirming our hyothesis that the contraction-induced secretomes are distinct under physiological and pathological conditions (Figure 44). The following proteins were induced by EPS in both cell models: complement factor D (CFD) and desmocollin-3 (DSC3), both predicted as "classical secreted myokines" (SP+), translation initiation factor eIF-2B subunit alpha (EIF2B1), which was secreted unconventionally (Outcyte+), and another capZ-interacting protein (RCSD1), which was not predicted as a "secretory myokine" (NP).

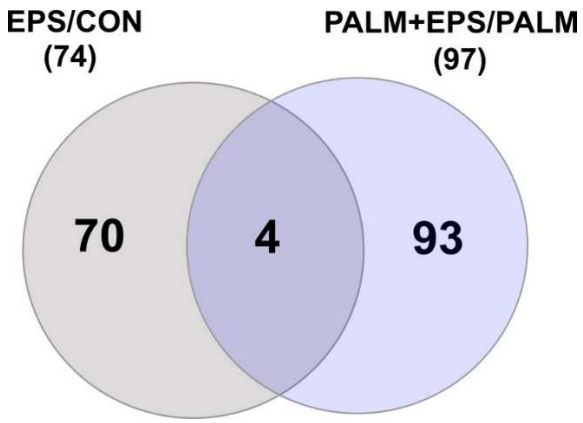

Figure 44: Comparison of EPS-regulated myokines in the CM of insulin sensitive versus insulin resistant human myotubes. Human myotubes were pretreated with either BSA (insulin sensitive cells) or 800 µM palmitate (insulin resistant cells) and then subjected to 6h of low-frequency EPS. Venn diagram analysis shows the differentially regulated proteins by EPS in both muscle secretomes. Secretome of EPS-treated insulin sensitive cells is shown in grey, while secretome of EPS-treated insulin resistant cells is displayed in blue. Primary HSkMCs derived from five donors *(n=5)*. Analysis was performed based on UniprotKB IDs. CON: control, EPS: electrical pulse stimulation, HSkMCs: human skeletal muscle cells, PALM: palmitate, CM: conditioned media

4 Discussion

Skeletal muscle functions as an endocrine organ, producing and secreting myokines in an autocrine, paracrine and endocrine manner. Previous studies have shown that myokines mediate crosstalk between skeletal muscle and other organs to regulate metabolic homeostasis and therefore may serve as potential prognostic biomarkers for future therapies of metabolic diseases (e.g. T2DM, insulin resistance) (41-43). In particular, myokines released in response to exercise (exerkines), are thought to mediate the health-promoting effects of exercise, such as improved insulin sensitivity and glucose metabolism (48). Therefore, in-depth analysis of the myokinome using a non-targeted approach is of great importance to contribute to the knowledge of the muscle secretome and to discover novel myokines associated with exercise and metabolic diseases.

Previous proteomic studies have followed this approach by performing muscle secretome analyses of CM derived from different cell culture models using high-resolution MS (52). The most commonly used cell culture models for the analysis of myokine secretion under physiological and pathological conditions are murine C2C12 cells and primary HSkMCs, in addition to the rat L6 myoblast cell line. Since the secretion profile of myokines is altered in disease or after strength and endurance training, recent MS-based studies have aimed to characterize the muscle secretome along its changes during myogenesis (206-208), different *in vivo* exercise interventions (209, 210) and obesity (211) to expand the knowledge of the myokinome in heath and disease.

4.1 Contraction-induced muscle secretomes of C2C12 cells and HSkMCs differ

The first objective of this thesis was to compare the muscle secretomes of murine C2C12 and human myotubes after acute low-frequency EPS exposure, as they are widely used as skeletal muscle models despite limited comparative studies (179). To date, only two MS-based studies have investigated the effects of EPS on the muscle secretome of C2C12 and human myotubes, both using chronic low-frequency EPS protocols (70, 192), but none of these studies directly compared muscle secretomes across cell culture models. This study fills this gap by comparing and analyzing the secretomes of contracting C2C12 and human myotubes after acute low-frequency EPS using high-resolution MS, providing new insights into the muscle secretome after an acute bout of exercise.

C2C12 and human myotubes, obtained from three donors were exposed to acute low-frequency EPS, the supernatant was collected and processed within the bottom-up proteomics workflow. To date, hundreds of myokines have been identified using high-resolution MS (212).

In this study, we compared our data with data from the literature, resulting in the identification of 1,440 and 385 novel myokines secreted by murine and human myotubes, respectively. LC-MS/MS secretome analysis further revealed that the murine and human muscle secretomes overlap in 2,556 proteins, with 80% of human myokines also detected in the murine secretome. However, C2C12 cells secreted a larger amount of proteins (5,710), of which 12% were classified as “classically secreted” (SP+). In contrast, human myotubes secreted fewer proteins (3,285), but twice as many myokines were classified as “SP+” proteins as in C2C12 cells, suggesting that the human species secretes a larger number of myokines through the classical secretory pathway. Comparison of the secretome and proteome data showed that the C2C12 secretome is similar to the proteome, as demonstrated by a large overlap of 4,718 proteins (83%). Interestingly, GOCC analysis revealed that the C2C12 secretome and proteome were much more similar in cellular components than in HSkMCs. A possible explanation may be that a greater amount of lysed cells was present in the C2C12 secretome, however, no morphological damage to the cells was observed, nor were higher levels of LDH measured in the supernatant. Another possible reason could be that myokines secreted by C2C12 cells follow a different secretion pattern compared to human cells. We observed that twice as many myokines were secreted via the classical secretory pathway in HSkMCs (24%) compared to C2C12 cells, whereas the percentage of unconventionally secreted myokines was similar in both species (38-40%), suggesting that C2C12 cells have a different secretion pattern than HSkMCs. This theory could be experimentally validated by exposing both cell culture models to brefeldin A, an inhibitor of protein trafficking via the classical secretory pathway (ER-to-Golgi). Comparative analysis would reveal whether the same number of myokines is secreted via the classical pathway in both species of whether protein secretion routes are distinct. Furthermore, GOCC analysis showed that the cellular components of secreted proteins in both species are different with respect to myokines annotated as “extracellular exosomes” and “mitochondrial proteins”. While the amount of mitochondrial proteins in the murine secretome and proteome was very similar, this was not observed for the HSkMCs. One possibility could be that more mitochondrial proteins are expressed in the C2C12 cells and therefore more proteins are secreted. A recent study showed that whole mitochondria can be released into the extracellular space by vesicular trafficking (213). This suggests that mitochondrial proteins most likely were released via UPS pathways involving vesicular structures (exosomes), which may be one explanation why less myokines were secreted via the classical secretory pathway in the C2C12 secretome. This speculation that secretion mechanisms differ between C2C12 cells and HSKMCs could be further tested by measuring mitochondrial proteins in the supernatant of both cell culture models using targeted assays such as ELISA or MIA. It is also striking that the proportion of extracellular exosomes in the HSkMC secretome is very high (>1000 proteins), whereas the proportion of proteins with this annotation in the C2C12

secretome is very low (approx. 50), suggesting that murine myokines are less secreted by exosomes (Type III pathway) and perhaps more secreted using other UPS pathways. However, bioinformatic tools such as SignalP, SecretomeP, Outcyte and GO are often used to predict protein secretion based on algorithms, but the validation of large MS-datasets remains a major challenge as most of the detected proteins are not yet annotated as “bonafide secreted proteins”, therefore results obtained by computational filtering should be interpreted with caution as these tools have their limitations (214). Grube et al. previously exposed C2C12 myotubes to brefeldin A treatment and suggested that bioinformatics tools (SignalP) detects classically secreted proteins with 93% certainty (215), so additional validation of protein secretion through experimental approaches may be a relevant aspect to consider before analyzing MS secretome data sets.

Furthermore, acute low-frequency EPS induced 518 differentially regulated myokines in the C2C12 secretome, while 336 myokines were differentially regulated in the human secretome. The majority of proteins were upregulated in the secretome of both cell models (C2C12: 346 proteins; HSkMCs: 199 proteins). Interestingly, the bioinformatic prediction analysis for EPS-induced myokines was very similar for both species. In fact, 11-16% of all “predicted secretory proteins” were secreted via the classical secretion pathway, while 42-45% were secreted via UPS pathways, indicating that both cells models responded similarly to the EPS treatment. Again, GOCC analysis revealed differences in the cellular components of contracting myotubes from C2C12 cells and HSkMCs, showing that twice as many mitochondrial proteins were secreted by C2C12 compared to HSkMCs, while in HSkMCs markedly more proteins were released by extracellular exosomes, suggesting that secretion mechanism in both cell models are distinct.

EPS-induced changes in the murine and human muscle secretome were comparable, but only 40 common myokines were regulated by EPS in both muscle secretomes, suggesting that proteins induced by acute low-frequency EPS differ in each cell culture model. We also compared our acute (6h) exercise model with a previously used chronic (24h) exercise model from the literature. Gonzalez-Franquesa et al. analyzed the muscle secretome of C2C12 myotubes after chronic exposure to EPS (11.5 V, 1 Hz, 2 ms) for 24 hours and quantified 75 myokines in the CM that were differentially regulated by EPS (192). Comparison of their results with ours showed that although the same EPS settings (11.5 V, 1 Hz, 2 ms) were used, only nine common proteins were detected in both secretomes after acute and chronic EPS, indicating that the duration of stimulation plays a critical role in EPS-induced protein secretion. Interestingly, among these nine common myokines was gremlin-1, a novel adipo-myokine that will be discussed in more detail in Section 4.4. Similar results were obtained for human myotubes when our EPS protocol was compared with another EPS protocol from the literature,

but it should be noted that the EPS settings were not identical. Mengeste et al. used a chronic low-frequency EPS protocol (24h, 10 V, 0.1 Hz, 2 ms) on human myotubes, which resulted in the quantification of 149 differentially regulated myokines by MS-analysis (70). When comparing our data with theirs, an overlap of only 10 myokines was found in the CM of contracting human myotubes, most likely due to the different EPS parameters as well as the different exposure times (6h *vs* 24h), suggesting that the composition of the muscle secretome is altered in response to different types of exercise. Furthermore, it should be kept in mind that a comparison of MS data is generally only relative, as the samples were processed in different proteomics workflows and the analyses were performed on different devices with different technical settings. In addition, cell culture conditions vary with respect to the cell culture models, passages, media, and donors used in each study. Comparative studies of the two cell models are rare, although C2C12 cells and HSkMCs are the most commonly used cell systems, especially for studying exercise-related effects in muscle. Abdelmoez et al. directly compared C2C12 and human myotubes at the transcriptomic level. Using the same EPS settings (40 V, 2 ms, 1 Hz) as we did, myotubes were exposed to EPS (3h) and mRNA expression levels of contraction-responsive genes were found to be differentially regulated in both cell models (166), suggesting that acute low-frequency EPS-induced differences can already by detected at the mRNA level.

To validate contractile activity in murine C2C12 and primary human myotubes after an acute bout of exercise *in vitro*, changes in AMPKα activity at the major regulatory phosphorylation site Thr-172 were detected by Western blot analysis. In human myotubes, acute low-frequency EPS (6h, 40 V, 1 Hz, 2 ms) significantly increased AMPKα (Thr172) phosphorylation, which is consistent with previous data from Christensen et al. showing the same effect after exposing human myotubes to the same EPS (6h, 40 V, 1 Hz, 2 ms) protocol (177). Another study reported increased AMPKα activity after exposure to acute (8h) and chronic (24h) low-frequency EPS (11.5 V, 1 Hz, 2 ms) in primary human myotubes, showing significant changes in AMPKα phosphorylation (Thr172), with the highest activity after eight hours (171). The same acute low-frequency EPS protocol was used for C2C12 myotubes in this thesis, except that the voltage settings were changed from 40 V to 11.5 V, which was necessary to compare the MS-secretome data of C2C12 cells from this study with the literature. EPS (6h, 11.5 V, 1 Hz, 2 ms) notably increased AMPKα phosphorylation (Thr172) in C2C12 myotubes, but without statistical significance, which may be due to the lower number of experiments performed for C2C12 cells compared to HSkMCs. Another possible reason could be that AMPKα activity in murine C2C12 cells significantly increases only after long-term chronic exposure to EPS (> 24 hours), which was previously shown when C2C12 myotubes were exposed to the same EPS parameters (11.5 V, 1 Hz, 2 ms) (191), suggesting that the exposure time of EPS significantly affects AMPKα activity, which seems to be regulated differently in both cell models (C2C12 *vs*

HSkMCs). However, the use of EPS as an *in vitro* contraction model has limitations, as not all *in vivo* characteristics of skeletal muscle can be simulated. Physiological contraction is caused by the involvement of motor neurons and neuromuscular junctions (216), whereas *in vitro* contraction is induced by electrical impulses due to the lack of interaction with other cells. Cell culture systems also lack other physiological features such as blood flow and innervation, which are essential for feedback regulation to meet the metabolic needs of the working muscle. In addition, *in vivo* muscle cells are belted by connective tissue and extracellular matrix that are important characteristics in terms of muscle contraction and regulation of physiological functions that are lacking in cell culture models (217). As the study of primary HSkMCs may provide an even better understanding of the health-promoting effects of exercise in humans, it remains inevitable to further investigate the role of myokines by non-targeted MS-based approaches and in-depth analyses regarding their role in exercise adaptations and molecular functions.

4.2 The muscle secretomes of insulin sensitive and insulin resistant human myotubes differ

To date, only two MS-based secretome studies have investigated the muscle secretome of insulin resistant muscle cells, both using rodent skeletal muscle cell lines (C2C12 and L6) pretreated with palmitate to induce insulin resistance (200, 205). The FFA palmitate has been extensively studied in the context of insulin resistance over the last two decades and has been shown to be a suitable model to simulate insulin resistance *in vitro* (167, 218). Since HSkMCs provide characteristics closer to native muscle (e.g. donor variability), the second aim of this thesis was to generate insulin resistant human myotubes obtained by five donors by exposure to palmitate (800 µM, 12 hours in starvation medium). Subsequently, the CM was processed within the bottom-up proteomics workflow and analyzed by high-resolution MS to unravel the complex network of the muscle secretome of lipid-induced insulin resistant human myotubes and to extend the knowledge gained to the human system. Muscle secretome analysis of insulin sensitive and resistant human myotubes revealed the presence of 4,185 myokines, of which 865 proteins were considered as “classically secreted proteins” (SP+) and 1,471 proteins were assigned to UPS pathways (SP-, Outcyte-). This was further confirmed by GOCC analysis, showing that the majority of myokines were annotated as “extracellular exosomes”, “plasma membrane”, “vesicles” or “mitochondria”, indicating that most myokines were secreted via UPS pathways, for instance using Type III organelle-based translocation to traffic in vesicles (e.g. exosomes) towards the plasma membrane. Palmitate differentially regulated 170 myokines, of which 22% trafficked to the plasma membrane surface via the classical secretion pathway and the majority of 42% via UPS pathways. PCA of both secretomes showed clear

segregation, indicating that the secretomes of insulin sensitive and resistant myotubes are sufficiently distinct. Taken together, detailed secretome profiling identified a unique myokine signature in an insulin resistant state that was observed in all five donors.

Deshmukh et al. performed an MS-based secretome analysis using C2C12 myotubes pretreated with 500 µM palmitate in starvation medium for 16 hours, followed by another 12 hours of starvation in the absence of palmitate. Lipid-induced insulin resistance was validated by impaired insulin signaling, which was assessed by immunoblotting showing reduced insulin-stimulated phosphorylation of AKT (Ser473) in palmitate-treated cells (200). In total, the MS-analysis identified 4,491 proteins in the CM, of which 779 proteins were categorized by SignalP as “classically secreted proteins” (SP+), which is very similar to the results of our MS-based secretome analysis of insulin sensitive and insulin resistant human myotubes. In addition, approximately 3,000 proteins were quantified in the CM of each replicate, of which approximately 23% were considered to be putative secreted proteins (200). We quantified a similar number of proteins in the CM (approximately 2,800 per donor), however, we were able to identify three times as many proteins as “predicted secretory proteins” in the CM of human myotubes, which may be due to the fact that a different species was analyzed and also that bioinformatic analysis tools have become more precise in recent years. In addition, we used an additional algorithm (Outcyte) to predict and access proteins secreted via UPS pathways, which may be another reason for the higher number of putative secreted proteins. Moreover, they showed that the lipid-induced muscle secretome (500 µM palmitate) clearly segregated from its control (BSA-treated myotubes) (200), which is consistent with our findings in the human model.

To validate palmitate-induced insulin resistance in human myotubes, changes in phosphorylation were assessed by immunoblotting, which revealed significantly decreased levels of phosphorylation of AKT at Ser473 and Thr308. In addition, phosphorylation of GSK3α (Ser21), GSK3β (Ser9) and PRAS40 (Thr-246) was also notably disrupted, although not statistically significant. Presumably, a larger number of donors (>*n=5*) would lead to statistically significant results. These findings are consistent with previous data from Batista et al., who monitored specific targets of the insulin signaling pathway in induced pluripotent stem (iPS) cells derived from healthy and T2DM patients and differentiated into myoblasts. Immunoblotting results showed that insulin-induced changes in the phosphorylation of AKT (Thr308), GSK3α (Ser21) and FoxO1 (Thr24) were still significant in both healthy controls and T2DM patients, but the response to insulin treatment was significantly reduced in T2DM patients compared to controls (219). In addition, insulin-stimulated glycogen synthesis in skeletal muscle cells was assessed after pretreatment of human myotubes with palmitate, which resulted in a significant reduction in glycogen synthesis in palmitate-treated cells

compared to untreated cells. However, it is important to note that these results were obtained using an alternative palmitate regimen, but it is worth considering as the concentration of palmitate used was lower (300 µM) and therefore similar results can be expected when using the higher concentration (800 µM).

4.3 Contraction-induced muscle secretomes of insulin sensitive and insulin resistant human myotubes differ

Exercise is an important component of non-pharmacological therapy for T2DM and insulin resistance, and many recent studies have shown that exercise can increase insulin sensitivity even in insulin resistant patients. To date, there is no secretome analysis that provides insight into the muscle secretome of insulin resistant skeletal muscle cells previously exposed to exercise. Therefore, the third objective of this thesis was to extend the knowledge on the effects of an acute bout of exercise on the muscle secretome of insulin resistant human skeletal muscle cells. Human myotubes obtained from five donors were pretreated with palmitate, then exposed to acute low-frequency EPS (6h, 40V, 2 ms, 1 Hz) and CM was processed within a bottom-up proteomics workflow. EPS induced the secretion of 97 proteins in the CM of insulin resistant myotubes, whereas 74 proteins were induced in the CM of insulin sensitive myotubes. PCA showed that both EPS-induced secretomes clearly segregated, indicating differences in the myokine secretion profile of contracting insulin sensitive and resistant human myotubes. Therefore, we directly compared the EPS-induced myokines in both cell models and found an overlap of only four proteins. This low number of common myokines in the CM of insulin sensitive and resistant myotubes suggests that different myokines are regulated by acute low-frequency EPS in both cell models.

In addition, protein secretion levels of the contraction-induced myokine IL-6 were measured in the CM of insulin sensitive and insulin resistant myotubes using MIA. In both cell models, IL-6 protein levels were significantly increased after acute low-frequency EPS, validating our acute low-frequency EPS model. However, protein secretion was significantly reduced in insulin resistant myotubes compared to control, supporting our hypothesis that the EPS-induced muscle secretome is altered in insulin resistance. These results are consistent with previous findings by Lambernd et al. who exposed human myotubes to acute (8h) and chronic (24h) low-frequency EPS (11.5 V, 1 Hz, 2 ms) and detected significantly higher levels of IL-6 in the CM after both acute and chronic EPS (171). Using MIA, we aimed to simultaneously detect other known exercise-induced myokines, but only a modest increase (LIF, VEGF, MCP-1) or no increase (IL-8, SPARC) was observed for the tested exerkines in the CM of insulin sensitive myotubes, which also appeared to be donor-dependent. Previous studies validated EPS-induced muscle contraction by measuring significantly increased levels of the exerkines LIF

and IL-8 after 48 hours (30 V, 1 Hz, 2 ms) (70) and VEGF after 24 hours (11.5 V, 1 Hz, 2 ms) (171) in human myotubes or MCP-1 after 24 hours (11.5 V, 1 Hz, 2 ms) in C2C12 myotubes (191), suggesting that the duration of low-frequency EPS significantly affects the myokine secretion profile in both C2C12 and human myotubes. Interestingly, pro-inflammatory factors, such as MIF, MCP-1 and IL-8 were upregulated in the CM of insulin resistant cells, suggesting that palmitate treatment affected the secretion of these cytokines.

Using our cell culture model, we were able to show that insulin signaling was significantly impaired after exposure of human myotubes to 800 µM palmitate, which is consistent with previously reported results from Batista et al., monitoring impaired insulin signaling in muscle cells from diabetic (T2DM) patients (219). Furthermore, non-targeted MS secretome analysis showed that the contraction-induced myokine secretion profile is altered in insulin resistance, which was further confirmed by targeted secretome analysis showing a significant decrease in IL-6 secretion in response to acute low-frequency EPS in insulin resistant cells.

4.4 Different mechanisms that may cause alterations in the secretome in insulin resistance

In this study, we observed that the secretomes of insulin sensitive and resistant myotubes are distinct under resting and contracting conditions. Therefore, potential mechanisms responsible for these changes remain to be elucidated and should be addressed in future experiments. One possibility is that gene expression into proteins is altered by epigenetic modifications such as DNA methylation and post-translational histone modification. These modifications can be caused by environmental factors such as diet, sedentary behavior, lack of exercise and obesity, all of which promote insulin resistance. It has been shown that the regulation of inflammatory genes is mainly regulated by the transcription factors NF-κB, signal transducers and activators of transcription (STAT), forkhead box protein P3 (FOXP3), interferon regulatory factor (IRF) as well as by epigenetic modifications, resulting in increased synthesis of inflammatory cytokines such as IL-1β, IL-6 and TNF-α, triggering inflammation and promoting the development of insulin resistance (220). Interestingly, we observed that total IL-6 secretion levels were increased in palmitate-treated myotubes, hence it could be hypothesized that IL-6 secretion in the insulin resistant state could be caused by epigenetic modifications at the transcriptional level, which could be validated by qPCR.

Moreover, another level of regulation is the post-transcriptional control of gene expression by microRNAs (miRNAs) and RNA-binding proteins (RBS), which play a critical role in metabolic homeostasis and are altered in metabolic diseases, including insulin resistance and T2DM. Some RBS and miRNAs have a major direct impact on insulin signaling pathway, for instance,

by influencing the expression of key components such as IR and IRS, resulting in dysregulation of insulin signaling cascade (221). Therefore, post-transcriptional gene expression alterations may also affect protein secretion pathways, which may explain why the two muscle secretomes differ.

Furthermore, we observed changes in the secretory pattern in insulin resistant myotubes, as notably more myokines were secreted by conventional and unconventional secretory pathways. Another possible reason for these differences may be that protein trafficking routes are affected and altered in insulin resistance. For instance, 31% of the EPS-induced myokines secreted by insulin resistant cells were transported and released via the classical secretory pathway, which increased the number of “SP+” proteins by 7% compared to the secretome of contracting insulin sensitive myotubes. Interestingly, the percentage of unconventionally secreted “SP-” myokines was doubled, as 24% were secreted by insulin resistant contracting myotubes. This unique myokine signature in the insulin resistant state suggests that more myokines are secreted via UPS pathways, such as the Type III pathway using vesicular structures (e.g. MVB) to translocate to the plasma membrane. Fusion of vesicles with the plasma membrane (exocytosis) to translocate proteins into the extracellular space is also regulated by SNARE proteins (222). In response to insulin, SNARE proteins mediate the docking and fusion of the GSV with the plasma membrane, allowing GLUT4 to be inserted into the plasma membrane and cargo proteins released into the extracellular space. Exocytosis is regulated by two SNARE proteins: v-SNAREs (e.g. VAMP2) located on the membrane of the transport vesicle (e.g. GSV) and t-SNAREs (syntaxin) located on the target membrane (e.g. plasma membrane). It has been reported that defective GLUT4 translocation in insulin resistance and T2DM is associated with defects in SNARE proteins (223, 224). Deficiencies in these exocytosis proteins could be another reason why the myokine secretion profile is altered in insulin resistant myotubes.

Moreover, the activity of most proteins in T2DM is modulated by the presence of post-translational modifications (PTM) such as phosphorylation, N-glycosylation, O-GlcNAcylation, acetylation and advanced glycation end products, which can be assessed using proteomic technologies (225). Batista et al. performed phosphoproteomics of insulin resistant cells from T2DM patients and showed that over 1,000 protein events were dysregulated in diabetic patients, most of them in an insulin-dependent manner (219). These changes in PTM in insulin resistant cells may also affect secretory pathways and therefore may be another explanation for the differences in muscle secretomes between insulin resistant and insulin sensitive cells. Moreover, we showed that insulin signaling was disrupted in insulin resistant myotubes as indicated by significant changes in AKT phosphorylation (Ser-417, Thr-308). Since exercise is known to improve insulin sensitivity, it could be speculated that EPS may ameliorate these

changes in PTM in insulin resistant cells and have a beneficial effect on insulin signaling by reversing palmitate-induced insulin resistance.

Direct comparison of EPS-induced secretomes from insulin sensitive and resistant myotubes revealed striking differences in myokine secretion patterns with only four common proteins in the regulated secretomes. EPS-induced IL-6 secretion was significantly altered in insulin resistant myotubes, raising the question of what drives the differences in protein secretion. One possible mechanism may be changes in histone deacetlyase 5 (HDAC5) in insulin resistance, which has recently been proposed to be the major regulator of IL-6 synthesis and secretion from skeletal muscle (226). Our group previously showed that knockdown of *Hdac5* in C2C12 myotubes promoted an increase in IL-6 gene expression and secretion. Moreover, EPS (24h, 11.5 V, 1 Hz, 2 ms) of *Hdac5* deficient C2C12 myotubes further increased IL-6 transcription (226). Another study showed that contraction-induced AMPK activation led to increased phosphorylation of HDAC5, possibly resulting in its nuclear exclusion and subsequent alterations in histone acetylation (227). Therefore, insulin resistance may be caused by epigenetic modifications on HDAC5 that can be reversed by EPS, explaining why IL-6 secretion was altered in insulin resistant cells, but still significant in response to EPS. This speculation could be tested by measuring *Hdac5* expression by RT-qPCR or changes in histone acetylation in unstimulated and EPS-stimulated insulin resistant cells. It therefore remains to be clarified to what extent epigenetic changes influence myokine secretion.

In conclusion, we have shown that the muscle secretomes of insulin sensitive and resistant myotubes are distinct, under resting and contracting conditions. These differences may be driven by different factors, including epigenetic modifications, post-transcriptional changes and dysfunctional vesicle trafficking, which affect protein secretion caused by insulin resistance. However, these hypotheses remain speculative and need to be tested in further approaches.

4.5 Exercise-induced myokines as biomarkers

It has been hypothesized that contraction-induced myokines (exerkines) promote the beneficial health effects of exercise, but the underlying mechanisms are still unclear. Recent studies have shown that CM obtained from skeletal muscle after exercise/muscle contraction has a beneficial effect on glucose and lipid metabolism in the periphery. Laurens et al. exposed HSkMCs to an acute intense EPS protocol (3h, 10 V, 24 ms, 0.5 Hz) and a chronic moderate EPS protocol (24h, 10 V, 2 ms, 0.1 Hz) and exposed human adipocytes to the EPS-induced CM to identify novel exerkines that promote lipolysis in adipose tissue. Indeed, they found that adipose tissue lipolysis was significantly increased after exposure to CM from contracting skeletal muscle cells and identified growth and differentiation factor 15 (GDF15) as a novel

exerkine that promotes lipolysis (176). Another cross-talk study by Barlow et al. investigated the effect of contraction-induced CM on insulin secretion in pancreatic beta cells. Therefore, C2C12 myotubes were exposed to a chronic EPS protocol (24h, 40 V, 1 Hz, 2 ms) and CM was transferred to INS-1 832/3 cells (pseudoislets) in real time. Interestingly, EPS-induced CM significantly increased insulin secretion in INS-1 832/3 cells. Furthermore, CM was shown to significantly increase insulin secretion in palmitate-pretreated pseudoislets as well as insulin secretion in T2DM patients (178). Taken together, these findings confirm that contraction-induced myokines are involved in mediating the health-promoting effects of exercise. It remains to be elucidated whether it is the combination of exerkines or single factors that mediate these effects, and therefore it is of paramount importance to further investigate the muscle secretome to identify novel contraction-induced factors and subsequently determine their autocrine, paracrine and endocrine effects on substrate metabolism.

In this thesis, we propose a selection of novel contraction-induced myokines that are differentially regulated in response to acute low-frequency EPS of either C2C12 or human myotubes, which will be discussed in the following sections. All myokines described below have been classified as “classically secreted proteins” (SP+) and further information is provided in Supplemental Table 8.

Angiopoietin-related protein 4

Angiopoietin-related protein 4 (ANGPTL4) is a ubiquitously expressed protein that is released into the systemic circulation by various cell types and is involved in lipid and glucose metabolism (46, 72). It acts as an inhibitor of lipoprotein lipase (LPL), an enzyme that hydrolyzes triacylglycerol-rich lipoproteins into fatty acids that are taken up by adipose tissue and skeletal muscle, promoting elevated plasma triacylglycerol levels associated with obesity and insulin resistance (228). Its role in diet-induced obesity and related metabolic dysfunctions remains unclear. Janssen et al. generated ANGPTL$^{-/-}$ mice and fed them a Western-style diet rich in unsaturated fatty acids and cholesterol. Interestingly, metabolic characterization of the knockout animals revealed improved glucose tolerance compared to wildtype animals (228). Thus targeting and inhibiting ANGPTL4 could ameliorate metabolic dysfunctions such as glucose intolerance. Another study by Cinkajzlová et al. measured elevated plasma levels of circulating ANGPTL4 in obese patients with or without T2DM (72), suggesting that elevated levels of ANGPTL4 might serve as a potential biomarker for the onset of metabolic diseases (e.g. T2DM). In contrast, angiopoietin-related protein 4 has previously been described as an exercise-induced myokine and is also released from hepatocytes in response to exercise (229, 230). Scheler et al. exposed primary HSkMCs to EPS (14 V, 5 Hz, 2 ms) and measured significantly increased mRNA expression levels of ANGPTL4 after four hours of stimulation and increased plasma levels after eight hours of EPS (69). In contrast, Catoire et al. conducted

an *in vivo* one-legged acute endurance exercise study (1h of cycling) in humans and described higher circulating levels of ANGPTL4 in the non-exercising leg compared to the exercising leg (231).

In this study, we identified angiopoietin-related protein 4 as a myokine in the CM of C2C12 and human myotubes. In previous MS-based secretome studies, Angiopoietin-related protein 4 was also detected as a muscle-secreted protein in the cell culture supernatant of C2C12 myotubes (192, 200) and human myotubes (208). We observed that palmitate treatment significantly increased ANGPTL4 protein levels in the CM of insulin resistant human myotubes. Furthermore, EPS significantly induced ANGPTL4 protein secretion in the muscle secretome of insulin resistant human myotubes compared to EPS-treated insulin sensitive cells. However, it remains uncertain whether this effect is due to EPS or the pretreatment with palmitate. In conclusion, further studies are needed to elucidate the extracellular function of secreted muscle-derived angiopoietin-related protein 4 in the context of exercise, as the literature is still controversial. Cell culture-based studies can help to explore the molecular functions of angiopoietin-related protein 4 by exposing myocytes and adipocytes to higher ANGPTL4 levels measuring its effect on substrate metabolism (e.g. insulin-stimulated glucose uptake, glycogen synthesis, fatty acid oxidation, glucose-stimulated insulin secretion).

Osteopontin

Osteopontin (OPN) or secreted phosphoprotein 1 (SPP1) is an extracellular matrix protein originally identified by Franzén et al. as a major component of bone tissue (232), but now known to be involved in several physiological and pathological processes, including adipose tissue inflammation, insulin resistance and diabetes (233, 234). In addition to being expressed in osteoblasts and osteocytes, osteopontin is also found in several other cell types such as macrophages, T-cells and skeletal muscle cells (234). Osteopontin acts as a cytokine and macrophage chemoattractant that recruits macrophages to adipose tissue and causes an inflammatory state. Especially adipose tissue secreted cytokines (adipokines) such as IL-6, MCP-1 and TNF-α are associated with obesity and the development of insulin resistance (235). Recent studies have reported that obesity-induced low grade inflammation in adipose tissue led to increased levels of OPN in both adipose tissue and plasma (236, 237). In another study, higher levels of circulating OPN were observed in T2DM patients compared to non-diabetic patients, which correlated positively with IL-6, MCP-1 and TNF-α secretion (238). Furthermore, in a diet-induced obesity model in mice, increased plasma OPN levels were observed, while knockout animals (*opn*$^{-/-}$) improved insulin sensitivity (239), suggesting that pharmacological targeting of osteopontin may enhance insulin sensitivity. These previous findings suggest that osteopontin, when secreted at higher levels by macrophages, promotes inflammation in adipose tissue and therefore could serve as a potential biomarker for the onset of metabolic

disorders. However, little is known about the extracellular functions of osteopontin, which is derived from contracting skeletal muscle cells.

In this study, we detected osteopontin as a myokine in the CM of C2C12 myotubes, which interestingly was not identified in the CM of primary human myotubes. Previous MS-based secretome studies also detected osteopontin in the CM of C2C12 myotubes (192, 200), yet it has not been described in any human MS-based secretome study, hence skeletal muscle secretion of osteopontin might be species dependent. We observed that osteopontin was secreted from C2C12 myotubes in response to muscle contraction and was significantly increased in the CM after six hours of acute low-frequency EPS. These findings are consistent with previous results of our group that also described increased osteopontin secretion in the CM of C2C12 myotubes exposed to acute (6h) and chronic (24h) low-frequency EPS (11.5 V, 2 ms, 1 Hz) (MD thesis, Carolin Brügge, 2024). In contrast, Verheggen et al. showed that plasma levels of circulating osteopontin did not change before and after exercise interventions. They also found no differences in osteopontin mRNA levels at the mRNA levels in skeletal muscle cells between the two groups, leading them to conclude that osteopontin is not associated with exercise-induced improvements in insulin sensitivity (240). In summary, osteopontin may be a novel contraction-regulated myokine that mediates anti-inflammatory effects when released by skeletal muscle in response to exercise, but exercise studies are scarce and findings are controversial. For some cytokines (e.g. IL-6) both anti-inflammatory and pro-inflammatory effects have been described, depending on the origin of the secreting cell and the signaling pathways (241). Therefore, future studies are needed to investigate the role and function of contraction-induced muscle secreted osteopontin in the context of insulin sensitivity and glucose and lipid metabolism. Cell culture studies can help to explore the function of muscle-derived osteopontin on glucose-stimulated insulin secretion in pancreatic beta cells or insulin-stimulated glucose uptake in myocytes and adipocytes.

CD44 antigen

The CD44 antigen is a cell surface glycoprotein with an extracellular domain (ectodomain) that binds to its classical ligands hyaluronan (HA) and osteopontin (OPN). There is increasing evidence that CD44 is implicated in the regulation of glucose and lipid homeostasis and therefore plays an important role in the development of metabolic diseases such as obesity and diabetes, but the underlying mechanisms have yet to be uncovered (242). CD44 receptor is expressed in various metabolic organs. High levels of CD44 promote the development of insulin resistance and diabetes by facilitating immune cell infiltration and inflammation in adipose tissue and the liver and by reducing insulin sensitivity and glucose uptake in skeletal muscle (242). Hasib et al. determined the role of CD44 in skeletal muscle by confirming that global CD44-deficient (*cd44*$^{-/-}$) mice fed a high-fat diet were less susceptible to develop skeletal

muscle insulin resistance. Pharmacological intervention then confirmed that the HA-CD44 interaction was required for diet-induced insulin resistance in skeletal muscle (243), suggesting a critical role for the CD44 receptor in the development of muscle insulin resistance and therefore a potential pharmacological target for diabetes therapy. The ectodomain of CD44 is released from the cell surface as a soluble protein (98), which is mediated by an irreversible post-translational modification process called ectodomain shedding (UPS), in which the ectodomain is cleaved by a sheddase (protease) (97). The extracellular functions of the soluble CD44 secretory protein in the context of skeletal muscle secretion and exercise have not yet been described.

In this study we identified CD44 as a myokine, which was secreted in the CM of C2C12 and human myotubes. Previous MS-studies also detected CD44 in the cell culture supernatant released by C2C12 cells (192, 200, 206) and HSkMCs (208, 210, 244). Interestingly, acute low-frequency EPS significantly decreased CD44 levels in the CM of C2C12 myotubes. These results suggest that CD44 may be a novel exercise-regulated myokine. Downregulation of CD44 may improve insulin sensitivity by reducing binding to its pro-inflammatory ligands osteopontin and hyaluronan. However, these results were not be reproduced in human myotubes. Therefore, further functional experiments are needed to clarify the role and function of muscle-derived extracellular CD44 and to determine whether targeting this protein could increase insulin sensitivity in skeletal muscle and possibly other metabolic organs.

Apolipoprotein D

Apolipoprotein D (ApoD) is a small (29 kDa) glycoprotein that is part of the human plasma lipoprotein system and involved in the regulation of the transport of small hydrophobic molecules. It is widely distributed in several tissues and strongest expressed in the central nervous system (245). In particular, the neuroprotective and anti-inflammatory functions of apolipoprotein D in neurodegenerative diseases have been the focus of many research studies in recent years (246-250). Apparently, apolipoprotein D is also linked to insulin signaling and lipid metabolism in humans, as an association between apolipoprotein D polymorphism and diabetes, obesity and hyperinsulinemia was reported (251, 252). Recently, Desmarais et al. demonstrated that high protein levels of ApoD in the adipose tissue (round ligament) of obese women correlated positively with lower plasma insulin levels and insulin resistance as well as increased insulin sensitivity. In addition, lower circulating levels of the pro-inflammatory cytokine TNF-α were also linked to higher adipose tissue ApoD protein levels, indicating that higher ApoD levels are associated with improved metabolic health parameters in obese women (253). Moreover, apolipoprotein D has been associated with osteopontin, a critical regulator of adipose tissue inflammation, as it recruits and activates macrophages, as described above. Interestingly, apolipoprotein D was shown by Jin et al. to reduce osteopontin-

mediated macrophage tissue infiltration (254), suggesting that apolipoprotein D may serve as a pharmaceutical target, as it suppresses osteopontin-mediated inflammatory functions and therefore may mediate health benefits such as reducing adipose tissue inflammation.

In this study, apolipoprotein D was identified as a myokine secreted in the CM of C2C12 and human myotubes. It was previously detected by MS-analyses in the muscle secretome of C2C12 myotubes (200) and HSkMCs (244). Acute low-frequency EPS significantly increased ApoD protein levels in the cell culture supernatant of insulin sensitive human myotubes, suggesting that it is released by skeletal muscle in response to exercise. It can be hypothesized that contraction-induced muscle-derived apolipoprotein D may mediate beneficial health effects by blocking osteopontin and thereby reducing macrophage tissue infiltration. To test this theory, *in vitro* studies using 3T3-L1 cells (adipocytes) and myocytes (C2C12, HSkMCs) are required that expose these cells to muscle-derived apolipoprotein D and subsequently measure OPN levels (mRNA and protein levels) in these insulin resistant metabolic tissues using targeted approaches such as RT-qPCR and enzyme-linked immunosorbent assay (ELISA) or MIA.

Gremlin-1

Gremlin-1 (GREM1) is a member of the transforming growth factor-beta (TGF-β) superfamily and has been implicated in several physiological and pathological processes, including wound healing, inflammation, cancer, and tissue fibrosis (255). In addition, several studies have reported a link between increased circulating levels of gremlin-1 and metabolic diseases such as obesity, insulin resistance and T2DM (256, 257). Recently, Hedjazifar et al. suggested that the major source of circulating gremlin-1 is likely to be the adipose tissue therefore defined gremlin-1 as a novel adipokine that plays a critical role in glucose metabolism and insulin sensitivity (256). Gustafson et al. showed that gremlin-1 mRNA expression was increased in hypertrophic obese patients, which was positively correlated with adipose cell size, body mass index (BMI) (258) and percentage of body fat (256). Furthermore, Hedjazifar et al. confirmed that both gremlin-1 mRNA levels and plasma protein levels were increased in patients with insulin resistance and T2DM patients. Additionally, they showed that circulating gremlin-1 directly antagonizes insulin signaling, as it significantly impaired insulin-induced phosphorylation of AKT (Ser473) in all three insulin target tissues (adipose tissue, skeletal muscle, liver) (256). Interestingly, physical exercise promoted normalization of elevated gremlin-1 levels, which correlated with a reduced risk of developing further complications (e.g. cardiovascular) associated with metabolic diseases (259). Furthermore, massive weight loss (approx. 50 kg) after bariatric surgery significantly reduced gremlin-1 expression levels in the adipose tissue. However, the extracellular role of circulating gremlin-1 is far from being

understood, but it may serve as a potential biomarker to monitor pathogenic processes in patients with metabolic diseases (256).

In this study, gremlin-1 was secreted by C2C12 and human myotubes in the cell culture supernatant and was therefore identified as a myokine. Previous MS-based secretome studies also confirmed gremlin-1 as a myokine released by C2C12 cells (192, 200) and HSkMCs (208). Moreover, we identified gremlin-1 as a classically secreted protein (SP+), which was previously confirmed by other studies, as it structure shows that it contains a signal peptide sequence at the N-terminus (255, 260). Acute low-frequency EPS significantly increased gremlin-1 protein levels in the CM of C2C12 myotubes. Interestingly, further results from our workgroup confirmed that gremlin-1 acts as an exercise-induced myokine, as significantly increased secreted protein levels were detected in the CM from insulin resistant C2C12 myotubes that were subjected to a chronic (24h) low-frequency EPS protocol (11.5 V, 2 ms, 1 Hz) (MD thesis, Michelle Deatc, 2024). Furthermore, data alignment with the literature revealed that Gonzalez-Franquesa et al. also identified gremlin-1 as a contraction-induced myokine in the CM of C2C12 myotubes also subjected to the same chronic low-frequency EPS protocol (24h, 11.5 V, 2 ms, 1 Hz) (192). Taken together, these findings suggest that gremlin-1 is secreted by skeletal muscle in addition to adipose tissue and can therefore be described as an adipo-myokine. Moreover, our results and recent literature suggest that gremlin-1 is a novel exercise-induced myokine (exerkine) that responds to both, acute (6h) and chronic (24h) low-frequency EPS, even in insulin resistant muscle cells (MD thesis, Michelle Deatc, 2024). Dual roles of adipo-myokines (e.g. IL-6) have been described, exterting anti-inflammatory and pro-inflammatory effects (241). Therefore, it is possible that exercise-induced gremlin-1 released from skeletal muscle has positive effects on metabolic organs. Hence, future cell-based functional assays are required to determine the role and function of gremlin-1 on glucose metabolism (e.g. insulin-stimulated glucose uptake, glycogen synthesis), lipid metabolism (e.g. fatty acid oxidation) or insulin sensitivity (e.g. glucose-stimulated insulin secretion) in metabolic organs (adipose tissue, skeletal muscle, pancreas)

Adiponectin

Adiponectin (ADIPOQ) was originally described as an adipokine involved in the regulation of numerous metabolic processes such as glycemic control and fatty acid oxidation (261-263). It is also expressed in various organs, including skeletal muscle, where it improves insulin sensitivity (264). Under pathological conditions, adiponectin mediates protective effects in various cell types by suppressing cell death, inhibiting inflammation and increasing cell survival (262). Moreover, adiponectin plasma levels negatively correlate with obesity-related metabolic disorders such as insulin resistance and T2DM, as they were reduced in these patients (263). Recently, adiponectin has been identified as a myokine that acts in an autocrine and paracrine

fashion via binding to its receptors AdipoR-1 (skeletal muscle) and AdipoR-2 (liver) (265-267). Apparently, adiponectin is induced in skeletal muscle by various metabolic stimuli (e.g. inflammation, oxidative stress, exercise) and is involved in the regulation of several processes in skeletal muscle, such as insulin signaling, intramyocellular Ca^{2+} concentration, muscle mass, inflammation and autophagy (263, 264). Furthermore, it has been suggested that muscle-derived adiponectin mainly affects oxidative pathways and mitochondrial function (264). The effects of exercise on skeletal muscle adiponectin induction have also been studied using various *in vivo* exercise regimens (e.g. treadmill training, swimming) in rodents, but the results were controversial. One study reported an increase in adiponectin mRNA expression in the *gastrocnemius* muscle of rats as well as elevated circulating protein levels after six months of treadmill training. They also showed increased expression of AdipoR-1 and phosphorylation of AMPKα in L6 myoblasts exposed to the serum of previously exercising rats (268). Another group confirmed these results as they found significantly increased mRNA expression of adiponectin in *gastrocnemius* muscle in mice after 10 weeks of constant-moderate intensity treadmill training (269). However, another study observed no exercise-induced changes in total adiponectin protein in the *soleus* muscle of rats following 12 weeks of low, moderate and high-intense treadmill training (270). In addition, various animal models of obesity have been developed to investigate the effects of exercise (e.g. treadmill training, swimming) on adiponectin induction in skeletal muscle. Several research groups observed significantly increased adiponectin mRNA expression after nine weeks of swimming in the *gastrocnemius* muscle of obese rats (271) and higher protein levels of AdipoR-1 after 12 weeks of swimming in muscle of obese mice (272). In contrast, another study observed no exercise-induced changes in AdipoR-1 protein levels in obese C57BL5 mice at moderate intensity on a treadmill for eight weeks (273). That said, it is important to clarify the role of different muscle groups and types of exercise in the induction of skeletal muscle adiponectin in future studies.

In this study, we identified adiponectin as a muscle-derived secreted protein in the CM of C2C12 and human myotubes. Previous MS secretome studies also detected adiponectin as a myokine in the cell culture supernatant of C2C12 myotubes (192, 215), yet we are the first to quantify adiponectin in the CM of HSkMCs by MS analysis. Moreover, acute low-frequency EPS significantly increased secreted adiponectin protein levels in the CM of C2C12 myotubes, however, this effect was not observed in human myotubes. To date, there are no studies on exercise-induced adiponectin and its role in human skeletal muscle (264). Therefore, the extracellular function of exercise-induced muscle-derived adiponectin and its autocrine, paracrine and endocrine effects on other metabolic tissues need to be elucidated. Cell-culture based assays can help to uncover whether adiponectin has health-promoting effects on glucose and lipid metabolism in metabolically active organs (e.g. adipose tissue, skeletal

muscle). Therefore, adipocytes and myocytes could be exposed to adiponectin to measure its influence on insulin-stimulated glucose uptake.

Adipsin/ complement factor D

Adipsin, also known as complement factor D (CFD), was originally defined in 1987 by the Spiegelman and Flier laboratories as the first adipokine produced and secreted by 3T3 adipocytes, a small protein (28 kDa) belonging to the serine protease family (274, 275). It is responsible for maintaining adipose tissue homeostasis and induces glucose-mediated insulin secretion in pancreatic beta cells. Moreover, it also regulates the alternative complement pathway by catalyzing C3a (activated component 3 (C3)) production, which promotes insulin secretion from pancreatic beta cells (276-278). Several studies reported that C3a levels are a risk factor for the development of diabetes (279-281) and Song et al. recently suggested an association between familial C3a deficiency and obesity including its related metabolic diseases (282). Tafere et al. reviewed multiple studies that measured decreased circulating levels of adipsin in patients with T2DM. Since it was shown that adipose tissue-derived adipsin plays an important role in regulating adipose tissue homeostasis and increasing glucose-stimulated insulin secretion, it is a promising novel biomarker for monitoring the early onset of T2DM, hence further studies are required to unravel the mechanism by which adipsin enhances insulin secretion in pancreatic beta cells (278). Furthermore, adipsin is also expressed in other organs including skeletal muscle (283) and was previously identified by our group in the muscle secretome of primary human myotubes using high-resolution MS (244).

In this study, we also identified adipsin as a myokine in the muscle secretome of primary human myotubes, but we did not detect it in the CM of C2C12 myotubes, nor was it detected as a myokine released by C2C12 cells in previous MS-based secretomes. Acute low-frequency EPS significantly increased the secreted levels of adipsin in the CM of insulin sensitive human myotubes. Interestingly, the same effect was observed for EPS-induced secreted adipsin from insulin resistant human myotubes. These findings suggest that adipsin is a novel adipo-myokine induced by exercise in both insulin sensitive and resistant skeletal muscle (exerkine). Therefore, it may mediate insulin sensitizing effects even in insulin resistant muscle, and further experimental cell-culture based studies are required in order to determine the function of extracellular muscle-derived adipsin on substrate metabolism. An interesting approach would be to test whether muscle-derived adipsin also has a positive effect on glucose-stimulated insulin secretion in pancreatic islet cells (beta cells).

Complement c1q tumor necrosis factor-related protein 3

C1q/TNF-related protein-3 (CTRP3) (previously referred to as CORS26 or alternatively cartducin and cartonectin) is a novel adipokine containing a globular C1q domain that is also

expressed in other cytokines such as TNF-α and adiponectin. Together, they all belong to the C1q/TNF superfamily, which is involved in metabolism, inflammation and survival signaling in various tissues (284). It is a hydrophobic secreted protein that most likely mediates its physiological functions through endocrine mechanisms (285, 286). *In vitro* and *in vivo* studies have confirmed that C1q/TNF-related protein-3 is predominantly expressed in differentiated adipocytes (286-288), but it is also present in multiple other tissues, including skeletal muscle (289). *In vitro* studies have shown that as an adipokine, it promotes the secretion of other adipokines, weakens inflammatory signaling, enhances proliferation and differentiation, and increases haptic lipid oxidation. (285, 290-292). The role of C1q/TNF-related protein-3 in the context of T2DM and obesity is controversial in the literature. Circulating C1q/TNF-related protein-3 levels have been reported to be increased, unaffected or reduced in patients with obesity and/or T2DM (284). Several studies reported that circulating C1q/TNF-related protein-3 levels were decreased when circulating pro-inflammatory factors such as TNF-α, IL-6 and C-reactive protein (CRP) were increased in obese/T2DM patients, describing a negative correlation, which may suggest that C1q/TNF-related protein-3 may mediate anti-inflammatory effects (293-295). It was also observed that circulating C1q/TNF-related protein-3 levels were significantly increased in women compared to men (296-298), suggesting that gender plays a critical role. Furthermore, Choi et al. showed that circulating C1q/TNF-related protein-3 levels were reduced by 15% in obese Korean women after three months of exercise. However, it is uncertain whether the reduction in circulating C1q/TNF-related protein-3 levels was due to the exercise program or the loss of body weight (296), so the role of exercise on circulating C1q/TNF-related protein-3 levels remains to be elucidated.

In this study, we identified C1q/TNF-related protein-3 as a skeletal muscle-derived secreted protein in the CM of C2C12 and human myotubes. Previous MS-based secretome studies also detected C1q/TNF-related protein-3 in the cell culture supernatant of C2C12 cells (192, 200, 206, 215), yet we are the first to describe this protein also secreted from human myotubes. Bioinformatic analysis classified C1q/TNF-related protein-3 as a classically secreted myokine (SP+), which is likely as previous literature described that the protein structure contains an N-terminal hydrophobic signaling peptide sequence (299). In addition, its sequence has been described to be 38% homologous to adiponectin in mice and 36% in humans (284), suggesting that it may have similar endocrine effects, as both proteins belong to the C1q/TNF superfamily. Acute low-frequency EPS induced a significant increase in extracellular C1q/TNF-related protein-3 levels in the CM of insulin sensitive human myotubes, indicating that it may be a novel exercise-induced myokine. Hence, we propose that C1q/TNF-related protein-3 is a novel adipo-myokine secreted by skeletal muscle in response to exercise. It is possible that the anti-inflammatory effects of circulating C1q/TNF-related protein-3 are additionally mediated by

muscle-derived C1q/TNF-related protein-3. This theory needs to be tested in future experiments. For instance, insulin sensitivity and anti-inflammatory effects mediated by C1q/TNF-related protein-3 could be tested by exposing insulin resistant adipocytes and myocytes to high levels of C1q/TNF-related protein-3 and then measuring insulin-stimulated glucose uptake in both tissues as well as mRNA levels (e.g. RT-qPCR) and protein secretion levels (ELISA, MIA) of representative pro-inflammatory cytokines such as IL-6 and TNF-α.

5 Conclusion

In this thesis, the secretomes of murine and human skeletal muscle cells were studied using a non-targeted MS-based approach to expand the knowledge of the secretory profile of myokines under physiological and pathological conditions. We were the first to compare contraction-induced muscle secretomes across the two species and were able to show that the muscle secretome changes depend on the cell culture model. This was demonstrated by different myokines induced by EPS in the CM of C2C12 and human myotubes. Also, comparison of our data with the literature showed that myokine secretion varies depending on the EPS protocol. Moreover, we were the first to analyze the muscle secretome of resting and contracting insulin resistant primary human myotubes and showed that the myokine profile was altered in the insulin resistant state. A comprehensive analysis of the muscle secretomes revealed striking differences in the myokine pattern in contracting insulin resistant compared to insulin sensitive human myotubes. Furthermore, bioinformatic prediction analysis suggests changes in secretory pathways in the insulin resistant state, resulting in a shift in the balance between classical and unconventional secretory pathways. These changes may affect, at least in part, the metabolic response to exercise in patients with T2DM.

Taken together, we extended the knowledge on i) the contraction-induced myokine secretion profile of C2C12 myotubes and ii) the contraction-induced myokine secretion profile of insulin sensitive and resistant human myotubes in response to acute (6h) low-frequency EPS. Furthermore, we proposed novel exercise-induced myokines, some of which have already been described as adipokines and are most likely involved in muscle-organ crosstalk mediating health-promoting effects on whole-body metabolism. The discovery of potential novel exercise-induced myokines could significantly enhance our comprehension of the health benefits associated with physical activity and pave the way for the elucidation of the underlying mechanisms. In addition, the identification of contraction-induced myokines and their beneficial influence on substrate metabolism could also be of great importance for individuals who do not respond to exercise (“non-responders”). To conclude, these secreted factors could serve as biomarkers for different training interventions (anaerobic *vs* aerobic training) in order to tailor a personalized training therapy to suit individual needs.

Moreover, comparative secretome analyses underscore the importance of studies using HSkMCs to translate the knowledge gained to the human system. Therefore, further studies are needed to determine i) the underlying mechanisms causing the changes in the myokine profile of insulin resistant HSkMCs and ii) the impact of contraction-induced myokines on the substrate metabolism.

6 References

1. Chatterjee S, Khunti K, Davies MJ. Type 2 diabetes. Lancet. 2017;389(10085):2239-51.
2. Federation ID. IDF Atlas 10th edition: IDF; 2021 [Available from: https://diabetesatlas.org/atlas/tenth-edition/.
3. Eizirik DL, Pasquali L, Cnop M. Pancreatic β-cells in type 1 and type 2 diabetes mellitus: different pathways to failure. Nat Rev Endocrinol. 2020;16(7):349-62.
4. Atkinson MA, Eisenbarth GS, Michels AW. Type 1 diabetes. Lancet. 2014;383(9911):69-82.
5. Galicia-Garcia U, Benito-Vicente A, Jebari S, Larrea-Sebal A, Siddiqi H, Uribe KB, et al. Pathophysiology of Type 2 Diabetes Mellitus. Int J Mol Sci. 2020;21(17).
6. Roden M, Shulman GI. The integrative biology of type 2 diabetes. Nature. 2019;576(7785):51-60.
7. Sparks LM. Exercise training response heterogeneity: physiological and molecular insights. Diabetologia. 2017;60(12):2329-36.
8. Stephens NA, Sparks LM. Resistance to the beneficial effects of exercise in type 2 diabetes: are some individuals programmed to fail? J Clin Endocrinol Metab. 2015;100(1):43-52.
9. Pesta DH, Goncalves RLS, Madiraju AK, Strasser B, Sparks LM. Resistance training to improve type 2 diabetes: working toward a prescription for the future. Nutr Metab (Lond). 2017;14:24.
10. Ross R, Goodpaster BH, Koch LG, Sarzynski MA, Kohrt WM, Johannsen NM, et al. Precision exercise medicine: understanding exercise response variability. Br J Sports Med. 2019;53(18):1141-53.
11. Merz KE, Thurmond DC. Role of Skeletal Muscle in Insulin Resistance and Glucose Uptake. Compr Physiol. 2020;10(3):785-809.
12. Keshel TE, Coker RH. Exercise Training and Insulin Resistance: A Current Review. J Obes Weight Loss Ther. 2015;5(Suppl 5).
13. Guerreiro VA, Carvalho D, Freitas P. Obesity, Adipose Tissue, and Inflammation Answered in Questions. J Obes. 2022;2022:2252516.
14. Al-Beltagi M, Bediwy AS, Saeed NK. Insulin-resistance in paediatric age: Its magnitude and implications. World J Diabetes. 2022;13(4):282-307.
15. Czech MP. Insulin action and resistance in obesity and type 2 diabetes. Nat Med. 2017;23(7):804-14.
16. da Silva Rosa SC, Nayak N, Caymo AM, Gordon JW. Mechanisms of muscle insulin resistance and the cross-talk with liver and adipose tissue. Physiol Rep. 2020;8(19):e14607.
17. Petersen MC, Shulman GI. Mechanisms of Insulin Action and Insulin Resistance. Physiol Rev. 2018;98(4):2133-223.
18. Sampath Kumar A, Maiya AG, Shastry BA, Vaishali K, Ravishankar N, Hazari A, et al. Exercise and insulin resistance in type 2 diabetes mellitus: A systematic review and meta-analysis. Ann Phys Rehabil Med. 2019;62(2):98-103.
19. Guilherme A, Virbasius JV, Puri V, Czech MP. Adipocyte dysfunctions linking obesity to insulin resistance and type 2 diabetes. Nat Rev Mol Cell Biol. 2008;9(5):367-77.
20. Hardy OT, Czech MP, Corvera S. What causes the insulin resistance underlying obesity? Curr Opin Endocrinol Diabetes Obes. 2012;19(2):81-7.
21. Li M, Chi X, Wang Y, Setrerrahmane S, Xie W, Xu H. Trends in insulin resistance: insights into mechanisms and therapeutic strategy. Signal Transduct Target Ther. 2022;7(1):216.
22. Samuel VT, Shulman GI. The pathogenesis of insulin resistance: integrating signaling pathways and substrate flux. J Clin Invest. 2016;126(1):12-22.
23. Frontera WR, Ochala J. Skeletal muscle: a brief review of structure and function. Calcif Tissue Int. 2015;96(3):183-95.

24. Mukund K, Subramaniam S. Skeletal muscle: A review of molecular structure and function, in health and disease. Wiley Interdiscip Rev Syst Biol Med. 2020;12(1):e1462.
25. Isesele PO, Mazurak VC. Regulation of Skeletal Muscle Satellite Cell Differentiation by Omega-3 Polyunsaturated Fatty Acids: A Critical Review. Front Physiol. 2021;12:682091.
26. Jiwlawat S, Lynch E, Glaser J, Smit-Oistad I, Jeffrey J, Van Dyke JM, et al. Differentiation and sarcomere formation in skeletal myocytes directly prepared from human induced pluripotent stem cells using a sphere-based culture. Differentiation. 2017;96:70-81.
27. Sweeney HL, Hammers DW. Muscle Contraction. Cold Spring Harb Perspect Biol. 2018;10(2).
28. Iberite F, Gruppioni E, Ricotti L. Skeletal muscle differentiation of human iPSCs meets bioengineering strategies: perspectives and challenges. NPJ Regen Med. 2022;7(1):23.
29. Hikida RS. Aging changes in satellite cells and their functions. Curr Aging Sci. 2011;4(3):279-97.
30. Macaluso F, Myburgh KH. Current evidence that exercise can increase the number of adult stem cells. J Muscle Res Cell Motil. 2012;33(3-4):187-98.
31. Hernandez-Hernandez JM, Garcia-Gonzalez EG, Brun CE, Rudnicki MA. The myogenic regulatory factors, determinants of muscle development, cell identity and regeneration. Semin Cell Dev Biol. 2017;72:10-8.
32. Zammit PS. Function of the myogenic regulatory factors Myf5, MyoD, Myogenin and MRF4 in skeletal muscle, satellite cells and regenerative myogenesis. Semin Cell Dev Biol. 2017;72:19-32.
33. Collins CA, Gnocchi VF, White RB, Boldrin L, Perez-Ruiz A, Relaix F, et al. Integrated functions of Pax3 and Pax7 in the regulation of proliferation, cell size and myogenic differentiation. PLoS One. 2009;4(2):e4475.
34. Akizawa Y, Kanno H, Kawamichi Y, Matsuda Y, Ohta H, Fujii H, et al. Enhanced expression of myogenic differentiation factors and skeletal muscle proteins in human amnion-derived cells via the forced expression of MYOD1. Brain Dev. 2013;35(4):349-55.
35. Kassar-Duchossoy L, Gayraud-Morel B, Gomès D, Rocancourt D, Buckingham M, Shinin V, et al. Mrf4 determines skeletal muscle identity in Myf5:Myod double-mutant mice. Nature. 2004;431(7007):466-71.
36. Przewozniak M, Czaplicka I, Czerwinska AM, Markowska-Zagrajek A, Moraczewski J, Streminska W, et al. Adhesion proteins--an impact on skeletal myoblast differentiation. PLoS One. 2013;8(5):e61760.
37. Karstoft K, Pedersen BK. Skeletal muscle as a gene regulatory endocrine organ. Curr Opin Clin Nutr Metab Care. 2016;19(4):270-5.
38. Severinsen MCK, Pedersen BK. Muscle-Organ Crosstalk: The Emerging Roles of Myokines. Endocr Rev. 2020;41(4):594-609.
39. McPherron AC, Lawler AM, Lee SJ. Regulation of skeletal muscle mass in mice by a new TGF-beta superfamily member. Nature. 1997;387(6628):83-90.
40. Pedersen BK, Steensberg A, Fischer C, Keller C, Keller P, Plomgaard P, et al. Searching for the exercise factor: is IL-6 a candidate? J Muscle Res Cell Motil. 2003;24(2-3):113-9.
41. Pedersen BK, Febbraio MA. Muscles, exercise and obesity: skeletal muscle as a secretory organ. Nat Rev Endocrinol. 2012;8(8):457-65.
42. Laurens C, Bergouignan A, Moro C. Exercise-Released Myokines in the Control of Energy Metabolism. Front Physiol. 2020;11:91.
43. Garneau L, Aguer C. Role of myokines in the development of skeletal muscle insulin resistance and related metabolic defects in type 2 diabetes. Diabetes Metab. 2019;45(6):505-16.
44. Eckardt K, Gorgens SW, Raschke S, Eckel J. Myokines in insulin resistance and type 2 diabetes. Diabetologia. 2014;57(6):1087-99.

45. Kwon JH, Moon KM, Min KW. Exercise-Induced Myokines can Explain the Importance of Physical Activity in the Elderly: An Overview. Healthcare (Basel). 2020;8(4).
46. Leal LG, Lopes MA, Batista ML, Jr. Physical Exercise-Induced Myokines and Muscle-Adipose Tissue Crosstalk: A Review of Current Knowledge and the Implications for Health and Metabolic Diseases. Front Physiol. 2018;9:1307.
47. Safdar A, Saleem A, Tarnopolsky MA. The potential of endurance exercise-derived exosomes to treat metabolic diseases. Nat Rev Endocrinol. 2016;12(9):504-17.
48. Chow LS, Gerszten RE, Taylor JM, Pedersen BK, van Praag H, Trappe S, et al. Exerkines in health, resilience and disease. Nat Rev Endocrinol. 2022;18(5):273-89.
49. Feraco A, Gorini S, Armani A, Camajani E, Rizzo M, Caprio M. Exploring the Role of Skeletal Muscle in Insulin Resistance: Lessons from Cultured Cells to Animal Models. Int J Mol Sci. 2021;22(17).
50. Ciaraldi TP, Ryan AJ, Mudaliar SR, Henry RR. Altered Myokine Secretion Is an Intrinsic Property of Skeletal Muscle in Type 2 Diabetes. PLoS One. 2016;11(7):e0158209.
51. Garcia-Martin R, Brandao BB, Thomou T, Altindis E, Kahn CR. Tissue differences in the exosomal/small extracellular vesicle proteome and their potential as indicators of altered tissue metabolism. Cell Rep. 2022;38(3):110277.
52. Florin A, Lambert C, Sanchez C, Zappia J, Durieux N, Tieppo AM, et al. The secretome of skeletal muscle cells: A systematic review. Osteoarthr Cartil Open. 2020;2(1):100019.
53. Aguer C, Loro E, Di Raimondo D. Editorial: The Role of the Muscle Secretome in Health and Disease. Front Physiol. 2020;11:1101.
54. So B, Kim HJ, Kim J, Song W. Exercise-induced myokines in health and metabolic diseases. Integr Med Res. 2014;3(4):172-9.
55. Hoffmann C, Weigert C. Skeletal Muscle as an Endocrine Organ: The Role of Myokines in Exercise Adaptations. Cold Spring Harb Perspect Med. 2017;7(11).
56. Trovato E, Di Felice V, Barone R. Extracellular Vesicles: Delivery Vehicles of Myokines. Front Physiol. 2019;10:522.
57. Görgens SW, Eckardt K, Jensen J, Drevon CA, Eckel J. Exercise and Regulation of Adipokine and Myokine Production. Prog Mol Biol Transl Sci. 2015;135:313-36.
58. Whitham M, Febbraio MA. The ever-expanding myokinome: discovery challenges and therapeutic implications. Nat Rev Drug Discov. 2016;15(10):719-29.
59. Pedersen BK, Febbraio MA. Muscle as an endocrine organ: focus on muscle-derived interleukin-6. Physiol Rev. 2008;88(4):1379-406.
60. Ahsan M, Garneau L, Aguer C. The bidirectional relationship between AMPK pathway activation and myokine secretion in skeletal muscle: How it affects energy metabolism. Front Physiol. 2022;13:1040809.
61. Petersen AM, Pedersen BK. The anti-inflammatory effect of exercise. J Appl Physiol (1985). 2005;98(4):1154-62.
62. Wang X, Bao W, Liu J, Ouyang YY, Wang D, Rong S, et al. Inflammatory markers and risk of type 2 diabetes: a systematic review and meta-analysis. Diabetes Care. 2013;36(1):166-75.
63. Lowe G, Woodward M, Hillis G, Rumley A, Li Q, Harrap S, et al. Circulating inflammatory markers and the risk of vascular complications and mortality in people with type 2 diabetes and cardiovascular disease or risk factors: the ADVANCE study. Diabetes. 2014;63(3):1115-23.
64. Qu D, Liu J, Lau CW, Huang Y. IL-6 in diabetes and cardiovascular complications. Br J Pharmacol. 2014;171(15):3595-603.
65. Kraakman MJ, Kammoun HL, Allen TL, Deswaerte V, Henstridge DC, Estevez E, et al. Blocking IL-6 trans-signaling prevents high-fat diet-induced adipose tissue macrophage recruitment but does not improve insulin resistance. Cell Metab. 2015;21(3):403-16.
66. Catoire M, Kersten S. The search for exercise factors in humans. Faseb j. 2015;29(5):1615-28.
67. Pedersen BK. Muscles and their myokines. J Exp Biol. 2011;214(Pt 2):337-46.

68. Covington JD, Tam CS, Bajpeyi S, Galgani JE, Noland RC, Smith SR, et al. Myokine Expression in Muscle and Myotubes in Response to Exercise Stimulation. Med Sci Sports Exerc. 2016;48(3):384-90.
69. Scheler M, Irmler M, Lehr S, Hartwig S, Staiger H, Al-Hasani H, et al. Cytokine response of primary human myotubes in an in vitro exercise model. Am J Physiol Cell Physiol. 2013;305(8):C877-86.
70. Mengeste AM, Nikolic N, Dalmao Fernandez A, Feng YZ, Nyman TA, Kersten S, et al. Insight Into the Metabolic Adaptations of Electrically Pulse-Stimulated Human Myotubes Using Global Analysis of the Transcriptome and Proteome. Front Physiol. 2022;13:928195.
71. Busquets S, Figueras M, Almendro V, Lopez-Soriano FJ, Argiles JM. Interleukin-15 increases glucose uptake in skeletal muscle. An antidiabetogenic effect of the cytokine. Biochim Biophys Acta. 2006;1760(11):1613-7.
72. Cinkajzlova A, Mraz M, Lacinova Z, Klouckova J, Kavalkova P, Kratochvilova H, et al. Angiopoietin-like protein 3 and 4 in obesity, type 2 diabetes mellitus, and malnutrition: the effect of weight reduction and realimentation. Nutr Diabetes. 2018;8(1):21.
73. Evers-van Gogh IJ, Oteng AB, Alex S, Hamers N, Catoire M, Stienstra R, et al. Muscle-specific inflammation induced by MCP-1 overexpression does not affect whole-body insulin sensitivity in mice. Diabetologia. 2016;59(3):624-33.
74. Vandanmagsar B, Haynie KR, Wicks SE, Bermudez EM, Mendoza TM, Ribnicky D, et al. Artemisia dracunculus L. extract ameliorates insulin sensitivity by attenuating inflammatory signalling in human skeletal muscle culture. Diabetes Obes Metab. 2014;16(8):728-38.
75. Sell H, Dietze-Schroeder D, Kaiser U, Eckel J. Monocyte chemotactic protein-1 is a potential player in the negative cross-talk between adipose tissue and skeletal muscle. Endocrinology. 2006;147(5):2458-67.
76. Vella L, Caldow MK, Larsen AE, Tassoni D, Della Gatta PA, Gran P, et al. Resistance exercise increases NF-kappaB activity in human skeletal muscle. Am J Physiol Regul Integr Comp Physiol. 2012;302(6):R667-73.
77. Della Gatta PA, Garnham AP, Peake JM, Cameron-Smith D. Effect of exercise training on skeletal muscle cytokine expression in the elderly. Brain Behav Immun. 2014;39:80-6.
78. Tantiwong P, Shanmugasundaram K, Monroy A, Ghosh S, Li M, DeFronzo RA, et al. NF-κB activity in muscle from obese and type 2 diabetic subjects under basal and exercise-stimulated conditions. Am J Physiol Endocrinol Metab. 2010;299(5):E794-801.
79. Peake JM, Suzuki K, Hordern M, Wilson G, Nosaka K, Coombes JS. Plasma cytokine changes in relation to exercise intensity and muscle damage. Eur J Appl Physiol. 2005;95(5-6):514-21.
80. Bonifacino JS, Glick BS. The mechanisms of vesicle budding and fusion. Cell. 2004;116(2):153-66.
81. Lee MC, Miller EA, Goldberg J, Orci L, Schekman R. Bi-directional protein transport between the ER and Golgi. Annu Rev Cell Dev Biol. 2004;20:87-123.
82. Rabouille C. Pathways of Unconventional Protein Secretion. Trends Cell Biol. 2017;27(3):230-40.
83. Malhotra V. Unconventional protein secretion: an evolving mechanism. EMBO J. 2013;32(12):1660-4.
84. Dimou E, Nickel W. Unconventional mechanisms of eukaryotic protein secretion. Curr Biol. 2018;28(8):R406-R10.
85. Kim J, Gee HY, Lee MG. Unconventional protein secretion - new insights into the pathogenesis and therapeutic targets of human diseases. J Cell Sci. 2018;131(12).
86. Ding J, Wang K, Liu W, She Y, Sun Q, Shi J, et al. Pore-forming activity and structural autoinhibition of the gasdermin family. Nature. 2016;535(7610):111-6.
87. Zacherl S, La Venuta G, Muller HM, Wegehingel S, Dimou E, Sehr P, et al. A direct role for ATP1A1 in unconventional secretion of fibroblast growth factor 2. J Biol Chem. 2015;290(6):3654-65.

88. Steringer JP, Bleicken S, Andreas H, Zacherl S, Laussmann M, Temmerman K, et al. Phosphatidylinositol 4,5-bisphosphate (PI(4,5)P2)-dependent oligomerization of fibroblast growth factor 2 (FGF2) triggers the formation of a lipidic membrane pore implicated in unconventional secretion. J Biol Chem. 2012;287(33):27659-69.
89. McGrath JP, Varshavsky A. The yeast STE6 gene encodes a homologue of the mammalian multidrug resistance P-glycoprotein. Nature. 1989;340(6232):400-4.
90. Maricchiolo E, Panfili E, Pompa A, De Marchis F, Bellucci M, Pallotta MT. Unconventional Pathways of Protein Secretion: Mammals vs. Plants. Front Cell Dev Biol. 2022;10:895853.
91. Pallotta MT, Nickel W. FGF2 and IL-1β - explorers of unconventional secretory pathways at a glance. J Cell Sci. 2020;133(21).
92. Gustafson D, Veitch S, Fish JE. Extracellular Vesicles as Protagonists of Diabetic Cardiovascular Pathology. Front Cardiovasc Med. 2017;4:71.
93. Dupont N, Jiang S, Pilli M, Ornatowski W, Bhattacharya D, Deretic V. Autophagy-based unconventional secretory pathway for extracellular delivery of IL-1beta. EMBO J. 2011;30(23):4701-11.
94. Zhang M, Kenny SJ, Ge L, Xu K, Schekman R. Translocation of interleukin-1beta into a vesicle intermediate in autophagy-mediated secretion. Elife. 2015;4.
95. Gee HY, Kim J, Lee MG. Unconventional secretion of transmembrane proteins. Semin Cell Dev Biol. 2018;83:59-66.
96. Tsumagari K, Chang CH, Ishihama Y. Exploring the landscape of ectodomain shedding by quantitative protein terminomics. iScience. 2021;24(4):102259.
97. Lichtenthaler SF, Lemberg MK, Fluhrer R. Proteolytic ectodomain shedding of membrane proteins in mammals-hardware, concepts, and recent developments. Embo j. 2018;37(15).
98. Hayashida K, Bartlett AH, Chen Y, Park PW. Molecular and cellular mechanisms of ectodomain shedding. Anat Rec (Hoboken). 2010;293(6):925-37.
99. Song P, Kwon Y, Joo JY, Kim DG, Yoon JH. Secretomics to Discover Regulators in Diseases. Int J Mol Sci. 2019;20(16).
100. Zhao L, Poschmann G, Waldera-Lupa D, Rafiee N, Kollmann M, Stuhler K. OutCyte: a novel tool for predicting unconventional protein secretion. Sci Rep. 2019;9(1):19448.
101. Nielsen H, Tsirigos KD, Brunak S, von Heijne G. A Brief History of Protein Sorting Prediction. Protein J. 2019;38(3):200-16.
102. Teufel F, Almagro Armenteros JJ, Johansen AR, Gislason MH, Pihl SI, Tsirigos KD, et al. SignalP 6.0 predicts all five types of signal peptides using protein language models. Nat Biotechnol. 2022;40(7):1023-5.
103. Nielsen H, Petsalaki EI, Zhao L, Stuhler K. Predicting eukaryotic protein secretion without signals. Biochim Biophys Acta Proteins Proteom. 2019;1867(12):140174.
104. Bendtsen JD, Jensen LJ, Blom N, Von Heijne G, Brunak S. Feature-based prediction of non-classical and leaderless protein secretion. Protein Eng Des Sel. 2004;17(4):349-56.
105. Karlsson HK, Zierath JR. Insulin signaling and glucose transport in insulin resistant human skeletal muscle. Cell Biochem Biophys. 2007;48(2-3):103-13.
106. Boucher J, Kleinridders A, Kahn CR. Insulin receptor signaling in normal and insulin-resistant states. Cold Spring Harb Perspect Biol. 2014;6(1).
107. Sun XJ, Rothenberg P, Kahn CR, Backer JM, Araki E, Wilden PA, et al. Structure of the insulin receptor substrate IRS-1 defines a unique signal transduction protein. Nature. 1991;352(6330):73-7.
108. Shaw LM. The insulin receptor substrate (IRS) proteins: at the intersection of metabolism and cancer. Cell Cycle. 2011;10(11):1750-6.
109. Huang C, Thirone AC, Huang X, Klip A. Differential contribution of insulin receptor substrates 1 versus 2 to insulin signaling and glucose uptake in l6 myotubes. J Biol Chem. 2005;280(19):19426-35.
110. Bouzakri K, Roques M, Gual P, Espinosa S, Guebre-Egziabher F, Riou JP, et al. Reduced activation of phosphatidylinositol-3 kinase and increased serine 636

phosphorylation of insulin receptor substrate-1 in primary culture of skeletal muscle cells from patients with type 2 diabetes. Diabetes. 2003;52(6):1319-25.
111. Sylow L, Tokarz VL, Richter EA, Klip A. The many actions of insulin in skeletal muscle, the paramount tissue determining glycemia. Cell Metab. 2021;33(4):758-80.
112. Alessi DR, James SR, Downes CP, Holmes AB, Gaffney PR, Reese CB, et al. Characterization of a 3-phosphoinositide-dependent protein kinase which phosphorylates and activates protein kinase Balpha. Curr Biol. 1997;7(4):261-9.
113. Sarbassov DD, Guertin DA, Ali SM, Sabatini DM. Phosphorylation and regulation of Akt/PKB by the rictor-mTOR complex. Science. 2005;307(5712):1098-101.
114. Oh WJ, Jacinto E. mTOR complex 2 signaling and functions. Cell Cycle. 2011;10(14):2305-16.
115. Zheng X, Cartee GD. Insulin-induced Effects on the Subcellular Localization of AKT1, AKT2 and AS160 in Rat Skeletal Muscle. Sci Rep. 2016;6:39230.
116. Mann G, Riddell MC, Adegoke OAJ. Effects of Acute Muscle Contraction on the Key Molecules in Insulin and Akt Signaling in Skeletal Muscle in Health and in Insulin Resistant States. Diabetology. 2022;3(3):423-46.
117. Duvel K, Yecies JL, Menon S, Raman P, Lipovsky AI, Souza AL, et al. Activation of a metabolic gene regulatory network downstream of mTOR complex 1. Mol Cell. 2010;39(2):171-83.
118. Tzivion G, Dobson M, Ramakrishnan G. FoxO transcription factors; Regulation by AKT and 14-3-3 proteins. Biochim Biophys Acta. 2011;1813(11):1938-45.
119. Espelage L, Al-Hasani H, Chadt A. RabGAPs in skeletal muscle function and exercise. J Mol Endocrinol. 2020;64(1):R1-R19.
120. Sano H, Kane S, Sano E, Miinea CP, Asara JM, Lane WS, et al. Insulin-stimulated phosphorylation of a Rab GTPase-activating protein regulates GLUT4 translocation. J Biol Chem. 2003;278(17):14599-602.
121. Sakamoto K, Holman GD. Emerging role for AS160/TBC1D4 and TBC1D1 in the regulation of GLUT4 traffic. Am J Physiol Endocrinol Metab. 2008;295(1):E29-37.
122. Chadt A, Immisch A, de Wendt C, Springer C, Zhou Z, Stermann T, et al. "Deletion of both Rab-GTPase-activating proteins TBC1D1 and TBC1D4 in mice eliminates insulin- and AICAR-stimulated glucose transport [corrected]. Diabetes. 2015;64(3):746-59.
123. Hermida MA, Dinesh Kumar J, Leslie NR. GSK3 and its interactions with the PI3K/AKT/mTOR signalling network. Adv Biol Regul. 2017;65:5-15.
124. Kim KH, Song MJ, Yoo EJ, Choe SS, Park SD, Kim JB. Regulatory role of glycogen synthase kinase 3 for transcriptional activity of ADD1/SREBP1c. J Biol Chem. 2004;279(50):51999-2006.
125. Negoita F, Addinsall AB, Hellberg K, Bringas CF, Hafen PS, Sermersheim TJ, et al. CaMKK2 is not involved in contraction-stimulated AMPK activation and glucose uptake in skeletal muscle. Mol Metab. 2023;75:101761.
126. Koh HJ, Brandauer J, Goodyear LJ. LKB1 and AMPK and the regulation of skeletal muscle metabolism. Curr Opin Clin Nutr Metab Care. 2008;11(3):227-32.
127. Hardie DG, Ross FA, Hawley SA. AMPK: a nutrient and energy sensor that maintains energy homeostasis. Nat Rev Mol Cell Biol. 2012;13(4):251-62.
128. Thomson DM. The Role of AMPK in the Regulation of Skeletal Muscle Size, Hypertrophy, and Regeneration. Int J Mol Sci. 2018;19(10).
129. Peifer-Weiß L, Al-Hasani H, Chadt A. AMPK and Beyond: The Signaling Network Controlling RabGAPs and Contraction-Mediated Glucose Uptake in Skeletal Muscle. Int J Mol Sci. 2024;25(3).
130. Winder WW, Thomson DM. Cellular energy sensing and signaling by AMP-activated protein kinase. Cell Biochem Biophys. 2007;47(3):332-47.
131. Carling D. AMPK signalling in health and disease. Curr Opin Cell Biol. 2017;45:31-7.
132. Hawley SA, Selbert MA, Goldstein EG, Edelman AM, Carling D, Hardie DG. 5'-AMP activates the AMP-activated protein kinase cascade, and Ca2+/calmodulin activates the calmodulin-dependent protein kinase I cascade, via three independent mechanisms. J Biol Chem. 1995;270(45):27186-91.

133. Davies SP, Helps NR, Cohen PT, Hardie DG. 5'-AMP inhibits dephosphorylation, as well as promoting phosphorylation, of the AMP-activated protein kinase. Studies using bacterially expressed human protein phosphatase-2C alpha and native bovine protein phosphatase-2AC. FEBS Lett. 1995;377(3):421-5.
134. Hardie DG. Keeping the home fires burning: AMP-activated protein kinase. J R Soc Interface. 2018;15(138).
135. Mafakheri S, Chadt A, Al-Hasani H. Regulation of RabGAPs involved in insulin action. Biochem Soc Trans. 2018;46(3):683-90.
136. de Wendt C, Espelage L, Eickelschulte S, Springer C, Toska L, Scheel A, et al. Contraction-Mediated Glucose Transport in Skeletal Muscle Is Regulated by a Framework of AMPK, TBC1D1/4, and Rac1. Diabetes. 2021;70(12):2796-809.
137. Kjøbsted R, Chadt A, Jørgensen NO, Kido K, Larsen JK, de Wendt C, et al. TBC1D4 Is Necessary for Enhancing Muscle Insulin Sensitivity in Response to AICAR and Contraction. Diabetes. 2019;68(9):1756-66.
138. Kjøbsted R, Kristensen JM, Eskesen NO, Kido K, Fjorder K, Damgaard DF, et al. TBC1D4-S711 Controls Skeletal Muscle Insulin Sensitization After Exercise and Contraction. Diabetes. 2023;72(7):857-71.
139. DeFronzo RA, Tripathy D. Skeletal muscle insulin resistance is the primary defect in type 2 diabetes. Diabetes Care. 2009;32 Suppl 2(Suppl 2):S157-63.
140. Shulman GI. Ectopic fat in insulin resistance, dyslipidemia, and cardiometabolic disease. N Engl J Med. 2014;371(23):2237-8.
141. Lee SH, Park SY, Choi CS. Insulin Resistance: From Mechanisms to Therapeutic Strategies. Diabetes Metab J. 2022;46(1):15-37.
142. Kitessa SM, Abeywardena MY. Lipid-Induced Insulin Resistance in Skeletal Muscle: The Chase for the Culprit Goes from Total Intramuscular Fat to Lipid Intermediates, and Finally to Species of Lipid Intermediates. Nutrients. 2016;8(8).
143. Li Y, Xu S, Zhang X, Yi Z, Cichello S. Skeletal intramyocellular lipid metabolism and insulin resistance. Biophys Rep. 2015;1:90-8.
144. Dilworth L, Facey A, Omoruyi F. Diabetes Mellitus and Its Metabolic Complications: The Role of Adipose Tissues. Int J Mol Sci. 2021;22(14).
145. Mastrototaro L, Roden M. Insulin resistance and insulin sensitizing agents. Metabolism. 2021;125:154892.
146. Roden M. Does endurance training protect from lipotoxicity? Diabetes. 2012;61(10):2397-9.
147. Erion DM, Shulman GI. Diacylglycerol-mediated insulin resistance. Nat Med. 2010;16(4):400-2.
148. Qiu T, Yang X, Wang J, Pan C, Chu X, Xiong J, et al. Obesity-induced elevated palmitic acid promotes inflammation and glucose metabolism disorders through GPRs/NF-κB/KLF7 pathway. Nutr Diabetes. 2022;12(1):23.
149. Palomer X, Pizarro-Delgado J, Barroso E, Vázquez-Carrera M. Palmitic and Oleic Acid: The Yin and Yang of Fatty Acids in Type 2 Diabetes Mellitus. Trends Endocrinol Metab. 2018;29(3):178-90.
150. Chandra K. JV, Jain S. K. Plasma Non-Esterified Fatty Acids (NEFA) in Type 2

Diabetes Mellitus: Evidence on Pathophysiology. Journal of Diabetes and Clinical Research. 2021;Volume 3(Issue 2).
151. Glatz JF, Luiken JJ, Bonen A. Membrane fatty acid transporters as regulators of lipid metabolism: implications for metabolic disease. Physiol Rev. 2010;90(1):367-417.
152. Bandet CL, Tan-Chen S, Bourron O, Le Stunff H, Hajduch E. Sphingolipid Metabolism: New Insight into Ceramide-Induced Lipotoxicity in Muscle Cells. Int J Mol Sci. 2019;20(3).
153. Kwon B, Querfurth HW. Palmitate activates mTOR/p70S6K through AMPK inhibition and hypophosphorylation of raptor in skeletal muscle cells: Reversal by oleate is similar to metformin. Biochimie. 2015;118:141-50.

154. Hirabara SM, Curi R, Maechler P. Saturated fatty acid-induced insulin resistance is associated with mitochondrial dysfunction in skeletal muscle cells. J Cell Physiol. 2010;222(1):187-94.
155. Ebersbach-Silva P, Poletto AC, David-Silva A, Seraphim PM, Anhe GF, Passarelli M, et al. Palmitate-induced Slc2a4/GLUT4 downregulation in L6 muscle cells: evidence of inflammatory and endoplasmic reticulum stress involvement. Lipids Health Dis. 2018;17(1):64.
156. Jove M, Planavila A, Laguna JC, Vazquez-Carrera M. Palmitate-induced interleukin 6 production is mediated by protein kinase C and nuclear-factor kappaB activation and leads to glucose transporter 4 down-regulation in skeletal muscle cells. Endocrinology. 2005;146(7):3087-95.
157. Dimopoulos N, Watson M, Sakamoto K, Hundal HS. Differential effects of palmitate and palmitoleate on insulin action and glucose utilization in rat L6 skeletal muscle cells. Biochem J. 2006;399(3):473-81.
158. Jove M, Planavila A, Sanchez RM, Merlos M, Laguna JC, Vazquez-Carrera M. Palmitate induces tumor necrosis factor-alpha expression in C2C12 skeletal muscle cells by a mechanism involving protein kinase C and nuclear factor-kappaB activation. Endocrinology. 2006;147(1):552-61.
159. Weigert C, Brodbeck K, Staiger H, Kausch C, Machicao F, Haring HU, et al. Palmitate, but not unsaturated fatty acids, induces the expression of interleukin-6 in human myotubes through proteasome-dependent activation of nuclear factor-kappaB. J Biol Chem. 2004;279(23):23942-52.
160. Li H, Malhotra S, Kumar A. Nuclear factor-kappa B signaling in skeletal muscle atrophy. J Mol Med (Berl). 2008;86(10):1113-26.
161. Cogolludo A, Villamor E, Perez-Vizcaino F, Moreno L. Ceramide and Regulation of Vascular Tone. Int J Mol Sci. 2019;20(2).
162. Ly LD, Xu S, Choi SK, Ha CM, Thoudam T, Cha SK, et al. Oxidative stress and calcium dysregulation by palmitate in type 2 diabetes. Exp Mol Med. 2017;49(2):e291.
163. Cao SS, Kaufman RJ. Endoplasmic reticulum stress and oxidative stress in cell fate decision and human disease. Antioxid Redox Signal. 2014;21(3):396-413.
164. Wong CY, Al-Salami H, Dass CR. C2C12 cell model: its role in understanding of insulin resistance at the molecular level and pharmaceutical development at the preclinical stage. J Pharm Pharmacol. 2020;72(12):1667-93.
165. Aas V, Bakke SS, Feng YZ, Kase ET, Jensen J, Bajpeyi S, et al. Are cultured human myotubes far from home? Cell Tissue Res. 2013;354(3):671-82.
166. Abdelmoez AM, Sardon Puig L, Smith JAB, Gabriel BM, Savikj M, Dollet L, et al. Comparative profiling of skeletal muscle models reveals heterogeneity of transcriptome and metabolism. Am J Physiol Cell Physiol. 2020;318(3):C615-C26.
167. Aas V, Rokling-Andersen M, Wensaas AJ, Thoresen GH, Kase ET, Rustan AC. Lipid metabolism in human skeletal muscle cells: effects of palmitate and chronic hyperglycaemia. Acta Physiol Scand. 2005;183(1):31-41.
168. Nintou E, Karligiotou E, Vliora M, Ioannou LG, Flouris AD. Characteristics of the Protocols Used in Electrical Pulse Stimulation of Cultured Cells for Mimicking In Vivo Exercise: A Systematic Review, Meta-Analysis, and Meta-Regression. Int J Mol Sci. 2022;23(21).
169. Nedachi T, Fujita H, Kanzaki M. Contractile C2C12 myotube model for studying exercise-inducible responses in skeletal muscle. Am J Physiol Endocrinol Metab. 2008;295(5):E1191-204.
170. Park S, Turner KD, Zheng D, Brault JJ, Zou K, Chaves AB, et al. Electrical pulse stimulation induces differential responses in insulin action in myotubes from severely obese individuals. J Physiol. 2019;597(2):449-66.
171. Lambernd S, Taube A, Schober A, Platzbecker B, Gorgens SW, Schlich R, et al. Contractile activity of human skeletal muscle cells prevents insulin resistance by inhibiting pro-inflammatory signalling pathways. Diabetologia. 2012;55(4):1128-39.

172. Nikolic N, Bakke SS, Kase ET, Rudberg I, Flo Halle I, Rustan AC, et al. Electrical pulse stimulation of cultured human skeletal muscle cells as an in vitro model of exercise. PLoS One. 2012;7(3):e33203.
173. Raschke S, Eckardt K, Bjorklund Holven K, Jensen J, Eckel J. Identification and validation of novel contraction-regulated myokines released from primary human skeletal muscle cells. PLoS One. 2013;8(4):e62008.
174. Tarum J, Folkesson M, Atherton PJ, Kadi F. Electrical pulse stimulation: an in vitro exercise model for the induction of human skeletal muscle cell hypertrophy. A proof-of-concept study. Exp Physiol. 2017;102(11):1405-13.
175. Shainberg A, Burstein M. Decrease of acetylcholine receptor synthesis in muscle cultures by electrical stimulation. Nature. 1976;264(5584):368-9.
176. Laurens C, Parmar A, Murphy E, Carper D, Lair B, Maes P, et al. Growth and differentiation factor 15 is secreted by skeletal muscle during exercise and promotes lipolysis in humans. JCI Insight. 2020;5(6).
177. Christensen CS, Christensen DP, Lundh M, Dahllof MS, Haase TN, Velasquez JM, et al. Skeletal Muscle to Pancreatic beta-Cell Cross-talk: The Effect of Humoral Mediators Liberated by Muscle Contraction and Acute Exercise on beta-Cell Apoptosis. J Clin Endocrinol Metab. 2015;100(10):E1289-98.
178. Barlow J, Solomon TPJ. Conditioned media from contracting skeletal muscle potentiates insulin secretion and enhances mitochondrial energy metabolism of pancreatic beta-cells. Metabolism. 2019;91:1-9.
179. Nikolic N, Gorgens SW, Thoresen GH, Aas V, Eckel J, Eckardt K. Electrical pulse stimulation of cultured skeletal muscle cells as a model for in vitro exercise - possibilities and limitations. Acta Physiol (Oxf). 2017;220(3):310-31.
180. Beiter T, Hudemann J, Burgstahler C, Niess AM, Munz B. Effects of extracellular orotic acid on acute contraction-induced adaptation patterns in C2C12 cells. Mol Cell Biochem. 2018;448(1-2):251-63.
181. Burch N, Arnold AS, Item F, Summermatter S, Brochmann Santana Santos G, Christe M, et al. Electric pulse stimulation of cultured murine muscle cells reproduces gene expression changes of trained mouse muscle. PLoS One. 2010;5(6):e10970.
182. Valero-Breton M, Warnier G, Castro-Sepulveda M, Deldicque L, Zbinden-Foncea H. Acute and Chronic Effects of High Frequency Electric Pulse Stimulation on the Akt/mTOR Pathway in Human Primary Myotubes. Front Bioeng Biotechnol. 2020;8:565679.
183. Manabe Y, Miyatake S, Takagi M, Nakamura M, Okeda A, Nakano T, et al. Characterization of an acute muscle contraction model using cultured C2C12 myotubes. PLoS One. 2012;7(12):e52592.
184. Furuichi Y, Manabe Y, Takagi M, Aoki M, Fujii NL. Evidence for acute contraction-induced myokine secretion by C2C12 myotubes. PLoS One. 2018;13(10):e0206146.
185. Feng YZ, Nikolic N, Bakke SS, Kase ET, Guderud K, Hjelmesaeth J, et al. Myotubes from lean and severely obese subjects with and without type 2 diabetes respond differently to an in vitro model of exercise. Am J Physiol Cell Physiol. 2015;308(7):C548-56.
186. Kugler BA, Deng W, Francois B, Anderson M, Hinkley JM, Houmard JA, et al. Distinct Adaptations of Mitochondrial Dynamics to Electrical Pulse Stimulation in Lean and Severely Obese Primary Myotubes. Med Sci Sports Exerc. 2021;53(6):1151-60.
187. Tamura Y, Kouzaki K, Kotani T, Nakazato K. Electrically stimulated contractile activity-induced transcriptomic responses and metabolic remodeling in C(2)C(12) myotubes: twitch vs. tetanic contractions. Am J Physiol Cell Physiol. 2020;319(6):C1029-C44.
188. Broholm C, Laye MJ, Brandt C, Vadalasetty R, Pilegaard H, Pedersen BK, et al. LIF is a contraction-induced myokine stimulating human myocyte proliferation. J Appl Physiol (1985). 2011;111(1):251-9.
189. Son YH, Lee SM, Lee SH, Yoon JH, Kang JS, Yang YR, et al. Comparative molecular analysis of endurance exercise in vivo with electrically stimulated in vitro myotube contraction. J Appl Physiol (1985). 2019;127(6):1742-53.

190. Miyatake S, Bilan PJ, Pillon NJ, Klip A. Contracting C2C12 myotubes release CCL2 in an NF-kappaB-dependent manner to induce monocyte chemoattraction. Am J Physiol Endocrinol Metab. 2016;310(2):E160-70.
191. Evers-van Gogh IJ, Alex S, Stienstra R, Brenkman AB, Kersten S, Kalkhoven E. Electric Pulse Stimulation of Myotubes as an In Vitro Exercise Model: Cell-Mediated and Non-Cell-Mediated Effects. Sci Rep. 2015;5:10944.
192. Gonzalez-Franquesa A, Stocks B, Borg ML, Kuefner M, Dalbram E, Nielsen TS, et al. Discovery of thymosin beta4 as a human exerkine and growth factor. Am J Physiol Cell Physiol. 2021;321(5):C770-C8.
193. Gorgens SW, Benninghoff T, Eckardt K, Springer C, Chadt A, Melior A, et al. Hypoxia in Combination With Muscle Contraction Improves Insulin Action and Glucose Metabolism in Human Skeletal Muscle via the HIF-1alpha Pathway. Diabetes. 2017;66(11):2800-7.
194. Kanzleiter T, Rath M, Gorgens SW, Jensen J, Tangen DS, Kolnes AJ, et al. The myokine decorin is regulated by contraction and involved in muscle hypertrophy. Biochem Biophys Res Commun. 2014;450(2):1089-94.
195. Schmitz-Peiffer C, Craig DL, Biden TJ. Ceramide generation is sufficient to account for the inhibition of the insulin-stimulated PKB pathway in C2C12 skeletal muscle cells pretreated with palmitate. J Biol Chem. 1999;274(34):24202-10.
196. Coll T, Eyre E, Rodriguez-Calvo R, Palomer X, Sanchez RM, Merlos M, et al. Oleate reverses palmitate-induced insulin resistance and inflammation in skeletal muscle cells. J Biol Chem. 2008;283(17):11107-16.
197. Cazzolli R, Carpenter L, Biden TJ, Schmitz-Peiffer C. A role for protein phosphatase 2A-like activity, but not atypical protein kinase Czeta, in the inhibition of protein kinase B/Akt and glycogen synthesis by palmitate. Diabetes. 2001;50(10):2210-8.
198. Chavez JA, Summers SA. Characterizing the effects of saturated fatty acids on insulin signaling and ceramide and diacylglycerol accumulation in 3T3-L1 adipocytes and C2C12 myotubes. Arch Biochem Biophys. 2003;419(2):101-9.
199. Pickersgill L, Litherland GJ, Greenberg AS, Walker M, Yeaman SJ. Key role for ceramides in mediating insulin resistance in human muscle cells. J Biol Chem. 2007;282(17):12583-9.
200. Deshmukh AS, Cox J, Jensen LJ, Meissner F, Mann M. Secretome Analysis of Lipid-Induced Insulin Resistance in Skeletal Muscle Cells by a Combined Experimental and Bioinformatics Workflow. J Proteome Res. 2015;14(11):4885-95.
201. Wiśniewski JR, Zougman A, Nagaraj N, Mann M. Universal sample preparation method for proteome analysis. Nat Methods. 2009;6(5):359-62.
202. Boyle EI, Weng S, Gollub J, Jin H, Botstein D, Cherry JM, et al. GO::TermFinder--open source software for accessing Gene Ontology information and finding significantly enriched Gene Ontology terms associated with a list of genes. Bioinformatics. 2004;20(18):3710-5.
203. Heberle H, Meirelles GV, da Silva FR, Telles GP, Minghim R. InteractiVenn: a web-based tool for the analysis of sets through Venn diagrams. BMC Bioinformatics. 2015;16(1):169.
204. Metsalu T, Vilo J. ClustVis: a web tool for visualizing clustering of multivariate data using Principal Component Analysis and heatmap. Nucleic Acids Res. 2015;43(W1):W566-70.
205. Yoon JH, Kim D, Jang JH, Ghim J, Park S, Song P, et al. Proteomic analysis of the palmitate-induced myotube secretome reveals involvement of the annexin A1-formyl peptide receptor 2 (FPR2) pathway in insulin resistance. Mol Cell Proteomics. 2015;14(4):882-92.
206. Henningsen J, Pedersen BK, Kratchmarova I. Quantitative analysis of the secretion of the MCP family of chemokines by muscle cells. Mol Biosyst. 2011;7(2):311-21.
207. Chan CY, Masui O, Krakovska O, Belozerov VE, Voisin S, Ghanny S, et al. Identification of differentially regulated secretome components during skeletal myogenesis. Mol Cell Proteomics. 2011;10(5):M110 004804.

208. Le Bihan MC, Bigot A, Jensen SS, Dennis JL, Rogowska-Wrzesinska A, Lainé J, et al. In-depth analysis of the secretome identifies three major independent secretory pathways in differentiating human myoblasts. J Proteomics. 2012;77:344-56.
209. Norheim F, Raastad T, Thiede B, Rustan AC, Drevon CA, Haugen F. Proteomic identification of secreted proteins from human skeletal muscle cells and expression in response to strength training. Am J Physiol Endocrinol Metab. 2011;301(5):E1013-21.
210. Whitham M, Parker BL, Friedrichsen M, Hingst JR, Hjorth M, Hughes WE, et al. Extracellular Vesicles Provide a Means for Tissue Crosstalk during Exercise. Cell Metab. 2018;27(1):237-51.e4.
211. Hittel DS, Berggren JR, Shearer J, Boyle K, Houmard JA. Increased secretion and expression of myostatin in skeletal muscle from extremely obese women. Diabetes. 2009;58(1):30-8.
212. Zunner BEM, Wachsmuth NB, Eckstein ML, Scherl L, Schierbauer JR, Haupt S, et al. Myokines and Resistance Training: A Narrative Review. Int J Mol Sci. 2022;23(7).
213. Liang W, Sagar S, Ravindran R, Najor RH, Quiles JM, Chi L, et al. Mitochondria are secreted in extracellular vesicles when lysosomal function is impaired. Nat Commun. 2023;14(1):5031.
214. Knecht S, Eberl HC, Kreisz N, Ugwu UJ, Starikova T, Kuster B, et al. An Introduction to Analytical Challenges, Approaches, and Applications in Mass Spectrometry-Based Secretomics. Mol Cell Proteomics. 2023;22(9):100636.
215. Grube L, Dellen R, Kruse F, Schwender H, Stuhler K, Poschmann G. Mining the Secretome of C2C12 Muscle Cells: Data Dependent Experimental Approach To Analyze Protein Secretion Using Label-Free Quantification and Peptide Based Analysis. J Proteome Res. 2018;17(2):879-90.
216. Vila OF, Qu Y, Vunjak-Novakovic G. In vitro models of neuromuscular junctions and their potential for novel drug discovery and development. Expert Opin Drug Discov. 2020;15(3):307-17.
217. Zhang W, Liu Y, Zhang H. Extracellular matrix: an important regulator of cell functions and skeletal muscle development. Cell Biosci. 2021;11(1):65.
218. Yudhani RD, Sari Y, Nugrahaningsih DAA, Sholikhah EN, Rochmanti M, Purba AKR, et al. In Vitro Insulin Resistance Model: A Recent Update. J Obes. 2023;2023:1964732.
219. Batista TM, Jayavelu AK, Wewer Albrechtsen NJ, Iovino S, Lebastchi J, Pan H, et al. A Cell-Autonomous Signature of Dysregulated Protein Phosphorylation Underlies Muscle Insulin Resistance in Type 2 Diabetes. Cell Metab. 2020;32(5):844-59 e5.
220. Klimczak S, Śliwińska A. Epigenetic regulation of inflammation in insulin resistance. Semin Cell Dev Biol. 2024;154(Pt C):185-92.
221. Pérez-García A, Torrecilla-Parra M, Fernández-de Frutos M, Martín-Martín Y, Pardo-Marqués V, Ramírez CM. Posttranscriptional Regulation of Insulin Resistance: Implications for Metabolic Diseases. Biomolecules. 2022;12(2).
222. Koike S, Jahn R. SNARE proteins: zip codes in vesicle targeting? Biochem J. 2022;479(3):273-88.
223. Hwang J, Thurmond DC. Exocytosis Proteins: Typical and Atypical Mechanisms of Action in Skeletal Muscle. Front Endocrinol (Lausanne). 2022;13:915509.
224. Aslamy A, Thurmond DC. Exocytosis proteins as novel targets for diabetes prevention and/or remediation? Am J Physiol Regul Integr Comp Physiol. 2017;312(5):R739-r52.
225. Chatterjee B, Thakur SS. Investigation of post-translational modifications in type 2 diabetes. Clin Proteomics. 2018;15:32.
226. Klymenko O, Brecklinghaus T, Dille M, Springer C, de Wendt C, Altenhofen D, et al. Histone deacetylase 5 regulates interleukin 6 secretion and insulin action in skeletal muscle. Mol Metab. 2020;42:101062.
227. McGee SL, van Denderen BJ, Howlett KF, Mollica J, Schertzer JD, Kemp BE, et al. AMP-activated protein kinase regulates GLUT4 transcription by phosphorylating histone deacetylase 5. Diabetes. 2008;57(4):860-7.
228. Janssen AWF, Katiraei S, Bartosinska B, Eberhard D, Willems van Dijk K, Kersten S. Loss of angiopoietin-like 4 (ANGPTL4) in mice with diet-induced obesity uncouples

visceral obesity from glucose intolerance partly via the gut microbiota. Diabetologia. 2018;61(6):1447-58.
229. Raschke S, Eckel J. Adipo-myokines: two sides of the same coin--mediators of inflammation and mediators of exercise. Mediators Inflamm. 2013;2013:320724.
230. Ingerslev B, Hansen JS, Hoffmann C, Clemmesen JO, Secher NH, Scheler M, et al. Angiopoietin-like protein 4 is an exercise-induced hepatokine in humans, regulated by glucagon and cAMP. Mol Metab. 2017;6(10):1286-95.
231. Catoire M, Mensink M, Kalkhoven E, Schrauwen P, Kersten S. Identification of human exercise-induced myokines using secretome analysis. Physiol Genomics. 2014;46(7):256-67.
232. Franzén A, Heinegård D. Isolation and characterization of two sialoproteins present only in bone calcified matrix. Biochem J. 1985;232(3):715-24.
233. Fitter S, Zannettino ACW. Osteopontin in the pathophysiology of obesity: Is Opn a fat cell foe? Obes Res Clin Pract. 2018;12(3):249-50.
234. Icer MA, Gezmen-Karadag M. The multiple functions and mechanisms of osteopontin. Clin Biochem. 2018;59:17-24.
235. Kahles F, Findeisen HM, Bruemmer D. Osteopontin: A novel regulator at the cross roads of inflammation, obesity and diabetes. Mol Metab. 2014;3(4):384-93.
236. Gómez-Ambrosi J, Catalán V, Ramírez B, Rodríguez A, Colina I, Silva C, et al. Plasma osteopontin levels and expression in adipose tissue are increased in obesity. J Clin Endocrinol Metab. 2007;92(9):3719-27.
237. Kiefer FW, Zeyda M, Todoric J, Huber J, Geyeregger R, Weichhart T, et al. Osteopontin expression in human and murine obesity: extensive local up-regulation in adipose tissue but minimal systemic alterations. Endocrinology. 2008;149(3):1350-7.
238. Daniele G, Guardado Mendoza R, Winnier D, Fiorentino TV, Pengou Z, Cornell J, et al. The inflammatory status score including IL-6, TNF-α, osteopontin, fractalkine, MCP-1 and adiponectin underlies whole-body insulin resistance and hyperglycemia in type 2 diabetes mellitus. Acta Diabetol. 2014;51(1):123-31.
239. Nomiyama T, Perez-Tilve D, Ogawa D, Gizard F, Zhao Y, Heywood EB, et al. Osteopontin mediates obesity-induced adipose tissue macrophage infiltration and insulin resistance in mice. J Clin Invest. 2007;117(10):2877-88.
240. Verheggen RJ, Poelkens F, Roerink SH, Ramakers RE, Catoire M, Hermus AR, et al. Exercise Improves Insulin Sensitivity in the Absence of Changes in Cytokines. Med Sci Sports Exerc. 2016;48(12):2378-86.
241. Scheller J, Chalaris A, Schmidt-Arras D, Rose-John S. The pro- and anti-inflammatory properties of the cytokine interleukin-6. Biochim Biophys Acta. 2011;1813(5):878-88.
242. Weng X, Maxwell-Warburton S, Hasib A, Ma L, Kang L. The membrane receptor CD44: novel insights into metabolism. Trends Endocrinol Metab. 2022;33(5):318-32.
243. Hasib A, Hennayake CK, Bracy DP, Bugler-Lamb AR, Lantier L, Khan F, et al. CD44 contributes to hyaluronan-mediated insulin resistance in skeletal muscle of high-fat-fed C57BL/6 mice. Am J Physiol Endocrinol Metab. 2019;317(6):E973-E83.
244. Hartwig S, Raschke S, Knebel B, Scheler M, Irmler M, Passlack W, et al. Secretome profiling of primary human skeletal muscle cells. Biochim Biophys Acta. 2014;1844(5):1011-7.
245. Rassart E, Desmarais F, Najyb O, Bergeron KF, Mounier C. Apolipoprotein D. Gene. 2020;756:144874.
246. Terrisse L, Poirier J, Bertrand P, Merched A, Visvikis S, Siest G, et al. Increased levels of apolipoprotein D in cerebrospinal fluid and hippocampus of Alzheimer's patients. J Neurochem. 1998;71(4):1643-50.
247. Kalman J, McConathy W, Araoz C, Kasa P, Lacko AG. Apolipoprotein D in the aging brain and in Alzheimer's dementia. Neurol Res. 2000;22(4):330-6.
248. Sutcliffe JG, Thomas EA. The neurobiology of apolipoproteins in psychiatric disorders. Mol Neurobiol. 2002;26(2-3):369-88.
249. Thomas EA, Copolov DL, Sutcliffe JG. From pharmacotherapy to pathophysiology: emerging mechanisms of apolipoprotein D in psychiatric disorders. Curr Mol Med. 2003;3(5):408-18.

250. Rickhag M, Deierborg T, Patel S, Ruscher K, Wieloch T. Apolipoprotein D is elevated in oligodendrocytes in the peri-infarct region after experimental stroke: influence of enriched environment. J Cereb Blood Flow Metab. 2008;28(3):551-62.
251. Baker WA, Hitman GA, Hawrami K, McCarthy MI, Riikonen A, Tuomilehto-Wolf E, et al. Apolipoprotein D gene polymorphism: a new genetic marker for type 2 diabetic subjects in Nauru and south India. Diabet Med. 1994;11(10):947-52.
252. Vijayaraghavan S, Hitman GA, Kopelman PG. Apolipoprotein-D polymorphism: a genetic marker for obesity and hyperinsulinemia. J Clin Endocrinol Metab. 1994;79(2):568-70.
253. Desmarais F, Bergeron KF, Lacaille M, Lemieux I, Bergeron J, Biron S, et al. High ApoD protein level in the round ligament fat depot of severely obese women is associated with an improved inflammatory profile. Endocrine. 2018;61(2):248-57.
254. Jin D, El-Tanani M, Campbell FC. Identification of apolipoprotein D as a novel inhibitor of osteopontin-induced neoplastic transformation. Int J Oncol. 2006;29(6):1591-9.
255. Grillo E, Ravelli C, Colleluori G, D'Agostino F, Domenichini M, Giordano A, et al. Role of gremlin-1 in the pathophysiology of the adipose tissues. Cytokine Growth Factor Rev. 2023;69:51-60.
256. Hedjazifar S, Khatib Shahidi R, Hammarstedt A, Bonnet L, Church C, Boucher J, et al. The Novel Adipokine Gremlin 1 Antagonizes Insulin Action and Is Increased in Type 2 Diabetes and NAFLD/NASH. Diabetes. 2020;69(3):331-41.
257. Alregaiey KA, Alfadda AA, Alsaber NS, Bedaiwi AM, Almubarak FR, Bin Muammar AF, et al. Analysis of Gremlin 1 Levels Following Sleeve Gastrectomy. Cureus. 2023;15(11):e48738.
258. Gustafson B, Hammarstedt A, Hedjazifar S, Hoffmann JM, Svensson PA, Grimsby J, et al. BMP4 and BMP Antagonists Regulate Human White and Beige Adipogenesis. Diabetes. 2015;64(5):1670-81.
259. Saeidi A, Seifi-Ski-Shahr F, Soltani M, Daraei A, Shirvani H, Laher I, et al. Resistance training, gremlin 1 and macrophage migration inhibitory factor in obese men: a randomised trial. Arch Physiol Biochem. 2023;129(3):640-8.
260. Elemam NM, Malek AI, Mahmoud EE, El-Huneidi W, Talaat IM. Insights into the Role of Gremlin-1, a Bone Morphogenic Protein Antagonist, in Cancer Initiation and Progression. Biomedicines. 2022;10(2).
261. Nicholson T, Church C, Baker DJ, Jones SW. The role of adipokines in skeletal muscle inflammation and insulin sensitivity. J Inflamm (Lond). 2018;15:9.
262. Wang ZV, Scherer PE. Adiponectin, the past two decades. J Mol Cell Biol. 2016;8(2):93-100.
263. Krause MP, Milne KJ, Hawke TJ. Adiponectin-Consideration for its Role in Skeletal Muscle Health. Int J Mol Sci. 2019;20(7).
264. Martinez-Huenchullan SF, Tam CS, Ban LA, Ehrenfeld-Slater P, McLennan SV, Twigg SM. Skeletal muscle adiponectin induction in obesity and exercise. Metabolism. 2020;102:154008.
265. Jortay J, Senou M, Delaigle A, Noel L, Funahashi T, Maeda N, et al. Local induction of adiponectin reduces lipopolysaccharide-triggered skeletal muscle damage. Endocrinology. 2010;151(10):4840-51.
266. Jortay J, Senou M, Abou-Samra M, Noel L, Robert A, Many MC, et al. Adiponectin and skeletal muscle: pathophysiological implications in metabolic stress. Am J Pathol. 2012;181(1):245-56.
267. Krause MP, Liu Y, Vu V, Chan L, Xu A, Riddell MC, et al. Adiponectin is expressed by skeletal muscle fibers and influences muscle phenotype and function. Am J Physiol Cell Physiol. 2008;295(1):C203-12.
268. Dai Y, Pang J, Gong H, Fan W, Zhang TM. Roles and tissue source of adiponectin involved in lifestyle modifications. J Gerontol A Biol Sci Med Sci. 2013;68(2):117-28.
269. Martinez-Huenchullan SF, Maharjan BR, Williams PF, Tam CS, McLennan SV, Twigg SM. Skeletal muscle adiponectin induction depends on diet, muscle type/activity, and exercise modality in C57BL/6 mice. Physiol Rep. 2018;6(20):e13848.

270. Garekani ET, Mohebbi H, Kraemer RR, Fathi R. Exercise training intensity/volume affects plasma and tissue adiponectin concentrations in the male rat. Peptides. 2011;32(5):1008-12.
271. Safwat Y, Yassin N, Gamal El Din M, Kassem L. Modulation of skeletal muscle performance and SERCA by exercise and adiponectin gene therapy in insulin-resistant rat. DNA Cell Biol. 2013;32(7):378-85.
272. Farias JM, Maggi RM, Tromm CB, Silva LA, Luciano TF, Marques SO, et al. Exercise training performed simultaneously to a high-fat diet reduces the degree of insulin resistance and improves adipoR1-2/APPL1 protein levels in mice. Lipids Health Dis. 2012;11:134.
273. Pierard M, Conotte S, Tassin A, Boutry S, Uzureau P, Boudjeltia KZ, et al. Interactions of exercise training and high-fat diet on adiponectin forms and muscle receptors in mice. Nutr Metab (Lond). 2016;13:75.
274. Cook KS, Groves DL, Min HY, Spiegelman BM. A developmentally regulated mRNA from 3T3 adipocytes encodes a novel serine protease homologue. Proc Natl Acad Sci U S A. 1985;82(19):6480-4.
275. Cook KS, Min HY, Johnson D, Chaplinsky RJ, Flier JS, Hunt CR, et al. Adipsin: a circulating serine protease homolog secreted by adipose tissue and sciatic nerve. Science. 1987;237(4813):402-5.
276. Lo JC, Ljubicic S, Leibiger B, Kern M, Leibiger IB, Moede T, et al. Adipsin is an adipokine that improves β cell function in diabetes. Cell. 2014;158(1):41-53.
277. Gómez-Banoy N, Guseh JS, Li G, Rubio-Navarro A, Chen T, Poirier B, et al. Adipsin preserves beta cells in diabetic mice and associates with protection from type 2 diabetes in humans. Nat Med. 2019;25(11):1739-47.
278. Tafere GG, Wondafrash DZ, Zewdie KA, Assefa BT, Ayza MA. Plasma Adipsin as a Biomarker and Its Implication in Type 2 Diabetes Mellitus. Diabetes Metab Syndr Obes. 2020;13:1855-61.
279. Baldo A, Sniderman AD, St-Luce S, Avramoglu RK, Maslowska M, Hoang B, et al. The adipsin-acylation stimulating protein system and regulation of intracellular triglyceride synthesis. J Clin Invest. 1993;92(3):1543-7.
280. Engström G, Hedblad B, Eriksson KF, Janzon L, Lindgärde F. Complement C3 is a risk factor for the development of diabetes: a population-based cohort study. Diabetes. 2005;54(2):570-5.
281. Mamane Y, Chung Chan C, Lavallee G, Morin N, Xu LJ, Huang J, et al. The C3a anaphylatoxin receptor is a key mediator of insulin resistance and functions by modulating adipose tissue macrophage infiltration and activation. Diabetes. 2009;58(9):2006-17.
282. Song NJ, Kim S, Jang BH, Chang SH, Yun UJ, Park KM, et al. Small Molecule-Induced Complement Factor D (Adipsin) Promotes Lipid Accumulation and Adipocyte Differentiation. PLoS One. 2016;11(9):e0162228.
283. Kyohara M, Shirakawa J, Okuyama T, Togashi Y, Inoue R, Li J, et al. Soluble EGFR, a hepatokine, and adipsin, an adipokine, are biomarkers correlated with distinct aspects of insulin resistance in type 2 diabetes subjects. Diabetol Metab Syndr. 2020;12:83.
284. Li Y, Wright GL, Peterson JM. C1q/TNF-Related Protein 3 (CTRP3) Function and Regulation. Compr Physiol. 2017;7(3):863-78.
285. Peterson JM, Wei Z, Wong GW. C1q/TNF-related protein-3 (CTRP3), a novel adipokine that regulates hepatic glucose output. J Biol Chem. 2010;285(51):39691-701.
286. Wong GW, Krawczyk SA, Kitidis-Mitrokostas C, Revett T, Gimeno R, Lodish HF. Molecular, biochemical and functional characterizations of C1q/TNF family members: adipose-tissue-selective expression patterns, regulation by PPAR-gamma agonist, cysteine-mediated oligomerizations, combinatorial associations and metabolic functions. Biochem J. 2008;416(2):161-77.
287. Schaffler A, Ehling A, Neumann E, Herfarth H, Tarner I, Gay S, et al. Genomic organization, chromosomal localization and adipocytic expression of the murine gene for CORS-26 (collagenous repeat-containing sequence of 26 kDa protein). Biochim Biophys Acta. 2003;1628(1):64-70.

288. Schaffler A, Weigert J, Neumeier M, Scholmerich J, Buechler C. Regulation and function of collagenous repeat containing sequence of 26-kDa protein gene product "cartonectin". Obesity (Silver Spring). 2007;15(2):303-13.
289. Otani M, Furukawa S, Wakisaka S, Maeda T. A novel adipokine C1q/TNF-related protein 3 is expressed in developing skeletal muscle and controls myoblast proliferation and differentiation. Mol Cell Biochem. 2015;409(1-2):271-82.
290. Li X, Jiang L, Yang M, Wu YW, Sun SX, Sun JZ. CTRP3 modulates the expression and secretion of adipokines in 3T3-L1 adipocytes. Endocr J. 2014;61(12):1153-62.
291. Peterson JM, Seldin MM, Wei Z, Aja S, Wong GW. CTRP3 attenuates diet-induced hepatic steatosis by regulating triglyceride metabolism. Am J Physiol Gastrointest Liver Physiol. 2013;305(3):G214-24.
292. Schmid A, Kopp A, Aslanidis C, Wabitsch M, Müller M, Schäffler A. Regulation and function of C1Q/TNF-related protein-5 (CTRP-5) in the context of adipocyte biology. Exp Clin Endocrinol Diabetes. 2013;121(5):310-7.
293. Ban B, Bai B, Zhang M, Hu J, Ramanjaneya M, Tan BK, et al. Low serum cartonectin/CTRP3 concentrations in newly diagnosed type 2 diabetes mellitus: in vivo regulation of cartonectin by glucose. PLoS One. 2014;9(11):e112931.
294. Petersen PS, Wolf RM, Lei X, Peterson JM, Wong GW. Immunomodulatory roles of CTRP3 in endotoxemia and metabolic stress. Physiol Rep. 2016;4(5).
295. Qu H, Deng M, Wang H, Wei H, Liu F, Wu J, et al. Plasma CTRP-3 concentrations in Chinese patients with obesity and type II diabetes negatively correlate with insulin resistance. J Clin Lipidol. 2015;9(3):289-94.
296. Choi HY, Park JW, Lee N, Hwang SY, Cho GJ, Hong HC, et al. Effects of a combined aerobic and resistance exercise program on C1q/TNF-related protein-3 (CTRP-3) and CTRP-5 levels. Diabetes Care. 2013;36(10):3321-7.
297. Deng W, Li C, Zhang Y, Zhao J, Yang M, Tian M, et al. Serum C1q/TNF-related protein-3 (CTRP3) levels are decreased in obesity and hypertension and are negatively correlated with parameters of insulin resistance. Diabetol Metab Syndr. 2015;7:33.
298. Wolf RM, Steele KE, Peterson LA, Magnuson TH, Schweitzer MA, Wong GW. Lower Circulating C1q/TNF-Related Protein-3 (CTRP3) Levels Are Associated with Obesity: A Cross-Sectional Study. PLoS One. 2015;10(7):e0133955.
299. Maeda T, Abe M, Kurisu K, Jikko A, Furukawa S. Molecular cloning and characterization of a novel gene, CORS26, encoding a putative secretory protein and its possible involvement in skeletal development. J Biol Chem. 2001;276(5):3628-34.

7 Supplement

7.1 Contribution to manuscripts

Michael Turewicz, Christine Skagen, Sonja Hartwig, Stephan Majda, Kristina Thedinga, Ralf Herwig, Christian Binsch, D., Delsi Altenhofen, Margriet Ouwens, **Pia Marlene Förster**, Torben Stermann, Alexandra Chadt, Stefan Lehr, Tobias Marschall6, G. Hege Thoresen, Hadi Al-Hasani. Temporal phosphoproteomics reveals circuitry of phased propagation in insulin signaling. *Nature Communications.* The manuscript is currently under revision (2024).

Contribution: I was involved in the interpretation of the data.

Further, parts of this thesis shall be published in a separate paper. The manuscript is currently under preparation:

Pia Marlene Förster, Moira Fee Pottgießer, Christian Binsch, Awovi Didi Humpert, Carolin Brügge, Michelle Isabel Deatc, Regina Ensenauer, Alexandra Chadt, Hege Thoresen, Margriet Ouwens, Sonja Hartwig, Stefan Lehr, Hadi Al-Hasani.

7.2 Abbreviations

AGC	Automatic gain control
AMPK	5'-adenosine monophosphate-activated protein kinase
ANGPTL4	Angiopoietin-related protein 4
ApoD	Apolipoprotein D
APS	Ammonium persulfate
BCA	Bicinchonic acid assay
BDNF	Brain-derived neurotrophic factor
BMI	Body mass index
BSA	Bovine serum albumin
CaMKK	Ca2+/ calmodulin-dependent protein kinase kinase
CFD	Complement factor 1 / Adipisin
CFTR	Cystic fibrosis transmembrane conductance regulator
CM	Conditioned media
DAG	Diacylglycerol(s)
DDA	Data dependent acquisition
DMEM	Dulbecco´s Modified Eagle Medium
DMSO	Dimethyl sulfoxide
DPBS	Dulbecco´s Phosphate Buffered Saline
DTT	Dithiothreitol
EDTA	Ethylenediaminetetraacetic acid
EGTA	Ethyleneglycol-bis(aminoethylether)-N,N,N′,N′-tetraacetic acid
EPS	Electrical pulse stimulation
EtOH	Ethanol
EV	Extracellular vesicles
FAIMS	High field asymmetric waveform ion mobility spectrometry
FASP	Filter-aided sample preparation
FBS	Fetal bovine serum
FFA	Free fatty acid(s)
FGF-2	Fibroblast growth factor 2
FGF-21	Fibroblast growth factor 21
FST	Follistatin
FSTL1	Follistatin-like 1
GAPDH	Glyceraldehyde 3-phosphate dehydrogenase
GLUT4	Glucose transporter type 4
GOCC	Gene Ontology cellular component

GREM1	Gremlin-1
GSK3	Glycogen synthase kinase 3
H_2O	Water
HCD	Higher-energy collisional dissociation
HCl	Hydrochloric acid
HPLC	High Performance Liquid Chromatography
HRP	Horseradish peroxidase
HS	Horse serum
HSkMCs	Human skeletal muscle cells
HSMM	Human skeletal muscle myoblasts
IAA	Iodoacetamide
IGF-1	Insulin-like growth factor 1
IL	Interleukin
IMCL	Intramyocellular lipids
IRS	Insulin receptor substrate
KCl	Potassium chloride
KOH	Potassium hydroxide
LC	Liquid Chromatography
LDH	Lactate dehydrogenase
LIF	Leukemia inhibitory factor
LKB1	Liver kinase B1
LY	LY294002
MCP-1	Monocyte chemoattractant protein-1
MeCN	Acetonitrile
MeOH	Methanol
$MgSO_4$	x7H2O Magnesium sulphate heptahydrate
MIA	Multiplex immunoassays
MP	Milk powder
MRF	Myogenic regulator factor
MS	Mass spectrometry
MVB	Multivesicular bodies
Myf5	Myogenic factor 5
MyoD	Myoblast determination protein 1
MyoG	Myogenin
Na_2HPO_4	Disodium hydrogen phosphate
NaCl	Sodium chloride
$NaHCO_3$	Sodium hydrogen carbonate

o-H_3PO_4	Ortho-phosphoric acid
OPN / SPP1	Osteopontin / secreted phosphoprotein 1
PBS	Phosphate buffered saline
PCA	Principle component analysis
PD™	Proteome Discoverer™
PI3K	Phosphoinositide 3-kinases
PIP_2	Phosphatidylinositol-4,5-bisphosphate
PIP_3	Phosphatidylinositol (3,4,5)-triphosphate
PKB/AKT	Protein kinase B
PRAS40	Proline-rich AKT substrate 40 kDa
PSM	Peptide spectrum match
qRT-PCR	Reverse transcription-quantitative polymerase chain reaction
ROS	Reactive oxygen species
SDS	Sodium dodecyl sulfate
SDS-PAGE	Sodium-dodecylsulfate-polyacrylamide gel electrophoresis
SEM	Standard error of the mean
SNARE	Soluble N-ethylmaleimide sensitive factor attachment protein receptor
SP	Signal peptide
SPARC	Secreted protein acidic and rich in cysteine
T1DM	Type 1 diabetes mellitus
T2DM	Type 2 diabetes mellitus
TBC1D1/4	TBC1 domain familiy D1/D4
TBS-T	Tris-buffered saline with Tween®
TEMED	N,N,N′,N′-Tetramethyl-ethylendiamin
TFA	Trifluoroacetic acid
TG	Triglyceride(s)
TNF-α	Tumor necrosis factor alpha
UPS	Unconventional protein secretion
VEGF	Vascular endothelial growth factor

7.3 Supplemental Tables

Supplemental Table 1: Donors used for cell culture experiments in this thesis.

Donor	Muscle Tissue	Cell type	Sex	Race	Age	BMI
Donor 1	*Quadriceps femoris*	Myoblasts	Male	Caucasian	35 years	25 kg/m^2
Donor 2	*Quadriceps femoris*	Myoblasts	Male	Caucasian	35 years	24 kg/m^2
Donor 3	*Quadriceps femoris*	Myoblasts	Male	Caucasian	16 years	N/A
Donor 4	*Quadriceps femoris*	Myoblasts	Male	Black	22 years	26 kg/m^2
Donor 5	*Quadriceps femoris*	Myoblasts	Male	Caucasian	21 years	19 kg/m^2

Supplemental Table 2: EPS-induced differentially regulated unconventionally secreted proteins in the muscle secretome of C2C12 cells (EPS/CON).

UniProtKB	Gene symbol	Protein description	*p*-value	Log_2FC	Secretion type
Q8VDS8	Stx18	Syntaxin-18	1.00E-17	6.64	SP-
Q9CQY1	Atg12	Ubiquitin-like protein ATG12	1.00E-17	6.64	SP-
Q8VIN1	Pbp2	Phosphatidylethanolamine-binding protein 2	1.00E-17	6.64	SP-
P00329	Adh1	Alcohol dehydrogenase 1	1.00E-17	6.64	SP-
Q8R2K1	Fuom	Fucose mutarotase	1.00E-17	6.64	SP-
Q9EPN1	Nbea	Neurobeachin	1.00E-17	6.64	SP-
Q8R088	Golph3l	Golgi phosphoprotein 3-like	1.00E-17	6.64	SP-
P12710	Fabp1	Fatty acid-binding protein, liver	1.00E-17	6.64	Outcyte+
P02088	Hbb-b1	Hemoglobin subunit beta-1	1.00E-17	6.64	Outcyte+
O55022	Pgrmc1	Membrane-associated progesterone receptor component 1	1.00E-17	6.64	Outcyte+
Q80V26	Bpnt2	Golgi-resident adenosine 3',5'-bisphosphate 3'-phosphatase	1.00E-17	6.64	Outcyte+
O88559	Men1	Menin	1.00E-17	6.64	Outcyte+
P30115	Gsta3	Glutathione S-transferase A3	1.00E-17	6.64	Outcyte+
Q9D1L9	Lamtor5	Ragulator complex protein LAMTOR5	1.00E-17	6.64	Outcyte+
Q8C196	Cps1	Carbamoyl-phosphate synthase [ammonia], mitochondrial	1.00E-17	6.64	Outcyte+
Q9EQU5	Set	Protein SET	1.00E-17	0.95	Outcyte+
P09602	Hmgn2	Non-histone chromosomal protein HMG-17	2.41E-12	0.92	SP-
Q8C5Q4	Grsf1	G-rich sequence factor 1	3.75E-05	0.77	SP-
Q8BJK1	Kctd7	BTB/POZ domain-containing protein KCTD7	1.97E-04	0.75	SP-
P23249	Mov10	Putative helicase MOV-10	1.13E-09	0.61	Outcyte+

Q62425	Ndufa4	Cytochrome c oxidase subunit NDUFA4	5.33E-07	0.56	SP-
P01942	Hba	Hemoglobin subunit alpha	8.34E-05	0.52	Outcyte+
Q9Z2D8	Mbd3	Methyl-CpG-binding domain protein 3	2.37E-03	0.52	Outcyte+
O35143	Atp5if1	ATPase inhibitor, mitochondrial	5.66E-12	0.47	SP-
P56565	S100a1	Protein S100-A1	1.66E-04	0.43	Outcyte+
P52503	Ndufs6	NADH dehydrogenase [ubiquinone] iron-sulfur protein 6, mitochondrial	4.17E-06	0.42	SP-
Q8BXK9	Clic5	Chloride intracellular channel protein 5	5.82E-03	0.41	Outcyte+
Q91V01	Lpcat3	Lysophospholipid acyltransferase 5	3.12E-02	0.41	Outcyte+
Q9CWI3	Bccip	BRCA2 and CDKN1A-interacting protein	1.56E-03	0.39	SP-
Q9ESN6	Trim2	Tripartite motif-containing protein 2	2.98E-03	0.39	SP-
P56394	Cox17	Cytochrome c oxidase copper chaperone	1.34E-07	0.38	SP-
P62309	Snrpg	Small nuclear ribonucleoprotein G	4.24E-09	0.37	SP-
P62984	Uba52	Ubiquitin-60S ribosomal protein L40	1.26E-02	0.37	SP-
O08997	Atox1	Copper transport protein ATOX1	1.77E-07	0.36	SP-
P62274	Rps29	40S ribosomal protein S29	2.07E-07	0.35	SP-
P62862	Fau; FAU	40S ribosomal protein S30	4.90E-05	0.35	SP-
Q8CFE2	Hpf1	Histone PARylation factor 1	8.80E-07	0.34	SP-
Q8BMD8	Slc25a24	Calcium-binding mitochondrial carrier protein SCaMC-1	2.88E-06	0.34	SP-
Q8R1R3	Stard7	StAR-related lipid transfer protein 7, mitochondrial	1.13E-02	0.34	SP-
Q9JL56	Gde1	Glycerophosphodiester phosphodiesterase 1	3.93E-02	0.34	SP-
Q64433	Hspe1	10 kDa heat shock protein, mitochondrial	1.19E-08	0.33	Outcyte+
Q9D6J6	Ndufv2	NADH dehydrogenase [ubiquinone] flavoprotein 2, mitochondrial	1.35E-04	0.33	SP-
Q9DCB1	Hmgn3	High mobility group nucleosome-binding domain-containing protein 3	1.80E-04	0.33	SP-
Q9CQ40	Mrpl49	39S ribosomal protein L49, mitochondrial	5.18E-03	0.33	SP-
Q9QUH0	Glrx	Glutaredoxin-1	8.21E-03	0.33	Outcyte+
P62307	Snrpf	Small nuclear ribonucleoprotein F	1.74E-05	0.32	Outcyte+
Q9DCZ4	Apoo	MICOS complex subunit Mic26	1.10E-02	0.32	Outcyte+
Q8BGD8	Coa6	Cytochrome c oxidase assembly factor 6 homolog	1.49E-02	0.32	SP-
Q6PNC0	Dmxl1	DmX-like protein 1	1.82E-02	0.32	Outcyte+
Q8BHG1	Nrdc	Nardilysin	3.44E-07	0.31	Outcyte+
Q99JI1	Mustn1	Musculoskeletal embryonic nuclear protein 1	9.10E-07	0.31	SP-
P32848	Pvalb	Parvalbumin alpha	4.12E-04	0.31	Outcyte+

Q9WV98	Timm9	Mitochondrial import inner membrane translocase subunit Tim9	5.18E-03	0.31	SP-
Q60935	Art1	GPI-linked NAD(P)(+)--arginine ADP-ribosyltransferase 1	6.22E-03	0.31	Outcyte+
P56391	Cox6b1	Cytochrome c oxidase subunit 6B1	2.41E-06	0.3	SP-
Q61937	Npm1	Nucleophosmin	3.12E-06	0.3	SP-
O54781	Srpk2	SRSF protein kinase 2	4.92E-06	0.3	Outcyte+
Q9CR60	Golt1b	Vesicle transport protein GOT1B	2.78E-02	0.28	SP-
P14069	S100a6	Protein S100-A6	2.47E-05	0.27	Outcyte+
Q99LY9	Ndufs5	NADH dehydrogenase [ubiquinone] iron-sulfur protein 5	1.72E-04	0.27	SP-
Q9CRD0	Ociad1	OCIA domain-containing protein 1	2.88E-04	0.27	SP-
Q8CII2	Cdc123	Cell division cycle protein 123 homolog	2.16E-02	0.27	Outcyte+
Q9CQH8	Rpp14	Ribonuclease P protein subunit p14	3.82E-02	0.27	SP-
P62983	Rps27a	Ubiquitin-40S ribosomal protein S27a	5.46E-06	0.26	SP-
Q9CQR2	Rps21	40S ribosomal protein S21	7.10E-06	0.26	SP-
Q9R000	Itgb1bp2	Integrin beta-1-binding protein 2	3.40E-04	0.26	Outcyte+
Q9D3D9	Atp5f1d	ATP synthase subunit delta, mitochondrial	2.79E-03	0.26	Outcyte+
Q9CQH7	Btf3l4	Transcription factor BTF3 homolog 4	2.46E-05	0.25	Outcyte+
Q61335	Bcap31	B-cell receptor-associated protein 31	6.27E-04	0.25	SP-
Q9DB15	Mrpl12	39S ribosomal protein L12, mitochondrial	6.36E-04	0.25	Outcyte+
Q8R429	Atp2a1	Sarcoplasmic/endoplasmic reticulum calcium ATPase 1	7.53E-05	0.24	SP-
Q9D1R9	Rpl34	60S ribosomal protein L34	1.42E-04	0.24	SP-
A2AMM0	Cavin4	Caveolae-associated protein 4	1.93E-04	0.24	SP-
Q60737	Csnk2a1	Casein kinase II subunit alpha	1.14E-03	0.24	SP-
P19536	Cox5b	Cytochrome c oxidase subunit 5B, mitochondrial	1.02E-02	0.24	SP-
Q9D517	Agpat3	1-acyl-sn-glycerol-3-phosphate acyltransferase gamma	1.32E-02	0.24	SP-
Q9Z2P8	Vamp5	Vesicle-associated membrane protein 5	4.17E-02	0.24	Outcyte+
P25444	Rps2	40S ribosomal protein S2	7.03E-05	0.23	SP-
O54962	Banf1	Barrier-to-autointegration factor	1.58E-03	0.23	Outcyte+
Q8VC70	Rbms2	RNA-binding motif, single-stranded-interacting protein 2	1.08E-02	0.23	SP-
P99028	Uqcrh	Cytochrome b-c1 complex subunit 6, mitochondrial	3.35E-02	0.23	SP-
Q9JJI8	Rpl38	60S ribosomal protein L38	3.79E-04	0.22	SP-
P83882	Rpl36a	60S ribosomal protein L36a	6.01E-04	0.22	SP-
Q9EQS3	Mycbp	c-Myc-binding protein	8.68E-04	0.22	SP-
Q9D6K8	Fundc2	FUN14 domain-containing protein 2	1.95E-03	0.22	SP-
Q8R5J9	Arl6ip5	PRA1 family protein 3	1.85E-04	0.21	Outcyte+

P62301	Rps13	40S ribosomal protein S13	2.51E-04	0.21	SP-
P62918	Rpl8	60S ribosomal protein L8	3.97E-04	0.21	SP-
P47964		60S ribosomal protein L36	4.00E-04	0.21	SP-
O55143	Atp2a2	Sarcoplasmic/endoplasmic reticulum calcium ATPase 2	6.37E-04	0.21	SP-
P61514	Rpl37a	60S ribosomal protein L37a	2.28E-03	0.21	SP-
Q8BX35	Eda2r	Tumor necrosis factor receptor superfamily member 27	3.46E-03	0.21	SP-
Q8CC21	Ttc19	Tetratricopeptide repeat protein 19, mitochondrial	1.98E-02	0.21	SP-
Q9CR67	Tmem33	Transmembrane protein 33	2.35E-02	0.21	Outcyte+
Q924T3	Xrcc4	DNA repair protein XRCC4	3.76E-02	0.21	SP-
P20801	Tnnc2	Troponin C, skeletal muscle	4.68E-04	0.2	SP-
P62305	Snrpe	Small nuclear ribonucleoprotein E	1.29E-03	0.2	SP-
P61957	Sumo2	Small ubiquitin-related modifier 2	3.03E-03	0.2	SP-
Q9CR68	Uqcrfs1	Cytochrome b-c1 complex subunit Rieske, mitochondrial	4.68E-03	0.2	SP-
Q61686	Cbx5	Chromobox protein homolog 5	6.27E-03	0.2	SP-
A2RSX7	Tyw5	tRNA wybutosine-synthesizing protein 5	1.27E-02	0.2	Outcyte+
P62852	Rps25	40S ribosomal protein S25	9.92E-04	0.19	Outcyte+
O70622-2	Rtn2	Isoform 2 of Reticulon-2	2.06E-03	0.19	Outcyte+
P67871	Csnk2b	Casein kinase II subunit beta	9.87E-03	0.19	SP-
Q99P72-1	Rtn4	Isoform C of Reticulon-4	1.26E-02	0.19	SP-
P11031	Sub1	Activated RNA polymerase II transcriptional coactivator p15	3.21E-02	0.19	SP-
Q9JI08	Bin3	Bridging integrator 3	4.13E-02	0.19	SP-
P58771	Tpm1	Tropomyosin alpha-1 chain	1.50E-03	0.18	SP-
Q6ZWU9	Rps27	40S ribosomal protein S27	1.66E-03	0.18	Outcyte+
P97461		40S ribosomal protein S5	1.86E-03	0.18	SP-
P97352	S100a13	Protein S100-A13	3.70E-03	0.18	SP-
Q9CQ62	Decr1	2,4-dienoyl-CoA reductase [(3E)-enoyl-CoA-producing], mitochondrial	2.16E-02	0.18	Outcyte+
Q99JF8	Psip1	PC4 and SFRS1-interacting protein	1.32E-02	0.17	SP-
P83870	Phf5a	PHD finger-like domain-containing protein 5A	1.34E-02	0.17	SP-
P09542	Myl3	Myosin light chain 3	2.20E-02	0.17	SP-
Q62084	Ppp1r14b	Protein phosphatase 1 regulatory subunit 14B	2.30E-02	0.17	SP-
Q9DCW4	Etfb	Electron transfer flavoprotein subunit beta	2.50E-02	0.17	Outcyte+
P13412	Tnni2	Troponin I, fast skeletal muscle	3.50E-03	0.16	SP-
Q9CZX8	Rps19	40S ribosomal protein S19	3.69E-03	0.16	SP-
P97351	Rps3a	40S ribosomal protein S3a	3.83E-03	0.16	SP-
P63325	Rps10	40S ribosomal protein S10	3.92E-03	0.16	SP-
P67984	Rpl22	60S ribosomal protein L22	5.81E-03	0.16	SP-
O89086	Rbm3	RNA-binding protein 3	7.11E-03	0.16	SP-
P39689	Cdkn1a	Cyclin-dependent kinase inhibitor 1	8.73E-03	0.16	SP-
Q4KML4	Abracl	Costars family protein ABRACL	2.47E-02	0.16	SP-

Q8K4F5	Abhd11	Protein ABHD11	2.72E-02	0.16	SP-
P99025	Gchfr	GTP cyclohydrolase 1 feedback regulatory protein	3.09E-02	0.16	SP-
Q9D7M1	Gid8	Glucose-induced degradation protein 8 homolog	7.59E-03	0.15	Outcyte+
P62830	Rpl23	60S ribosomal protein L23	9.78E-03	0.15	SP-
Q9JK92	Hspb8	Heat shock protein beta-8	1.51E-02	0.15	SP-
P14115	Rpl27a	60S ribosomal protein L27a	1.65E-02	0.15	SP-
Q9JKB3	Ybx3	Y-box-binding protein 3	1.74E-02	0.15	SP-
P97449	Anpep	Aminopeptidase N	1.77E-02	0.15	SP-
O35459	Ech1	Delta(3,5)-Delta(2,4)-dienoyl-CoA isomerase, mitochondrial	2.13E-02	0.15	SP-
P60824	Cirbp	Cold-inducible RNA-binding protein	3.41E-02	0.15	SP-
P14131	Rps16	40S ribosomal protein S16	1.03E-02	0.14	SP-
P63276	Rps17	40S ribosomal protein S17	1.13E-02	0.14	SP-
P62245	Rps15a	40S ribosomal protein S15a	1.29E-02	0.14	SP-
P62702	Rps4x	40S ribosomal protein S4, X isoform	1.36E-02	0.14	SP-
Q60870	Reep5	Receptor expression-enhancing protein 5	1.39E-02	0.14	Outcyte+
P62843	Rps15	40S ribosomal protein S15	1.46E-02	0.14	SP-
Q9CYR0	Ssbp1	Single-stranded DNA-binding protein, mitochondrial	1.52E-02	0.14	SP-
P84089	Erh	Enhancer of rudimentary homolog	1.85E-02	0.14	SP-
Q3TVI8	Pbxip1	Pre-B-cell leukemia transcription factor-interacting protein 1	2.52E-02	0.14	SP-
P62751	Rpl23a	60S ribosomal protein L23a	2.74E-02	0.14	Outcyte+
P97457	Myl11	Myosin regulatory light chain 11	1.66E-02	0.13	Outcyte+
P60867	Rps20	40S ribosomal protein S20	1.79E-02	0.13	SP-
Q9EPL8	Ipo7	Importin-7	1.84E-02	0.13	Outcyte+
P0DP27	Calm2	Calmodulin-2	2.13E-02	0.13	SP-
Q99L04	Dhrs1	Dehydrogenase/reductase SDR family member 1	3.20E-02	0.13	SP-
P0C0S6	H2az1	Histone H2A.Z	3.24E-02	0.13	Outcyte+
Q9R0Q7	Ptges3	Prostaglandin E synthase 3	3.36E-02	0.13	SP-
Q6ZWV3	Rpl10	60S ribosomal protein L10	3.41E-02	0.13	SP-
Q78ZA7	Nap1l4	Nucleosome assembly protein 1-like 4	3.52E-02	0.13	Outcyte+
P00920	Ca2	Carbonic anhydrase 2	3.62E-02	0.13	Outcyte+
Q9CQQ8	Lsm7	U6 snRNA-associated Sm-like protein LSm7	3.72E-02	0.13	Outcyte+
Q61425	Hadh	Hydroxyacyl-coenzyme A dehydrogenase, mitochondrial	4.01E-02	0.13	Outcyte+
P49962	Srp9	Signal recognition particle 9 kDa protein	4.11E-02	0.13	SP-
A2AN08	Ubr4	E3 ubiquitin-protein ligase UBR4	4.13E-02	0.13	SP-
P10639	Txn	Thioredoxin	2.71E-02	0.12	SP-
P62281	Rps11	40S ribosomal protein S11	2.73E-02	0.12	SP-
P09541	Myl4	Myosin light chain 4	2.75E-02	0.12	SP-
P19123	Tnnc1	Troponin C, slow skeletal and cardiac muscles	3.14E-02	0.12	Outcyte+

P50543	S100a11	Protein S100-A11	3.21E-02	0.12	SP-
P62960	Ybx1	Y-box-binding protein 1	3.28E-02	0.12	SP-
P62897	Cycs	Cytochrome c, somatic	3.42E-02	0.12	Outcyte+
P62082	Rps7	40S ribosomal protein S7	3.62E-02	0.11	SP-
P05977	Myl1	Myosin light chain 1/3, skeletal muscle isoform	4.02E-02	0.11	SP-
Q9CQW1	Ykt6	Synaptobrevin homolog YKT6	3.75E-02	-0.13	Outcyte+
Q99PL5	Rrbp1	Ribosome-binding protein 1	3.96E-02	-0.14	Outcyte+
Q01768	Nme2	Nucleoside diphosphate kinase B	4.03E-02	-0.14	Outcyte+
Q9EPC1	Parva	Alpha-parvin	2.22E-02	-0.15	SP-
Q9WUM3	Coro1b	Coronin-1B	3.51E-02	-0.15	SP-
Q8VE70	Pdcd10	Programmed cell death protein 10	4.14E-02	-0.15	Outcyte+
P0C872	Jmjd7	Bifunctional peptidase and (3S)-lysyl hydroxylase Jmjd7	4.08E-02	-0.16	Outcyte+
Q9D9V3	Echdc1	Ethylmalonyl-CoA decarboxylase	4.46E-02	-0.16	SP-
Q99K51	Pls3	Plastin-3	7.44E-03	-0.17	Outcyte+
Q5FWK3	Arhgap1	Rho GTPase-activating protein 1	9.93E-03	-0.17	SP-
Q8R1F9	Rpp40	Ribonuclease P protein subunit p40	2.23E-02	-0.17	Outcyte+
Q3UFY7	Nt5c3b	7-methylguanosine phosphate-specific 5'-nucleotidase	2.54E-02	-0.17	Outcyte+
Q64674	Srm	Spermidine synthase	3.09E-02	-0.17	Outcyte+
Q9R0P5	Dstn	Destrin	4.41E-03	-0.18	SP-
P22935	Crabp2	Cellular retinoic acid-binding protein 2	4.87E-03	-0.18	SP-
Q91YR1	Twf1	Twinfilin-1	1.03E-02	-0.18	SP-
Q8C4Q6	Aida	Axin interactor, dorsalization-associated protein	3.36E-02	-0.18	Outcyte+
P23492	Pnp	Purine nucleoside phosphorylase	4.14E-03	-0.19	Outcyte+
Q8CI51	Pdlim5	PDZ and LIM domain protein 5	9.37E-03	-0.19	Outcyte+
Q8BJH1	Zc2hc1a	Zinc finger C2HC domain-containing protein 1A	2.95E-02	-0.19	Outcyte+
P58774-2	Tpm2	Isoform 2 of Tropomyosin beta chain	2.97E-02	-0.19	Outcyte+
P40124	Cap1	Adenylyl cyclase-associated protein 1	1.61E-03	-0.2	Outcyte+
Q9CQI6	Cotl1	Coactosin-like protein	1.85E-03	-0.2	SP-
P47757-4	Capzb	Isoform 3 of F-actin-capping protein subunit beta	3.82E-03	-0.2	SP-
Q9D1G5	Lrrc57	Leucine-rich repeat-containing protein 57	8.75E-03	-0.2	Outcyte+
Q9WVA4	Tagln2	Transgelin-2	9.51E-04	-0.21	SP-
Q80XC2	Trmt61a	tRNA (adenine(58)-N(1))-methyltransferase catalytic subunit TRMT61A	1.41E-02	-0.21	SP-
Q8BK75	Elp6	Elongator complex protein 6	1.41E-02	-0.21	SP-
Q6PE15	Abhd10	Palmitoyl-protein thioesterase ABHD10, mitochondrial	1.86E-02	-0.21	SP-
Q9QZA0	Ca5b	Carbonic anhydrase 5B, mitochondrial	3.23E-02	-0.21	SP-
Q6IRU2	Tpm4	Tropomyosin alpha-4 chain	4.92E-04	-0.22	Outcyte+
Q91VH2	Snx9	Sorting nexin-9	3.44E-03	-0.22	Outcyte+

P43275	H1-1	Histone H1.1	4.22E-03	-0.24	Outcyte+
Q9JM14	Nt5c	5'(3')-deoxyribonucleotidase, cytosolic type	4.37E-03	-0.24	SP-
Q80WB5	Ntaq1	Protein N-terminal glutamine amidohydrolase	3.11E-03	-0.25	SP-
P37804	Tagln	Transgelin	1.84E-05	-0.27	SP-
Q6P8J7	Ckmt2	Creatine kinase S-type, mitochondrial	4.16E-04	-0.27	SP-
Q505K2	Fhip1a	FHF complex subunit HOOK interacting protein 1A	2.60E-04	-0.28	SP-
Q9D7A6	Srp19	Signal recognition particle 19 kDa protein	1.65E-02	-0.28	SP-
Q9D1F3	Eola1	Protein EOLA1	2.65E-02	-0.28	Outcyte+
Q61595-9	Ktn1	Isoform 9 of Kinectin	2.31E-04	-0.29	Outcyte+
P41731	Cd63	CD63 antigen	7.00E-06	-0.31	SP-
Q9QXE7	Tbl1x	F-box-like/WD repeat-containing protein TBL1X	1.50E-02	-0.32	SP-
Q8VDC0	Lars2	Probable leucine--tRNA ligase, mitochondrial	2.29E-05	-0.34	SP-
Q812E0	Cpeb2	Cytoplasmic polyadenylation element-binding protein 2	8.37E-03	-0.34	SP-
P70429	Evl	Ena/VASP-like protein	1.19E-02	-0.34	SP-
G5E8F4	Fpgt	Fucose-1-phosphate guanylyltransferase	1.77E-02	-0.34	SP-
Q09324	Gcnt1	Beta-1,3-galactosyl-O-glycosyl-glycoprotein beta-1,6-N-acetylglucosaminyltransferase	1.24E-02	-0.35	Outcyte+
P50295	Nat2	Arylamine N-acetyltransferase 2	4.91E-03	-0.36	Outcyte+
Q8CBY0	Gatc	Glutamyl-tRNA(Gln) amidotransferase subunit C, mitochondrial	6.00E-06	-0.38	SP-
Q8K1H1	Tdrd7	Tudor domain-containing protein 7	7.68E-03	-0.4	Outcyte+
Q9DC77	Smpx	Small muscular protein	1.38E-02	-0.4	SP-
A2AIG8	Accs	1-aminocyclopropane-1-carboxylate synthase-like protein 1	7.61E-03	-0.42	SP-
Q8VDM1	Zgpat	Zinc finger CCCH-type with G patch domain-containing protein	4.29E-03	-0.48	SP-
Q9D8Z6	Atg101	Autophagy-related protein 101	5.58E-03	-0.51	Outcyte+
P84078	Arf1	ADP-ribosylation factor 1	5.35E-04	-0.55	Outcyte+
P63147	Ube2b	Ubiquitin-conjugating enzyme E2 B	1.00E-17	-6.64	SP-
Q3U0V2	Tradd	Tumor necrosis factor receptor type 1-associated DEATH domain protein	1.00E-17	-6.64	SP-
Q3TYD6	Lmtk2	Serine/threonine-protein kinase LMTK2	1.00E-17	-6.64	SP-
Q9D287	Bcas2	Pre-mRNA-splicing factor SPF27	1.00E-17	-6.64	SP-
P19973	Lsp1	Lymphocyte-specific protein 1	1.00E-17	-6.64	Outcyte+
B9EJ80	Pdzd8	PDZ domain-containing protein 8	1.00E-17	-6.64	Outcyte+
P62631	Eef1a2	Elongation factor 1-alpha 2	1.00E-17	-6.64	Outcyte+
Q8BKT8	Haus7	HAUS augmin-like complex subunit 7	1.00E-17	-6.64	Outcyte+

Q9CPT3	Nanp	N-acylneuraminate-9-phosphatase	1.00E-17	-6.64	Outcyte+

Supplemental Table 3: EPS-induced differentially regulated unconventionally secreted proteins in the muscle secretome of HSkMCs obtained from three donors (EPS/CON).

UniProtKB	Gene symbol	Protein description	*p*-value	Log_2FC	Secretion type
P40394	ADH7	All-trans-retinol dehydrogenase [NAD(+)] ADH7	1.00E-17	6.64	Outcyte+
O60218	AKR1B10	Aldo-keto reductase family 1 member B10	1.00E-17	6.64	Outcyte+
Q8N2F6	ARMC10	Armadillo repeat-containing protein 10	1.00E-17	6.64	Outcyte+
Q9Y2V2	CARHSP1	Calcium-regulated heat-stable protein 1	1.00E-17	6.64	SP-
O95833	CLIC3	Chloride intracellular channel protein 3	1.00E-17	6.64	SP-
Q12926	ELAVL2	ELAV-like protein 2	1.00E-17	6.64	SP-
P01877	IGHA2	Immunoglobulin heavy constant alpha 2	1.00E-17	6.64	SP-
Q8IUC1	KRTAP11-1	Keratin-associated protein 11-1	1.00E-17	6.64	SP-
Q3LI77	KRTAP13-4	Keratin-associated protein 13-4	1.00E-17	6.64	SP-
P09960-4	LTA4H	Isoform 4 of Leukotriene A-4 hydrolase	1.00E-17	6.64	Outcyte+
P26572	MGAT1	Alpha-1,3-mannosyl-glycoprotein 2-beta-N-acetylglucosaminyltransferase	1.00E-17	6.64	SP-
Q96EY5	MVB12A	Multivesicular body subunit 12A	1.00E-17	6.64	Outcyte+
Q9Y3R4	NEU2	Sialidase-2	1.00E-17	6.64	SP-
Q8N573	OXR1	Oxidation resistance protein 1	1.00E-17	6.64	Outcyte+
P20962	PTMS	Parathymosin	1.00E-17	6.64	SP-
O43548	TGM5	Protein-glutamine gamma-glutamyltransferase 5	1.00E-17	6.64	SP-
Q9NUM4	TMEM106B	Transmembrane protein 106B	1.00E-17	6.64	SP-
P11441	UBL4A	Ubiquitin-like protein 4A	1.00E-17	6.64	SP-
P36543	ATP6V1E1	V-type proton ATPase subunit E 1	1.00E-17	3.2	Outcyte+
P29034	S100A2	Protein S100-A2	1.13E-08	2	Outcyte+
O75351	VPS4B	Vacuolar protein sorting-associated protein 4B	1.42E-04	1.64	SP-
Q9Y2G3	ATP11B	Phospholipid-transporting ATPase IF	1.05E-07	1.34	SP-
P49207	RPL34	60S ribosomal protein L34	5.18E-05	1.34	SP-
Q9BYE4	SPRR2G	Small proline-rich protein 2G	3.34E-06	1.31	SP-
Q7L523	RRAGA	Ras-related GTP-binding protein A	2.38E-03	1.31	SP-
Q9BYZ2	LDHAL6B	L-lactate dehydrogenase A-like 6B	2.26E-07	1.3	Outcyte+
P31151	S100A7	Protein S100-A7	1.12E-06	1.24	SP-
Q9Y385	UBE2J1	Ubiquitin-conjugating enzyme E2 J1	3.89E-04	1.19	Outcyte+

Q12792	TWF1	Twinfilin-1	9.33E-06	1.16	SP-
Q969L2	MAL2	Protein MAL2	1.32E-02	0.91	SP-
Q01469	FABP5	Fatty acid-binding protein 5	5.48E-04	0.87	Outcyte+
P06702	S100A9	Protein S100-A9	7.27E-04	0.86	Outcyte+
P63098	PPP3R1	Calcineurin subunit B type 1	1.51E-03	0.86	Outcyte+
P05109	S100A8	Protein S100-A8	6.58E-04	0.85	Outcyte+
Q9NZ01	TECR	Very-long-chain enoyl-CoA reductase	2.41E-02	0.83	Outcyte+
Q3ZCW2	LGALSL	Galectin-related protein	1.82E-02	0.81	Outcyte+
P07451	CA3	Carbonic anhydrase 3	4.29E-03	0.78	Outcyte+
O95147	DUSP14	Dual specificity protein phosphatase 14	2.36E-02	0.78	SP-
Q04695	KRT17	Keratin, type I cytoskeletal 17	2.05E-03	0.77	SP-
P04406-2	GAPDH	Isoform 2 of Glyceraldehyde-3-phosphate dehydrogenase	4.12E-02	0.71	Outcyte+
O95486	SEC24A	Protein transport protein Sec24A	5.72E-03	0.7	SP-
Q14320	FAM50A	Protein FAM50A	3.43E-02	0.68	Outcyte+
O75531	BANF1	Barrier-to-autointegration factor	8.18E-03	0.65	Outcyte+
Q7L5L3	GDPD3	Lysophospholipase D GDPD3	2.71E-02	0.65	Outcyte+
P62837	UBE2D2	Ubiquitin-conjugating enzyme E2 D2	8.11E-03	0.64	SP-
P47929	LGALS7; LGALS7B	Galectin-7	9.07E-03	0.64	SP-
P80294	MT1H	Metallothionein-1H	8.71E-03	0.63	SP-
Q96P63-2	SERPINB12	Isoform 2 of Serpin B12	1.12E-02	0.63	Outcyte+
P36952	SERPINB5	Serpin B5	3.26E-02	0.62	Outcyte+
Q96FQ6	S100A16	Protein S100-A16	1.36E-02	0.6	SP-
Q9HCY8	S100A14	Protein S100-A14	1.43E-02	0.6	SP-
Q9ULZ3	PYCARD	Apoptosis-associated speck-like protein containing a CARD	2.14E-02	0.6	SP-
P01834	IGKC	Immunoglobulin kappa constant	1.91E-02	0.59	SP-
Q96FX8	PERP	p53 apoptosis effector related to PMP-22	2.00E-02	0.58	Outcyte+
P63302	SELENOW	Selenoprotein W	2.49E-02	0.56	Outcyte+
P05089	ARG1	Arginase-1	2.98E-02	0.54	Outcyte+
Q53FT3	HIKESHI	Protein Hikeshi	4.21E-02	0.52	SP-
Q8WWM9	CYGB	Cytoglobin	3.61E-02	0.48	SP-
P30419	NMT1	Glycylpeptide N-tetradecanoyltransferase 1	4.33E-02	0.48	Outcyte+
P39019	RPS19	40S ribosomal protein S19	4.02E-02	-0.53	SP-
P08865	RPSA	40S ribosomal protein SA	2.72E-02	-0.58	SP-
P16949	STMN1	Stathmin	1.78E-02	-0.61	SP-
Q13642-5	FHL1	Isoform 5 of Four and a half LIM domains protein 1	1.65E-02	-0.62	Outcyte+
P62263	RPS14	40S ribosomal protein S14	3.72E-02	-0.65	SP-
P61247	RPS3A	40S ribosomal protein S3a	1.14E-02	-0.66	SP-
P62277	RPS13	40S ribosomal protein S13	3.49E-02	-0.66	SP-
P62280	RPS11	40S ribosomal protein S11	3.74E-02	-0.67	SP-
P60866	RPS20	40S ribosomal protein S20	9.41E-03	-0.68	SP-
P24534	EEF1B2	Elongation factor 1-beta	8.74E-03	-0.69	Outcyte+

Q9UPY8	MAPRE3	Microtubule-associated protein RP/EB family member 3	2.66E-02	-0.69	Outcyte+
A0AVT1	UBA6	Ubiquitin-like modifier-activating enzyme 6	4.09E-02	-0.69	Outcyte+
O15372	EIF3H	Eukaryotic translation initiation factor 3 subunit H	2.58E-02	-0.7	SP-
P63173	RPL38	60S ribosomal protein L38	3.68E-02	-0.71	SP-
P01112	HRAS	GTPase HRas	4.12E-02	-0.71	SP-
Q8WWI5	SLC44A1	Choline transporter-like protein 1	3.18E-02	-0.73	SP-
P46783	RPS10	40S ribosomal protein S10	4.74E-03	-0.76	SP-
P62851	RPS25	40S ribosomal protein S25	1.14E-02	-0.76	Outcyte+
O95361	TRIM16	Tripartite motif-containing protein 16	2.03E-02	-0.78	Outcyte+
Q8IWA5	SLC44A2	Choline transporter-like protein 2	3.19E-02	-0.78	SP-
Q5BKX8	CAVIN4	Caveolae-associated protein 4	9.87E-03	-0.8	SP-
Q12931	TRAP1	Heat shock protein 75 kDa, mitochondrial	1.69E-03	-0.81	SP-
P18077	RPL35A	60S ribosomal protein L35a	1.81E-02	-0.81	SP-
P62316	SNRPD2	Small nuclear ribonucleoprotein Sm D2	6.17E-03	-0.83	SP-
Q9BVM4	GGACT	Gamma-glutamylaminecyclotransferase	1.19E-02	-0.83	SP-
P62070	RRAS2	Ras-related protein R-Ras2	3.08E-02	-0.84	SP-
P62304	SNRPE	Small nuclear ribonucleoprotein E	1.15E-02	-0.85	SP-
P62701	RPS4X	40S ribosomal protein S4, X isoform	2.31E-03	-0.86	SP-
Q9UKK3	PARP4	Protein mono-ADP-ribosyltransferase PARP4	1.89E-02	-0.86	Outcyte+
P46782	RPS5	40S ribosomal protein S5	1.60E-03	-0.87	SP-
Q71UM5	RPS27L	40S ribosomal protein S27-like	2.10E-02	-0.91	Outcyte+
P61353	RPL27	60S ribosomal protein L27	4.58E-03	-0.92	SP-
O15427	SLC16A3	Monocarboxylate transporter 4	2.93E-02	-0.93	Outcyte+
P51114	FXR1	RNA-binding protein FXR1	3.46E-03	-0.94	SP-
P42766	RPL35	60S ribosomal protein L35	4.41E-02	-0.94	SP-
P83881	RPL36A	60S ribosomal protein L36a	1.61E-02	-0.96	SP-
P08473	MME	Neprilysin	7.82E-04	-0.99	Outcyte+
P50502	ST13	Hsc70-interacting protein	2.44E-04	-1.02	SP-
P62249	RPS16	40S ribosomal protein S16	6.36E-05	-1.03	SP-
O43236	SEPTIN4	Septin-4	1.27E-03	-1.03	SP-
P62750	RPL23A	60S ribosomal protein L23a	9.97E-04	-1.06	Outcyte+
O75508	CLDN11	Claudin-11	4.21E-03	-1.12	Outcyte+
Q96F85	CNRIP1	CB1 cannabinoid receptor-interacting protein 1	2.09E-02	-1.12	Outcyte+
Q5VST9	OBSCN	Obscurin	3.05E-03	-1.13	SP-
O14817	TSPAN4	Tetraspanin-4	7.92E-03	-1.18	SP-
O43847	NRDC	Nardilysin	1.85E-02	-1.18	Outcyte+
P27105	STOM	Stomatin	3.89E-05	-1.19	Outcyte+
Q8NBI5	SLC43A3	Equilibrative nucleobase transporter 1	1.29E-02	-1.19	Outcyte+
O14653	GOSR2	Golgi SNAP receptor complex member 2	1.23E-03	-1.2	SP-

P63027	VAMP2	Vesicle-associated membrane protein 2	1.34E-03	-1.21	SP-
O94788	ALDH1A2	Retinal dehydrogenase 2	7.53E-05	-1.22	SP-
Q99961	SH3GL1	Endophilin-A2	2.76E-03	-1.24	SP-
P63172	DYNLT1	Dynein light chain Tctex-type 1	5.24E-03	-1.25	Outcyte+
P27701	CD82	CD82 antigen	1.74E-05	-1.33	SP-
P41732	TSPAN7	Tetraspanin-7	2.85E-05	-1.33	SP-
P53985	SLC16A1	Monocarboxylate transporter 1	4.53E-04	-1.39	Outcyte+
P46776	RPL27A	60S ribosomal protein L27a	3.31E-06	-1.41	SP-
P48788	TNNI2	Troponin I, fast skeletal muscle	2.93E-05	-1.41	SP-
Q5TDH0	DDI2	Protein DDI1 homolog 2	1.53E-08	-1.45	SP-
Q9UBI6	GNG12	Guanine nucleotide-binding protein G(I)/G(S)/G(O) subunit gamma-12	3.20E-05	-1.46	SP-
P55854	SUMO3	Small ubiquitin-related modifier 3	1.37E-07	-1.72	SP-
Q8TAV4	STOML3	Stomatin-like protein 3	1.16E-07	-1.73	SP-
P16333	NCK1	Cytoplasmic protein NCK1	1.43E-06	-1.89	Outcyte+
Q9BQI0	AIF1L	Allograft inflammatory factor 1-like	1.00E-17	-6.64	SP-
Q9NWV8	BABAM1	BRISC and BRCA1-A complex member 1	1.00E-17	-6.64	Outcyte+
Q6ZP82	CCDC141	Coiled-coil domain-containing protein 141	1.00E-17	-6.64	Outcyte+
Q9UKF6	CPSF3	Cleavage and polyadenylation specificity factor subunit 3	1.00E-17	-6.64	SP-
P38919	EIF4A3	Eukaryotic initiation factor 4A-III	1.00E-17	-6.64	SP-
Q13491	GPM6B	Neuronal membrane glycoprotein M6-b	1.00E-17	-6.64	Outcyte+
Q12849	GRSF1	G-rich sequence factor 1	1.00E-17	-6.64	SP-
Q92819	HAS2	Hyaluronan synthase 2	1.00E-17	-6.64	Outcyte+
P02100	HBE1	Hemoglobin subunit epsilon	1.00E-17	-6.64	Outcyte+
Q8IUC0	KRTAP13-1	Keratin-associated protein 13-1	1.00E-17	-6.64	SP-
Q6IAA8	LAMTOR1	Ragulator complex protein LAMTOR1	1.00E-17	-6.64	SP-
P53384	NUBP1	Cytosolic Fe-S cluster assembly factor NUBP1	1.00E-17	-6.64	SP-
O43809	NUDT21	Cleavage and polyadenylation specificity factor subunit 5	1.00E-17	-6.64	Outcyte+
Q15149-8	PLEC	Isoform 8 of Plectin	1.00E-17	-6.64	SP-
Q86TP1	PRUNE1	Exopolyphosphatase PRUNE1	1.00E-17	-6.64	SP-
P11234	RALB	Ras-related protein Ral-B	1.00E-17	-6.64	Outcyte+
Q96AT9	RPE	Ribulose-phosphate 3-epimerase	1.00E-17	-6.64	Outcyte+
P11166	SLC2A1	Solute carrier family 2, facilitated glucose transporter member 1	1.00E-17	-6.64	Outcyte+
Q9BZX2	UCK2	Uridine-cytidine kinase 2	1.00E-17	-6.64	SP-

Supplemental Table 4: EPS-induced differentially regulated unconventionally secreted proteins in the muscle secretome of insulin sensitive HSkMCs obtained from five donors (EPS/CON).

UniProtKB	Gene symbol	Protein description	*p*-value	Log_2FC	Secretion type
Q96QA5	GSDMA	Gasdermin-A	1.88E-02	1.5	Outcyte+
P48509	CD151	CD151 antigen	2.10E-03	1.06	SP-
Q9UBV8	PEF1	Peflin	4.45E-02	1	SP-
P05089	ARG1	Arginase-1	2.25E-02	0.81	Outcyte+
P29034	S100A2	Protein S100-A2	1.67E-02	0.55	Outcyte+
Q99584	S100A13	Protein S100-A13	4.10E-02	0.48	Outcyte+
Q8IWV7	UBR1	E3 ubiquitin-protein ligase UBR1	1.27E-02	0.44	Outcyte+
Q96IW2	SHD	SH2 domain-containing adapter protein D	2.05E-02	0.42	SP-
P80217	IFI35	Interferon-induced 35 kDa protein	3.75E-03	0.41	Outcyte+
Q9HBL8	NMRAL1	NmrA-like family domain-containing protein 1	2.42E-03	0.38	Outcyte+
P55011	SLC12A2	Solute carrier family 12 member 2	3.06E-03	-0.31	SP-
O96019	ACTL6A	Actin-like protein 6A	1.94E-02	-0.36	Outcyte+
P08240	SRPRA	Signal recognition particle receptor subunit alpha	4.20E-02	-0.42	Outcyte+
Q8N1Q1	CA13	Carbonic anhydrase 13	3.62E-02	-0.44	Outcyte+
Q8NCH0	CHST14	Carbohydrate sulfotransferase 14	3.15E-02	-0.45	Outcyte+
Q9NTX5	ECHDC1	Ethylmalonyl-CoA decarboxylase	2.58E-02	-0.52	Outcyte+
P10301	RRAS	Ras-related protein R-Ras	4.37E-02	-0.78	SP-
Q9H0A8	COMMD4	COMM domain-containing protein 4	4.19E-02	-0.83	SP-
Q14232	EIF2B1	Translation initiation factor eIF-2B subunit alpha	1.03E-02	-0.84	Outcyte+
O14908	GIPC1	PDZ domain-containing protein GIPC1	2.67E-02	-0.85	SP-
Q8N428	GALNT16	Polypeptide N-acetylgalactosaminyltransferase 16	2.74E-02	-1.24	Outcyte+

Supplemental Table 5: PALM-induced differentially regulated unconventionally secreted proteins in the muscle secretome of insulin resistant HSkMCs obtained from five donors (PALM/CON).

UniProtKB	Gene symbol	Protein description	*p*-value	Log_2FC	Secretion type
Q12797	ASPH	Aspartyl/asparaginyl beta-hydroxylase	9.98E-03	2.36	SP-
O15372	EIF3H	Eukaryotic translation initiation factor 3 subunit H	2.69E-02	1.25	SP-
P53999	SUB1	Activated RNA polymerase II transcriptional coactivator p15	4.62E-04	1.24	SP-
Q86UE4	MTDH	Protein LYRIC	1.63E-02	1.16	Outcyte+
Q9UKM7	MAN1B1	Endoplasmic reticulum mannosyl-oligosaccharide 1,2-alpha-mannosidase	1.06E-02	1.11	SP-
P23193	TCEA1	Transcription elongation factor A protein 1	1.18E-02	1.03	SP-
O60502	OGA	Protein O-GlcNAcase	2.94E-02	1.01	Outcyte+

P18077	RPL35A	Large ribosomal subunit protein eL33	3.33E-02	1	SP-
O00487	PSMD14	26S proteasome non-ATPase regulatory subunit 14	4.23E-02	0.95	SP-
Q96QA5	GSDMA	Gasdermin-A	2.00E-02	0.9	Outcyte+
O14980	XPO1	Exportin-1	1.51E-02	0.89	SP-
Q9UMS4	PRPF19	Pre-mRNA-processing factor 19	2.45E-02	0.67	Outcyte+
P18085	ARF4	ADP-ribosylation factor 4	2.78E-02	0.66	SP-
A9UHW6	MIF4GD	MIF4G domain-containing protein	2.07E-02	0.63	Outcyte+
Q9P2E9	RRBP1	Ribosome-binding protein 1	2.53E-02	0.62	Outcyte+
Q9P0P0	RNF181	E3 ubiquitin-protein ligase RNF181	2.73E-02	0.62	SP-
O43678	NDUFA2	NADH dehydrogenase [ubiquinone] 1 alpha subcomplex subunit 2	2.39E-02	0.61	SP-
P61289	PSME3	Proteasome activator complex subunit 3	3.30E-02	0.6	Outcyte+
Q86SF2	GALNT7	N-acetylgalactosaminyltransferase 7	1.51E-03	0.57	Outcyte+
P51809	VAMP7	Vesicle-associated membrane protein 7	3.04E-02	0.55	Outcyte+
Q9H173	SIL1	Nucleotide exchange factor SIL1	4.41E-02	0.52	SP-
O75828	CBR3	Carbonyl reductase [NADPH] 3	4.24E-02	0.48	SP-
Q96P63-2	SERPINB12	Isoform 2 of Serpin B12	3.82E-02	0.47	Outcyte+
O15305	PMM2	Phosphomannomutase 2	3.36E-02	0.45	SP-
P21283	ATP6V1C1	V-type proton ATPase subunit C 1	1.47E-02	0.43	Outcyte+
O00214	LGALS8	Galectin-8	3.98E-02	0.4	Outcyte+
Q14204	DYNC1H1	Cytoplasmic dynein 1 heavy chain 1	1.49E-02	0.37	SP-
Q9P283	SEMA5B	Semaphorin-5B	2.36E-03	0.36	Outcyte+
Q96JY6	PDLIM2	PDZ and LIM domain protein 2	2.45E-02	0.33	SP-
Q15149-3	PLEC	Isoform 3 of Plectin	4.99E-03	0.33	SP-
Q16851-2	UGP2	Isoform 2 of UTP--glucose-1-phosphate uridylyltransferase	1.58E-02	0.31	Outcyte+
Q10471	GALNT2	Polypeptide N-acetylgalactosaminyltransferase 2	2.12E-02	0.3	SP-
Q96GG9	DCUN1D1	DCN1-like protein 1	2.51E-02	0.27	Outcyte+
Q9NP79	VTA1	Vacuolar protein sorting-associated protein VTA1 homolog	1.67E-02	0.24	Outcyte+
Q92520	FAM3C	Protein FAM3C	3.92E-02	0.24	SP-
P60673	PFN3	Profilin-3	5.19E-03	0.19	SP-
Q9HD42	CHMP1A	Charged multivesicular body protein 1a	3.39E-04	0.18	Outcyte+
Q15286	RAB35	Ras-related protein Rab-35	4.38E-02	0.18	Outcyte+
P01040	CSTA	Cystatin-A	3.95E-02	0.18	Outcyte+
P18669	PGAM1	Phosphoglycerate mutase 1	4.29E-02	-0.1	Outcyte+
O00764	PDXK	Pyridoxal kinase	2.89E-02	-0.11	Outcyte+
O43488	AKR7A2	Aflatoxin B1 aldehyde reductase member 2	4.32E-02	-0.13	SP-
Q8NCW5	NAXE	NAD(P)H-hydrate epimerase	3.14E-02	-0.16	SP-

P07738	BPGM	Bisphosphoglycerate mutase	3.75E-02	-0.18	Outcyte+
P13929	ENO3	Beta-enolase	3.08E-02	-0.18	Outcyte+
O95834	EML2	Echinoderm microtubule-associated protein-like 2	3.99E-02	-0.19	SP-
P11766	ADH5	Alcohol dehydrogenase class-3	4.12E-03	-0.2	Outcyte+
P61457	PCBD1	Pterin-4-alpha-carbinolamine dehydratase	6.53E-03	-0.21	Outcyte+
O43708	GSTZ1	Maleylacetoacetate isomerase	3.14E-04	-0.23	SP-
Q9HB07	MYG1	MYG1 exonuclease	8.35E-03	-0.23	SP-
O94903	PLPBP	Pyridoxal phosphate homeostasis protein	1.01E-02	-0.23	Outcyte+
P30086	PEBP1	Phosphatidylethanolamine-binding protein 1	1.71E-02	-0.24	SP-
Q9BW91	NUDT9	ADP-ribose pyrophosphatase, mitochondrial	2.76E-02	-0.26	SP-
Q08257	CRYZ	Quinone oxidoreductase	1.98E-02	-0.28	Outcyte+
Q9NWV4	CZIB	CXXC motif containing zinc binding protein	3.47E-02	-0.28	Outcyte+
Q9Y235	APOBEC2	C->U-editing enzyme APOBEC-2	1.72E-02	-0.29	Outcyte+
Q9UNP9	PPIE	Peptidyl-prolyl cis-trans isomerase E	2.60E-02	-0.33	Outcyte+
Q13228	SELENBP1	Methanethiol oxidase	2.21E-02	-0.34	Outcyte+
P15144	ANPEP	Aminopeptidase N	2.07E-02	-0.36	Outcyte+
P07108	DBI	Acyl-CoA-binding protein	1.15E-02	-0.36	Outcyte+
Q9UBQ6	EXTL2	Exostosin-like 2	1.87E-02	-0.36	SP-
Q9NPH2-2	ISYNA1	Isoform 2 of Inositol-3-phosphate synthase 1	3.20E-02	-0.38	SP-
Q9UFN0	NIPSNAP3A	Protein NipSnap homolog 3A	2.22E-02	-0.39	SP-
Q5JS37	NHLRC3	NHL repeat-containing protein 3	3.78E-03	-0.4	SP-
P55011	SLC12A2	Solute carrier family 12 member 2	1.76E-02	-0.46	SP-
O95749	GGPS1	Geranylgeranyl pyrophosphate synthase	4.48E-02	-0.47	Outcyte+
Q9GZT8	NIF3L1	NIF3-like protein 1	4.10E-02	-0.49	SP-
O43924	PDE6D	Retinal rod rhodopsin-sensitive cGMP 3',5'-cyclic phosphodiesterase subunit delta	3.05E-02	-0.5	Outcyte+
Q5T013	HYI	Putative hydroxypyruvate isomerase	2.94E-02	-0.56	SP-
P23470	PTPRG	Receptor-type tyrosine-protein phosphatase gamma	3.87E-02	-0.62	Outcyte+
Q16773	KYAT1	Kynurenine--oxoglutarate transaminase 1	1.71E-02	-0.76	Outcyte+
Q9UNA0	ADAMTS5	A disintegrin and metalloproteinase with thrombospondin motifs 5	1.43E-02	-0.79	Outcyte+

Supplemental table 6: EPS-induced differentially regulated unconventionally secreted proteins in the muscle secretome of insulin resistant HSkMCs obtained from five donors (PALM+EPS/PALM).

UniProtKB	Gene symbol	Protein description	*p*-value	Log_2FC	Secretion type
Q8TET4	GANC	Neutral alpha-glucosidase C	2.31E-02	3.41	SP-
O75923-13	DYSF	Isoform 13 of Dysferlin	1.73E-02	1.58	SP-
Q96IJ6	GMPPA	Mannose-1-phosphate guanyltransferase alpha	7.84E-04	1.46	SP-
P20929-2	NEB	Isoform 2 of Nebulin	6.68E-03	1.31	SP-
Q9NUQ7	UFSP2	Ufm1-specific protease 2	4.71E-03	1.11	Outcyte+
P49356	FNTB	Protein farnesyltransferase subunit beta	4.48E-02	0.89	SP-
Q96EY5	MVB12A	Multivesicular body subunit 12A	3.36E-02	0.75	Outcyte+
Q5T013	HYI	Putative hydroxypyruvate isomerase	7.34E-03	0.64	SP-
Q9UPT8	ZC3H4	Zinc finger CCCH domain-containing protein 4	3.36E-02	0.63	NP
Q6ZRP7	QSOX2	Sulfhydryl oxidase 2	3.12E-02	0.6	Outcyte+
Q9H773	DCTPP1	dCTP pyrophosphatase 1	1.48E-02	0.59	SP-
Q86X55	CARM1	Histone-arginine methyltransferase CARM1	3.26E-02	0.54	SP-
Q8WZ42-6	TTN	Isoform 6 of Titin	1.71E-02	0.47	SP-
Q9NZJ9	NUDT4	Diphosphoinositol polyphosphate phosphohydrolase 2	2.19E-02	0.42	SP-
Q9BSJ8	ESYT1	Extended synaptotagmin-1	2.66E-02	0.36	Outcyte+
Q8TB22	SPATA20	Spermatogenesis-associated protein 20	3.72E-02	0.32	Outcyte+
O95834	EML2	Echinoderm microtubule-associated protein-like 2	3.00E-02	0.29	SP-
P49914	MTHFS	5-formyltetrahydrofolate cyclo-ligase	2.21E-02	0.28	SP-
P46926	GNPDA1	Glucosamine-6-phosphate isomerase 1	4.47E-02	0.27	Outcyte+
O43399	TPD52L2	Tumor protein D54	5.97E-03	0.27	SP-
P16083	NQO2	Ribosyldihydronicotinamide dehydrogenase [quinone]	3.72E-02	0.26	Outcyte+
Q15382	RHEB	GTP-binding protein Rheb	1.46E-02	0.24	SP-
P04732	MT1E	Metallothionein-1E	1.36E-02	0.21	SP-
P78527	PRKDC	DNA-dependent protein kinase catalytic subunit	5.62E-03	0.19	SP-
O95292	VAPB	Vesicle-associated membrane protein-associated protein B/C	2.03E-02	0.18	Outcyte+
P05976	MYL1	Myosin light chain 1/3, skeletal muscle isoform	3.30E-02	0.17	SP-
O00233	PSMD9	26S proteasome non-ATPase regulatory subunit 9	3.10E-02	0.14	SP-
Q9UJ68	MSRA	Mitochondrial peptide methionine sulfoxide reductase	2.94E-02	0.13	SP-
P13693	TPT1	Translationally-controlled tumor protein	3.25E-02	-0.25	Outcyte+
O75503	CLN5	Ceroid-lipofuscinosis neuronal protein 5	2.90E-02	-0.36	SP-
P09874	PARP1	Poly [ADP-ribose] polymerase 1	2.66E-03	-0.38	Outcyte+

P06753	TPM3	Tropomyosin alpha-3 chain	3.94E-02	-0.47	Outcyte+
P09493-7	TPM1	Isoform 7 of Tropomyosin alpha-1 chain	2.40E-02	-0.57	Outcyte+
Q6BCY4	CYB5R2	NADH-cytochrome b5 reductase 2	1.20E-02	-0.57	SP-
Q14232	EIF2B1	Translation initiation factor eIF-2B subunit alpha	2.33E-02	-0.6	Outcyte+
Q10472	GALNT1	Polypeptide N-acetylgalactosaminyltransferase 1	4.05E-02	-0.65	Outcyte+
P09493-10	TPM1	Isoform 10 of Tropomyosin alpha-1 chain	8.65E-03	-0.67	SP-
Q9NQ48	LZTFL1	Leucine zipper transcription factor-like protein 1	3.47E-02	-1.27	SP-

Supplemental Table 7: EPS-induced differentially regulated conventionally secreted proteins in the muscle secretome of insulin resistant versus insulin sensitive HSkMCs obtained from five donors (PALM+EPS/EPS).

UniProtKB	Gene symbol	Protein description	*p*-value	Log_2FC	Secretion type
Q9H2U2	PPA2	Inorganic pyrophosphatase 2, mitochondrial	3.42E-02	3.17	Outcyte+
Q9UBB6	NCDN	Neurochondrin	2.23E-02	1.76	SP-
P38919	EIF4A3	Eukaryotic initiation factor 4A-III	3.75E-02	1.7	SP-
Q7LGC8	CHST3	Carbohydrate sulfotransferase 3	1.50E-02	1.68	SP-
Q9NWV8	BABAM1	BRISC and BRCA1-A complex member 1	8.15E-03	1.5	Outcyte+
O94929	ABLIM3	Actin-binding LIM protein 3	2.29E-02	1.48	SP-
Q00796	SORD	Sorbitol dehydrogenase	2.02E-02	1.43	Outcyte+
P54619	PRKAG1	5'-AMP-activated protein kinase subunit gamma-1	1.80E-02	1.33	Outcyte+
P21964	COMT	Catechol O-methyltransferase	1.89E-02	1.32	SP-
Q5TDH0	DDI2	Protein DDI1 homolog 2	1.37E-02	1.23	SP-
O14908	GIPC1	PDZ domain-containing protein GIPC1	6.05E-03	1.18	SP-
Q86X55	CARM1	Histone-arginine methyltransferase CARM1	2.10E-02	1.12	SP-
Q96DI7	SNRNP40	U5 small nuclear ribonucleoprotein 40 kDa protein	5.10E-04	1.04	SP-
Q9Y3A5	SBDS	Ribosome maturation protein SBDS	2.66E-02	1.04	SP-
P16234	PDGFRA	Platelet-derived growth factor receptor alpha	3.83E-02	1.04	SP-
P61289	PSME3	Proteasome activator complex subunit 3	6.86E-03	1	Outcyte+
P22234	PAICS	Bifunctional phosphoribosylaminoimidazole carboxylase/ phosphoribosylaminoimidazole succinocarboxamide synthetase	3.39E-02	1	Outcyte+
P54920	NAPA	Alpha-soluble NSF attachment protein	3.43E-02	1	Outcyte+

Q7L2H7	EIF3M	Eukaryotic translation initiation factor 3 subunit M	1.27E-02	0.96	Outcyte+
P53618	COPB1	Coatomer subunit beta	3.88E-02	0.87	Outcyte+
Q8NBF2	NHLRC2	NHL repeat-containing protein 2	3.97E-02	0.87	SP-
Q8TBC4	UBA3	NEDD8-activating enzyme E1 catalytic subunit	3.06E-03	0.86	SP-
P17661	DES	Desmin	2.70E-02	0.85	SP-
P18754	RCC1	Regulator of chromosome condensation	4.33E-02	0.85	SP-
P15170-3	GSPT1	Isoform 3 of Eukaryotic peptide chain release factor GTP-binding subunit ERF3A	3.80E-02	0.84	Outcyte+
P08240	SRPRA	Signal recognition particle receptor subunit alpha	2.23E-02	0.81	Outcyte+
P21283	ATP6V1C1	V-type proton ATPase subunit C 1	2.98E-02	0.81	Outcyte+
P36507	MAP2K2	Dual specificity mitogen-activated protein kinase kinase 2	3.06E-02	0.79	SP-
Q9UNE7	STUB1	E3 ubiquitin-protein ligase CHIP	3.96E-02	0.78	SP-
Q7Z6Z7	HUWE1	E3 ubiquitin-protein ligase HUWE1	1.41E-02	0.77	SP-
P55210	CASP7	Caspase-7	3.35E-02	0.76	Outcyte+
O94979	SEC31A	Protein transport protein Sec31A	8.46E-03	0.75	Outcyte+
Q9P299	COPZ2	Coatomer subunit zeta-2	1.59E-02	0.74	SP-
P02511	CRYAB	Alpha-crystallin B chain	3.37E-02	0.74	SP-
A0AVT1	UBA6	Ubiquitin-like modifier-activating enzyme 6	7.02E-03	0.73	Outcyte+
Q96AC1	FERMT2	Fermitin family homolog 2	1.65E-02	0.72	Outcyte+
P27701	CD82	CD82 antigen	1.45E-02	0.71	SP-
Q9H173	SIL1	Nucleotide exchange factor SIL1	1.05E-02	0.7	SP-
O75935	DCTN3	Dynactin subunit 3	3.20E-02	0.7	Outcyte+
Q9Y224	RTRAF	RNA transcription, translation and transport factor protein	3.39E-02	0.68	Outcyte+
Q8WZ42-6	TTN	Isoform 6 of Titin	3.46E-02	0.66	SP-
P42224	STAT1	Signal transducer and activator of transcription 1-alpha/beta	2.28E-02	0.64	Outcyte+
O00154	ACOT7	Cytosolic acyl coenzyme A thioester hydrolase	2.79E-02	0.64	SP-
Q9NVD7	PARVA	Alpha-parvin	1.35E-02	0.62	SP-
P04899	GNAI2	Guanine nucleotide-binding protein G(i) subunit alpha-2	2.40E-02	0.62	SP-
Q9UDY4	DNAJB4	DnaJ homolog subfamily B member 4	3.59E-03	0.61	SP-
Q9H4W6	EBF3	Transcription factor COE3	1.87E-02	0.61	SP-
P30044	PRDX5	Peroxiredoxin-5, mitochondrial	4.25E-02	0.61	SP-
P50552	VASP	Vasodilator-stimulated phosphoprotein	4.22E-02	0.56	SP-
P30084	ECHS1	Enoyl-CoA hydratase, mitochondrial	3.06E-03	0.55	SP-
P48739	PITPNB	Phosphatidylinositol transfer protein beta isoform	3.47E-02	0.55	Outcyte+
Q15149-4	PLEC	Isoform 4 of Plectin	2.34E-03	0.54	SP-

Q96P70	IPO9	Importin-9	1.90E-02	0.48	Outcyte+
P37235	HPCAL1	Hippocalcin-like protein 1	6.82E-03	0.46	SP-
P13995	MTHFD2	Bifunctional methylenetetrahydrofolate dehydrogenase/ cyclohydrolase, mitochondrial	1.49E-02	0.46	SP-
Q16222	UAP1	UDP-N-acetylhexosamine pyrophosphorylase	4.18E-02	0.46	Outcyte+
P07741	APRT	Adenine phosphoribosyltransferase	2.17E-02	0.45	Outcyte+
O76003	GLRX3	Glutaredoxin-3	1.59E-02	0.44	Outcyte+
Q06323	PSME1	Proteasome activator complex subunit 1	2.16E-02	0.44	Outcyte+
Q13884	SNTB1	Beta-1-syntrophin	2.56E-02	0.42	SP-
P15927	RPA2	Replication protein A 32 kDa subunit	1.35E-02	0.41	SP-
P15559	NQO1	NAD(P)H dehydrogenase [quinone] 1	3.46E-02	0.39	SP-
O43617	TRAPPC3	Trafficking protein particle complex subunit 3	1.91E-02	0.37	Outcyte+
Q92499	DDX1	ATP-dependent RNA helicase DDX1	1.41E-02	0.33	Outcyte+
O14980	XPO1	Exportin-1	3.85E-02	0.33	SP-
Q15286	RAB35	Ras-related protein Rab-35	2.38E-02	0.32	Outcyte+
Q8TB22	SPATA20	Spermatogenesis-associated protein 20	2.58E-02	0.32	Outcyte+
Q86Y38	XYLT1	Xylosyltransferase 1	5.35E-03	0.3	Outcyte+
P00167	CYB5A	Cytochrome b5	3.21E-02	0.25	Outcyte+
P10253	GAA	Lysosomal alpha-glucosidase	4.16E-02	0.24	SP-
O60243	HS6ST1	Heparan-sulfate 6-O-sulfotransferase 1	1.15E-02	0.2	Outcyte+
Q01518-2	CAP1	Isoform 2 of Adenylyl cyclase-associated protein 1	3.92E-02	0.15	Outcyte+
Q86WR0	CCDC25	Coiled-coil domain-containing protein 25	1.54E-02	-0.14	SP-
Q99584	S100A13	Protein S100-A13	2.35E-02	-0.26	Outcyte+
Q9Y385	UBE2J1	Ubiquitin-conjugating enzyme E2 J1	3.11E-02	-0.36	Outcyte+
Q9UBQ6	EXTL2	Exostosin-like 2	4.34E-02	-0.37	SP-
P13073	COX4I1	Cytochrome c oxidase subunit 4 isoform 1, mitochondrial	4.38E-02	-0.4	Outcyte+
O75882	ATRN	Attractin	3.55E-02	-0.42	Outcyte+
P07686	HEXB	Beta-hexosaminidase subunit beta	3.39E-02	-0.43	SP-
P43251	BTD	Biotinidase	2.76E-02	-0.45	SP-
Q9UNP9	PPIE	Peptidyl-prolyl cis-trans isomerase E	1.95E-02	-0.5	Outcyte+
P07311	ACYP1	Acylphosphatase-1	4.36E-03	-0.53	Outcyte+
O75635	SERPINB7	Serpin B7	3.69E-02	-0.6	Outcyte+
O75326	SEMA7A	Semaphorin-7A	2.62E-03	-0.6	Outcyte+
Q8NBJ4	GOLM1	Golgi membrane protein 1	1.57E-02	-0.75	Outcyte+
Q8N573	OXR1	Oxidation resistance protein 1	6.48E-04	-0.8	Outcyte+

Q9NQ48	LZTFL1	Leucine zipper transcription factor-like protein 1	3.12E-02	-1.53	SP-
Q10472	GALNT1	Polypeptide N-acetylgalactosaminyltransferase 1	4.22E-02	-1.56	Outcyte+

Supplemental Table 8: Overview of novel exercise-induced myokines.

UniProtKB	Gene symbol	Cell model	Condition	Secretion	*p*-value
Q9BY76	ANGPTL4	HSkMCs	PALM+EPS/EPS PALM/CON	SP+	9.16E-03 3.54E-02
P05090	APOD	HSkMCs	EPS/CON	SP+	1.79E-02
Q9BXJ4	C1QTNF3/ CTRP3	HSkMCs	EPS/CON	SP+	1.88E-02
P00746	CFD	HSkMCs	EPS/CON PALM+EPS/PALM	SP+	1.60E-02 2.27E-02
Q60994	Adipoq	C2C12	EPS/CON	SP+	2.68E-02
P15379	Cd44	C2C12	EPS/CON	SP+	1.03E-02
O70326	Grem1	C2C12	EPS/CON	SP+	1.93E-03
P10923	Opn/ Spp11	C2C12	EPS/CON	SP+	1.00E-17

7.4 Supplemental Figures

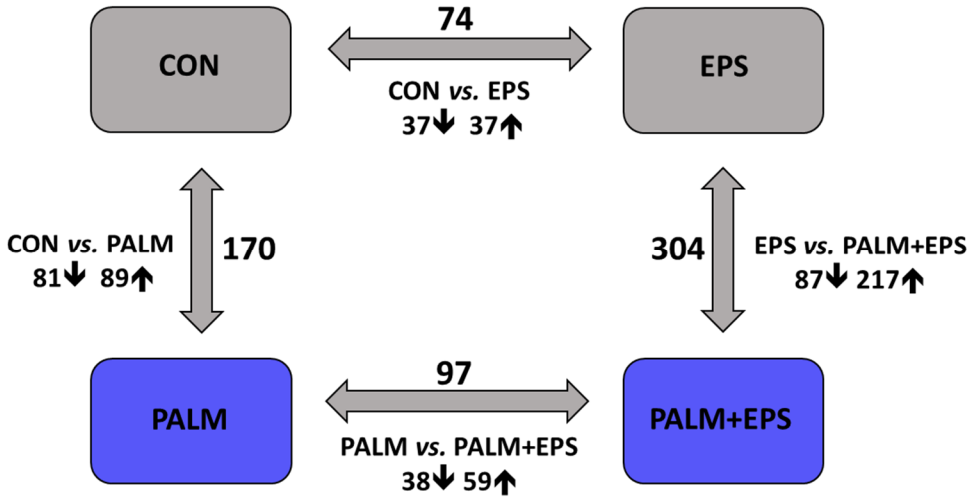

Supplemental Figure 1: Overview of differentially regulated myokines in the muscle secretomes of insulin sensitive and resistant human myotubes following acute low-frequency EPS. Human myotubes were pretreated with either BSA (insulin sensitive cells) or 800 µM palmitate (insulin resistant cells) and then subjected to 6h of low-frequency EPS**.** CM was processed within a bottom-up proteomics workflow and analyzed by high-resolution MS. HSkMCs: human skeletal muscle cells, EPS: electrical pulse stimulation, CM: conditioned media, MS: mass spectrometry

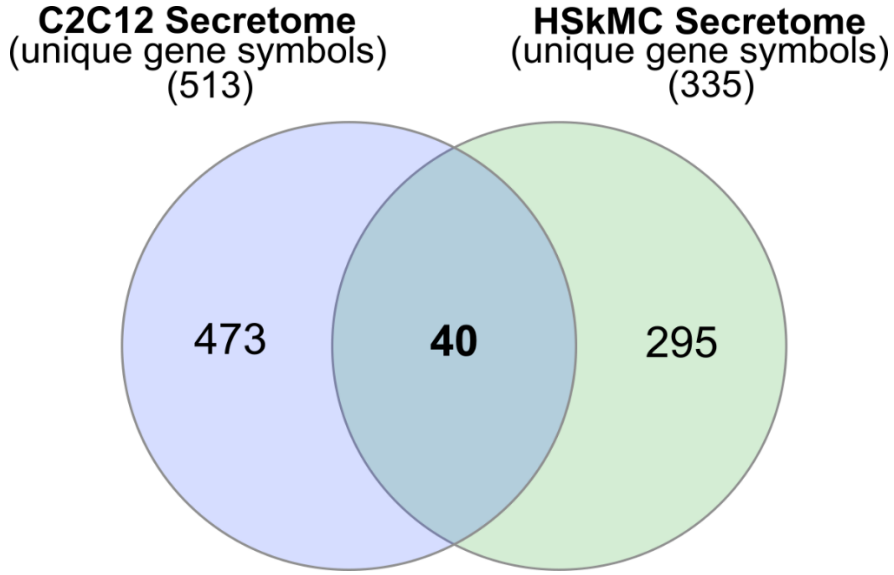

Supplemental Figure 2: Comparative analysis of EPS-induced muscle secretome of C2C12 and HSkMCs. Myotubes were subjected to acute (6h) low-frequency EPS and subsequently CM was processed within a bottom-up proteomics workflow and analyzed by high-resolution MS. HSkMCs: human skeletal muscle cells, EPS: electrical pulse stimulation, CM: conditioned media, MS: mass spectrometry

7.5 List of Figures

7.6 List of Tables

Danksagung

Mein besonderer Dank gilt Herrn Prof. Dr. Hadi Al-Hasani für die Überlassung dieses hochinteressanten Themas und das in mich gesetzte Vertrauen. Danke Hadi, für Deine große Unterstützung, Deine wertvollen Beiträge und Anregungen, die maßgeblich zum Gelingen dieser Arbeit beigetragen haben. Danke für die unzähligen wissenschaftlichen Diskussionen und aufmunternden Worte, die mich immer wieder inspiriert und motiviert haben, dieses Projekt voranzutreiben. Außerdem danke ich Dir für die besondere Möglichkeit, dass ich meine Doktorarbeit im Rahmen des Graduiertenkollegs Vivid absolvieren durfte, es war eine aufregende, spannende und lehrreiche Zeit.

Herrn Prof. Dr. Jürgen Scheller danke ich für die Übernahme des Zweitgutachtens, dem Interesse an meiner Arbeit sowie den hilfreichen Anregungen und Diskussionen im Rahmen des Graduiertenkollegs.

Ein großes Dankeschön geht an Dr. Alexandra Chadt. Danke Alexandra, für Deine wertvollen fachlichen Ratschläge zu meinem Projekt und Deine Bemühungen, wenn ich mal nicht weiterkam. Insbesondere danke ich Dir auch für Dein Engagement und Deine Unterstützung gerade zu Beginn meiner Promotionszeit, die mir trotz der COVID-19 Pandemie einen erfolgreichen Einstieg in die wissenschaftliche Arbeit im Labor ermöglicht haben.

Des Weiteren danke ich Dr. Stefan Lehr und Dr. Sonja Hartwig, für die tatkräftige Unterstützung in dieser intensiven Zeit, die vielen Proteomics Diskussionen und die aufbauenden Worte, wenn die Experimente nicht so geklappt haben wie erwartet. Ohne Eure Unterstützung wäre die vorliegende Arbeit in dieser Form nicht möglich gewesen. Außerdem möchte ich mich ganz herzlich bei Martina Schiller und Ulrike Kettel für die tolle Zusammenarbeit und Unterstützung bei den Proteomics Experimenten bedanken.

Ich danke allen gegenwärtigen und ehemaligen Kolleg*innen des Instituts für Klinische Biochemie und Pathobiochemie für eine unvergessliche Zeit. Insbesondere danke ich Anna Scheel, Aleksandra Nikolic, Dr. Lena Espelage und Didi Humpert, für die wunderbaren Erinnerungen, die wir in den letzten Jahren innerhalb und außerhalb des Labors gemeinsam erlebt haben. Vielen Dank auch an Moira Pottgießer, Michelle Deatc und Carolin Brügge für die tolle Zusammenarbeit auf Projekt 6 des Vivid Graduiertenkollegs. Es war mir eine große Freude, Euch bei eurer medizinischen Doktorarbeit zu begleiten und zu betreuen und vor allem die Höhen und Tiefen dieses Projektes mit Euch zu teilen. Außerdem ein großes Dankeschön an Dr. Christian Binsch für die immer offene Tür, die Geduld und die hilfreichen Anregungen bei meinen bioinformatischen Fragen. Ganz herzlich möchte ich mich bei Dagmar Grittner und Carina Heitmann für die tolle Zusammenarbeit und Unterstützung bei der Zellkultur bedanken. Danke Dagmar für die sorgfältige Einführung in die Arbeit mit Skelettmuskelzellen und dafür, dass du mir immer mit guten Ratschlägen zur Seite gestanden hast.

Ein besonderer Dank gilt meinem Onkel Prof. Dr. med. Ralf Stahlmann, der mich damals ermutigt hat, diese Stelle anzutreten. „Keine Angst vor neuen Herausforderungen“, hast Du gesagt. Ich bin froh und ewig dankbar, Deinen Rat befolgt zu haben.

Meinen Eltern, Ilona Stahlmann-Förster und Dr. Christian Förster, sowie meiner Schwester Leonie Paula Förster danke ich von ganzem Herzen für die unermüdliche Unterstützung in dieser intensiven, prägenden und herausfordernden Zeit. Danke, dass Ihr immer an mich geglaubt und mich auf meinem Weg begleitet habt. Ohne Euch wäre das alles nicht möglich

gewesen. Meiner besten Freundin Dr. Lavinia Bruno danke ich dafür, dass ich mich immer auf Dich verlassen konnte und Du mir immer zur Seite gestanden hast, sei es während der Schulzeit, des Studiums oder der Promotion.

Mein größter und tiefster Dank gilt jedoch meinem besten Freund und Partner, Calvin Castenow. Ich danke Dir für Deine Liebe, Geduld und Unterstützung in dieser intensiven Zeit.

Erklärung

Ich versichere an Eides Statt, dass die vorliegende Dissertation von mir eigenständig und ohne unzulässige fremde Hilfe unter Berücksichtigung der "Grundsätze zur Sicherung guter wissenschaftlicher Praxis an der Heinrich-Heine-Universität Düsseldorf" verfasst wurde.

Des Weiteren versichere ich, dass die Dissertation in der vorliegenden Form bei keiner anderen Institution vorliegt.

Düsseldorf, 10. April 2024

_____

Pia Marlene Förster